Modelling Topographic Uncertainty: Impacts on Large Scale Environmental Modelling

---

Dissertation
zur
Erlangung der naturwissenschaftlichen Doktorwürde
(Dr. sc. nat.)
vorgelegt der
Mathematisch-naturwissenschaftlichen Fakultät
der
Universität Zürich
von

Felix Hebeler

aus
Deutschland

Promotionskomitee:
Prof. Robert Weibel (Vorsitz)
Dr. Ross S. Purves (Leitung der Dissertation)
Dr. Nicholas Hulton

Zürich, 2008

Mit dem Wissen wächst der Zweifel.
– Johann Wolfgang von Goethe

To my grandfather Joseph Häusler

$*$ 14.4.1914 † 24.8.2004

Abstract

Uncertainty can be apprehended as lack of knowledge about a certain phenomenon. Decisions about whether and how to react to this uncertainty depend on a number of factors. These factors include the ability to estimate the amount of uncertainty and thus estimate the involved risk, available options to decrease either the uncertainty or its relevance, and the costs for responding or ignoring uncertainty.

In GIScience, the modelling of processes is subject to uncertainties from a number of sources. Above all, the abstraction inherent in any model results in uncertainty, created from the assumptions made to simplify complex processes and interrelations in order to formalise and model them. Additionally, uncertainty in any input data propagates through a model into the results. For topography-based models, i.e. models characterising and detecting topographic form, or models simulating processes that act upon this topography, digital elevation models (DEMs) are a potential source of uncertainty. DEMs consist of measured or digitised elevation values, and as such are subject to any error in the data capturing process. Widespread DEMs such as GLOBE or SRTM are distributed with accuracy figures that only give global measures such as root mean square error (RMSE) lacking any information on the spatial distribution of error. Where uncertainty from DEM accuracy has to be modelled to assess its impact on the results of associated topographic models, assumptions have to be made about the spatial distribution of uncertainty. Within this dissertation it has been shown that these assumptions influence the impact of uncertainty on modelled ice sheets.

Besides DEM accuracy, a number of factors in handling DEM data introduce additional uncertainty. These factors include the choice of data model, processing such as projecting and resampling of a DEM data, as well as algorithms used to extract and process elevation based information.

Within this dissertation, the influence of resampling on uncertainty in topography has been explored. This was done by assessing the variation in resampled DEMs introduced by changing the source and target resolution, choice of resampling algorithms and resampling origin. When these uncertainties were modelled and added to input

topographies for the GLIMMER ice sheet model, they had noticeable influence on modelled ice sheet configurations.

Where higher accuracy reference data for a DEM is available, error can be derived and analysed to provide information about spatial autocorrelation and possible dependencies of error with topographic attributes such as elevation, slope or roughness. Within the course of this dissertation, an uncertainty model was developed which allows modelling of GLOBE DEM uncertainty for areas without higher accuracy reference data such as Scandinavia. The model is based on derived dependencies of GLOBE error with topographic attributes, derived from areas where SRTM data was available to be used as a reference. The model includes both deterministic and stochastic components and reproduces GLOBE DEM uncertainty well for different test areas.

The developed uncertainty model was applied to investigate the impact of DEM uncertainty on different types of models in three case studies. The first case study applied a geomorphologic and hydrologic model (TARDEM), the second case study used two snow melt models, and in the third case study the GLIMMER ice sheet model was employed. Results showed the impact of uncertainty to be depending on a number of facts. Generally, modelled DEM uncertainty had less impact on derived global topographic variables such as mean slope length or the number of derived watersheds when applied to a hydrological model. Higher impacts were recorded where the model focus was on local processes, such as the delineation of a certain watershed and calculation of associated parameters such as hypsometry. For process models like the ice sheet model, factors such as terrain configuration (smooth vs. rough topography, abundant ridges or valleys) influenced the impact of DEM uncertainty on ice sheet model (ISM) results.

Additionally, the amount of uncertainty and its spatial correlation, as well as the relative influence of topography within a model were found to play key roles. This implies that for process models, the impact of uncertainty can vary over time. In the case of the ice sheet model, uncertainty had the greatest impact on ice sheet configuration during phases of inception and retreat, and its impact was shown to be dependent on the overall size of the ice masses.

In another set of experiments, a range of sensitivity tests using different ISM parameters and input data were conducted, and the results of these tests were used to conduct a full parametric uncertainty analysis (PUA) for a steady-state climate scenario on Fennoscandia. Results from this analysis allowed the comparison of the influence of uncertainty in other parameters to that of DEM uncertainty, which was found to be equivalent to a 1 °C change in climate. The impact of DEM uncertainty was found to

be comparable to that of various 'internal' ISM parameters. However modelled DEM uncertainty resulted in significantly different ice sheet configurations. This underlines the importance of DEM uncertainty to be considered in ice sheet modelling.

Using different temperature index models (TIM) to model potential snow melt across different resolutions revealed significant impact of scale and resampling on modelled melt rates. This effect was substantially decreased by the use of subgrid model approaches. While it was shown that these subgrid approaches are subject to an increased susceptibility to DEM uncertainty, this effect was more than compensated for by an increased performance in terms of modelled melt rates.

In summary, the results of this dissertation underline the necessity of detailed information on the statistical and spatial distribution of DEM uncertainty to be included with the data. Additionally, in topographic modelling, uncertainty from other sources such as resampling have shown to be of importance, and modellers and end-users should account for these uncertainties introduced into model results.

Zusammenfassung

Unsicherheit kann als ein Mangel an Wissen über ein bestimmtes Phänomen verstanden werden. Die Entscheidung, wie und ob auf diese Unsicherheit zu reagieren ist, hängt von einer Reihe von Faktoren ab. Diese Faktoren beinhalten die Fähigkeit, die Unsicherheit und das damit verbundene Risiko abzuschätzen, die Möglichkeit entweder die Unsicherheit selbst oder deren Relevanz zu verringern, sowie die mit einer Reaktion verbundenen Kosten.

Das Modellieren von Prozessen in den Geoinformationswissenschaften unterliegt Unsicherheiten aus einer Reihe von Quellen. Vor allem die in jedem Model implizit vorhandene Abstraktion erzeugt Unsicherheiten, z.B. durch Annahmen zur Vereinfachung komplexer Prozesse und Abhängigkeiten, welche getroffen werden um eine Modellierung zu ermöglichen. Zusätzlich pflanzen sich Unsicherheiten in den Eingangsdaten durch die Modelkette in die Ergebnisse fort. Für topographiebasierte Modelle, die zum Beispiel zur Beschreibung und Erkennung von topographischen Formen verwendet werden, oder für Modelle, die Prozesse auf topographischen Oberflächen simulieren, sind die verwendeten digitalen Höhenmodelle (DHM) eine potentielle Quelle von Unsicherheiten. DHM bestehen aus gemessenen oder digitalisierten Höhenwerten und sind daher Fehlern in der Datenerfassung unterworfen. Verbreitete DHM wie GLOBE und SRTM enthalten als einzige Angabe zur Datengenauigkeit die Wurzel der mittleren quadratischen vertikalen Abweichung, während Informationen zur deren räumlichen Verteilung vollständig fehlen. Um die Auswirkungen der Unsicherheit aus DHM Ungenauigkeiten auf topographiebasierte Modelle zu analysieren, muss diese Unsicherheit simulierte werden. Sind keine Angaben zur räumlichen Verteilung vorhanden, müssen diesbezüglich Annahmen getroffen werden. Im Rahmen der vorliegenden Dissertation konnte gezeigt werden, dass diese Annahmen sich auf den Einfluss von Unsicherheiten auswirken, im konkreten Fall auf Ergebnisse eines Eisschild Modells (ESM).

Bei der Verwendung von DHM können Unsicherheiten aus einer Reihe weiterer Faktoren herrühren. Diese Faktoren sind z.B. das verwendete Datenmodell, Datenver-

arbeitung wie Projizieren oder Resampling eines DHM, sowie die Wahl der Algorithmen bei der Extrahierung und Verarbeitung von Höhendaten. Im Rahmen dieser Dissertation wurde der Einfluss des Resamplings auf topographische Unsicherheiten untersucht. Dazu wurden Faktoren wie die Ausgangs und Zielauflösung, die verwendeten Algorithmen und der Ursprung variiert, und die Abweichungen in den resultierenden, niedriger aufgelösten DHM analysiert. Die für das GLIMMER ESM verwendeten Topographien wurden mit diesen Unsicherheiten variiert, was zu deutlichen Unterschieden in den Ergebnissen führte. Wo Referenzdaten mit höherer Genauigkeit für ein DHM vorliegen, können Fehler berechnet und analysiert werden, um Informationen zur räumlichen Autokorrelation sowie zu Abhängigkeiten der Fehler von topographischen Kennwerten wie Höhe, Hangneigung oder Rauigkeit abzuleiten. Im Rahmen dieser Dissertation wurde ein Unsicherheitsmodell entwickelt, das die Modellierung von GLOBE DHM Unsicherheiten erlaubt, für die keine Referenzdaten vorliegen. Dieses Modell basiert auf Abhängigkeiten von GLOBE DHM Fehlern von topographischen Kennwerten, die für Gebiete in denen SRTM als Referenz verfügbar ist ermittelt wurden. Das Modell besteht sowohl aus deterministischen wie stochastischen Komponenten, und reproduziert GLOBE DHM Unsicherheiten für verschiedene Testgebiete gut.

Das entwickelte Unsicherheitsmodell wurde verwendet um die Auswirkungen von DHM Unsicherheiten auf verschiedene Modelltypen zu testen. Hierzu wurden drei Fallstudien durchgeführt; jeweils eine mit einem geomorphologischen/hydrologischen Modell (TARDEM), eine zweite mit zwei unterschiedlichen Schmelzmodellen, und eine dritte unter Verwendung des GLIMMER Eisschild Modells. Die Ergebnisse zeigen, dass die Auswirkungen der DHM Unsicherheiten von einer Reihe von Faktoren abhängen. Bei der Verwendung mit einem hydrologischen Modell hatten Unsicherheiten grundsätzlich geringeren Einfluss auf die Berechnung globaler topographischer Kennwerte wie der mittleren Hanglänge oder der Anzahl der berechneten Einzugsgebiete in einem DHM. Der Einfluss wurde deutlich größer, wenn lokale Kennwerte bestimmt wurden, wie z.B. die Grenzen einzelner Einzugsgebiete, oder deren Hypsometrie. Der Einfluss der Unsicherheit in Prozessmodellen wie dem verwendeten ESM hing zusätzlich von Faktoren wie der Charakteristik des Geländes (gleichmäßige oder raue Oberfläche, vorhandene Bergrücken oder Täler) ab. Zusätzlich spielten die Menge und räumliche Korrelation der Unsicherheit, sowie der relative Einfluss der Topographie auf das betrachtete Modell eine wichtige Rolle. Dies bedeutet, dass der Einfluss der Unsicherheit auf Prozessmodelle zeitlich variieren kann. Im Fall des Eissschildmodells waren die größten Auswirkungen der DHM Unsicherheit bei der Neubildung

von Eisschilden sowie bei deren Rückzug zu verzeichnen. Außerdem war der relative Einfluss abhängig von der absoluten Größe des modellierten Eisschildes.

In weiteren Experimenten wurden Sensitivitätstests für eine Reihe von ESM Parametern und Eingangsdaten durchgeführt, und die Resultate wurden dazu verwendet, eine Parametrische Unsicherheitsanalyse (PUA) durchzuführen. Die Analyse wurde für simulierte Eisschilde im Gleichgewichtszustand in Skandinavien durchgeführt, um einen Vergleich des Einflusses der DHM Unsicherheit mit jenem der Unsicherheit anderer Parameter zu ermöglichen. Die Abweichung der ESM Ergebnisse aufgrund von DHM Unsicherheiten entspricht der klimatischen Veränderung von 1 °C, und ist vergleichbar mit dem Einfluss verschiedener 'interner' Modelparameter. Unsicherheiten in der Topographie resultierten jedoch in signifikanten Unterschieden in der räumlichen Anordnung der modellierten Eisschilde. Dies unterstreicht die Dringlichkeit, den Einfluss von topographischer Unsicherheit bei der Modellierung von Eisschilden zu berücksichtigen. Die Verwendung verschiedener Temperatur Index Modelle (TIM) zur Modellierung potentieller Schneeschmelze in verschiedenen Auflösungen zeigte deutliche Einflüsse von Auflösung und Resampling auf modellierte Schmelzraten. Dieser Effekt konnte durch die Verwendung sogenannter 'Subgrid' Modelle deutlich verringert werden. Allerdings zeigten die verwendeten Subgrid Parametrisierungen eine erhöhte Anfälligkeit gegenüber DHM Unsicherheiten, die jedoch durch die verbesserte Effizienz und Qualität der Ergebnisse mehr als ausgeglichen wurde.

Zusammenfassend unterstreichen die Ergebnisse dieser Dissertation die Notwendigkeit, dass DHM Daten detaillierte Informationen zur statistischen wie räumlichen Verteilung von Unsicherheiten beinhalten müssen. Zusätzlich sind bei der Verwendung von DHM Unsicherheiten anderen Ursprungs von Bedeutung und müssen von Modellierern und Benutzern berücksichtigt werden.

Contents

List of Tables

List of Figures

List of Appendices

List of Acronyms

DCW	Digital Chart of the World
DEM	Digital Elevation Model
DDF	Degree Day Factor
DTED	Digital Terrain Elevation Data
DTM	Digital Terrain Model
EBM	Energy Balance Model
ELA	Equilibrium Line Altitude
GIS	Geographic Information System
IDW	Inverse Distance Weighting
ISM	Ice Sheet Model(ing)
LGM	Last Glacial Maximum
LIDAR	LIght Detection And Ranging
LISA	Local Indicator of Spatial Association
MAAT	Mean Annual Air Temperature
MCS	Monte Carlo Simulation
PDD	Positive Degree Days
PDF	Probability Distribution Function
RVT	Regionalized Variable Theory
SIA	Shallow Ice Approximation
SRTM	Shuttle Radar Topography Mission
TIM	Triangulated Irregular Network
TWI	Topographic Wetness Index

List of Symbols

β	Clausius-Clapeyron gradient
$\dot{\varepsilon}$	Shear strain rate
∇	Horizontal gradient operator
ρ_i	Density (of ice)
σ	Longitudinal deviatoric stress
τ	Shear stress
A	Arrhenius value
a	Accumulation
b	Mass balance
c	Ablation
c_p	Specific heat capacity of ice
G	Geothermal heat flux
g	Acceleration by gravity (9.81 m s^{-2})
H	Ice thickness
h	Elevation at ice base
k	Conductivity of ice
m	Melt
n	Flow law exponent
Q	Activation energy for creep
Q_g	Deformation heat
R	Gas constant (8.314 J $mol^{-1}\,K^{-1}$)
S	Elevation at ice surface
T	Temperature
t	Time
u	Velocity (horizontal)
w	Velocity (vertical)

Acknowledgments

Above all, I would like to thank Dr. Ross Purves, who has been a great supervisor and friend, and showed great endurance helping and motivating me through the course of my dissertation. I am grateful for the countless times he was there with advice not only concerning scientific issues and his efforts in making my work a worthwhile experience.
I would also like to express my gratitude to Prof. Robert Weibel for making it possible to receive a doctorate at the GIS division of the GIUZ and the Swiss National Fund for financing my work.
Many thanks go to Dr. Nicholas Hulton for co-supervising my dissertation and to Dr. Magnus Hagdorn and Stewart Jamieson, without whom my work with the GLIMMER ice sheet model would not have been so successful.
I would also like to thank Prof. Peter Fisher and Dr. Jo Wood for their valuable input formulating some of the ideas in this thesis, and Dr. Phaedon Kyriakidis for providing me with his valuable Matlab Geostatistics toolbox.
I am indebted to Dr. Felix Morsdorf for being my personal Matlab guru. Honest thanks appertain to Ralph Straumann for being a great officemate and an excellent proofreader. Thanks also to Dr. Daniel Wirz who has helped me through those first month of UNIX, and the whole IT Team who kept me going. Finally, I would like to thank everyone at the GIUZ for making my time not all work, but also fun.
I of course also owe gratitude to my parents who had to understand that I was writing yet another thesis.

I am much obliged to Katja Adl-Amini, who went through all those ups and downs with me – again. I could not have done it without you!

Chapter 1

Introduction

1.1 Motivation

1.1.1 The Phenomenon of Uncertainty

Uncertainty is a part of our everyday life – individuals and the society they form can (usually) handle uncertainty depending on its context using different strategies. During a day, we are continuously making decisions about whether uncertainty in a certain situation is relevant and needs to be dealt with or can be ignored. If we are uncertain about the time it takes to transfer from our hotel to the train station in an unfamiliar city, we try to assess this uncertainty. We might estimate for example that if a shuttle exists transfer time might be 5 minutes, while walking might take us 30 minutes. Additionally, we estimate the risk, in this case missing the train. Based on the amount of uncertainty - often associated with likeliness - and the respective risk, we judge whether this impact is relevant to us. If the relevance is high enough, we might decide to respond to the uncertainty by reducing it through acquiring additional information, in this case about the transfer times and distances, beforehand. Or we might decide to leave the hotel earlier, thus reducing the relevance of the uncertainty, at the cost of a long wait at the station.

Uncertainty and its relevance to us is obviously dependent on a number of factors, such as context: in the above example we would judge the risk very differently depending on whether we can take a later train at no additional cost leaving every 10 minutes, or whether there is only one train a day, and we have to make the connection to get to an important job interview on time. Similarly, relevance of uncertainty depends on previous experiences, character, the phenomenon that is uncertain, and the possi-

ble consequences – for different people from different cultures in different situations, uncertainty in the same context might be either relevant or irrelevant.

How relevant uncertainty in a certain situation is to us also depends on our abilities and the possibilities to act upon it. If we have to walk from a location A to another location B, and we estimate the time it will take to be about 20 minutes, it might not matter to us how accurate the estimate is. If we have to catch a train at B, relevance of the estimate quality is increased - the threshold for a concerning amount of uncertainty is lowered. While we are walking from A to B, we can update our estimation based on the time it took to cover the first part of the distance, the traffic ahead, etc. and create some knowledge from this experience. If we decide it is more likely the walk will take longer than expected, we will respond to it by speeding up. Formally, the quality of our decision is a function of risk, costs and benefits (Agumya and Hunter, 2002), in this case the risk of missing the train, the cost of an exhausting and embarrassing run with luggage (or a long wait in case of early arrival) and the benefit of making the connection with minimal effort. Coping with uncertainty in this way requires the possibility to constantly or repeatedly reassess the situation - time elapsed, distance travelled - and possibly notion and experience about the environment we navigate in or environments similar to it. Our experience from this trip and any previous ones and the knowledge gained will build up and enable us to even better estimate our next travel time and to make a decision whether the uncertainty inherent in it needs to be tackled and if so, how.

The decision making process inherent in coping with day to day uncertainty can be captured in a decision tree (Fig. 1.1). While this procedure is similar for dealing with uncertainty in the more formalised and abstract situation of decision making and modelling, a number of differences exist. Because in our daily life we most often cope with uncertainty and its relevance to ourselves, the aim is usually to reduce it to a point we can live with it – meaning to a convenient point where we can usually ignore it – and we do this intuitively and do not have to communicate it. On the contrary in decision making or modelling, we have to formalise uncertainty in order to assess it, and also all the knowledge on its amount, impact and relevance gained along the decision tree, in order to communicate it to decision makers or end-users. Also, the sources of uncertainty and the factors influencing the necessary judgments can differ.
For example a key aspect of modelling is that it is an abstraction of reality - it might be just the inherent simplification that enables us to understand and explore a complex process chain - yet this abstraction introduces uncertainty. This implies that every model per definition is subject to uncertainty, which has to be accounted for, evaluated

and decided upon. While geographic information systems (GIS) can be very powerful tools for modelling, e.g. of environmental systems, modelling in itself has a number of shortcomings compared to our ability of handling uncertainty in everyday life: there is (usually) no option of continuous reassessment and measuring of data, and a GIS can process information, but it cannot convert the information it receives to knowledge (Couclelis, 2003). We however can, and using a GIS, we therefore have to assess the uncertainty inherent in any associated data or model, estimate its impact and make decisions about possible actions to take – we might even build a knowledgebase. In any case, the quality of the decision whether and how to handle uncertainty is again a function of risk, cost and benefit, and a range of literature is dealing with fitness of use assessment of data, decision making and risk assessment in GIScience (Harrower, 2004; Agumya and Hunter, 2002).

Identifying and understanding the source and the nature of uncertainty, for example of a data set, is essential for detecting, measuring and modelling uncertainty, which in turn is necessary to decide whether it is negligible, can be reduced or should be communicated (Plewe, 2002; Veregin, 1989). In GIScience, we are most commonly working with sets of data that have been acquired using techniques and sensors we are often not (completely) familiar with, that we have not acquired ourselves, and that we seldom have the option to verify or refine. We are applying methods and tools we have not developed ourselves, to manage and analyse the data. We are using models that might be black boxes to produce results and visualise them in order to convey them to others. Each of these steps has many sources of uncertainty that might be difficult to assess, propagate through the modelling chain and interrelate to an overburdening complexity - and no GIS can estimate which uncertainty is relevant for which data and which task without human interaction. However, GIS have been developed for precise and accurate engineering and helping with complex tasks, for example to improve the accuracy, assessment, management and updating of land register data over single paper maps, and we would like to think of computer aided map production and risk assessment as reliable and flawless. Therefore it requires both awareness of the fact that uncertainty is inevitable and often considerable effort to investigate it, and more often than not, uncertainty is voluntarily or involuntarily ignored – Agumya and Hunter (2002) call this phenomenon often seen in the use of geographical data ‘risk retention’.

While in everyday live differentiating between the uncertainty inherent in a phenomenon itself (indeterminacy) or in the assertions of this phenomenon is hardly relevant, in order to understand how uncertainty propagates through a system we try to model using a GIS, we have to differentiate (Plewe, 2002). If we want to know how

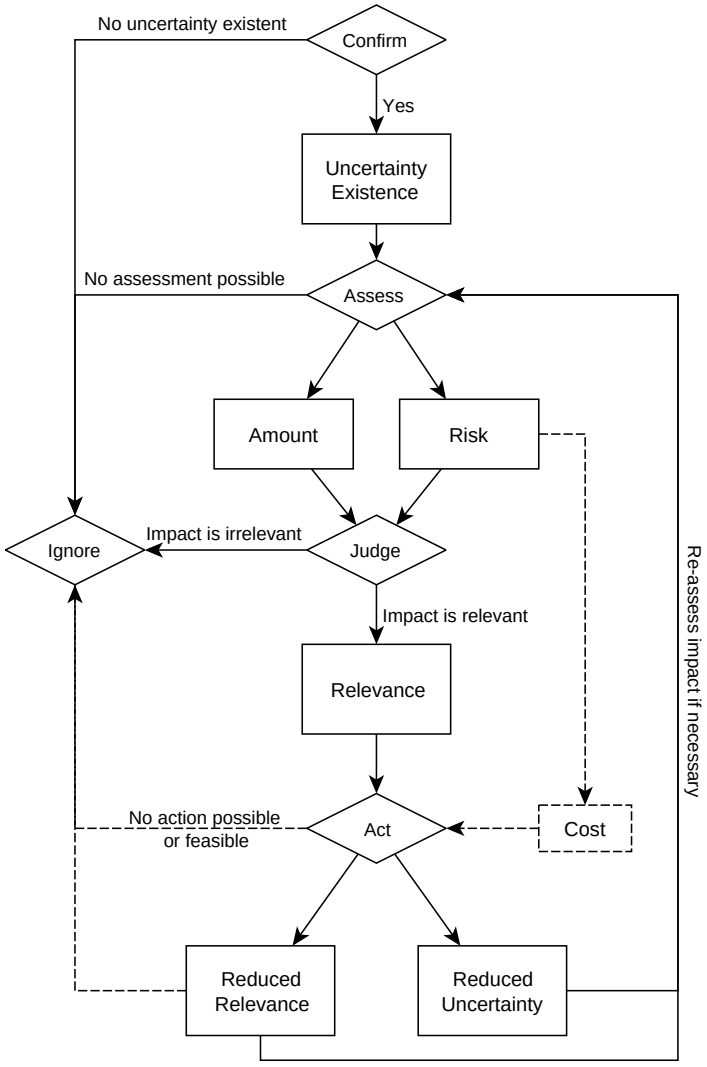

Figure 1.1: Decision tree for handling uncertainty. Once the existence of uncertainty in a decision, task or phenomenon is confirmed, the possible impact of this uncertainty has to be estimated by assessing the amount of uncertainty (often via the likeliness of extreme events) and the associated risk. It is then judged whether this impact is relevant or not, and possible actions can be chosen based on risk/cost analysis, that either reduce the amount of uncertainty or its relevance. While in everyday life uncertainty at some point ceases to play a role and can be ignored, in decision making or modelling tasks, information about uncertainty must not be discarded.

accurate or likely a prognosis we made based on a flood model is, we need to know about the accuracy of the input data, the degree of abstraction the conceptual flood model applies, the uncertainty introduced through our choice of algorithms, and even the comprehensibility of the output maps we give to decision makers.

A vast number of potential uncertainty sources exist, and for object boundaries alone, Couclelis (1996) has identified 120 kinds of uncertainty. For models that simulate processes based on topography, the digital elevation models (DEM) that are commonly used are an important source of uncertainty, and some aspects such as data accuracy, scale and algorithms used to derive topographic attributes have been examined in relative depths for their contribution to uncertainty in model results (e.g.

Oksanen and Sarjakoski, 2005a; Kienzle, 2004; Armstrong and Martz, 2003; Jones, 1998, and others). On the other hand, aspects such as the influence of the conceptual model applied to represent the continuous surface of the earth in digital form, or the preprocessing of data such as projecting and resampling, have been widely ignored (with some notable exceptions such as Schneider, 2001a,b). While it is common knowledge that elevation and its derivatives are influenced by the resolution of a DEM (e.g. Florinsky, 1998), the uncertainty introduced by factors such as the origin of resampling or the choice of resampling methods has - to my knowledge - been the subject of only a single publication (Fisher, 1996). This might be due to the fact that resampling a DEM to a lower resolution is commonly associated with lower accuracy, and any additional uncertainty introduced to this data is commonly disregarded as being of minor importance in comparison. The same holds for data accuracy of DEMs that have been resampled: in the light of the lower 'inaccurate' resolution, any uncertainty present in the original data appears to become irrelevant in the eye of the user, despite Hebeler and Purves (2005a) have shown that uncertainty in 1km data propagates to resolutions of 10 and 20km with noticeable impact on model results.

1.1.2 Modelling of Ice

Much of today's shape of the earth has been formed by ice sheets during the ice ages, and present day global circulation is largely influenced by the vast ice masses at the poles. Therefore understanding the dynamics of the cryosphere is often a key to understanding the dynamics of the earth's climate and geomorphology - past, present and future. The waxing and waning of ice sheets through the glacial stages has formed most of the landscapes around us, and the boundaries of these different stages, as marked by glaciomorphologic features such as moraines, kames and osers, serve as proxies in the examination and understanding of past climates and their impact on the earths climate and ecosystems. The advance and retreat of glaciers – remnants of the ice ages – has been observed and documented for more than 400 years, with increasing intensity since the 'Little Ice Age' in the middle of the 1800s (Benn and Evans, 1998). Dynamic modelling of the cryosphere, particulary of glaciers, ice sheets and permafrost, evolved soon after microcomputers became available (e.g. Budd and Jenssen, 1975), and has contributed significantly to our understanding of the global climate and the possible implications of climate change.

Glaciers are known to be important factors in hydrological modelling, as they function as freshwater resources and retention ponds (Jansson et al., 2003). Despite their impor-

tance in regional hydrology, only approximately 0.2% of the worlds freshwater stored as ice is made up by glaciers, while 98.5% is stored in the large ice sheets of Greenland and Antarctica (Slaymaker and Kelly, 2007). If both of these ice sheets would melt completely, an estimated global sea-level rise of approximately 70m would be the result (Alley et al., 2005). Consequently, because of their importance in climate research, geomorphology, sea level change prognosis and even risk analysis (e.g. for nuclear waste ultimate disposal places), a range of ice sheet models have been developed over time by different research groups. The original aims in the development of these models were diverse, with the foci on different regions such as Antarctica, Greenland, Patagonia, the Laurentide or Fennoscandian ice sheet, as well as on different aspects of ice sheet modelling, such as climate interaction, calving, ice streams or isostatic response (Hindmarsh, 1993). Gradually, these different models have spread and evolved, and currently about a dozen generic models with widespread application exist, such as GLIMMER (Hagdorn et al., 2007) or SICOPOLIS (Calov et al., 1998). In the EISMINT intercomparison initiative (Payne et al., 2000; Huybrechts et al., 1996), amongst others ten models applying the shallow ice approximation (SIA) have been used to model a set of scenarios (Huybrechts et al., 1996).

With the introduction and the subsequent constant improvement of remote sensing techniques, data collection for remote and difficult to access areas is also improving. Amongst others, climate and topographic data on the large inland ice sheets of Greenland and the Antarctica is becoming accessible in sufficient quality and extent (e.g. Lythe et al., 2001) to better understand the mechanisms of the wax and wane of ice sheets through the recent glacial series. Simulation of ice sheet growth and retreat through the past glacial series is not only of interest in terms of earth history, but also the verification of these simulations through empirical data, for example on maximum ice sheet extents during the Last Glacial Maximum (LGM), allows to improve these models. This in turn is crucial to create reliable scenarios of ice sheet growth and retreat under possible future climate change, and the impact this will have on sea-level rise, precipitation patterns and other climatic factors.
A substantial number of sensitivity studies focussing on different climate and model parameters as well as different regions have been conducted (e.g. Essery and Etchevers, 2004; Pattyn, 2003b; Purves and Hulton, 2000a; Huybrechts and de Wolde, 1999; Ritz et al., 1997; Fabre et al., 1995; van de Wal and Oerlemans, 1994). However, despite the recognition of the importance of topography for the modelling of both glaciers and ice sheets (Kerr, 1993), few studies on the influence of topography and associated uncertainties on simulated ice sheets exist.

Bedrock topography however is an important factor in ISM, as it influences ice sheet behaviour via its influence on both climate and ice dynamics. Since elevation is directly related to temperature, it influences mass balance via ablation for temperatures above 0 °C and precipitation for temperatures below freezing. Air temperature also determines ice temperature and thus influences ice dynamics through the dependency of ice velocity on viscosity. The influence of topography on climate, for example through the effect of rain shadow or continentality is modelled implicitly via the input climate forcing schemes. Geomorphology, as captured in the input topography, also influences ice sheet configuration by constraining, reducing or enhancing ice flow, either directly through the slope gradient, or through the arrangement of landscape features such as ridges or through valleys (Jamieson et al., 2008). Studies on the nucleation of ice sheets have emphasised the importance of certain landscape features such as peaks and high intermontane valleys, and have confirmed that ablation processes are poorly resolved in low resolution ISM (Marshall, 2002; Sugden et al., 2002; Marshall and Clarke, 1999).

Models of physical systems such as ice sheets are usually complex and non-linear, and changes of one parameter can influence the system both directly and indirectly through a number of feedback mechanisms, making an analytical estimation of the impact difficult or even impossible. Repeated modelling with varying parameters using Monte Carlo Simulation is a common approach for testing sensitivity of ISM to input parameters (van der Veen, 2002).

1.2 Thesis Rationale

Despite a wide range of existing work on uncertainty in GIS and geographic data, further investigation of the nature of topographic uncertainty is both a necessary and promising task. A large variety of potential sources of uncertainty related to topography exist, which need to be assessed and examined. The impact of this uncertainty on applications that make use of topographies, such as techniques used to extract landforms or models that simulate physical processes such as ISMs, needs to be understood, quantified and compared. In order to do so, topographic uncertainties of a specific source have to be modelled. While for some uncertainties, such as DEM accuracy, approaches for uncertainty modelling have been developed, a number of shortcomings exist, e.g. where only global DEM accuracy figures are available. Other sources of uncertainty from topographic representation such as resampling to lower resolutions,

have not yet been explored or modelled.
This leads to the formulation of a set of research question and objectives:

1.2.1 Research Questions

The research questions of this work can be divided into three categories. The first are concerned with the nature of topographic uncertainty:

1. What are the sources of uncertainty in/from topographic representation?
2. How can this uncertainty be quantified and modelled?

The second deals with the impact this uncertainty has on topography-based applications:

3. What impact does uncertainty from topographic representation have on topography-based modelling?
   Two case studies are used:
   - Geomorphological modelling
   - Ice sheet modelling
4. Where (on what topography/landform), when (during which phases) and how (through which mechanisms) does uncertainty from topographic representation impact ice sheet modelling?

The third category focuses on handling uncertainty and using the insights gained from answers to the previous research questions.

5. How can the effect of uncertainty from topographic representation be quantified and communicated?
6. How can the impact of uncertainty from topographic representation on ice sheet modelling be minimised?

1.2.2 Research Objectives

From the research questions formulated in the previous section, three main research objectives have been identified:

1. To identify sources of uncertainty from topographic representation and model uncertainty to assess its impact in environmental modelling.
2. To understand the mechanisms of uncertainty impact on form and process models.
3. To develop methods that minimise the impact of uncertainty from topographic representation in ISM.

1.2.3 Structure of the Thesis

In the following chapter 2, the subject of error and uncertainty in GIScience as discussed in the literature is presented, with an emphasis on spatial uncertainty. Because topographic uncertainty is the key topic of this dissertation, the state of the art of modelling topography as digital elevation models, and the inherent uncertainty will be presented, as well as existing approaches for assessing and modelling this uncertainty. As models are usually linked to topography via topographic attributes, their derivation and uncertainty within it is presented in a separate section, followed by a presentation of the state of the art of ice sheet modelling, associated uncertainties and approaches to overcome these uncertainties. The section finishes with an overview of the development and discussion of methods to communicate and visualise uncertainty, and implications of this state of the art to the dissertation at hand.

In chapter 3, an overview of the methodology used within the five papers included in this dissertation is given, including methods for assessing and modelling topographic uncertainty, as well as assessing and comparing its impact on geomorphologic models, melt models and full-scale ice sheet models.

The respective results from all five papers are briefly given in chapter 4, and are being comprehensively discussed in chapter 5, structured into the main subjects of assessing and quantifying uncertainty, modelling uncertainty, the impact of uncertainty on different models, and ways of minimising and reducing the impact of uncertainty. The dissertation concludes with chapter 6, giving an outlook for future work.

The five papers included in this dissertation can be found in the appendix:

A. Hebeler, F. & Purves, R.S. 2004: Representation of topography and its role in uncertainty: a case study in ice sheet modelling. *Proceedings of the GIScience 2004 conference, College Park, Maryland, Oct 19-24 2004, p.118-121*

B. Hebeler, F. & Purves, R.S. in press: The influence of elevation uncertainty on derivation of topographic indices. *Geomorphology*

C. Hebeler, F. & Purves, R.S. 2008: Modelling DEM data uncertainties for Monte Carlo Simulations of Ice Sheet Models. *In: A. Stein, J. Shi & W. Bijker: Quality Aspects in Spatial Data Mining, CRC Press, Boca Raton, p.175-196*

D. Hebeler, F. & Purves, R.S. 2008: The influence of resolution and topographic uncertainty on melt modelling using hypsometric subgrid parameterisation. *Hydrological Processes 22(19), p.3887-4021*

E. Hebeler, F., Purves, R.S. & Jamieson, S.S.R., in press: The impact of parametric uncertainty and topographic error in ice sheet modelling. *Journal of Glaciology*

Chapter 2

State of the Art

2.1 Error and Uncertainty in GIScience

"Vagueness is the inescapable punishment for cutting up a mostly continuous, heterogeneous and dynamic world into discrete, homogeneous and static categories" – Couclelis (2003)

In trying to underline the problem of introducing uncertainty through abstraction, Plewe (2002) claims that 'reality itself cannot be uncertain'. This standpoint is arguable, even if one does not go as far as relating it to Heisenberg's uncertainty principle (Couclelis, 2003), as uncertainty is all around our everyday life, and most of us would at least like to assume that this is indeed reality. In the same work, Plewe (2002) later on distinguishes between uncertainty in a phenomenon (indeterminacy) and uncertainty in assertions of that phenomenon, somewhat refuting his first statement.

Irrespective of whether uncertainty originates from a phenomenon or our assertion of it, our ability to deal with this **uncertainty in time, space or attributes** in our lives is reflected in many ways that are relevant for GIScience. One example are colloquial concepts of time that are often uncertain, e.g. 'soon', 'later', 'old', and many geographical concepts are also uncertain, such as descriptions of spatial objects like 'Indian Ocean' or relationships like 'near', 'below', 'north of' (compare Longley et al., 2005; Purves et al., 2005; Goodchild, 1992). Because we have the intuitive ability to interpolate, approximate, judge and clarify these loose or imprecise notions where necessary, they are convenient to deal with the many continuous everyday phenomena around use. On the contrary, GIS being developed as a tool for technical tasks like surveying or constructions, with the focus on the need to represent and model our geographi-

cal world as accurately as possible, *per se* lack these abilities to deal with imprecise notions or regions.

According to Plewe (2002), uncertainties are the result of complexities and problems in two processes, namely conceptualisation and measurement. For a GIS the common **entity model** (vector) is appropriate for modelling objects with crisp boundaries, such as buildings, streets or lakes, and uncertainty is usually associated with accuracy (how close a measured value is to the true value) and precision (how close similar measurements of the same value are). Both accuracy and precision mainly relate to the process of measurement – for example how accurate the outline of a building is captured in a map. Nevertheless, even a simple task like delineating a lake is already prone to uncertainty due to the continuous change of waterlevel and therefore shoreline over time – trying to represent a varying object in a static (vector) model is related to the second process of conceptualisation. It is this dilemma that the citation of Couclelis (2003) in the beginning of this section is referring to: the conceptual problem of capturing and depicting phenomena that are continuous in time or space such as temperature or soil pH, with crisp polygon boundaries is unsatisfying (Heuvelink, 1998). The problem is often illustrated using the Sorites paradox (e.g. Foody, 2003; Duckham et al., 2001; Fisher, 2000): when trying to define a heap, one would agree that 1 grain is certainly not a heap, so 1+1 grains cannot be a heap, neither can 2+1, 3+1 . . . 9999+1 grains and thus any number of grains. Setting a threshold to define a certain number of grains as a heap must thus inevitably be arbitrary.

Using regular tesselated grids or triangular irregular networks (TIN) is better suited to represent continuous data than vectors, as different data models have their advantages or disadvantages for certain applications (Burrough and McDonnell, 1998). However all variables modelled using these data types are subject to uncertainty, if only through the accuracy or precision of the model and the data. While finite difference grids might be much more suitable to represent continuous data, the resolution of the grid cell still represents a crisp boundary, imposed on a continuous phenomenon through a conceptual model and limited digital resources.

Burrough and McDonnell (1998) give an exhaustive list of possible sources of uncertainty and error for spatial data, including accuracy of content, measurement error, locational accuracy and the “human factor”. Apart from uncertainties introduced by humans during data capture and processing, since GIS are used to produce knowledge products, uncertainty can also arise from misinterpretations of valid data by (novice) end-users (Couclelis, 2003). Independent of the source of uncertainty, it needs to be judged whether the uncertainty inherent in a model or data makes it fit to be used for

a certain application or not, for example by checking whether the data resolution and accuracy is sufficient for the target process under observation, or whether the input data is representative for the analytical task (Hebeler, 2003). Unfortunately, computers do not have our natural ability to instinctively assess and judge upon uncertainty, but they need to be 'taught and trained', which requires us to realise and formalise how we shall deal with uncertainties in GIScience.

In his work on accuracy of spatial data, Veregin (1989) has identified five goals for handling error, extended to include uncertainty by Plewe (2002), where identifying and understanding of the sources and nature of uncertainty or error is diagnosed to be the essential base for all successive tasks (Fig. 2.1).

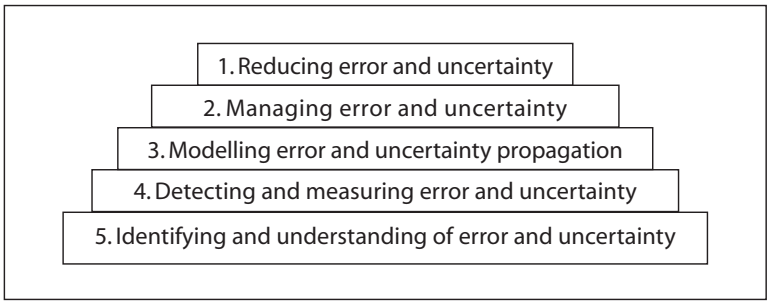

Figure 2.1: Five goals for handling error and uncertainty after Veregin (1989).

Definition: To avoid misconceptions often encountered due to the interchanging use of terms like error, fault, vagueness and uncertainty, at this point a definition of the terms used within this dissertation is given. Contrary to the relatively wide use of the term 'error' by Burrough and McDonnell (1998), that also includes 'variation', within this work the term **error** is used where a value x' (attribute or location) is deviating from its true value x by an error value ε. The term **uncertainty** u is used where a value x' is known to contain some error ε, but either the magnitude, location, or time of the error, or any combination of these, is unknown (MacEachren et al., 2005).

This implies that error can only be measured where higher accuracy reference data is available (Kyriakidis et al., 1999). If the error at a certain location z is known, the error at a neighbouring location z' can be estimated using geostatistics (Holmes et al., 2000), but since the the true error value at z' is not known, according to the definition in this work it is termed uncertainty.

Using a GIS, many common operations are effectively models: any algorithm used to calculate slope from gridded elevation values fits a (local) continuous surface through these points in order to derive a gradient, and thus effectively applies a surface model (Schneider, 2001b; Wood, 1998). Thus in addition to the uncertainty contained in the data, or **input error**, uncertainty from the operation itself, or **model error**, is present (Heuvelink, 1998). Thus propagation of both input and model error needs

to be considered when working with spatial data, and a number of methods exist for modelling error propagation, such as Taylor series (Heuvelink et al., 1989) and Monte Carlo Simulation (Davis and Keller, 1997a,b). While generally this applies to all digital spatial data, both vector and raster, continuous and discrete, the focus of this work is on the digital modelling of topography, the inherent uncertainty and the propagation of it to results of different form and process models.

Despite uncertainty being an unavoidable and intrinsic part of any model, the notion itself is still negatively associated with terms like faulty, inadequate or inaccurate – often reflected even in terminologies such as 'fighting uncertainty' (Couclelis, 2003). While efforts should obviously been taken to reduce uncertainty for any model, it is necessary to be aware of the fact that uncertainty can not be eradicated completely, and it therefore needs to be considered when deriving, distributing or displaying results.

Essence: Uncertainty is a natural phenomenon which is not necessarily a problem for GIS based spatial modelling, but understanding the nature of uncertainty associated with a data product or model can help to judge the **reliability** and **quality of results** and **prognoses**. Since all spatial data is subject to error and therefore uncertainty, where data is used in an application, uncertainty **propagates** through the modelling chain into the results. If decisions need to be made on the basis of these results, the impact of uncertainty on these results as well as possible decisions needs to be assessed. While this is often trivial for everyday life phenomena, a systematic approach is needed for GIS.

Need: Sources of uncertainty need to be **identified** and **quantified**. The **impact of uncertainty** on model results need to be assessed, for example via uncertainty modelling. It is critical to chose an adequate uncertainty model based on the available information and the intended use of the results. Based on this impact assessment, **decisions can be made** whether measures to minimise uncertainty need to be taken or not.
In general, efforts have to be made to increase acceptance of the need to **assess** and **communicate** uncertainty along with the respective data product.

2.2 Modelling Topography

Topographic models depicting the surface of the earth in three dimensions have been used as aids in navigation and construction for considerable time, and before digital modelling of terrain became possible, these models where actually made from materials like stone, clay, sand or plaster (Li et al., 2005). Maps, seen as a two dimensional form of terrain model, have been around aiding in property delineation and navigation for thousands of years. Consequently, with the invention of computers and subsequently GIS and digital terrain models, geographic data was commonly digitised from existing paper maps (Weibel and Heller, 1991) until remote sensing techniques became available for direct capturing of data at sufficient quality.

2.2.1 Digital Elevation Models

Globally available DEMs like GTOPO30 and GLOBE (U.S. Geological Survey, 1996; GLOBE Task Team & others, 1999) at resolutions of approximately 1km became available during the mid-1990s and were compiled from various data sources such as digitised contour maps of varying quality, resulting in inhomogeneous accuracy and overall quality, and abundant errors (Fig. 2.2). With the rapid advances in remote sensing, digital elevation models with resolutions of 100m such as the SRTM data (Farr et al., 2007) are available almost globally, and are considerably more homogenous in their quality. With LIDAR data becoming more and more popular (Sun et al., 2003), DEMs with resolutions up to 0.5m are already available in many areas (e.g. DTM-AV for Switzerland for areas below 2000m at 2m resolution - Swisstopo, 2007).

While data collected using higher resolution sensors is usually more accurate than that from lower resolution sensors, higher resolution is often falsely used as a synonym for ‘better’ data, while using the adequate DEM resolution is crucial for both form and process models (Armstrong and Martz, 2003). Not only may the use of too high resolutions DEM slow down computations with no apparent benefit, but potentially increased cost (time, money for high resolution data or better hardware); high resolution DEMs may also prevent the use of certain process models, e.g. where models are parameterising processes at a lower scale, their use at higher scales might render this parameterisation unusable (Purves and Hulton, 2000a).

In general, DEMs are used to model the continuous surface of the earth (or any other surface), but due to their digital nature, they are a mere collection of points, which need to be interpolated in order to model a surface. Generally, digital models of terrain can comprise either regular or irregular tessellations of point data, which

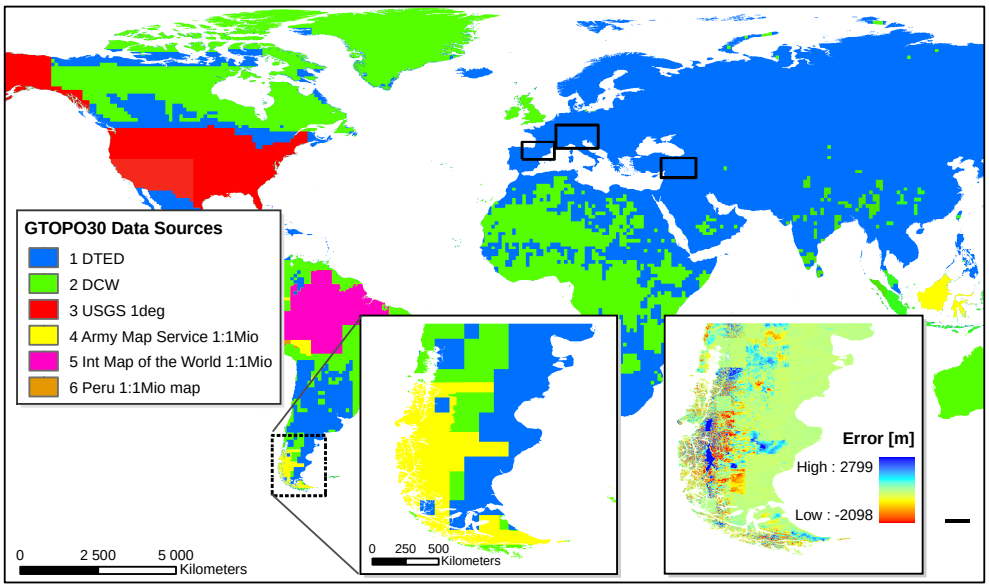

Figure 2.2: Sources used to compile GTOPO30 DEM data. The same source data, though with differing interpolation schemes were used in the production of GLOBE data. The study areas used to derive the GLOBE uncertainty model are marked solid black. Inset of Patagonia with data sources (left) and GLOBE deviation from SRTM (right). Note the variation in magnitude and spatial correlation of error for Patagonia (right inset), depending on the data sources used (left inset). Source: USGS 1996.

can contain additional data on structural features not explicitly contained in the point data otherwise, such as breaklines or drainage divides (Weibel and Heller, 1991). Different **data models** and interpolation approaches exist, including linear interpolation, quadratic patches, Bezier splines, and others. A considerable amount of work has focussed on the appropriateness and usability of these approaches for different tasks (e.g. Chaplot et al., 2006; Hutchinson and Gallant, 2000; Wise, 2000, 1998; Wood and Fisher, 1993), but besides the triangulated irregular network approach TIN (e.g. Hugentobler et al., 2004), regularly spaced, gridded elevation values, or rasters, are the most common data model used for DEM. Their advantage of very efficient operation using matrices is countered by the relative high amount of storage capacity needed, and the fixed resolution independent of the local variation of the modelled variable (Shortridge and Clarke, 1999).

A number of synonyms like digital elevation model DEM, digital terrain model DTM, digital height model DHM etc. exist, that commonly all relate to elevation data, but can have different meanings in different disciplines, and might refer to simple gridded elevation values as well as their interpolated surfaces (Li et al., 2005). The present

work focuses exclusively on gridded elevation data, and the term **DEM** will be used to refer to regular spaced measured elevation values.

Operations on a DEM, such as calculation of derivatives or querying of values located between the gridded elevation values, require interpolation. Methods for interpolating grid points can be categorised into global and local approaches. **Global functions** try to acknowledge all available information in a grid, for example by fitting higher order polynomial surfaces through all available data points (Wood, 1998). This can result in very high order polynomials and unrealistic surfaces, but assures continuity. **Local approaches** are using only immediate neighbours for interpolation, for example through bilinear interpolation or by fitting square or cubic surfaces through the four adjacent grid points (e.g. Zevenbergen and Thorne, 1987). Because surfaces are constructed of many local subsurfaces, local approaches can further be classified in discontinuous and continuous methods. Methods that produce global surfaces where at least the elevation function is continuous are named continuous or G_0 continuous; if the first and second derivatives are also continuous these function are said to be G_1 and G_2 continuous, respectively, and are often called smooth (Li et al., 2005; Hugentobler, 2004).

The standard representation of continuous data in a DEM in most GIS is in the form of a raster, where every grid cell is assigned the elevation value representative for the area it covers (e.g. from a sample measurement). This is equivalent to a local nearest neighbour interpolation and would result in a stepped, discontinuous surface when viewed uninterpolated (Fig. 2.3).

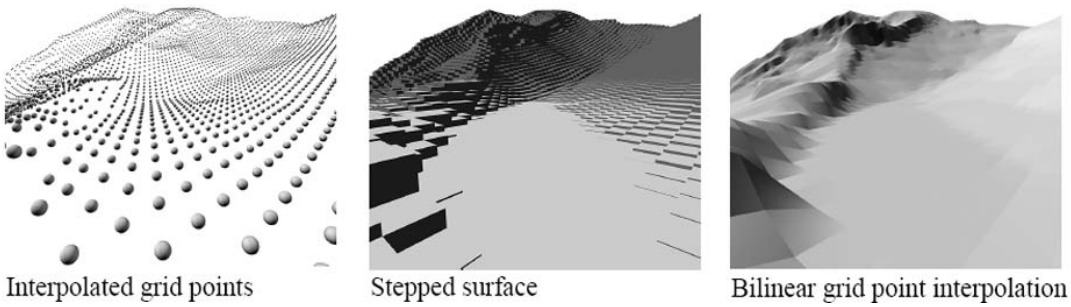

Figure 2.3: Example for interpolating surfaces from regular grid points (Martinoni, 2002).

2.2.2 Digital Elevation Model Uncertainty

Working with DEMs is subject to two categories of uncertainty: one is originating in the DEM itself, where uncertainties are associated with the DEM quality (data-based uncertainty - Shortridge, 2001). The other is originating from the use of the DEM, where the uncertainty stems from algorithms used to query, manipulate or visualise the DEM (data model-based uncertainty - Shortridge, 2001) and from models used to derive forms or simulate processes based on the DEM (Florinsky, 1998). Uncertainty related to DEM quality is mostly related to the data capture and preprocessing (Florinsky, 2002), and includes the following sources:

- Sensor precision, accuracy and reliability
- Sampling strategy
- Coordinate transformation
- Loss of precision
- Human factors

These factors all result in a deviation of the measured values at the sample locations from their true values, and are therefore usually deemed to be errors. Wise (2000) describes three types of error, namely blunders, systematic and random error. **Blunders** are gross errors and the results of, for example, failing measurement equipment or digitising errors, and are infrequent in recent commercial grade DEMs. **Systematic errors** are characterised by a common trend or dependency, and can be the result of both data capturing (radar shadow effects - Shortridge, 2006) or processing (terracing from poorly interpolated contour lines - Wood, 1996). These systematic *input errors* can potentially be eliminated or reduced, and a number of methods have been devised to achieve this (Wechsler and Kroll, 2006). **Random error** as the third type can originate from a variety of sources such as measurement and data processing and show no trends. The only way to eliminate or reduce nonsystematic errors is by repeating measurements, where possible using higher accuracy and precision methods.

This classification of error into three categories is built upon the '**regionalized variable theory**' (RVT) developed by Matheron (1969), which is the theoretical basis for geostatistical methods like Kriging (Oliver and Webster, 1990).

Additionally, almost any operation using a DEM as a continuous surface introduces further uncertainty (*model error*), because of the associated need for interpolation, referred to in section 2.2.1. These sources of uncertainty include

- Projecting to different spatial reference systems

- Resampling/Generalising of DEM data to different resolutions
- Interpolation applied in basically all operations that require continuous surfaces like value querying, calculation of derivatives, generalising, process modelling

and might also be termed *uncertainty of topographic representation*, as they are not depending on the elevation values of the DEM themselves (e.g. Fisher and Tate, 2006). This last source is an often underestimated or even completely neglected aspect of uncertainty in working with DEM, even though the resolution and representation of a terrain surface introduces ambiguities in any derived results (Schneider, 2001b).

A simple example might illustrate this: calculating slope and curvature using ESRIs Arc/Info, the SLOPE function uses finite differences between the eight adjacent neighbours of a cell to calculate slope gradient, whereas CURVATURE uses piecewise quadratic surfaces. Both functions are thus effectively calculating their respective derivatives using different surfaces (Hugentobler, 2004). If this inconsistency is known, it can be accounted for, for example if the derivatives are used for further modelling. However, using a different GIS that implements a different slope algorithm, is likely to produce different slope and curvature values for the same data set. The choice of algorithms thus influences model results, and results in uncertainty, where no clear modelling framework is given (Schneider and Martinoni, 2001).

2.2.3 Modelling DEM Error and Uncertainty

Because working with DEMs is subject to the errors and uncertainties discussed above, it is vital to examine and understand error propagation through the modelling chain and assess the impact of uncertainty associated with using a certain DEM. Uncertainty propagation can be examined analytically, e.g. using Taylor series (essentially breaking down complex, non-linear functions into a series of linear terms - Heuvelink, 1998). Where analytical solutions are not possible, DEM error, respectively uncertainty needs to be modelled in order to assess its impact on a certain process. This however, requires some information on the statistical and spatial distribution of uncertainty. Where higher accuracy reference data for a DEM is available, it can be used to derive error, in the simplest case by simple subtraction. However strictly speaking, even a higher reference elevation model can per definition not be error-free, and would thus give only an estimate of error.

Depending on whether the reference data is a simple set of validation points, or a higher accuracy DEM subset, the derived error will be in the form of single point observations or an error surface. Either way, the error can then be analysed to identify

characteristics of statistical and spatial distribution that allow modelling of uncertainty at locations without reference measurements.

In geostatistical modelling, following the regionalised variable theory (RVT), three components of error are known: the first are **global trends** overlaying local patterns, which can for example be detected using directional variograms or profile plots (Holmes et al., 2000; Liu and Jezek, 1999). The second component is a **spatially correlated component**, which is related to the fact that most natural variables (elevation, slope, pH, temperature) gradually change over space, and locations close to each other are more likely to have similar values than distant ones, a phenomenon often termed '**Tobler's First Law**' (e.g. Laube et al. (2005), after Tobler (1970)). As error usually depends on the absolute values of a variable, it exhibits similar amounts of spatial correlation as its associated variable. Often, a characteristic range of spatial correlation can be observed, showing error patterns that are highly correlated with the underlying terrain (Hunter and Goodchild, 1997). The third component is **random error** or noise, where no spatial dependency is apparent. The amount of random error can be captured as the nugget in variograms. When analysing and modelling uncertainty, all three components are attempted to be captured where they exist.

Where no reference data is available to derive error properties, uncertainty can only be modelled based on information about DEM accuracy and error distribution given in the metadata. However, despite the recognition of the necessity for detailed error models to be distributed with DEMs (Kyriakidis et al., 1999; Shortridge and Goodchild, 1999; Fisher, 1998; Ehlschlaeger and Goodchild, 1994), digital elevation models are still commonly distributed with global error or accuracy measures at most (Fisher, 1998). These measures are usually in the form of root mean square error (RMSE) or standard deviation for horizontal and vertical accuracy for a small number of control points, for example GLOBE, GTOPO30 or SRTM data. Since no information on the spatial distribution of error, or on dependencies with topographic attributes such as elevation or roughness is given (Oksanen and Sarjakoski, 2005b; Holmes et al., 2000), these global values are of limited use for modelling uncertainty. Assumptions about the spatial correlation of uncertainty have to be made where no information is available, and error is thus often assumed to be normally distributed and random (Oksanen and Sarjakoski, 2006; Wechsler, 2006; Fisher, 1998). However it is disputable whether this assumption is generally valid and it has been suggested that more complex error distribution functions should be used where possible (Holmes et al., 2000; Ehlschlaeger et al., 1997; Hunter and Goodchild, 1997).

Measures of spatial correlation are needed in order to analyse and model spatially autocorrelated uncertainty surfaces (Fisher, 1999). Common indices such as local indicators of spatial association (LISA, Anselin, 1995), Geary's c and Moran's I (Moran, 1950) exist, that essentially all measure the local or global degree of similarity of values. Moran's I compares the (weighted) ratio of the variance at a location against the variance of its neighbourhood with indices lying in the range of -1 to 1, where highly autocorrelated regions have values around 1 and anti-correlated (alternating) regions show values close to -1 (Shortridge, 2001). Moran's I is a simple and robust estimator for spatial correlation that is useful for determining locally varying spatial correlation, e.g. for different landforms or terrain types. However, as indices are relative for each survey area, comparing autocorrelation for different DEMs can be biased. Additionally, choosing the analysis window range and weights influences the analysis, and requires some prior information about the data to be examined (Liu and Jezek, 1999).

Another very common measure originating from geostatistics is the range of spatial autocorrelation determined using semivariograms (Burrough and McDonnell, 1998). Here, the variance of different value pairs is plotted against their distance (lag), again assuming that closer locations are more likely to have similar values, which results in increased variance for higher lags. The distance at which the variance reaches its maximum (sill) is the range at which the local correlation ceases to dominate values (Fig. 2.4). Using local or directional variograms can detect local trends and directional effects in the autocorrelation, and the resulting variograms are commonly used in interpolation methods such as Kriging. However, tuning of the analysis parameters and fitting of a theoretical variogram requires expert knowledge and automatic analysis is often unreliable and data specific.

Different **approaches for modelling spatial correlation** in elevation uncertainty exist which apply the measures described above. Fisher (1998) uses a simple **random cell swapping** algorithm with repeated measurements of Moran's I to increase autocorrelation of a white noise surface until a target correlation threshold is reached. The initial error is assumed to be normally distributed around a mean of zero with a standard deviation equal to the RMSE given in the DEM metadata, and independent of external variables such as topography. While this approach is simple to implement, for large grids and high degrees of spatial correlation, computational times increase exponentially. However, the approach could potentially be optimised using for example simulated annealing or any other sophisticated cell swapping algorithms. Because the spatial correlation is not introduced by filtering, the resulting surfaces are relatively

rough, which, when added to original topography might be problematic for some applications e.g. can cause instabilities in physical models due to unrealistically high slopes.

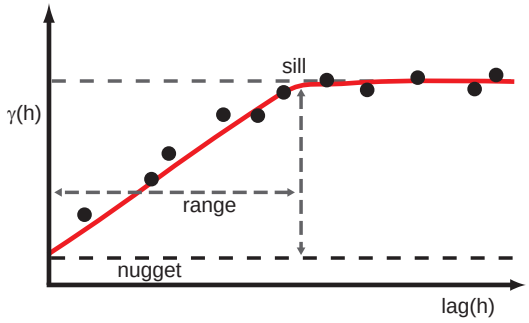

Figure 2.4: In a semivariogram, the difference in attribute values $\gamma(h)$ of two locations is plotted against the distance (lag) of the locations h for a set of (random) points. Following the assumption that closer locations are more likely to have similar values than distant ones, the difference in attribute values will increase with distance until it reaches a maximum distance (range), where the mean difference does not increase, marking the sill. Where random, uncorrelated error is present, it will show as nugget in the variogram.

Oksanen and Sarjakoski (2005b) model finescale DEM error as a Gaussian random field, also assuming external dependencies as well as systematic error to be absent. Using a Monte Carlo approach, they use sequential **Gaussian simulation** (Goovaerts, 1997) with variogram ranges derived from the literature, to assess the impact of different amounts of autocorrelation of error on the calculation of primary and secondary topographic attributes such as slope gradient and aspect and topographic wetness index (TWI). In a similar approach Oksanen and Sarjakoski (2005a) use process convolution, or **spatial moving averages**, to introduce autocorrelation to a Gaussian random field. However, both the range of the filter and the amount of error, expressed as standard deviation around a mean of zero of the random field, are chosen somewhat arbitrarily.

Although the assumption of **homoscedasticity** (in this case the DEM error being independent of underlying terrain) might be convenient (Kyriakidis et al., 1999), especially when no information about dependencies is available, it is usually not correct (Hunter and Goodchild, 1997). Taking into consideration the typical sources of uncertainties in DEM, such as measuring accuracy during data capture or interpolation from point observations, a dependency of uncertainty on terrain is self-evident: a measuring beam for example is more likely to be scattered over very rough than over smooth terrain, and the selection of a sample site location in rugged terrain will affect the measured elevation more than on a plain.

Having a DEM containing uncertainty (termed ‘soft data’), Kyriakidis et al. (1999) use a set of higher accuracy reference data (termed ‘hard data’) to directly simulate what is called the ‘higher accuracy reference elevation surface’ using stochastic simulation without explicitly generating an uncertainty surface. To do so, they use local uncertainty models at each grid node, which incorporate the covariance between hard data, soft data, and the sum of both, effectively using sequential Gaussian simulation with Cokriging to produce a suite of equiprobable surfaces. These surfaces are exact, as they replicate the elevation values at the hard data locations and **heteroscedastic**, as the simulated error depends on the elevation at each location, and the amount of spatial correlation. This approach allows statistical assessment of uncertainty by means of probabilities, and incorporates dependency of error on the underlying terrain. While the approach proved to be efficient for the authors’ case study on a 148x149 cell grid, a set of high accuracy reference data is again needed to (implicitly) assess and model the spatial autocorrelation of error, and for large data sets and high numbers of equiprobable surfaces needed for Monte Carlo Simulation, the approach is impractical.

Essence: Working with digital elevation models (DEM) is subject to both input and model error: uncertainty originates from both data capture (digitising error, sensor precision, pre-processing) as well as data handling (assumptions of the applied data model, interpolation algorithms). Commonly DEM data products are distributed with metadata containing only **global accuracy measures** such as RMSE. However DEM uncertainty is known to be spatially correlated and dependent on topographic attributes and global figures such as RMSE lack any spatial information. Modelling DEM uncertainty using only common global DEM accuracy measures such as RMSE is therefore subject to **potentially unrealistic assumptions**, such as normal distribution and homoscedasticity of uncertainty. Representing the correct **spatial correlation** of uncertainty is crucial, as it can lead to instabilities in associated models, but it can be arbitrary if no reference data is available. Where error properties can be deduced from higher accuracy reference data, sophisticated geostatistical methods can be applied, but these approaches require expert knowledge and extensive computational resources. Additionally, expensive higher accuracy reference data is needed.

Need: A method for fast simulation of DEM uncertainty at continental or global scales, that incorporates spatial correlation and the dependence of uncertainty on terrain properties, while using readily available reference data at most is needed in order to assess the impact of DEM uncertainty on environmental models at these large scales.

2.3 Topographic Attributes

DEMs are used in a wide range of applications, such as visualisation (Smith and Clark, 2005), hydrological and erosion modelling (Finlayson and Montgomery, 2003; Tucker and Whipple, 2002), solar radiation modelling (Kumar et al., 1997), viewshed analysis (Fisher, 1993) and landform detection (Fisher et al., 2004; MacMillan et al., 2000; Herrington and Pellegrini, 2000), all of which require the calculation of topographic attributes or topography-dependent indices. A wide range of topographic attributes/variables are known (e.g. Kienzle, 2004; Florinsky, 1998), which can be categorised into primary or **simple indices** and secondary or **compound indices**. Simple indices are calculated directly from the elevation values and can include basic statistic descriptives such as mean, maximum, standard deviation of elevation, the first and second order derivatives (slope gradient and aspect and plan and profile curvatures, respectively), as well as neighbourhood indices such as roughness and extremity (Carlisle, 2000). Moore et al. (1991) categorise these simple indices as **primary topographic attributes** together with more specific, secondary attributes such as catchment area, stream length or catchment slope. However, the later attributes are geomorphological or hydrological derived indices which are commonly used in applications of their related area, and all require the calculation of one or more additional attributes. e.g. catchment area for catchment slope, blurring the transition to **compound indices** such as the topographic wetness index (TWI, Beven and Kirkby, 1979) or the stream power index (Moore et al., 1991). These compound indices consist of two or more primary attributes and are dubbed **analytically derived compound topographic indices** by Moore et al. (1991). These indices are often used as proxies for physical properties or for parameterisation in specific applications, such as the TWI for soil-water related applications (Tarboton, 1997; Moore et al., 1991) or the 'topographic factor' for erosion modelling (Florinsky, 1998).

Where continuous surfaces are modelled from point elevation data, their first derivatives, slope gradient and aspect, are the most important topographic variables. Consequently, since the introduction of DEMs, a number of algorithms have been developed to derive slope from gridded elevation values, including linear interpolation and quadratic approximation (e.g. Zevenbergen and Thorne, 1987; Horn, 1981; Evans, 1980). Slope is a boundary condition for almost all physical processes (which are depending on gravity), and thus algorithms for deriving slope are used across a wide range of applications and scales (Florinsky, 1998). Consequently, a number of studies have examined the suitability of different algorithms for certain tasks and resolutions, (e.g. Kienzle, 2004; Zhang et al., 1999; Jones, 1998).

Second derivatives such as plan and profile curvature, denoting the change of slope, are also important, especially in hydrological applications (Florinsky, 1998), for example in flow path or run-off modelling. Similar to slope, a number of algorithms to derive (different) curvatures exist (Shary et al., 2002; Wood, 1996; Shary, 1995), and the effects of different algorithms, scales or window sizes on calculated curvature values have been investigated (e.g. Albani et al., 2004; Schmidt et al., 2003). While for regularly gridded elevation values, local interpolation methods to calculate first and second derivatives are fast and easy to implement, (e.g. Zevenbergen and Thorne, 1987; Evans, 1980), it has been shown that for some applications, fitting higher order polynomial surfaces and using an extended neighbourhood has advantages over simple quadratic fitting of immediate (max. 8 for grids) neighbours (Schmidt et al., 2003; Wood, 1996; Moore et al., 1991).

In general, applications can be categorized into deriving topographic attributes and thus characterising the form of the earth's surface (**form models**), and applying topographic attributes by modelling processes occurring on this surface (**process models**), or a combination of both, linking the relationship between form and process. Raper and Livingstone (1995) distinguish between approaches related to object identification and to object behaviour. Identifying and characterising form using topographic attributes is common across a range of geomorphological applications, such as landform detection to identify single features (e.g. mountains, Fisher et al., 2004) or classify terrain types (Chaplot et al., 2006; MacMillan et al., 2000).

Tools like TARDEM (Tarboton, 1999) have been developed for the automatic calculation of a wide range of topographic attributes, including delineation of watersheds or classification of streams using Strahler order. These attributes are often used as proxies in - mainly hydrological - form models, such as basin hydrology and run-off models (Kaser et al., 2003; Pike, 2000; Williams and Tarboton, 1999).

2.3.1 Uncertainty in Topographic Attributes

As topographic attributes are derived from continuous surfaces (modelled using gridded elevation values), they are both subject to input error of the elevation values and model error of the interpolation, used to model the DEM surface described in section 2.2.1. Consequently, calculation of any topographic attribute potentially introduces further uncertainty through the choice of algorithms, support size (the area respectively the number of points used in the calculation of the attribute) and scale. Because of their importance in topographic modelling, a number of studies have fo-

cused on the impact of scale and choice of algorithm (model error) on the derivation of slope gradient and aspect, both on natural topography (e.g. Zhang et al., 1999; Hunter and Goodchild, 1997) as well as artificial landscapes (e.g. Zhou and Liu, 2004; Corripio, 2003; Jones, 1998). Thanks to these studies, dependencies such as decreasing average slope gradient with coarser resolutions due to the smoothing effect of generalisation on topography today are common knowledge in GIS (compare Longley et al., 2005; Burrough and McDonnell, 1998). Walker and Willgoose (1999) and Lee (1996) have investigated the influence of input error by simulating DEM error and repeatedly extracting hydrological features such as floodplain cells and stream networks.

A number of authors have taking a further step in uncertainty analysis by examining the effect uncertainty of topographic attributes has on the derivation of compound indices and process model results, where dependencies are becoming too complex for analytical analysis. Endreny and Wood (2001) investigated the impact of both input and model uncertainty on simulated runoff using different algorithms, by modelling DEM uncertainty, producing probability maps by means of Monte Carlo Simulations. Essery and Marks (2007) studied the effects scaling and parameterisation have on a model of solar radiation, depending on slope gradient and aspect as well as relief shading.

Essence: Topographic attributes are the basis of virtually all applications that use DEMs to create, visualise, query or manipulate continuous topographic surfaces. As such, topographic attributes are subject to error and uncertainty of the DEM data. Additionally, derived topographic attributes are known to also be dependent on DEM **resolution**, the applied **data model** and **algorithms** used for calculation of attributes.
The impact uncertainty in topographic attributes has also depends on the type of model they are applied to: in **form models**, such as landform detection algorithms, uncertainty propagation is static, while in **process modelling**, such as runoff models or ISM, uncertainty impact is likely to vary over time and can be subject to feedback mechanisms.

Need: The impact of DEM uncertainty on the calculation of topographic attributes needs to be considered in topographic modelling. At the same time uncertainty created through the use of different algorithms, support size and scale in the derivation of these attributes has to be assessed and acknowledged with respect to results of any model based on these topographic attributes. Differentiating between the impact of input error and model error can be crucial for the understanding of the mechanisms of uncertainty impact.

2.4 Process Models

Process models are commonly using topography, respectively the derived topographic attributes, for the simulation of (geo-)physical processes, that can either take place on an existing topography, or simulate the shaping of topographic landforms (Codilean et al., 2006). Uncertainty propagates through process models and its amount and impact are non-static and vary over time, and thus can potentially multiply over the modelling timesteps. The impact of topographic uncertainty on process models is commonly more difficult to assess because of potential non-linear dependencies.

2.4.1 Ice Sheet Models

Ice sheets are usually modelled treating ice as a viscous mass (Paterson, 1994). As such, ice dynamics and flow velocity are predominantly controlled by the gradient both of the underlying bedrock as well as the ice surface, and the column height of ice, or ice thickness. Typically, an ice sheet model is composed of a core component ('Ice Sheet' in Fig. 2.5), where the physical properties of ice are modelled to resolve ice dynamics, and components which set the boundary conditions for this ice dynamics model. Commonly, these boundary conditions are the topography the ISM is running on ('Bedrock') and the climate acting on the ISM ('Environmental Input' , Fig. 2.5). As a result, the core ice sheet model component essentially outputs values of ice thickness for each grid cell in the model domain, at chosen time intervals ('Output', Fig. 2.5).

In ice sheet modelling, the topography is usually supplied as a DEM at the resolution appropriate to the model assumptions, typically in the range of 5-40km for ISM applying the shallow ice approximation (SIA) (Hagdorn et al., 2007; Payne, 1999; Greve, 1997; Oerlemans, 1980); a number of ISM modules can either directly or indirectly influence the ISM topography, for example isostasy, erosion or basal hydrology components. Climate forcing is controlling the mass balance of the ISM as well as the ice temperature, and the complexity of the climate component can vary from simple, constant parameters supplied at compilation time to a suite of complex coupled models that simulate climate from local to global scale and provide temperature, precipitation and wind data, calculate the response of the asthenosphere and lithosphere, derive sea level changes and more (Fig. 2.5).

Ice Dynamics

Higher order modelling of viscous mass dynamics including all stresses require the solving of around 12 equations per timestep, gridnode and thickness layer (see sec-

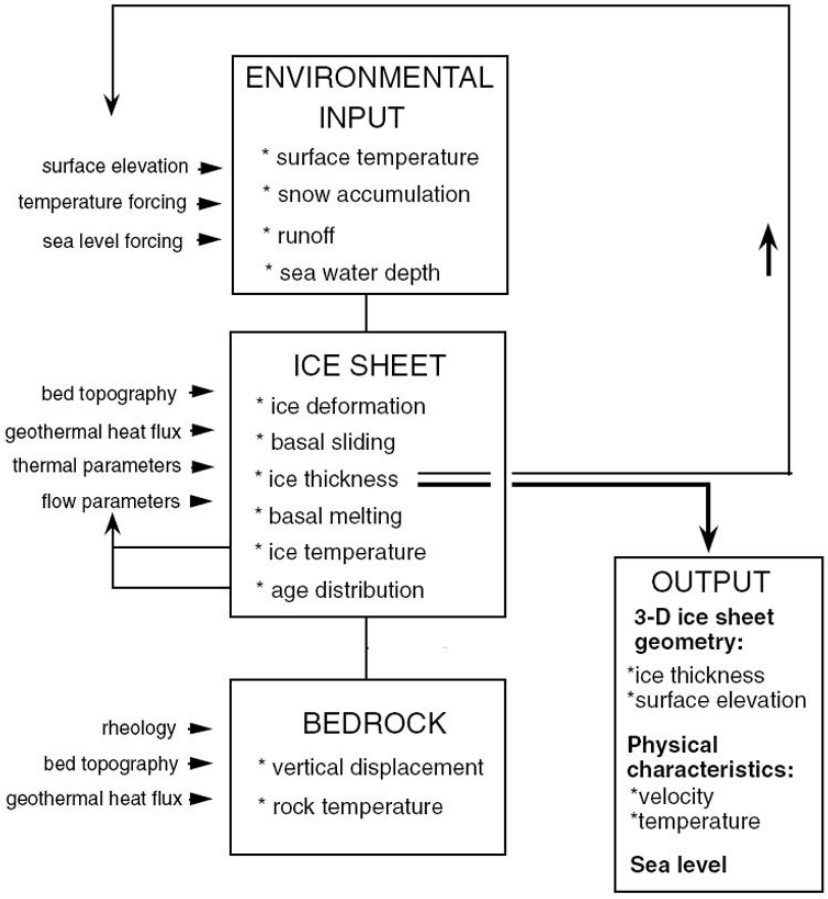

Figure 2.5: Principal structure of a basic 3D ice sheet model (not including ice shelves). Environmental input and bedrock are providing the boundary conditions for the core ice dynamics model. All three components are influenced by a number of external parameters (Modified after Huybrechts 2004).

tion 2.4.1), and as of today is still unfeasible for modelling across continental or even global scales because of the high computational demands. Under the **shallow ice approximation** (SIA, Nye, 1957) longitudinal stresses are neglected and ice sheets are assumed to be only under plane deformation, which essentially reduces the equations to be solved for modelling ice dynamics down to two (shear stresses in x and y direction) and enables modelling of large ice masses across large domains. The SIA is valid where bedrock and ice surface slopes are considered sufficiently small so that normal stress components can be neglected (Hutter, 1983). While this limits maximum model resolution through the assumption of small slope gradients, and does not resolve well certain features such as transition zones between fast and slow flowing ice, grounding

lines and ice shelves, it makes modelling of large scale ice masses possible. Following the SIA, the zero-order relation of shear (τ_{xz} and τ_{yz}) to ice thickness and surface slope according to Nye (1957) is:

$$\begin{aligned} \tau_{xz}(z) &= -\rho_{\mathrm{i}} g\,(S-z)\frac{\partial S}{\partial x} \\ \tau_{yz}(z) &= -\rho_{\mathrm{i}} g\,(S-z)\frac{\partial S}{\partial y} \end{aligned} \tag{2.1}$$

for height z in the ice column, where ρ_{i} is ice density and g is acceleration due to gravity. The ice surface elevation S is the sum of the ice thickness h and the elevation of the ice base H

$$S = H + h \tag{2.2}$$

For laminar flow (assuming flow-lines to be parallel to the surface and vertical flow velocity to be zero), effective strain rate $\dot{\varepsilon}$ relates to velocity u according to

$$\dot{\varepsilon}_{iz} = \frac{1}{2}\frac{\partial u}{\partial z} \qquad i = x, y \tag{2.3}$$

In addition to the driving stress, ice flow is dependent on temperature through its influence on ice viscosity. Temperature is controlled by three factors:

1. Temperature at the ice upper boundary, where the surface air temperature is depending on the local energy balance
2. Temperature at the ice lower boundary, where geothermal heat flux from the bedrock influences the basal temperature
3. The internal component of strain heating within the ice mass, important for solving the ice temperature regime

Glen's flow rate (Glen, 1958) relates shear strain rate $\dot{\varepsilon}_{xy}$ to shear stress τ_{xy} according to

$$\dot{\varepsilon}_{iz} = A\,\tau_{iz}^{n} \qquad i = x, y \tag{2.4}$$

where n is most commonly given the value 3 and A is the temperature dependant Arrhenius value. Ice temperature is therefore related to ice flow velocity according to the Arrhenius relation

$$A = f A_0 \exp\left(\frac{-Q}{RT}\right) \tag{2.5}$$

where A_0 is a temperature-independent material constant, R is the universal gas constant (8.314 J $\mathrm{mol}^{-1}\,\mathrm{K}^{-1}$) and Q is the activation energy for creep. f is a flow enhancement factor often used to tune ice flow (Ritz et al., 1997). For temperatures

T below -10 °C this implies that a strain rate produced by a given stress at -10 °C is 5 times that at -25 °C (Paterson, 1994). For temperatures above -10 °C empirical relations of strain rate and temperature are often used. Corrected for pressure melting, equation 2.4 is mostly used in ice sheet models as

$$\dot{\varepsilon}_{iz} = A\,T^{*}\,\tau_{*}^{n-1}\tau_{iz} \qquad i = x,y \tag{2.6}$$

where T^{*} is the correction term (Huybrechts, 1986).
Thus combining equations 2.1 and 2.6, one can approximate ice velocity at any height in the ice column by integrating

$$u(z) - u(h) = -2(\rho_{\mathrm{i}}g)^{n}\,(\nabla S \cdot \nabla S)^{\frac{n-1}{2}}\,\nabla S \int_{h}^{z} A(T^{*})(S-z)^{n}\,dz \tag{2.7}$$

where ∇ is the horizontal gradient operator (slope) and $u(h)$ is the basal velocity (sliding velocity). As shown in this equation, ice flow velocity varies to approximately the third power of surface slope and to about the fourth power of ice thickness, which makes topography a crucial factor controlling ice velocity and model stability.

Because ice flow is dependent on temperature, the internal field of the modelled ice mass has to be considered. Approximating this temperature field for poly-thermal glaciers is complex (Paterson, 1994). For this reason, ice sheets are often assumed to be cold or temperate. The associated **thermodynamics** can then be modelled by solving the time-dependent heat equation in ice as well as the underlying bed layer (usually for approx. 3-5km depth). Ice temperature (T) evolution can be calculated according to Payne et al. (2000):

$$\frac{\partial T}{\partial t} = \frac{k}{\rho_{\mathrm{i}}c_{\mathrm{p}}}\frac{\partial^{2}T}{\partial z^{2}} - \vec{u_a}\cdot\nabla T - w\frac{\partial T}{\partial z} - \frac{g(H+h-z)}{c}\nabla(H+h)\cdot\frac{\partial \vec{u_a}}{\partial z} \tag{2.8}$$

where $\vec{u_a}$ is the vertically averaged horizontal velocity vector, w is the vertical velocity (found diagnostically using the horizontal velocity field, derived from equation 2.7), k is ice conductivity and c_{p} is its specific heat capacity, H and h are ice thickness and elevation, respectively. The boundary conditions for integrating equation 2.8 are

1. heat flux at the ice sheet base depending solely on **geothermal heat flux** G and k:

$$\left.\frac{\partial T}{\partial t}\right|_{h} = -\frac{G}{k} \tag{2.9}$$

2. evolving temperature which cannot exceed the melting point

$$T' = T_0 - \beta\ (H + h - z) \tag{2.10}$$

where β is the Clausius-Clapeyron gradient.

The upper boundary condition is the ice sheet surface temperature, which is usually taken to be the air temperature for temperatures below 0 °C, or zero for air temperatures above the freezing point.

In addition to ice deformation or flow, movement of ice over its base can significantly contribute to overall velocity. Since motion at the base of an ice sheet can only be caused by sliding of ice over the ground (for ice reaching melting point) or deformation of the ground (for water saturated sediment bedrock), basal velocity for temperatures below the melting point is often taken to be zero as ice is assumed to be frozen to the bedrock (Ritz et al., 1997). However, temperate or polythermal glaciers and ice sheets show measurable **basal movement** (Fischer and Clarke, 2001), and the extend to which the basal component contributes to the overall ice movement depends on the bedrock characteristics, the basal hydrology, the geothermal heat flux and the temperature regime of the ice mass. For large existing ice sheets like the Greenland or Antarctic ice sheet, these characteristics are often not known or are difficult to average for coarse resolutions used in ice sheet models. Following the SIA, Ritz et al. (1997) use a simple law (derived from equation 2.7) for sliding and neglect bed deformation:

$$u_b(z) = k\,(-\rho_{\mathrm{i}} g\, H)^2\,(\nabla S \cdot \nabla S)^{1/2} \cdot \nabla S \tag{2.11}$$

with $u_b(z)$ being velocity at the bedrock and k a coefficient of the sliding law between 0 and 3 x 10^{-8}m a^{-1} Pa^{-2} accounting for bedrock characteristics (incorporating roughness and topography) in experiments carried out by the above mentioned authors (note: flow law exponent n has been set to 2 in equation 2.11). For glaciers, the ratio of basal velocity to surface velocity is typically between 0.2 and 0.9, often averaged as 0.5 (Paterson, 1994). Basal movement is often slow and therefore negligible in calculations of glacier movements over tens or hundreds of years. However when modelling surge-type glaciers or ice streams (Hubbard et al., 2005; Pattyn, 2003b) or modelling over evolutionary time spans, basal movement is an important factor that has to be considered. For a correct estimation of basal velocities, **basal hydrology** has to be considered (Fischer and Clarke, 2001; Murray, 1997). Even though Hubbard (1999) could not significantly improve results of his high resolution reconstruction of the Younger Dryas ice sheet in Scotland through the inclusion of basal hydrology, Engelhardt et al. (1990)

have shown that basal movement in ice streams can exceed the usual velocities by the factor of 100 as early as 1990. Neglecting bed deformation for some experiments is an acceptable practice because of the complexity of calculations; nevertheless, ice streams may move primarily by bed deformation (Anandakrishnan et al., 2007; Stokes et al., 2007), and measurements at Breidamerkurjökull, Iceland, indicate a 90% contribution of sediment deformation to total glacier forward movement (Fischer and Clarke, 2001). Blatter (1995) includes deformation by extending Nye (1957)'s equation (2.1) by a term for the vertically averaged, longitudinal deviatoric stress ($\bar{\sigma}'_x$ and $\bar{\sigma}'_y$, related to effective ice stretching), and Hubbard (1999) calculates basal shear stresses τ_{xz} and τ_{yz} according to

$$\tau_{iz} = -\rho_i g H \frac{\partial S}{\partial i_j} + 2 \frac{\partial (H \bar{\sigma}'_j)}{\partial i_j} \qquad i = x, y \tag{2.12}$$

where S is the ice surface elevation $(H + h)$ and i is the spatial index. Hubbard then calculates average horizontal velocity using a basal sliding term similar to equation 2.11 including a sliding parameter k and an exponent m (Paterson, 1994), added to the internal deformation, where the effective stress τ is given by

$$2\tau^2 = \bar{\sigma}'^2_x + \bar{\sigma}'^2_y + 2(\tau^2_{xz} + \tau^2_{yz}) \tag{2.13}$$

The heat Q_g caused by the deformation in ice sheet can be calculated following:

$$Q_g = \frac{\partial u_x}{\partial z} \tau_{xz} + \frac{\partial u_y}{\partial z} \tau_{yz} \tag{2.14}$$

with u_x/u_z the x/y component of the horizontal shear strain, z the height in the ice column and τ the shear stress, for a point within an ice sheet, contributing to the ice sheet temperature.

Mass balance

The mass balance of an ice sheet is determined by the amount of total accumulation and ablation. Accumulation is usually assumed to be dominated of by the amount of precipitation to fall as snow, but factors like snow drift and avalanches have been shown to contribute significantly to accumulation for glaciers (e.g. Kuhn, 2003; Purves et al., 1999), but these factors are less important for large ice sheets. Ablation is determined by the amount of melt an ice mass experiences, and through calving of ice at the marine margins. Essentially, the ice dynamic component is modelling the movement of ice from accumulation areas of positive mass balance to ablation areas of negative

mass balance. Ablation and accumulation areas are separated by an equilibrium line, where neither process prevails and mass balance becomes zero. For modelling, mass balance b needs to be provided at every node and can be derived according to

$$b = c + a = \int_{t1}^{t} (\dot{c} + \dot{a})\, dt \tag{2.15}$$

with c being accumulation, a ablation, t time. For every grid cell **accumulation** is calculated from precipitation as snow and ice flow into the cell. Accordingly, **ablation** is calculated by determining the amount of surface melt minus the amount of meltwater that refreezes, plus the amount of basal melt, calving at the marine margin and ice flow out of the cell.

In essence, an ISM is modelling the evolution of *ice thickness* at each grid node over time, which can be formulated in relation to the continuity equation (Payne, 1999) as

$$\frac{\partial H}{\partial t} = -\nabla(\overline{u}_a H) + b_\mathrm{s} - m_\mathrm{b} \tag{2.16}$$

where $\overline{u}$ is the vertically averaged ice velocity, derived by integrating equation 2.7, m_b is the basal melting and b_s is the surface mass balance, which is expressed as equivalent of volume of water per unit area relative to the previous ablation season. For the two-dimensional calculation of ice sheet thickness, ∇ is a term representing the vertically integrated horizontal ice flux divergence and convergence (ice flow to and from adjacent cells - Hubbard, 1999; Ritz et al., 1997).

The simplest form of prescribing mass balance to model an ice sheet has been used for the EISMINT intercomparison studies (Huybrechts et al., 1996), where mass balance is parameterised directly using the distance from the center of the modelling grid on a flat surface, producing radially symmetric ice sheets.

Climate Forcing

Where ISM are used for the simulation of past or present ice sheets, the necessary boundary conditions in the form of 'environmental input' to determine mass balance and ice dynamics have to be provided to the 'ice sheet' core component (Fig. 2.5), usually in the form of climate forcing. This can be done using a number of methods of different complexity and degrees of parameterisations.

A relatively simple method of representing climate (change) and its influence on mass balance of ice sheet models is through the **parameterisation of the equilibrium line altitute** ELA (Hagdorn, 2003). The idea is to simplify the complex implementations and interactions the change of climatic factors like temperature and precipitation

have, by representing them through their impacts on the ELA (Hulton et al., 1994; Ohmura et al., 1992). Mass balance in this case is parameterised and directly related to the elevation of a model grid cell relative to the ELA. In doing so, ice sheet models can be tuned to produce results that correspond with empirical data, which in turn allows to draw some conclusion on the climate likely to produce these results (Hulton et al., 2002). However, temperature needs to be provided as input to the ISM for the calculation of ice velocities, but as temperature in this setting is not influencing ablation, it is decoupled from the mass balance component, which can lead to unrealistic model setups. Additionally, equifinality is introducing some ambiguities in the results, as more than one combination of mass balance and temperature factors can produce the same final ice sheet configuration - a problem also occurring in other methods of climate forcing.

If mass balance is not parameterised directly in the ISM as described above, the relevant climatic factors contributing to ablation and accumulation need to be modelled, with the two most important parameters being temperature and precipitation. Additionally to its influence on ablation, temperature at the ice surface and the ice base is also needed as a boundary condition for the solving of ice dynamics (Eq. 2.8). While **basal temperature** is commonly estimated using a constant **geothermal heat flux** value (Eq. 2.9), ice surface and air temperature are determined using a climate forcing component.

Temperature index models: A number of studies have confirmed a strong relationship between temperature and ablation, such as Braithwaite (1995), and Schneeberger et al. (2003) who state that for larger ice masses, the average ice temperature influencing ice flow at a location is related mainly to elevation and latitude and to a much lesser degree to factors like net solar insolation. For glaciers, Schytt (1969) concluded the mean temperature of the ablation season to be the most important climatic factor controlling mass balance, while looking at the pre-conditions for the initiation of maritime ice caps, Kerr (1990) found the average sea temperature to play a key role. Temperature at a location can be approximated using for example a mean annual air temperature (MAAT) at sea level, seasonal temperature variation, and its dependency on elevation and latitude (Oerlemans, 2002). Ritz et al. (1997) calculate surface temperature for the Greenland ice sheet with an equation derived from parameterised temperature maps using surface elevation, latitude and and a factor representing climatic forcing according to:

$$T_{\mathrm{a}} = 49.13 - \left(7.992x10^{-3} * S\right) - 0.7576\,Lat + \Delta T_{\mathrm{clim}} \tag{2.17}$$

with T_a being the mean annual temperature, S (ice) surface elevation and ΔT_{clim} the climatic forcing factor. Hulton et al. (2002) use a 3rd order polynomial to represent temperature dependency on latitude.

Hence, melt is often parameterised using a temperature index model (TIM, Hock, 1999; Braithwaite, 1995). TIMs are based on the (empirical) relation of potential melt at a location being a function of the length of time an ice or snow mass is exposed to temperatures above the melting point. The time (days) above melting point for a location is usually given in positive degree days (PDD) per year (Reeh, 1991), while the available energy for melting is parameterised using a degree-day factor (DDF) which relates the temperature above 0 °C to melt. This way, TIMs can be used to approximate melt rates well where data for assessing the DDFs and temperature for a region is available (Braithwaite, 1995), while using a fraction of the computational resources necessary for EBMs following the basic form of

$$a_{pot} = \begin{cases} DDF \cdot T & T > T_t \\ 0 & T \leq T_t \end{cases} \tag{2.18}$$

where DDF is the degree days factor, usually given in m or $mm\ d^{-1}$ and T is the temperature in °C. Potential ablation a_{pot} is set to zero for temperatures below a certain threshold temperature T_t, usually 0 °C. Ablation is usually calculated daily and integrated over one year.

TIMs have been applied across a range of spatial and temporal resolutions (Hock, 2003), however where reference melt or temperature data is lacking, TIMs tend to locally over- or underestimate melt, and fail to reproduce spatial patterns of melt at higher resolutions. As potential radiation can be modelled to estimate temperature where no measurement data is available, a number of authors have enhanced TIMs using a radiation component to overcome these limitations (Pellicciotti et al., 2005; Schneeberger et al., 2003; Hock, 1999; Williams and Tarboton, 1999; Cazorzi and Fontana, 1996). Potential ablation at a location is then calculated following the basic scheme

$$a_{pot} = \begin{cases} F_t \cdot T + F_r \cdot (1-\alpha) \cdot swr & T > T_t \\ 0 & T \leq T_t \end{cases} \tag{2.19}$$

where F_t is a temperature factor equivalent to the DDF, T is the temperature, F_r is a radiation factor, α is albedo, swr is the shortwave radiation at the surface and $T_t = 0$ °C is the threshold temperature for melt to occur. These enhanced TIMs use topographic parameters like gradient slope and aspect to calculate solar radiation to model melt at

greater resolutions at the cost of increased computational demands. Calculating the potential incoming solar radiation is relatively straightforward, and for temporal resolutions of daily means or less, different parameterisations show fairly similar results (Kumar et al., 1997). However, in order to determine the net solar radiation at the surface a location is actually receiving, factors like surface albedo, cloud cover and relief shading have to be considered, which can be difficult to assess in some cases. Where factors like albedo or cloud cover are not available in sufficient spatial or temporal resolution, they are often based on assumptions, which introduces further uncertainty into the model. Albedo for example has a strong influence determining the potential solar radiation at a surface, and is known to vary over the extent of ice sheets and glaciers (Box et al., 2006; Oerlemans and Hoogendoorn, 1989) from values of 90% for fresh snow, 15% for debris covered ice and an average 4% for the earth surface (Paterson, 1994). Even though different values for snow, ice and barren ground are used when modelling energy balances Lefebre et al. (2003), because of the low resolution ice sheet models are usually run on, the spatial variability of albedo is often not captured.

Local energy balance models: Energy balance models (EBM) use the topography to calculate temperature at a location based on the radiation it receives just as enhanced TIMs do. EBMs however explicitly account for fluxes of sensible and latent heat in addition to the amount of incoming solar radiation at a certain location (and time) to determine the energy balance and thus the prevailing temperature and the energy available for melting snow or ice. EBMs are therefore characterised by a lesser degree of abstraction than eTIMs, and an increased demand for input data and computational resources. According to Oerlemans (2002), daily ablation a_t can be calculated according to

$$a_\mathrm{t} = shf_\mathrm{t} + lhf_\mathrm{t} + swr_\mathrm{t} + lwr_\mathrm{t} \tag{2.20}$$

where swr_t is the shortwave solar radiation and lwr_t is the longwave radiation influenced by albedo, cloudiness, exposition and slope. (lhf_t) and (shf_t) are the latent and sensible heat fluxes, respectively, influenced by factors like temperature gradient, wind, bedrock physics and humidity. Calculating the actual energy balance for large areas over long times can be extremely computational demanding on top of requiring a substantial amount of data that is not always available in the adequate quality. Additionally, energy balance calculation is only sensible at resolutions too high to be used with ISM applying the SIA, and thus is usually limited to simulating mountain glaciers or limited areas of interest within an ice sheet.

Both TIM and EBM require additional **precipitation** data to be input to the ISM to derive mass balance. While using the dependency of surface temperature on latitude and elevation allows to derive a spatially distributed temperature scheme sufficient for input to many ISM, spatially explicit precipitation schemes adapted to each topography are usually needed where mass balance is not modelled directly, for example based on ELA parameterisation. Precipitation schemes can be derived in a number of ways, but for modelling of past climates, a high degree of approximation is always inherent. One way of creating input precipitation schemes is to use present day precipitation, e.g. as supplied by CRU (2006) or IPCC (2006), and scale them to fit estimated mean values of past climates (compare Hebeler et al., in press), derived from proxies like GRIP (Johnsen et al., 1992). Another option is to apply snapshots from climate model reconstructions (Charbit et al., 2002) to drive an ISM. Where feedback effects of the modelled ice sheet with the regional climate should be considered, a coupled climate model has to be employed.

Coupled global climate models: Coupling an ISM to an (external) climate model allows to model feedback of ice sheets on regional and local climate, for example through orographic effects of the growing ice sheets, cooling effects that lead to reduced precipitation for continental regions, and their impact on the ice sheet configuration. Because global circulation models (GCM) usually have a very large model domain, their computational demands for use with regional ice sheet models are relatively high, despite the low resolution of the climate component. Alternatively, full-physics regional climate models can be used, which can support much higher resolutions, but despite the adapted modelling domain usually require unsuitable large computational capacities at the required resolutions. To overcome these limitations, Purves and Hulton (2000a) are using a limited area, reduced-process model of large-scale physics of precipitation, which considers the physics of moisture supply, transport and precipitation. With the atmosphere represented as vertically averaged air columns, their moisture content is determined using the underlying topography, temperature, wind speed and direction. Input variables are temperature as a function of latitude, elevation and continentality, wind as a verticaly averaged wind field, generated by the application of zonal pressure gradients and topography/elevation (considering up-wind slope), and topography for the calculation of elevation, up-wind slope and up-wind moisture removing obstacles. The model is coupled to a 3D thermomechanical ISM (Purves and Hulton, 2000b), with mass balance calculated from the proportion of precipitation falling as snow, ablation and ice temperature is derived using a TIM approach. Thus,

in their approach, effects of ice sheet evolution such as increase of ice extent and thickness, their effect on temperature and contintentality and the feedbacks on precipitation are explicitly integrated.

However, with ever increasing computational capacities, the use of GCMs for climate forcing of an ISM is becoming more and more feasible, and already a number of GCM of different complexity exist (Charbit et al., 2007). Examples include the community climate system model (Collins et al., 2006) used by Otto-Bliesner et al. (2006) to study climate and mass balance at the LGM, and the GENESIS GCM (Pollard and Thompson, 1997) used by Otto-Bliesner (1996). DeConto and Pollard (2003) use GENESIS to provide surface mass-balance forcing for an ISM, and include coupled surface models of ocean, soil, snow and vegetation. The GCM is asynchronously coupled to a 3-D ISM (Ritz et al., 1997; Huybrechts, 1990) including local bedrock response. Surface air temperature and precipitation is calculated from the GCM/surface models at resolutions of 3,75° x 3,75° / 2° x 2° , respectively, and interpolated to the 40 x 40km ISM resolution. For "computationally economical" reasons potential ablation is calculated from the GCM-derived monthly mean climatology using positive degree days (TIM) (DeConto and Pollard, 2003).

An alternative approach for using AGCM data with ice sheet models (ISM) despite the high computational demands is by coupling the ISM with AGCM snapshots (Fabre et al., 1998). However, this asynchronous coupling can result in long periods of static climate (10-100ka) in between snapshots. To overcome this limitation Charbit et al. (2002) interpolated six snapshots of modelled climate between the LGM and present taken at steps of 21ka over time to model the last deglaciation over the northern hemisphere using the ISM of Ritz et al. (1997).

Topography

The influence of topography in ISM is twofold: topography determines **ice dynamics** via the terrain configuration (ridges and troughs) and most important slope (Eq. 2.7). Additionally, topography influences **climate**, which has an effect on both mass balance via temperature and precipitation, as well as ice flow through its temperature relation (Eq. 2.5). Temperature is derived using the surface topography, which for ice free areas is the bedrock topography, usually supplied as a DEM at the model resolution, and the ice sheet surface for glaciated areas. Therefore bedrock topography plays an important role especially during inception (Oerlemans, 2002; Payne and Sugden, 1990), as the overall elevation as well as the terrain shape determines whether an ice sheet can form or not. High intermontane valleys for example support rapid growth

of ice sheets (Sugden et al., 2002), as cold temperatures support positive mass balance and low slope gradients prevent the ice from flowing rapidly to ablation areas. When considered in the model, orography can have an important influence on local precipitation patterns and therefore on mass balance through factors like advective rains, rain shadow or snow fence effects (Sugden et al., 2002). Oerlemans (2002) also points out the importance of isostatic response of the bed to orography and the evolution of ice sheets.

Even though an ice sheet is superimposed on the underlying bedrock topography by definition (Paterson, 1994), and for fully grown ice sheets the influence of ice surface topography typically dominates that of the bedrock topography, bedrock topography is still relevant for processes such as basal hydrology and sliding, and persisting terrain features such as ridges and troughs can influence ice flow directions and velocities (Jamieson et al., 2008).

Higher order ice physics

Models applying higher order physics, meaning they include both longitudinal and shear stresses for solving ice dynamics exist, using both finite difference and finite element approaches in two (Schoof, 2007b; Pattyn, 2003a) or three dimensions (Saito et al., 2006, 2003). These models are computational intensive and it is still not feasible to run continental or global scale ISM applying higher order physics. However, for most areas of a grown ice sheet such as the Antarctic ice sheets, applying the SIA is reasonable, as large ice thicknesses, low slope gradients and extremely cold temperatures permit fast ice flow where using higher order physics (HOP) is crucial. Therefore, HOP ISM are often used to study the behaviour of selected areas of interest in an ice sheet, such as the grounding line and ice shelves or ice streams (Schoof, 2007a), or in the modelling of glaciers (Schneeberger et al., 2003). Modelling approaches exist that try to combine both SIA and HOP using nested modelling approaches (e.g. Ritz et al., 2007).

2.4.2 Sources of Uncertainty in ISM

In an ISM, as in any model, the two categories of error resulting in uncertainty discussed in section 2.2.2 are input and model error.
Uncertainty arising from ISM input data can originate from **topography** and **climate** data, as well as **parameters** used to drive or tune the model, such as geothermal heat flux, lapse rate, or flow enhancement factor. These factors are often based on assump-

tions and subject to a substantial amount of simplification. ISM input data such as topography is subject to uncertainty that originates from measuring and processing (input and model error of the DEM). Additionally, algorithms applied within the ISM itself produce uncertainty (model error). Both types of uncertainty propagate through the modelling chain and therefore influences ISM results.

For simulations of existing ice sheets such as the Greenland ice sheet, uncertainties in the climate and mass balance estimates originate from the lack of temporal or spatial coverage, or natural variability of the measured phenomenon (Box et al., 2006; van der Veen, 2002). Recently high resolution regional climate models are becoming popular to fill these gaps. However, ablation processes that take place in zones of 1-50km width for example, are narrow in comparison to overall ice sheet sizes of thousands of kilometers in the case of Greenland and Antarctica. These ablation zones might only stretch across few model cells, and are still not well represented.

Running simulations of ice sheet model response to future climate change are prognostic and afflicted with a high degree of uncertainty, and require multiple runs with different climate scenarios to estimate the uncertainty in these simulations (e.g. IPCC, 2007; Alley et al., 2005). These uncertainties in the input climate are enhanced by the often high degree of parameterisation.

Even though ISM have developed rapidly from simple two-dimensional ice flow models (Pollard, 1982; Oerlemans, 1980) to three-dimensional (Huybrechts, 1990; Budd et al., 1984) and complex distributed systems integrating isostasy, basal hydrology, grounding line and ice shelf models (Charbit et al., 2007; Hagdorn et al., 2007; Huybrechts, 2004), many aspects of ice sheet dynamics and feedback systems are still not fully understood. One example are the basal boundary conditions of the ice shelf-ice sheet transition zone (compare Alley et al., 2005). Parameterisation is thus not always a means for efficient computing, but also for simple approximation of complex relations that cannot yet be be adequately captured. Possible misconceptions or oversimplifications in models are thus an important and difficult to assess source of uncertainty.

Uncertainty in the input DEM can be extremely large for topographies such as the Antarctic subglacial topography BEDMAP (Lythe et al., 2001), with potential uncertainties in elevation in the range of thousands of meters in remote areas of sparse data coverage. Areas with GLOBE data coverage such as Fennoscandia usually have accuracies stated in the meta-data of 16-30m RMSE. Nevertheless, the high degree of uncertainty in climate data and the high degree of abstraction and parameterisation still abundant in ice sheet modelling probably account for the fact that topography re-

lated uncertainty has not been widely recognised as an important source of uncertainty in ISM. This is likely to be sustained by the low resolutions ISMs commonly run on, where low accuracies are assumed to be of little relevance. However, previous experiments confirmed that even though the amount of DEM uncertainty is reduced through generalisation, it still has an impact on ISM. Above all, resampling a DEM to lower resolution introduces further uncertainties to the ISM input topography (Hebeler and Purves, 2004).
Thus, while all potential uncertainties in a DEM propagate to the ISM (compare section 2.2.2), additional uncertainty is introduced for example through the slope algorithms used for the calculation of ice velocities in the ISM. Because of the complexity of an ISM, these uncertainties are difficult to be traced analytically. Uncertainties in slope derivation for example, are likely to have larger effect on bedrock slopes than on ice surface slopes because of the steeper gradients at the base. Uncertainty in slope will thus have stronger impacts during inception than on fully grown ice sheets, and will impact basal hydrology more than surface melt. At the same time, elevation uncertainty will impact on both calculated slope and temperature, which might result in reverse effects. Thus for the analysis of uncertainty impact on ISM results, Monte Carlo methods are a suitable option (van der Veen, 2002).

2.4.3 Modelling using Subscale Information

Models such as ISM are a key tool in our understanding and exploration of systems. Since models are an abstraction of reality, the selection of appropriate **degrees of abstraction** is a key task. Complex processes need to be abstracted sufficiently so they can be understood and modelled, while their key properties and dependencies must be retained. Thus the scale and complexity of the processes to be modelled should determine the target model resolution - however in practice both the resolution and complexity of a model are often a trade-off between our ability to understand the system, the complexity of numerical solutions at a given resolution and computational capacities (Martin and Church, 2004; Armstrong and Martz, 2003; Malanson, 1999).

ISM are usually running on continental or global scale over extended periods of time. Because of the complexity of the model and the required computational resources, the spatial resolution of ISMs is often low at 5-20km or more, requiring a considerable amount of abstraction and simplification (such as applying the SIA). Applying these low resolutions in a model can however have significant drawbacks. For ISM, the smoothing of topographical features through the resampling of DEMs results

in an overall lowering of elevation and thus increase of temperature which might require unrealistic lowering of temperature for modelling ice nucleation (Marshall and Clarke, 1999). Additionally, resampling results in a decrease of average slope gradient which influences ice velocity calculations. Apart from the smoothing effects, ISM at low resolutions of 10-20km often fail to adequately resolve ablation processes (e.g. Marshall, 2002), because even for very large ice sheets such as in Greenland, ablation zones might be narrow and represented by only a few cells (Box et al., 2006; Ritz et al., 1997). This in turn requires unrealistically high high melt factors in order to fit ISM extents to empirical boundaries.

The described problems are typical in modelling of complex systems consisting of interrelated processes at different scales. These models often fail to capture the smallest scale processes because of limitations in maximum resolution, for example because of numerical or computational constraints. However, resolving these '**subscale**' processes can be crucial for realistic and reliable modelling (Marshall and Clarke, 1999). While **parameterisation** is *per se* an approach to include fine scale information in large scale modelling, the abstraction of processes fails to capture spatial variation at the subscale level, which might otherwise influence results (Essery and Marks, 2007; Hu and Islam, 1997). External coupling of two or more models at different resolutions is another option. One example is the coupling of global circulation models with regional climate models (e.g. Salzmann et al., 2007), however computational demands can be extensive and parameterisation is often preferable.

A scalable and computationally less demanding method to include subscale information at the model resolution is by the means of bins or **subgrids**. The approach is characterised by the use of additional layers of information on one or more variables at the model resolution. In geomorphological modelling, hypsometric information is commonly used (Essery, 2003; Marshall, 2002). In this case, instead of using one elevation value per grid cell, the hypsometry at the higher resolution is described, i.e. by using mean elevation of a number of elevation classes, stored in additional grid layers. Subgrid modelling is frequently applied in hydrological modelling of snowcover and melt across a range of scales (e.g. Liston, 2004; Strasser and Etchevers, 2003; Marshall, 2002; Marshall and Clarke, 1999; Luce and Tarboton, 2001; Luce et al., 1999; Leung et al., 1996). Taking subgrid modelling one step further is the approach of using nested grids (Calov and Marsi, 1998, e.g.). Here, areas where certain processes are ill-represented are identified either dynamically or prior to modelling, and the model resolution is selectively increased for these areas. Ritz et al. (2007) use the "Adaptive Grid Refinement In Fortran" (AGRIF, Debreu and Blayo, 2002) to model fast flowing

ice in outlet glaciers, and Pollard and DeConto (2007) apply a dynamic nested grid approach for modelling grounding line behaviour. This approach is of course only viable, where higher resolutions are not permitted by assumptions such as the SIA.

Essence: In general, uncertainty of input data such as DEMs have potentially **higher impact on process models** than on simple form models such as topographic attribute derivatives. Because of the higher complexity process models usually have, the impact of uncertainty is likely to be nonlinear and dynamic, and analytical analysis of uncertainty impact might not be feasible or possible at all.
Ice sheet models usually consist of a core component that solves **ice dynamics**, and associated components that supply the boundary conditions, such as bedrock topography, temperature and precipitation. These associated components can be of different complexity, from static values prescribed at compilation time to complex models of basal hydrology and coupled atmospheric circulation models. To adequately model the flow of ice, in the core ISM component the stresses that act on an ice mass have to be derived, which depend largely on the ice height and the **slope of the surface topography**. These stresses determine the **ice flow velocity** and together with **basal sliding** account for the total movement of ice. As flow velocity also depends on the ice temperature, the **temperature** regime of the ice, depending on air temperature, strain heating and the geothermal heat flux has to be solved. To model the evolution of the ice height, **mass balance**, essentially the difference between accumulation and ablation across an ice sheet has to be modelled. While mass balance can be parameterised directly, it is usually supplied via additional model components, such as **temperature index models (TIM)** which calculate ablation based on temperature.
(*continued on next page*)

(*continued*)
The different model components are interdependent and connected via complex feedback mechanisms of ice physics, climate and topography. Although highly sophisticated, many aspects of an ISM are subject to a **high degree of parameterisation**. As such, in order to assess and evaluate the **uncertainty impact** from one source category such as input DEM or climate drivers, uncertainty from other sources have to be reviewed as well, in order to identify particular **susceptible** model components. For a sensible assessment of ISM sensitivity to uncertainty from input topography, model parameterisation and applied algorithms, a profound understanding of the model interrelations is essential.
Where susceptible components such as ablation modelling in ISM have been detected, these components might be **isolated** in order to facilitate research on the causes of this susceptibility and to lessen or eliminate them. An example is the application of **subgrid approaches** to melt modelling, where the low resolution and small spatial extent the ablation area often has in ISM is compensated by incorporating higher resolution information.

Need: A profound understanding of the impact of uncertainty from topographic representation is needed in order to identify the susceptible processes within the model, and develop methods to minimise the impact. Limitations of the ISM, such as maximum resolution as well as computational limitations have to be accounted for. Additionally, the impact of parameter uncertainty needs to be assessed so topographic uncertainty impact can be related and efficiently communicated.

2.5 Dealing with uncertainty

"Communicating uncertainty is as much a challenge as understanding error in data and modeling" – Reinke and Hunter (2002)

As it has already been stated in section 2.1, uncertainty is present in many phenomena of everyday life as well as in most digital data models. Consequently, uncertainty does not necessarily pose a problem, but can even be used as a means for assessing the quality and probability of a prediction, accuracy of a map, etc. It is however crucial that producers and users of data such as DEM are aware of this uncertainty. Additionally, methods for assessing, describing and communication uncertainty associated with a product must be available, and applications using this data must be able to incorporate information on uncertainty. The need for the **distribution of detailed uncertainty models** with DEMs has been recognised for more than a decade, and has been stipulated by a multitude of authors (e.g. Kyriakidis et al., 1999; Shortridge and Goodchild, 1999; Fisher, 1998; Ehlschlaeger and Goodchild, 1994). Many GIS users are aware of the importance of uncertainties in DEMs, and a number of approaches for assessing, modelling and communicating uncertainty have been developed. However, despite this data users and applications rarely account for uncertainty (Wechsler, 2003).

Existing relations as well as needs for dealing with uncertainty, identified by different authors (Beven, 2007; Comber et al., 2006; Devillers et al., 2005; Shortridge and Goodchild, 1999) have been compiled and summarised (Fig. 2.6) to give an overview of the dependencies and processes that apply where data uncertainty is to be explicitly considered in an application: It is obvious that before uncertainty and its properties can efficiently be managed and communicated, it has to be understood and assessed, using meta data and/or higher accuracy reference data where available. This can be done for example by using spot height measurements as a reference for assessing the quality of a DEM, and will deliver a set of spatially distributed error values (Fig. 2.6,'Uncertainty Modelling'). Depending on the amount and type of information, a suitable uncertainty model has to be chosen; sticking to the example of reference data points, Kriging might be an adequate method to use (compare section 2.2.2), which may deliver a fitted semivariogram to describe the spatial correlation of the error. This specific uncertainty model for the data set can be visualised and communicated, and used within an application.

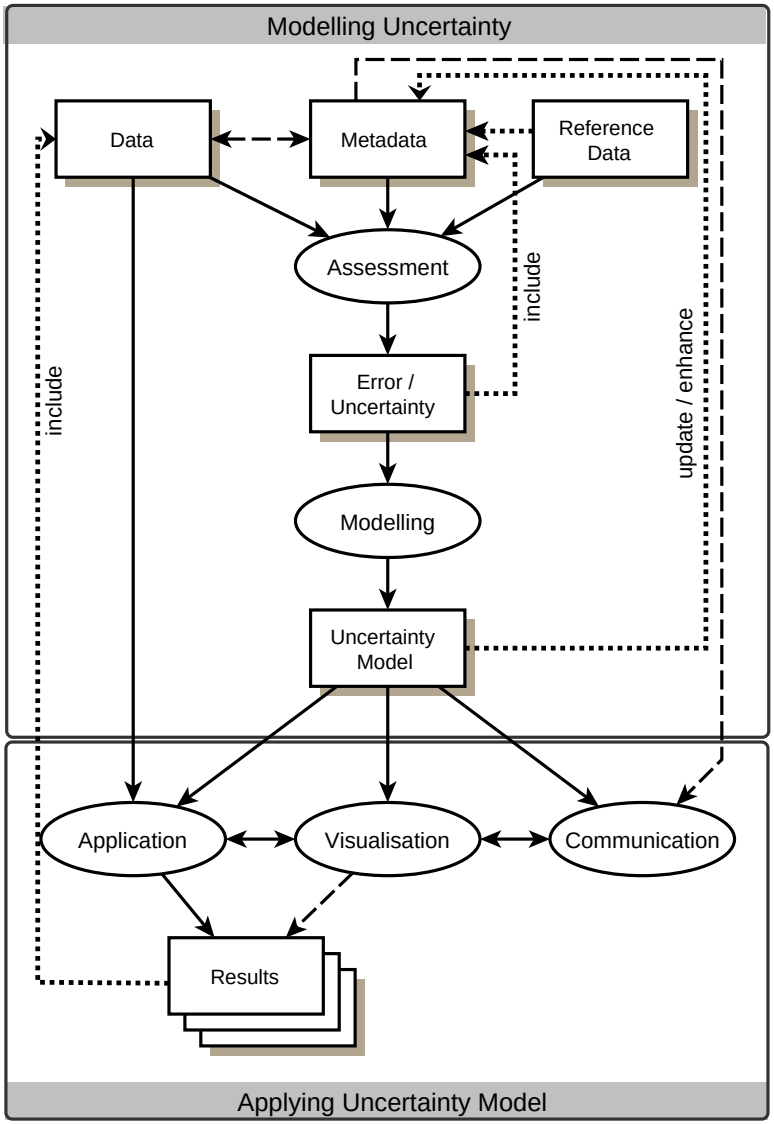

Figure 2.6: Processes, data and interdependencies in uncertainty assessment, modelling and application. Devillers et al. (2005) suggest a dynamic or proactive linkage of metadata and data. Once an uncertainty model has been developed for a certain dataset, it should be distributed as metadata, which will allow subsequent communication of the uncertainty (model) of the data without the need for assessment and model development.

2.5.1 Communicating Uncertainty

One necessity for improved **communication of uncertainty** is to distribute uncertainty information with corresponding data products. If higher order reference data exists, it should be distributed with the data. Alternatively, error derived using this reference data should be included in the metadata. Both cases would allow any data user to de-

velop their own uncertainty model.
However, as uncertainty modelling is complex and requires expert knowledge, in order to enhance the use of uncertainty models and to foster a **standardisation**, Shortridge and Goodchild (1999) suggest that an appropriate uncertainty model based on the available information should be developed and distributed with the data, including possible algorithms and dependencies. Alternatively, using this uncertainty model a number of equiprobable realisations of the data can be produced, that are either distributed along with the data or produced on the fly by user request (Shortridge and Goodchild, 1999). In order to facilitate the application of uncertainty information with for example DEMs, Shortridge and Goodchild (1999) identify the need for improvements of GIS, which are required to work with multiple surfaces and realisations. Beven (2007) proposes an integrated approach using multidisciplinary data, uncertainty and modelling constraints for the exploration and understanding of complex interrelations and models.
Devillers et al. (2005) suggest quality information should be linked to the data as **metadata**. This linkage could be realised using dynamic or 'proactive' content, that can act on the fly to provide uncertainty information for GIS analysis and prohibit "illegal operations". This again would require a **quality aware GIS** postulated by Shortridge and Goodchild (1999), and while information richness of this metadata would be drastically increased, the demand in terms of time to produce, understand and integrate this metadata correctly will also considerably increase (Fig. 2.7). Additionally, the notion of data allowing or prohibiting certain operations intuitively implies complications and restricted usability, and might appall many potential users. However, at this point efforts for standardising metadata even for static content have left almost a dozen different standards for DEM products alone. Despite the chance that proactive metadata will become a standard within the next few years are probably slim, efforts for communicating uncertainty in model results exist, both outside and within the GIS community.

In principal, two approaches of communicating data uncertainty exist (Buttenfield, 1993), namely reporting accuracy ("good aspect") which according to MacEachren et al. (2005) is usually favoured over reporting error ("bad aspect"). Reasons for this preference can include the implication of unreliability, the vagueness of the term uncertainty in itself and the lack of methods for depicting uncertainty together with data in sensible and understandable ways.

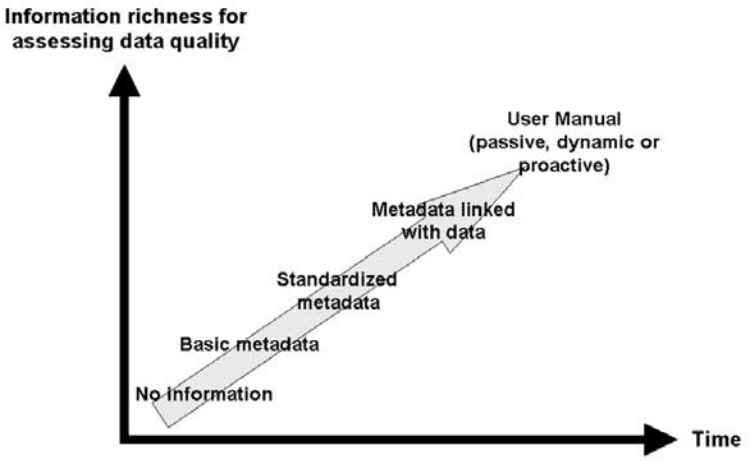

Figure 2.7: Information richness versus time costs for communicating data uncertainty via metadata. (Devillers et al., 2005)

2.5.2 Visualising Uncertainty

For digital geographic data using the entity model, concepts for **visualising** uncertainty have been proposed as early as the 1980's (compare Weibel and Buttenfield, 1992), and are usually based on the concept of graphical attributes (Bertin, 1983), adapted for cartographical data (Oehler, 2005; Buttenfield, 2000). Additional methods applicable for **entity based data models** include epsilon bands or buffers for lines and points and confusion matrices for classifications (Hunter and Goodchild, 1995). These methods are straightforward in two-dimensional depictions, e.g. maps, but are usually impracticable for three dimensions (Hunter and Goodchild, 1995) and cannot be easily transposed to **continuous data** using regular tesselated grids. A major problem for processing and visualising uncertainty of (large) raster data sets is the vast amount of data multiple equiprobable representations create. Griethe and Schumann (2006) give a general overview of uncertainty visualisation problems and methods applicable across scientific domains. Methods they present include the use of a framework where uncertainty data is used to parameterise or filter visualisation data. In studies on the use of uncertainty visualisation for decision making, data and its associated uncertainty information have been visualised using split displays, or by means of either user controlled or automatically toggled displays (Aerts et al., 2003; Evans, 1997). Another method of dynamic visualisation to convey uncertainty in continuous surfaces is by animation (Griethe and Schumann, 2006; Ehlschlaeger et al., 1997; Ehlschlaeger and Goodchild, 1994). Methods such as stochastic imaging (Journel, 1996) can be used to produce a number of equiprobable surfaces that are then animated on a timeline, e.g. discrete surfaces are interpolated for higher temporal resolutions (Ehlschlaeger et al., 1997; Ehlschlaeger and Goodchild, 1994) or the visualisation is integrated in the production of the surfaces in order to render smooth transitions (Griethe and Schumann, 2006).

In general, visualising uncertainty of a continuous surface or phenomenon in a single image is much more difficult than for discrete object boundaries. A relatively simple method applicable to both categorical and continuous data is the use of probability maps (Hunter and Goodchild, 1995) for the graphical display of uncertainty. Here, the probability of a grid cell to take on a certain value, range, or class across a number of realisations, for example produced using Monte Carlo Simulations, is calculated and plotted.

A number of studies exist that examine ways of representing uncertainty in maps (Harrower, 2004) and whether and how they benefit the user in the decision making process (Couclelis, 2003; Ziadat, 2007; Comber et al., 2006; Monmonier, 2006; Keuper, 2004; Foody and Atkinson, 2002).

An approach related to stochastic imaging that has become popular for communicating and visualising uncertain information is by the means of **fuzzy** sets (Zadeh, 1965). Approaches to represent uncertainty in GIS using fuzzy set theory have evolved in the early 1990's (Burrough et al., 1997). While probability maps depict the likeliness of an area or cell to have a certain attribute, fuzzy sets assign degrees of membership in two or more classes (of different attributes) to its elements. For each class a different membership function can be defined, and a cell or polygon can have different degrees of membership for a number of classes (Davis and Keller, 1997a). Fuzzy memberships concepts lend themselves to represent the conceptual vagueness of many geographical phenomena (Fisher et al., 2007). One example is the definition of geographical terms such as 'mountain' or the delineation of a landform such as a peak, where the membership function of a location (cell) belonging to the class 'peak' is not only depending on the applied concept, but also on its neighbouring landform and the observation scale (Fisher et al., 2004). Fuzzy theory has therefore frequently been applied to cope with uncertainties in morphometric analysis of DEMs and landform classification (e.g. Arrell et al., 2007; Burrough et al., 2000).

Despite their methodical adequacy for uncertain data, the visualisation of fuzzy memberships is non-trivial and their use give little, if at all, advantage over regular grids. In general, fuzzy set theory allows soft boundaries (Arrell et al., 2007), and multidimensional fuzzy membership functions are an option for representing multiple realisations of continuous surfaces produced using uncertainty models. For example Santos et al. (2002) use fuzzy numbers and fuzzy interpolation to produce 'envelopes' of uncertainty boundaries for surfaces.

Essence: As it has been stated in section 2.1, uncertainty in inherent any data or model. If it is dealt with adequately, uncertainty is not a problem, but can be used for assessing the quality and reliability of a model or prognosis. To facilitate a widespread use and understanding of the importance of uncertainty information and the potential it bears for decision making and quality assessment, **visualisation** techniques are essential. While a number of static and dynamic approaches for conveying uncertainty in geographic data have been developed, especially the communication of uncertainty in continuous, complex data has proven to be non-trivial.

Need: In order to be able to make use of uncertainty information, better means of **communicating uncertainty** have to be found and put to widespread use. This can include the distribution of equiprobable realisations of data, the distribution of uncertainty models and the standardisation and enhancement of metadata, as well as the development of quality aware GIS. Users of geographical data have to accept the fact that uncertainty is inevitable, which would eventually release the stigma that fosters suppression of uncertainty instead of assessment and utilisation.

2.6 Implications

The five goals for handling error and uncertainty by Veregin (1989) and Plewe (2002) (section 2.1)

1. Identifying and understanding of error and uncertainty
2. Detecting and measuring error
3. Modelling error and uncertainty propagation
4. Managing error and uncertainty
5. Reducing error and uncertainty

essentially are the basis for the research questions formulated in section 1.2. The first research question, the identification of potential uncertainty sources in topographic representation, is consistent with the first goal, laying the foundation of the work. Research question 2 deals with the quantification and modelling of uncertainty from topographic representation, equivalent to goal 2. This is essential for assessing the impact and thus propagation of uncertainty, and has been applied in the three case studies of geomorphological, melt and ice sheet modelling, relating to the third research question and goal 3. Research question 4 is seeking a deeper understanding of uncertainty propagation, partly relating back to the first goal, while the quantification and communication of uncertainty impact, formulated in the fifth research question is concordant with goal 4 of the list. Finally, finding methods to reduce the impact of topographic uncertainty on ice sheet models, is in close accordance with the fifth goal stipulated in the list.

Regular tesselated elevation grids are the most common form of DEM in modelling, also applied in the three case studies used in this dissertation. Uncertainty from three major categories have to be considered, which are data quality, data processing, and modelling uncertainty. In order to assess and model DEM data quality, metadata accuracy figures such as RMSE can be used, but to allow sensible impact analysis, reference data is necessary. The DEM data used for the two case studies undergoes two significant processing steps. One is the projection of the data to Albers Equal Area, which implicitly requires resampling. The second is adaption of the DEM resolution to meet the requirements of the model, which in the case of ISM requires downsampling of more than one order of magnitude. The impact of uncertainty from the third category, the modelling, is important to assess in order to understand the impact the degree of abstraction has on model results, and to allow comparison of uncertainty impact from other sources. Therefore, ways of assessing the importance of the differ-

ent potential uncertainty sources, as well as sensible ways of modelling the resulting uncertainty have to be found or developed.

Having developed adequate uncertainty models, the impact of topographic uncertainty can then be tested using topography based models. The impact on simpler form models, such as geomorphological or hydrological models that derive a suite of primary and secondary topographic attributes, can be compared with more complex process models, within which the derived topographic attributes are used to control simulated physical processes, e.g. ice flow in ISM. Assessing the impact of uncertainty in model parameter then allows a comparison.

Finally, using a profound understanding of the used ISM together with the insight gained from the different impact analysis studies, the goal is to develop ways to communicate uncertainty, and test and implement approaches for minimising uncertainty and/or it's impact on ISM results.

Chapter 3

Methodology

In the following chapter, a comprehensive overview of the methodology developed and applied within the papers included in this dissertation(Appendices A-E) is given.

Firstly, the approaches used to assess uncertainty from topographic representation are presented. The subsequent section introduces methods developed and applied for modelling this uncertainty. This modelled uncertainty has been used to assess the impact on different models. These models, namely a geomorphological/hydrological model, a snow melt model, and an ice sheet model, are introduced in consecutive sections. The approaches applied for subgrid modelling, and a parametric uncertainty analysis are ending this chapter. More detailed information is given in the respective paper referred to in each section, which can be found in the appendix.

3.1 Assessing Topographic Uncertainty

In order to model uncertainty, its amount, source, characteristic distribution and spatial configuration first needs to be assessed.
In our approach to modelling uncertainty associated with the use of common DEM products for environmental models, we investigated the two categories of possible sources presented in section 2.2.2, namely input and model error. As a range of sources from both categories exist, within the scope of this dissertation we had to focus on what was decided to be the most important and relevant ones for our case studies: data accuracy for input error, and resampling for model error.

Because ISM run on low resolutions of 5-20km, we assessed the impact of **resampling** DEMs from resolutions of approximately 100m (SRTM) to 5, 10 and 20km. To do so, we resampled SRTM data for the central European Alps using ArcGIS 9

standard resampling methods (bilinear interpolation and cubic convolution) as well as taking the total mean of all contributing cells. This resampling was repeated shifting the resampling origin cell-by-cell to generate 40 different target DEMs for each resampling method and target resolution. The standard deviation of elevation for each cell across the 40 realisations was then plotted against elevation, showing a dependency with elevation which was approximated using a 4th order polynomial and used in modelling uncertainty.

Additionally, the standard deviation of elevation of all cells at 90m resolution within each 5, 10 and 20km resolution cell was plotted against elevation, to give an estimate of the amount of generalisation and the range of elevations each low resolution cells represents (Fig. 3.1).

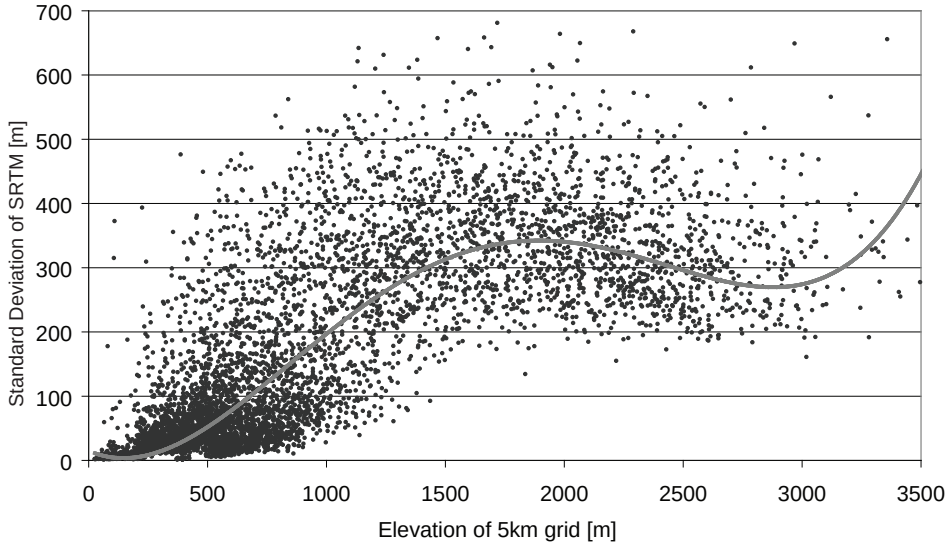

Figure 3.1: SRTM3 data of the Alps at approximately 77m resolution was resampled to 5km resolution using bilinear interpolation. The standard deviation of all SRTM elevation values at the original resolution within each 5km cell is plotted against elevation at 5km resolution. The distribution can be approximated using a 4th order polynomial giving an r^2 of 0.65. Note that applying this polynomial to model the dependency is only valid for elevations below 3500m.

Input error can only be derived using higher order reference data, which is commonly not available to the DEM user. Therefore, in a first approach to assess input error derived uncertainty, accuracy figures given for GLOBE and GTOPO30 DEMs as RMSE were used to create uncertainty surfaces for Fennoscandia. These RMSE vary for different sources from 18m for DTED to more than 300m for GLOBE Antarctica data, and no information on spatial distribution or dependencies is given.
In order to be able to model uncertainty from DEM data accuracy realistically, in-

cluding spatial correlation, a new method for modelling GLOBE DEM uncertainty was developed, assessing error properties based on SRTM data used as a reference (see appendices B, C and E). Using SRTM data as ground truth, error surfaces of different GLOBE datasets where created, and analysed for correlation with topographic attributes and indices such as gradient slope and aspect, curvature, roughness and extremity.

3.2 Uncertainty Modelling

Where accuracy information in DEM metadata is given as **RMSE**, no information on the spatial configuration is provided, and assumptions about the spatial autocorrelation of modelled error had to be made. In order to assess the potential difference in impact of **uncorrelated and correlated uncertainty surfaces**, random white noise with a mean of zero and standard deviations of 18, 30, 100 and 300m was added to GLOBE DEM of Scandinavia. The resulting disturbed DEMs were then resampled to 20km (see Hebeler and Purves, 2004), and used as input for Monte Carlo Simulations using the Edinburgh Ice Sheet climate driver (EIS, applying ELA parameterisation, Hagdorn, 2003) on the GLIMMER ISM.

In order to compare the impact of uncorrelated and correlated uncertainty surfaces on ISM results, random surfaces having the same mean and standard deviations were produced. Spatial correlation was then introduced to the surfaces following the approach of Fisher (1993) by randomly swapping cells with repeated calculation of Moran's I. However, for high rates of spatial autocorrelation (high Moran's I values), the method proved to be too inefficient when dealing with a large number of simulations (100+) over large areas needed as input to the ISM. In order to produce spatially correlated uncertainty surfaces of near normal distribution, sets of random points on the DEM were selected. Random values were then assigned to the points from a normal distribution, using a mean of zero and a standard deviation equivalent to the RMSE of the DEM metadata. These points where then interpolated using **inverse distance weighting** (IDW). IDW proved to provide smooth, correlated surfaces sufficiently fast for the generation of large sets of input topographies for the ISM.

In order to analyse the impact of uncertainty introduced by **resampling of DEMs**, the method described above was modified. The assessed uncertainty (described in section 3.1) showed strong spatial dependencies with elevation. In order to model this uncertainty, the statistical distribution of uncertainty was assumed to be normal, and the magnitude to correlate with elevation. For MCS of the Patagonian ice caps, spa-

tially correlated uncertainty surfaces were created by randomly selecting a set of 250 selected points on the input DEM, equivalent to every 100th cell of the DEM grid separated by a minimum distance of 2 cells. The derived elevation dependency of uncertainty was then applied to calculate a local standard deviation for each point. A random uncertainty value was then drawn from a normal distribution using this standard deviation and a mean of zero, giving a set of 250 uncertainty values for each DEM. IDW was again used to interpolate these points, resulting in **spatially correlated, elevation dependent** uncertainty surfaces. In this way, 150 random topographies were produced and used as input for MCS (see appendix A and Hebeler and Purves, 2005a).

In order to develop an **uncertainty model for GLOBE DEM error** that includes spatial autocorrelation as well as terrain dependencies, e.g. both deterministic and stochastic components (Appendices B, C & E), the derived dependencies of GLOBE error with terrain were used.

These dependencies were used to model a deterministic component of uncertainty by means of regression. The residuals of this regression, e.g. the part of uncertainty that did not show any correlation with topographic properties, were found to generally be normally distributed. These residuals were modelled using a random normal distribution, thus forming a stochastic component, which make the produced uncertainty surfaces suitable for MCS. The surfaces where then filtered using a convolution filter (Oksanen and Sarjakoski, 2005a) with a range determined through semivariogram analysis of the original error surfaces. Using this approach honours both systematic error (dependency of uncertainty on topographic attributes) as well as random error (Wise, 2000), reproducing the spatially correlated component as well as random noise, and partly also global trends (Fisher and Tate, 2006; Heuvelink, 1998). Using this approach to determine an uncertainty model for GLOBE DEM where higher order reference data (SRTM) is available allowed us to create a set of equiprobable uncertainty surfaces for Fennoscandia, where no reference data is available (compare Shortridge and Goodchild, 1999), which was then used as input for MCS.

3.3 Geomorphological Modelling

In a first set of experiments, the impact of GLOBE DEM uncertainty (derived using SRTM as a reference) on the derivation of topographic attributes and (static) form models was assessed (Hebeler and Purves, in press). A suite of 40 realisations of the uncertainty model was created and added to a GLOBE DEM of the European Alps. In each of the DEMs, sinks were filled using Arc/Info in order to create hydrologically cor-

rect topographies. From these topographies, a set of parameters was derived, namely elevation, gradient slope, number of watersheds, watershed boundaries, Strahler order, stream length and hypsometric integral, using TARDEM (Tarboton, 1999) for the calculation of the hydrological indices. For the two selected watersheds of the Inn and the Adda which are neighbouring at the headwater, additionally the membership likelihoods for DEM cells to belong to either one of the watersheds were calculated.

3.4 Ice Sheet Modelling using GLIMMER

Ice sheet modelling was done using the GLIMMER ISM, applying different climate drivers for modelling both reconstructions of the Last Glacial Maximum as well as steady-state runs using fixed climates on Fennoscandia and Patagonia. GLIMMER (General Land Ice Model for Multiply Enabled Regions, Payne, 1999) builds upon the foundations laid down by the modelling studies of Huybrechts (1986), Boulton and Payne (1992) and Payne and Dongelmans (1997). GLIMMER is a three-dimensional thermomechanical model that implements the shallow ice approximation (SIA) (Hutter, 1983) to solve ice dynamics calculations. Three example climate drivers are provided with the model in addition to an API allowing to couple GLIMMER with custom climate drivers or external models. For initial experiments, the original Edinburgh Ice Sheet driver (EIS) using ELA parameterisation described by Hagdorn (2003) was applied (Appendices A & C). Default model parameters were used to model ice sheets on topographies of Fennoscandia at 10 and 20km resolution, Patagonia at 10km resolution as well as on artificial topographies of various resolutions, in order to assess the general impact of different amounts of topographic uncertainty on basic ISM setups.

For Patagonia, recent temperature and precipitation distributions were used to derive climate forcing parameters, and altered to approximately represent conditions during the last LGM. The GLIMMER ISM was then run until modelled ice sheets were in equilibrium, with uncertainty surfaces created using random points interpolated using IDW (see section 3.2 and Hebeler and Purves, 2005a).
Reconstructions of the Fennoscandian ice sheet during the LGM based on the climate parameterisation developed by Hagdorn (2003) were run using uncorrelated topographic uncertainty and uncertainty correlated using random cell swapping and IDW, as well as GLOBE DEM uncertainty simulated using the regression model described in section 3.2.

Later experiments (Hebeler et al., in press) were conducted using an advanced climate driver (gen_pdd) developed by Jamieson and Sugden (2008), where calculation of ablation rates is done using a temperature index model (see section 2.4.1). Separate DDF for ice and snow are used, and a sinusoidal variation of air temperature of a set amplitude t_{range} is applied to account for seasonal variation. Additionally, diurnal variation is accounted for by random variation of temperature using a normal distribution N[0,5]. A firn model is incorporated via the calculation of a fraction of melted snow ($w_{\max}$) that refreezes to form superimposed ice. Surface temperature is calculated using a spatially distribution input grid of 20 year mean CRU (2006) and IPCC (2006) temperature data at sealevel, corrected for elevation using an atmospheric lapse rate ($lrate$). Temperature can be varied over time using time series files applying uniform absolute temperature changes across the grid. Where the derived temperature at the surface is smaller than a threshold temperature t_{snow}, precipitation is assumed to fall as snow, thus contributing to accumulation. Precipitation is also input to the model as spatially distributed 20 year mean precipitation values, derived from CRU and IPCC data. Variation over time can be done using time series files, where precipitation can be globally changed over the grid in percentage relative to the original values.

For all ISM setups, basal ice velocity v_{b} is derived according to

$$v_{\text{b}} = t_{\text{b}}\,\tau_{\text{b}} \tag{3.1}$$

with t_{b} being a basal slip coefficient and τ_{b} being shear stress according to equation 2.4. Sliding is assumed to occur where the ice base is melting, taking into account the geothermal heat flux, frictional heat components and corrections for pressure melting. While the early experiments used a constant basal slip coefficient for basal ice at pressure melting point, for the latest experiments for DEM and parametric uncertainty analyses (Hebeler et al., in press), basal slip is a function of basal water pressure (P_{w}):

$$t_{\text{b}} = \min(t_{\text{bmax}}\,, b_{\text{soft}} + t_{\text{bslope}} \times P_{\text{w}}) \tag{3.2}$$

where the slope of the function is given by t_{bslope}, the softness of the bed is given by a parameter b_{soft} and the basal traction is limited from becoming too large by the value of t_{bmax}. Variability in the basal traction parameter can significantly change the behaviour and form of the resulting ice mass.
A full outline of the numerics implemented in GLIMMER is provided by Hagdorn et al. (2007) and Paterson (1994) provides additional context to the derivation of these mechanics.

Monte Carlo Simulations were run in order to test the impact of uncertainty modelled using the approaches described in section 3.2. Suites of simulated uncertainty surfaces were added to the original topography at 1km resolution using GLOBE DEM data, and resampled to the target resolutions. The GLIMMER ISM was then run on each of the prepared input topographies using identical parameters and climate drivers. Modelled variables were output to a result file in the NetCDF format at discrete timesteps, usually modelled ice thickness every 100 model years, and variables such as horizontal and vertical ice velocities, basal sliding, ice temperature, ablation, basal melting etc. at lower temporal resolutions of 500 or 1000 model years. Using Python scripts and Matlab, ice extents and volume of all files and timesteps were calculated and analysed across all runs and finally visualised. Table 3.1 gives an overview of all experiments on topographic uncertainty impact on ISM conducted during the course of this dissertation.

Topography	Climate	Type	Res.	Uncertainty-Model	Uncertainty-Source	Reference
Fennoscandia	EIS	Steady State	20 km	Uncorrelated	RMSE, Generalisation	Appendix A
Fennoscandia	EIS	Steady State	20 km	RCS*/IDW	RMSE, Generalisation	Appendix A
Artificial	EIS	Steady State	5-20 km		No. of landscape features	Appendix A
Fennoscandia	EIS	LGM	20 km	IDW	RMSE, Generalisation	Hebeler et al. (2005); Hebeler and Purves (2005b)
Patagonia	EIS	Steady State	10 km	IDW	GLOBE DEM error	Hebeler and Purves (2005a)
Fennoscandia	EIS	LGM	10 km	Regression Model	GLOBE DEM error	Appendix C, Hebeler and Purves (2007a,b)
Fennoscandia	gen_pdd	Steady State	10 km	Regression Model	GLOBE DEM error	Appendix E
Fennoscandia	gen_pdd	Steady State	10 km	PU Model^{+}	ISM parameters	Appendix E
Alps	TIM/eTIM		0.1-10 km	Regression Model	GLOBE DEM error	Appendix D

Table 3.1: Overview of experiments on topographic uncertainty impact on ISM conducted during the course of this work. The 'climate' column states the respective climate driver used, e.g. the Edinburgh Ice Sheet driver (EIS) based on ELA parameterisation, and the generic pdd driver 'gen_pdd' based on a temperature index model. For completeness, experiments on GLOBE DEM uncertainty impact on pure melt models (TIM/eTIM) without ice dynamics are included. The applied uncertainty models are explained in detail in section 3.2. Experiments on artificial topographies were conducted without superimposed uncertainty surfaces, but using varying numbers of landscape features (peaks) to test their impact on ice sheet configuration for varying climates. *RCS= random cell swapping / $^{+}$Parametric Uncertainty Model.

3.5 Melt Modelling

In order to test the susceptibility of ablation to DEM uncertainty, scale and parameterisation, two melt models were implemented using Matlab. First, a simple temperature index model (TIM) was implemented following the concept of Braithwaite (1995). Potential melt is calculated as a function of degree days and temperature including a sinusoidal temperature variation with an amplitude of 5 °C representing seasonal temperature change, similar to the TIM used in the GLIMMER ISM. However, because potential melt was calculated without any coupled mass balance model, only one degree day factor (DDF) was used, instead of the usual separate DDFs for ice and snow.

The second model implemented was an enhanced TIM incorporating a solar radiation component, following the approach of Pellicciotti et al. (2005). For this enhanced TIM, albedo was assumed to be constant over time and space, and as for the TIM, only a single DDF was applied (Hebeler and Purves, 2008b).

Both models were run on a topography of the western European Alps, spanning an area of about 200'000km^2 and an elevation range of -4 to 4654m. Void-filled SRTM version 3 (Jarvis et al., 2006) data was used, projected to Albers Equal Area projection at resolutions of 100m, 1, 5 and 10km. Both models were tuned to approximately fit empirical melt rates reported by Strasser et al. (2004). For a list of parameters and their corresponding values used in the melt models, see Tab. 3.2.

Symbol	Parameter	Value	Units
α	Albedo	0.4	
a_{seas}	Seasonal temperature amplitude	5.0	°C
DDF	Degree day factor	5.2	mm d^{-1}
F_{r}	Shortwave radiation factor	0.012	m^2 mm W^{-1} h^{-1}
F_{t}	Temperature factor	0.05	m^2 h °C^{-1}
$lrate$	Atmospheric lapse rate	6.5	°C km^{-1}
$MAAT$	Mean annual air temperature at sealevel	15.0	°C
r	Ground reflectance coefficient	0.2	
S_0	Solar constant	1367	W m^{-2}
T_{t}	Temperature threshold for melt	0	°C

Table 3.2: Parameters used for the calculation of potential melt using the simple temperature index model and the enhanced solar radiation model.

3.6 Resolution Effects and Subscale Modelling

Because ablation/melt modelling is known to be insufficiently resolved in ISM running at low resolutions (Marshall and Clarke, 1999), within the scope of this dissertation alternative approaches for incorporating higher resolution terrain information were sought (compare research objective 4, section 1.2). One cause of the poor performance of ablation modelling in ISM is the low resolution, which has two effects, namely a high degree of smoothing of the topography, and a small relative extent (in number of cells) of the ablation zone. Thus, the aim was to identify the susceptibility of melt modelling to scale and parameterisation.

To examine resolution effects, melt was calculated at a high resolution (100m) using a TIM and eTIM (section 3.5). These melt rates were resampled to resolutions of $1, 5$ and 10km, using the mean melt of all contributing cells. In this way, the mean melt rate per area calculated at 100m resolution was preserved at each lower resolution, giving a 'reference'. These reference melt rates where then compared to a 'baseline' approach, where the respective melt model was applied directly to DEMs at $1, 5$ and 10km resolution.

In order to test the effect of subgrid modelling, an approach similar to that of Marshall and Clarke (1999) was chosen, where additional information on the topography within each low resolution cell is added as an additional layer at the same low model resolution. In the experiments presented here, instead of having one cell containing the mean elevation of the underlying area at each resolution, three cells containing the mean, upper and lower quartile elevation were used. This additional information can than be utilised for the calculation of melt, effectively lowering the degree of abstraction/parameterisation. For the first experiments, a simple parameterisation was chosen where melt was calculated separately for every subgrid and then a weighted average was taken. Using this subgrid approach allowed us to compare scale effects of the applied melt models (TIM and eTIM, section 3.5) using the unparameterised baseline approach as well as a subgrid approach.
In total, four different approaches for subgrid parameterisation have been developed and tested in the course of the experiments, all of which used different amounts of subgrid layers or varying hypsometric information.

In order to assess the impact of DEM uncertainty on both melt models, a Monte Carlo Simulation approach was chosen. The GLOBE DEM uncertainty model was used to add 100 uncertainty surfaces to input topographies at 1km, which were then resampled to 5 and 10km resolutions, giving a set of 100 different input topographies at each of the three resolutions. Melt was calculated at the 1km resolution using the TIM

and the results were resampled to 5 and 10km, again forming a 'reference' data set as use in the previously descriped experiments. Potential melt was then calculated on the 5 and 10km topographies, using the normal TIM ('baseline') as well as a subgrid parameterisation approach. This allowed a comparison of DEM uncertainty impact on the different methods (reference, baseline and subgrid) as well as the different resolutions (5 and 10km).

3.7 Parametric Uncertainty Analysis

As discussed previously, because of the complexity of the ISM, analytical examination of error propagation is not feasible. At the same time, combining separate single parameter sensitivity tests will not allow a sensible estimate of total parameter uncertainty of the ISM, because of the various interrelations and feedbacks of the model parameters, and the resulting non-linear behaviour. Therefore, in order to compare and rate the impact of uncertainty from DEM accuracy and resampling effects, a **parametric uncertainty analysis** (PUA) was conducted as proposed by van der Veen (2002). The main concept of a PUA is to assess the uncertainty of all model parameters, essentially assigning to each parameter a value range and a probability function for each parameter to take on a certain value within this range. This in turn allows the simultaneous variation of all model parameters across a number of Monte Carlo Simulation runs. Because probabilities have been assigned to the variation of each input parameter, the resulting variation in model results can also be assigned probabilities.

For the PUA, GLIMMER was run on the Fennoscandian topography at 10km resolution. To provide a stable baseline model configuration, which could then be varied for the PUA, a spatially distributed precipitation scheme was derived from present day CRU and IPCC data. Present mean annual air temperature and dependencies on latitude and elevation were used, and the MAAT was lowered about 12 °C to support the initial growth of an ice sheet. Both MAAT and precipitation could be controlled using global parameters to scale the initial values. A set of 12 parameters used in the GLIMMER ISM was then selected, on the basis of importance, assessed from the literature, i.e. the number of existing sensitivity test, as well as own experience. For each parameter, a range of plausible values (Tab. 3.3) as well as a possibility distribution function PDF was deducted from the literature, empirical data where it existed (e.g. CRU and IPCC climate data) as well as sensitivity tests using the GLIMMER ISM. A suite of 510 different GLIMMER configurations were created, with each of the 12 selected parameter values randomly drawn from their respective PDF. All initial parameter values

were kept constant over time, and the ISM was run until the modelled ice sheet was in equilibrium after about 30k years. This setup resulted in a suite of 510 different model results that were evaluated using Matlab.

Climate Forcing Parameter	**Range**	**Units**
Mean Annual Air Temperature	-8 to -18	°C[a]
Seasonal Temperature Half-Range	3 to 15	°C
Atmospheric Lapse Rate	-3 to -10	°C km^{-1}
Precipitation	50 to 150	%[a]
Degree Day Factor Ice	5 to 11	mm d^{-1} °C^{-1}
Degree Day Factor Snow	3 to 19	mm d^{-1} °C^{-1}
Geothermal Heat Flux	-30 to -70	mW m^{-2}
Snow Threshold Temperature	0.5 to 2.5	°C
Model Internal Parameter		
Flow Enhancement Factor	0.5 to 3.5	
Maximum Basal Traction	0.05 to 5	$\times 10^{-3}$m a^{-1} Pa^{-1}
Ice Thickness Threshold for Resolving Ice Physics	200 to 600	m
Meltwater refreezing fraction	0.4 to 0.8	

[a] *relative to present day climate*

Table 3.3: Parameters used in the parametric uncertainty test (Hebeler et al., in press)

Chapter 4

Results

This chapter gives a recapitulation of the results described in the five papers included in this dissertation. It also links the results obtained throughout the course of my PhD studies to provide an overview of the work and facilitate the understanding and integration of it.

4.1 Assessment of Topographic Uncertainty

Assessing the role of DEM resampling in topographic uncertainty revealed that both the resampling method as well as the grid origin used in the resampling have a major influence. Using different resampling algorithms and shifting the resampling origin resulted in substantial variation of resulting elevations within the target cells. This variation in elevation, and thus the corresponding uncertainty, is strongly dependent on elevation and terrain roughness. The resulting uncertainty in elevation values is well in excess of the given DEM accuracy figures. For example where SRTM data of the Alps at approximately 90m resolution was resampled to 5km using bilinear interpolation, the standard deviation of all original SRTM3 cells within the bounds of each 5km cell for mean elevations above 1000m was on average 350m (Fig. 3.1). Bilinear interpolation is the standard resampling method for many GIS such as ArcGIS. Commonly, this interpolation selects the center of the low resolution target cells, and interpolates the elevation values of only the four immediate neighbours of the underlying high resolution grid to interpolate the new value, irrespective of the actual total number of high resolution cells within the boundaries of a target resampled cell. Thus shifting the origin of the resampling (within the target cell boundaries) can result in noticeable differences in elevation values and the spatial configuration of landscape elements, as different values are used within the interpolation. Repeated resampling

of a DEM from 90m to 10km using fixed grid boundaries, but shifting resampling origins, resulted in variation of elevation in the resampled DEMs of 50-150m standard deviation on average for elevations above 1000m.

4.1.1 Assessment of GLOBE DEM Error

In our first experiments (compare Hebeler and Purves, 2004) we modelled DEM error and uncertainty based on information provided in the metadata, which is limited to a global RMSE usually derived using a (small) number of reference points.

Assessing GLOBE DEM error for the three selected test areas using SRTM as ground truth showed small systematic error of around 3.5m, and a standard deviation of approximately 70m (Tab. 4.1). Analysing the error properties (Hebeler and Purves, in press, 2008a)) revealed a number of findings:

- DEM error shows a distinct spatial correlation with main landscape features such as ridges, valleys etc. (Fig. 4.1a)
- Systematic error is abundant and varies for different examined regions; an example is an apparent systematic shift of GLOBE data relative to SRTM, which varies for different subsets and regions of GLOBE data
- Correlation and regression analysis revealed both error magnitude as well as sign of the error to be correlated with topographic attributes: error magnitude showed good correlation with elevation roughness (variation of elevation within a 3x3 neighbourhood), elevation, gradient slope and minimum extremity (divergence of center cell from minimum of 3x3 neighbourhood - Carlisle, 2000). Sign of error showed medium correlation with mean extremity (divergence of center cell from mean of 3x3 neighbourhood - Carlisle, 2000) and slope aspect. However a large amount of error was uncorrelated to the tested terrain attributes.
- Spatial autocorrelation of the derived error, assessed using semivariograms, showed directional effects, with mean maximum correlation ranges of three to five cells (km).

GLOBE error derived using SRTM thus showed systematic, spatially correlated and random components, in correspondence with the concepts by Fisher and Tate (2006) and others, as described in section 2.2.2.

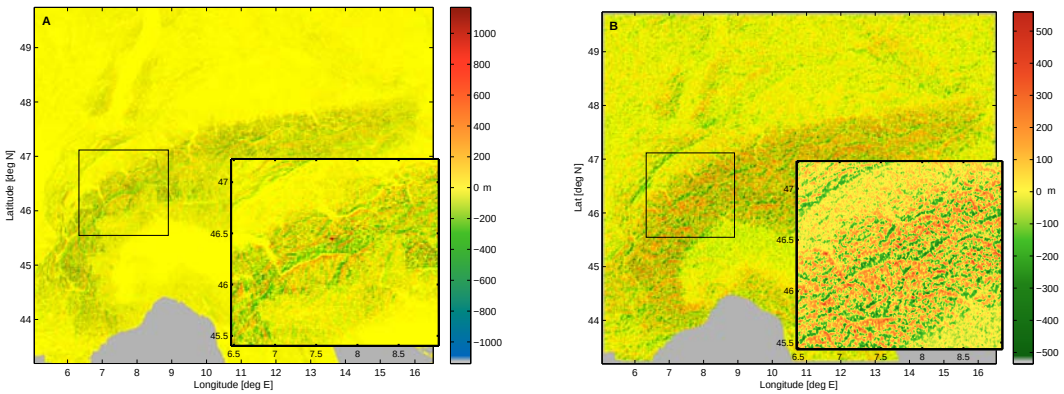

(a) Alps GLOBE DEM error

(b) Modelled DEM uncertainty

Figure 4.1: GLOBE DEM error of the European Alps (a) derived from the 1km GLOBE DEM data with SRTM data used as ground truth. Modelled GLOBE DEM uncertainty using the regression model for the same region captures the spatial distribution of uncertainty well (b).

Testregion	Mean	Standard Deviation	Range	Skewness	Kurtosis
Alps	3.3 m	82.2 m	-1140 – 1169 m	0.05	11.6
Pyrenees	4.2 m	68.8 m	-920 – 797 m	-0.14	14.2
Turkey	3.0 m	70.7 m	-817 – 964 m	-0.04	11.3

Table 4.1: GLOBE DEM error statistics, assessed using SRTM as ground truth for mountainous areas of three test regions of the Alps, the Pyrenees and Turkey.

4.2 Uncertainty Modelling

Modelling uncertainty from DEM accuracy on the basis of RMSE with random white noise produced very rough surfaces. The resulting topographies tended to lead to frequent model crashes due to the steep slopes and very rough, unrealistic surfaces (Hebeler and Purves, 2004).

Applying random cell swapping with calculation of Moran's I to introduce spatial autocorrelation of uncertainty produced much smoother, though still noisy surfaces (Fig. 4.2). This could be seen as in accordance with the regionalised variable theory introduced in chapter 2, which assumes that uncertainty consists of both correlated and random components. However, for medium to low rates of autocorrelation as measured by Moran's I, extreme outliers in the uncertainty surfaces such as single cell spikes and pits were still abundant (Fig. 4.2). These outliers again resulted in unrealistic topographies and still led to occasional model crashes. Additionally, using random cell swapping to create higher rates of spatial autocorrelation, proved to be very demand-

ing in terms of computational resources, above all time, and therefore was considered impractical for the use with large datasets.

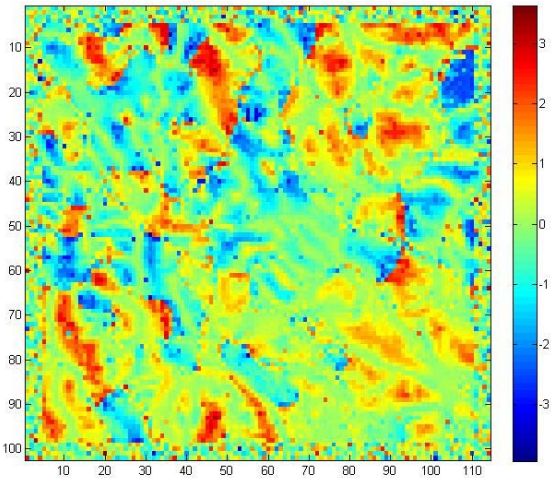

Figure 4.2: DEM uncertainty modelled using normally distributed random values. Spatial correlation introduced by random cell swapping with repeated measurement of Moran's I. Values of local Moran's I given in colour; mean (global) Moran's I for the surface is 0.42.

The alternative approach simulating uncertainty from generalisation used random points, interpolated using IDW. This method produced smooth surfaces without any outliers, that were suitable as input to the ISM much faster. Additionally, this approach allows to include dependencies of modelled uncertainty on DEM characteristics at the randomly selected locations. For the example of Patagonia, 250 random points were selected (1/100 fraction of gridcells) with a minimum distance of 2 cells, and interpolated using IDW of the nearest 15 neighbours. This resulted in surfaces of high autocorrelation, giving an average Moran's I of 0.76. However, for this method the amount of spatial correlation depended on the density of the selected random points and the chosen IDW parameters. Because these values could not be reliably based on empirical findings, the main selection criteria were to minimise the distortion of the original normal distribution, and a resulting 'smooth' topography without extreme outliers.

Using the properties of GLOBE DEM error (section 4.1) to develop an uncertainty model showed that the magnitude of error can be modelled well using a linear regression including the parameters 'elevation roughness' and 'minimum extremity' or 'elevation' with r^2 values between 0.4 and 0.5 using a global model (Hebeler and Purves, 2008a). If GLOBE DEM error is modelled for areas where SRTM was available and thus error can be calculated (i.e. the Alps), the residuals of this first regression can also be modelled using the magnitude of error, resulting in $r^2 > 0.8$ for a simple linear regression. Residuals of this second regression can then be modelled using a random normal distribution (Hebeler and Purves, in press).

If this GLOBE uncertainty is to be used in areas where no SRTM reference is available, such as Fennoscandia, the residuals of the error magnitude regression can

not be modelled. Analyses showed that the residuals of the first regression can be well approximated using a normal distribution around a mean of 0m with 45m standard deviation (N[0,45]).

It was also found that the sign of error can be modelled using a logistic regression including mean extremity and gradient aspect. Using these two variables allowed to model around 60% of the error sign correctly. The remainder was then assigned randomly, which essentially formed a second stochastic component. Finally, a convolution filter was applied to the so derived surfaces.

Using the described approach, the created uncertainty surfaces exhibited statistical distribution of uncertainty values very close to that of the derived error surfaces, and semivariograms indicating ranges of autocorrelation close to that of the original error. The created uncertainty surfaces reproduced correlation of uncertainty along prominent landscape features well, and since they contained both deterministic as well as stochastic elements, were fit for use in Monte Carlo Simulations. Modelled uncertainty surfaces are non-normally, symmetrically distributed, with a mean of approximately 3.8m and a standard deviation of approximately 80m for the Alps study area.

4.3 Impact of Topographic Uncertainty on Form and Process Models

4.3.1 Impact on Geomorphology Modelling

The impact of uncertainty derived from GLOBE DEM error on the calculation of topographic attributes was relatively small when focussing on global parameters calculated over the whole study area (Hebeler and Purves, in press). As an example, elevation and hypsometry for a larger study area are both hardly affected by modelled DEM uncertainty. When deriving topographic attributes for limited areas or delineating boundaries such as watersheds, some significant differences could be observed across MCS realisations, for example in the total number of delineated watersheds or the mean watershed slope. Simulated DEM accuracy uncertainty showed the greatest impact where the focus was on single, delineated areas (Fig. 4.3). Across 40 MCS runs, the area of a selected watershed was shown to vary up to 100%, resulting in comparably strong impact on derived attributes for these watersheds, such as calculated hypsometry (Hebeler and Purves, in press).

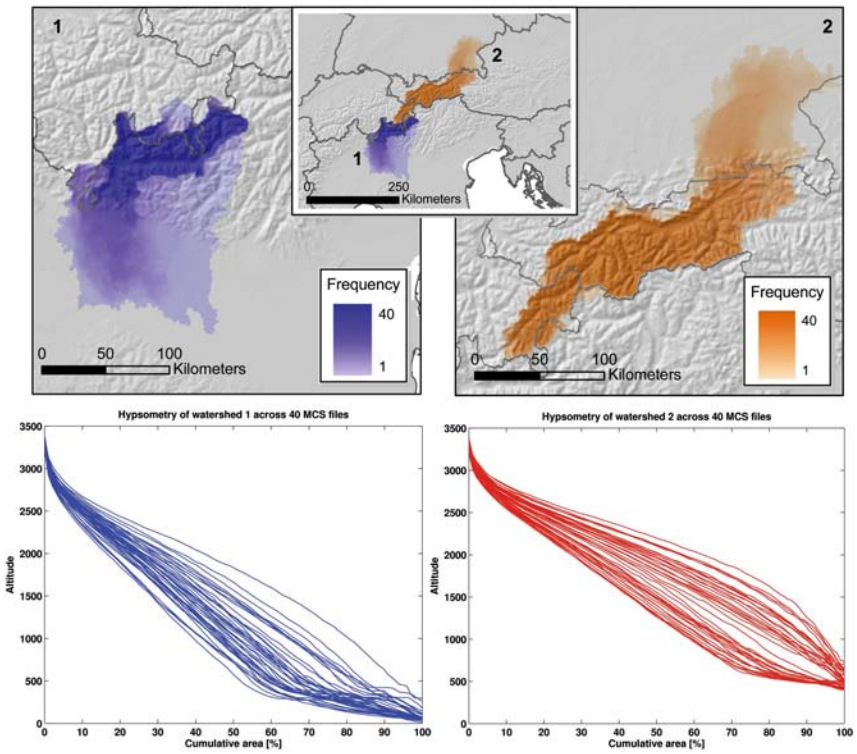

Figure 4.3: Variance in delineation of the Adda (1) and Inn (2) watersheds due to DEM uncertainty across 40 MCS runs (top). Variation in calculated hypsometry of the respective watershed across 40 MCS runs (bottom).

4.3.2 Impact on Ice Sheet Modelling

A first important result of introducing uncorrelated random error to ISM input topography was the relatively low variation of modelled ice sheet extent and volume using Monte Carlo Simulation. If random error with standard deviation above a certain threshold was added to topographies, the result were unrealistically noisy topographies which frequently caused ISM crashes due to instabilities. Introducing spatially correlated instead of uncorrelated random error produced smooth topographies that did not result in model crashes, even for high standard deviations (Hebeler and Purves, 2004).

An interesting observation was that the introduction of correlated error of lower mean and standard deviations as uncorrelated error, had a much greater impact on modelled ISM results, increasing variation of modelled ice extents and volumes by factors between three and eight (Fig. 4.4).

Applying the GLOBE DEM uncertainty model to Fennoscandia produced uncertainty surfaces with mean values of 0.64 ± 0.02m with standard deviations of 40.5 ± 0.02m. Statistical distributions were symmetrical around 0 (skewness=0) but

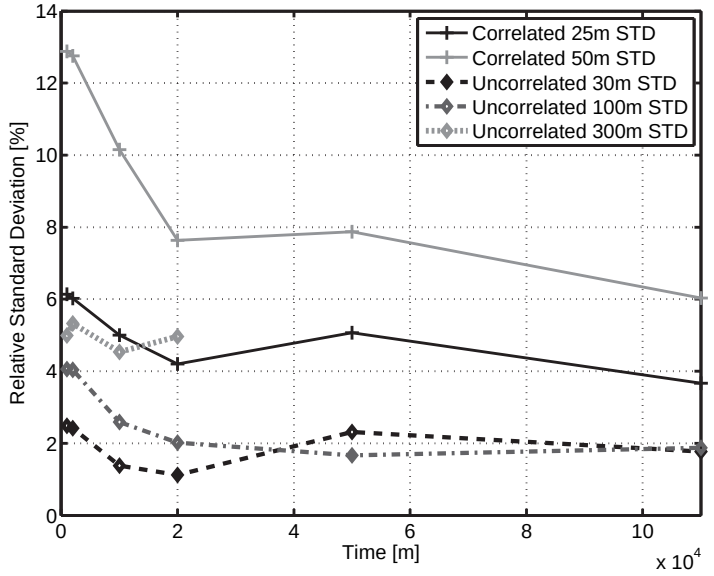

Figure 4.4: Impact of correlated (solid lines) and uncorrelated (broken lines) modelled uncertainty on modelled ice sheet extents on Fennoscandia, measured in percent relative standard deviation across 50 model runs. Using uncorrelated uncertainty simulated by a random normal distribution with standard deviation of 300m (gray dotted line) resulted in model crashes after 20ka due to instabilities caused by the high terrain roughness.

with a higher kurtosis (k=8.7) than a normal distribution (k=3). The influence of these uncertainty surfaces on modelled ice extent and volume for Fennoscandia was dependent on the total size as well as the phase (advance or retreat) of the modelled ice sheet. The relative standard deviation in ice extent varies between 2 and 15% for reconstructions of the Fennoscandian ice sheet during the LGM (Hebeler and Purves, 2008a). Strongest variations in modelled ice extent and volume across MCS runs at 10km resolution was recorded during inception and phases of ice retreat, and in general standard deviation is negatively correlated with ice volume and extent (Fig. 4.5). Variation in extent of fully grown ice sheets for these experiments lay between 2 and 7% (Fig. 4.5). This negative correlation of standard deviation with ice volume has been observed in previous experiments (Hebeler et al., 2005): testing the influence of uncertainty from generalisation on ISM results, comparable amounts of uncertainty have been introduced to topographies at 20km resolution, with resulting variation of MCS results of an average 10% for modelled ice extent of fully grown ice sheets. Relative standard deviation of ice extent and volume across 150 MCS runs plotted against normalised modelled ice sheet size (extent and volume) was strongly negatively correlated and could be approximated using a logarithmic function (approx. $-10ln(x)+3$) yielding an r^2 of 0.97.

However, for modelled ice caps in Patagonia calculated standard deviation of ice extent across MCS runs exhibited a positive correlation with overall ice sheet size. Because of the dominant influence of the Andean ridges in Patagonia, presumably the

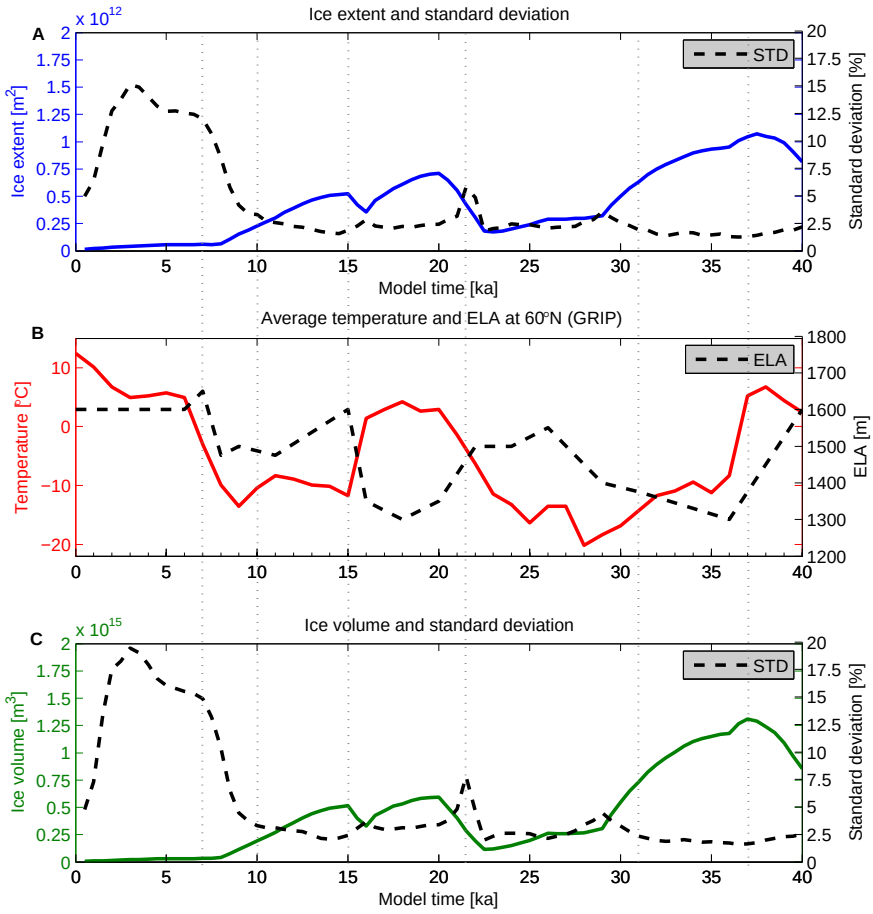

Figure 4.5: Mean and standard deviation of modelled ice extent and volume during the Fennoscandian LGM for the DEM uncertainty experiments. Mean ice extent (A) and volume (C) with their respective relative standard deviation (dashed lines) across 100 MCS runs plotted against modelling time. Climate forcing plotted over time (B) with temperature (solid) and forced ELA (dashed).

impact of topographic uncertainty on ISM results is also dependent on the characteristics of the topography the ISM is running on (Hebeler and Purves, 2005a).

Sensitivity tests of the impact of DEM uncertainty on ISM results to temperature confirmed the overall ice sheet size to influence results. MCS using modelled DEM uncertainty on Fennoscandia, applying steady-state climate showed a bifurcation in the PDF of modelled ice sheet extents where temperature was lowered by 10 °C relative to present day climate (Fig. 4.6(a)). This bifurcation is not detectable in the -12 °C and -14 °C scenarios which feature much larger ice sheets (Fig. 4.6(c),(e)).

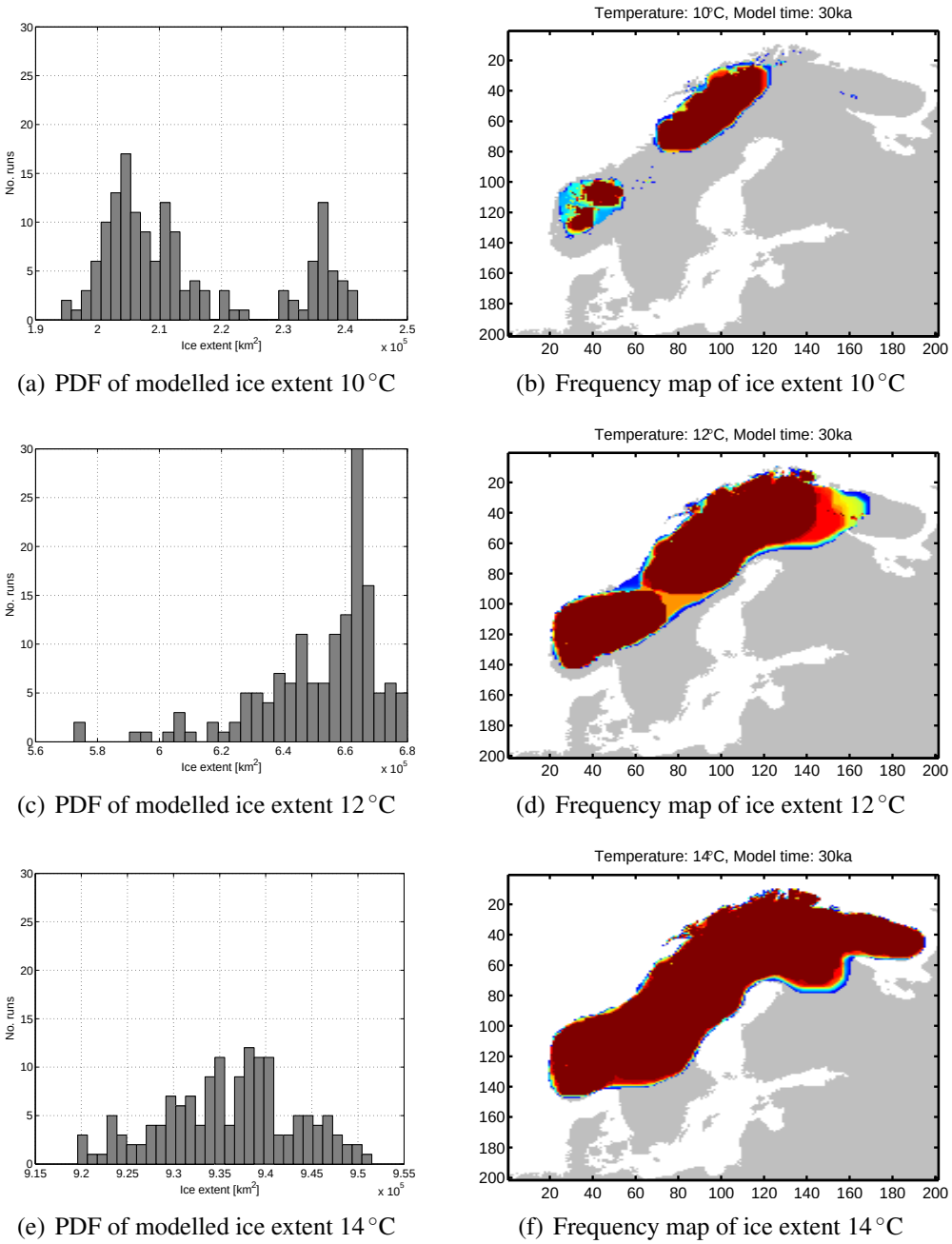

(a) PDF of modelled ice extent 10 °C

(b) Frequency map of ice extent 10 °C

(c) PDF of modelled ice extent 12 °C

(d) Frequency map of ice extent 12 °C

(e) PDF of modelled ice extent 14 °C

(f) Frequency map of ice extent 14 °C

Figure 4.6: PDF (a,c,e) and frequency maps (b,d,f) of modelled ice extent for the 10, 12 and 14 °C temperature lowering scenarios of the DEM uncertainty analysis.

4.3.3 ISM Parameter Sensitivity and Uncertainty Testing

Sensitivity tests revealed the modelled ISM extent and volumes to be highly sensitive to variation of input parameters that directly act on mass balance, such as temperature, precipitation and lapse rate (Hebeler et al., in press). Internal model parameters,

such as the flow enhancement factor or the threshold for ice dynamic calculation have relative little influence on modelled ice sheet configurations, but can control model stability. One example is basal traction, where certain parameter configurations can lead to model instabilities such as oscillations in ice flow. The tested parameter range of lapse rate, mean annual air temperature and seasonal variation as well as precipitation resulted in variation of up to 200% in modelled extent in the sensitivity tests. Up to 100% variation was recorded for DDF of ice and snow. While variation of both basal traction and flow enhancement factor showed negligible differences in modelled ice extent, changes in ice volume of up to 50% were observed.

Out of the total of 510 parametric uncertainty test runs, 4 model configurations prevented inception due to high temperatures and/or low precipitation and no ice formed at all; 6 out of 510 runs resulted in unreasonably large ice sheets with extents in excess of $2x10^6 km^2$ that grew out of the modelling domain. These total of 10 extreme outliers mark less then 2% of all runs, suggesting a reasonable setup of the PUA configuration.

The 10 outlier runs were removed prior to analysis. Across the remaining 500 runs, the calculated relative standard deviation was high, between 65-70% for grown ice sheets after 5000 model years. Relative standard deviation of extent over all runs decreased rapidly with growing ice masses, but slowly increased after 10'000 years. Modelled ice extent around a mean of $6x10^5 km^2$ $\pm 1\sigma$ varies between 2 and $8x10^5 km^2$. A bifurcation in modelled ice extents across the 500 runs is observable in the PDF (Fig. 4.7(a)). Additionally, a large peak of model runs with less than $0.35x10^5 km^2$ of modelled ice extents. The corresponding frequency maps shows two separate ice sheets in the southwest and northeast, that coalesce in around 50% of all runs (Fig. 4.7(b)).

4.4 The Influence of Scale and Subgrid Modelling

The resolution experiments comparing reference to baseline approaches for the two melt models revealed pronounced underestimation of melt with decreasing resolution for both melt models (Fig. 4.8(a), Hebeler and Purves (2008b)). This underestimation is observable for elevations which experience temperatures below zero at least once per year. Additionally, for the eTIM, melt rates around this 0 °C threshold are overestimated at lower resolutions, while they are underestimated for higher elevations (Fig. 4.8). Plotting mean melt rates against elevation in the resolution experiments also revealed an increased variation of melt for the different elevation classes with de-

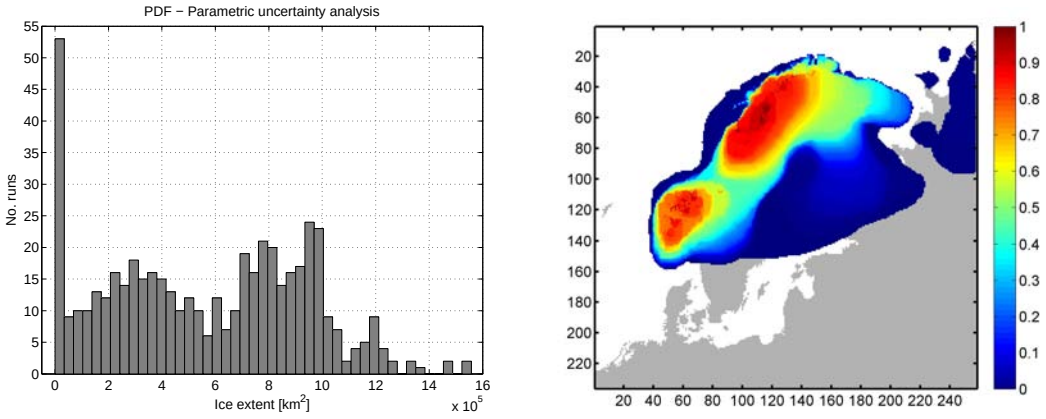

(a) PDF of the PUA ice extent

(b) Frequency map of the PUA ice extent

Figure 4.7: PDF and frequency maps of modelled ice extent for the parametric uncertainty analysis.

creasing resolutions, which are not captured in the baseline approach of both models (Hebeler and Purves, 2008b).

Using subgrid approaches can retain some of this variation and results in melt rates closer to that of the reference approach when compared with the baseline (Fig. 4.8(b)). However, the smoothing inherent in the averaging of melt applied in the reference approach, results in a loss of inception points at lower resolutions. Effectively, peaks above the ELA that have positive mass balance and can thus serve as nucleation points for ice, are reduced in elevation below the ELA during resampling. This effect, also less pronounced, is also observable in the subgrid approaches, while the baseline approach retains most potential inception points at the cost of an overall increased melt free area. For the eTIM, parameterisation of subgrids using mean slope for the four cardinal directions in addition to subgrid elevation improved model performance for low model resolutions of 5 and 10km.

Examining the susceptibility of the subgrid parameterisation approach to simulated DEM uncertainty compared to the reference and baseline approach using MCS, revealed a higher impact of uncertainty on subgrid approaches for lower elevations, while for higher elevations, susceptibility was comparable to that of the reference approach. The baseline approach proved to be more robust at high elevations with overall low melt rates.

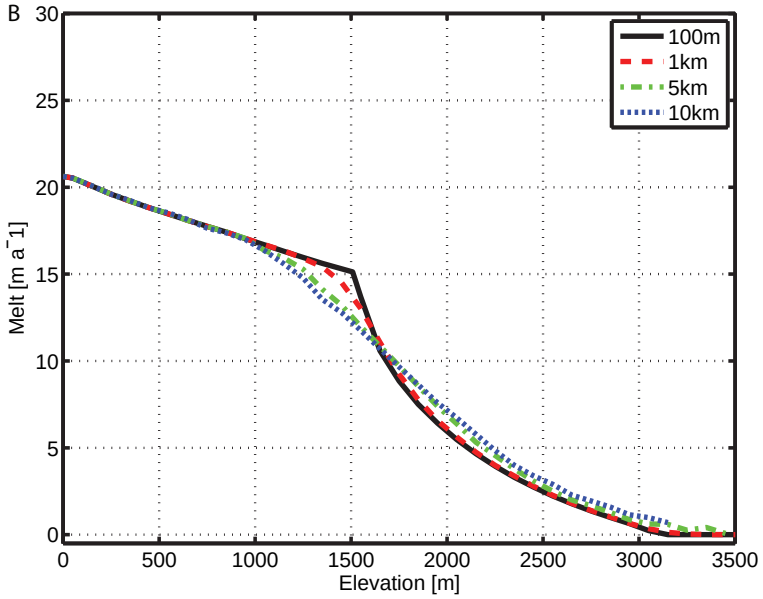

(a) Effect of resolution on modelled potential melt

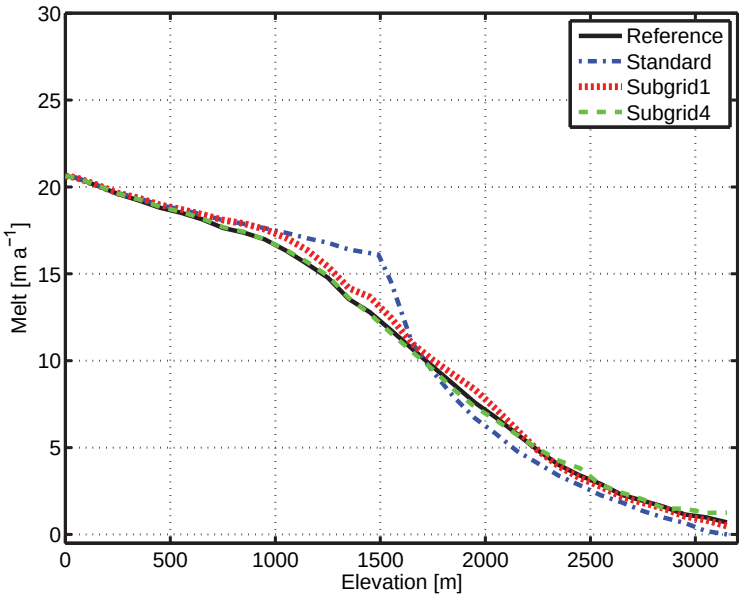

(b) Effect of parameterisation on modelled potential melt

Figure 4.8: Mean melt against elevation for the eTIM across 4 different resolutions (100, 1,5 and 10km) (a). Melt function becomes nonlinear above a threshold at approximately 1500m at the reference resolution of 100m. For areas above this threshold, temperatures are below 0 °C and melt becomes zero for increasing time spans during the year, and mean melt per elevation increases with decreasing resolution. While the baseline approach overestimates melt for elevations around 1500m and underestimates melt for elevations above 1700m at 10km resolution, the subgrid parameterisation approaches 1 and 4 show modelled melt rates close to the reference (b).

Chapter 5

Discussion

This chapter is intended to summarise and link the discussions of the research articles included in the appendix. The aim is to comprehensively discuss the research questions raised in the introduction, which are

1. To identify sources of uncertainty in topographic representation
2. To quantify and model these uncertainties
3. To assess the impact of these uncertainties on topography based models, in this case a geomorphological model (form) and a melt model as well as a full scale ice sheet model (process)
4. To understand the mechanisms through which topographic uncertainty influences these models
5. To assess ways of quantifying and communicating the impact of uncertainty on models and
6. To analyse ways of minimising this impact of uncertainty on the tested models

5.1 Assessing and Quantifying Uncertainty

5.1.1 Assessing DEM Uncertainty from Metadata

Where the uncertainty associated with the accuracy of a DEM needs to be assessed, one would assume that information given in the metadata would allow modelling of this uncertainty in a way suitable for studying the impact on related models using the DEM. In reality, researchers are faced with the problem that for common DEMs almost always the only information given is an RMSE, and arbitrary assumptions must be made about the statistical and spatial distribution (Raaflaub and Collins, 2006). During

a first set of experiments, uncertainty from DEM accuracy was simulated using normally distributed random white noise with a standard deviation deduced from GLOBE metadata RMSE (Hastings and Dunbar, 1998). DEMs resulting from the convolution of these uncertainty surfaces with the original DEMs showed frequent extreme outliers and had a very rough and noisy appearance for higher amounts of uncertainty (RMSE above 18m), and did not produce realistic topographic surfaces - even though the term 'realistic' for low resolution DEMs is likely to be biased by the expectation of what a DEM should look like from experience, which does not necessarily mean it is more correct or suitable for use.

However the noisiness of the resulting surfaces can be seen as a clear indication that DEM uncertainty of this amount is usually spatially correlated and needs to be modelled accordingly. Nevertheless the problem remains that no information on the distribution is given with the metadata, and this deficiency could only be compensated by using higher accuracy reference data or empirical data. Indeed, if a sufficiently large amount of studies on the properties of DEM error surfaces existed and were accessible, the uncertainty distribution properties might be derived using key information such as RMSE, terrain type or source data. However, such data is not readily available, and any survey of this kind would have been clearly beyond the scope of this dissertation.

Alternatively, assessing the properties of the spatial correlation of a DEM and applying it to the associated uncertainty is another option (e.g. Wechsler and Kroll, 2006). These approaches build on the assumption that the autocorrelation of topographic parameters such as elevation and slope is closely related to that of the DEM error (e.g. Oksanen and Sarjakoski, 2005b; Holmes et al., 2000; Hunter and Goodchild, 1997). Applying measures such as the range of spatial autocorrelation extracted from a DEM to uncorrelated random error is assuming this to be a more sensible approach than using arbitrarily chosen ranges (Raaflaub and Collins, 2006).

While a number of studies as well as own findings have confirmed DEM uncertainty to be closely related to topographic parameters such as elevation or terrain roughness, the amount of random, correlated and systematic error an uncertainty surface consists of depends on a number of potential factors such as data source, measuring sensors, preprocessing etc. Hence, if no information on the sources of data uncertainty are available, relating for example the variogram of a DEM to that of the associated error or uncertainty might be seen to be just as arbitrary, even if empirical data on the dependencies of DEM properties and associated uncertainty existed. Clearly, assessing uncertainty solely from metadata accuracy information given as RMSE is unsatisfac-

tory and barely allows for a rough estimation of the influence of DEM uncertainty on topographic models due to the unknown distribution properties.

5.1.2 Assessing Uncertainty from Resampling

Another important aspect of uncertainty from topographic representation in low resolution modelling is the effect the involved DEM resampling has. Trying to assess the different aspects of resampling, factors such as the resampling origin, the target resolution and the used algorithms were varied for resampling SRTM data to resolutions of 5 and 10km. The variation in the resulting DEMs allowed a correlation with elevation, which was implemented in an uncertainty model, and thus implicitly included information on the spatial distribution of uncertainty by linking it with elevation.

Users of standard tools like ArcGIS are often not aware of the potential variation in resampling of DEMs. and thus the implicitly introduced uncertainty, which is associated with arbitrary selection of resampling parameters, such as the resampling method, support, and the origins and cellsizes of source and target grids. Recording the variation of the original high resolution elevation values within each low resolution cell (Fig. 3.1) well depicts the amount of abstraction inherent in any (resampled) DEM, and conveys the uncertainty associated with the use of this kind of data. This method to assess uncertainty associated with DEM resampling was well suited for estimation of the amount of uncertainty, its dependency with elevation and its implicit spatial distribution, and allowed efficient modelling of DEM uncertainty surfaces. However, an explicit exploration of the spatial properties of this effect might allow an integration into spatial modelling of uncertainty such as Kriging.

5.1.3 Assessing DEM Uncertainty using Reference Data

In order to examine the influence of DEM data uncertainty on both geomorphological as well as ice sheet modelling, the limitations of modelling uncertainty on the basis of a global RMSE value had to be overcome. A direct assessment of error allows the capturing and reproduction of spatial dependencies and autocorrelation, which in turn supports the simulation of ‘realistic’ uncertainty surfaces. Analysing the impact of these realistic surfaces is required for a profound understanding of the influence topography and associated uncertainty have on terrain-based form and process modelling. Existing data of higher accuracy had to be used in order to assess DEM error properties, as taking reference field measurements was beyond the scope of this dissertation.

Deriving an uncertainty model for GLOBE DEM error was motivated by the fact that GLOBE data has a number of known flaws and inaccuracies, but despite this is still widely used for example in the cryosciences, as SRTM is only available up to 60° N. For modelling of the Fennoscandian or Laurentide ice sheet during the LGM, and for large scale modelling of Arctic permafrost for example, SRTM data cannot be used. Additionally, because SRTM data is relatively new, a substantial amount of existing experiments has been carried out using GLOBE data, and therefore is subject to the uncertainties associated with it. The derived GLOBE uncertainty model thus also allows assessment of other model results in retrospect.

Therefore, our aim was to assess uncertainty information in order to produce a robust uncertainty model for GLOBE based on readily available information. This uncertainty model was to be used to model the impact of DEM uncertainty on ISM of the Fennoscandian ice sheet through the Last Glacial Maximum. Because SRTM data is available for a large proportion of the GLOBE data coverage, and is compiled from homogenous sources and of significantly higher accuracy, we chose to use SRTM as a ground truth for assessing GLOBE DEM error. However care has to be taken as GLOBE source data differs for different regions (see Fig. 2.2 and U.S. Geological Survey, 1996), and the GLOBE uncertainty model developed here has been derived for DTED-based GLOBE DEM data. Preliminary tests using mixed DTED/DCW GLOBE DEM data showed different correlation coefficients and regression parameters. While this approach is probably valid for other source data, correlation of error with terrain characteristics for different source data is likely to require reanalysis.

Another option to test the developed uncertainty model would be to assess SRTM error properties using LIDAR or other data such as National Mapping Agency DEMs (e.g. Guth, 2006; Hofton et al., 2006; Carabajal and Harding, 2005), but higher resolution reference data spanning national borders is likely to be from different sources and thus heterogeneous, require substantial preprocessing and large amounts of storage and processing capacities. However, GLOBE DEM data at 1km resolution still supports sensible geomorphological modelling at regional or global scale for some processes, while SRTM at 100m resolution is of considerably higher accuracy, and thus suitable to be used as ground truth. Both datasets can be handled with moderately high demands on computation and storage capacities. The downside of using GLOBE data is that it is outdated by SRTM for large areas, and is known to be of very heterogeneous character, as it has been compiled from a wide range of source data, which is likely to have a negative effect on the quality of the derived regression model.

In principle, SRTM has already been used as ground truth for lower resolution DEMs in previous studies, for example by Hastings and Dunbar (1999) to assess GTOPO30 accuracy and by Jarvis et al. (2004) for comparison with GLOBE DEMs and local cartographic data. SRTM is however not deemed error-free, and the differences in data capture for SRTM and GLOBE are likely to results in potential systematic error of varying magnitude for the different types of GLOBE source data. This is a likely explanation of the systematic error of 3-4 m (Tab. 4.1) encountered in the error surfaces for the three test areas of the Alps, the Pyrenees and Turkey. Because reported/documented accuracy of SRTM is one order of magnitude higher than that of GLOBE, for our purpose we assumed SRTM to be suitable to use as ground truth and derive GLOBE error.

Deriving GLOBE error in this way for different regions resulted in a number of findings. First of all, besides the systematic error encoutered, the standard deviation of error was in the range of 70 to 80m, four to five times higher than the respective reported RMSE of 16m for GLOBE DEM based on DTED data (Hastings and Dunbar, 1998). However, care has to be taken as the analysis showed a systematic shift of GLOBE and SRTM data for different subregions, which, had it been eliminated before the analysis, might have reduced overall error. Additionally, all three selected test areas covered large proportions of mountainous terrain, and error was found to be much higher for rougher topographies. Error properties of less mountainous terrain in Southern Germany exhibited smaller standard deviations of 20-30m on average, which however is still up to twice that reported in the GLOBE documentation. Additionally, analysis of the derived error surface showed a clear spatial correlation of derived error with major topographic features of the DEM, which become obvious upon visual inspection. Correlation coefficients of different topographic attributes such as elevation, slope and aspect ranged from approximately 0.5 to 0.7, resulting in only medium r^2 values of the regression equations around 0.45. Despite this, especially the strong patterns of over- and underestimation of GLOBE elevations in respect to resampled SRTM on opposing sides of major ridges and valleys, visible in the derived error surfaces, suggested a stronger correlation of error and sign of error with aspect. A number of possible explanations for this phenomenon exist. First of all, our assumption of error-free SRTM might not hold, as semivariogram analysis of the error surfaces revealed directional effects for all three training areas (Alps, Turkey, Pyrenees), which might be caused by the SRTM shuttle flight path (Eineder et al., 2001). In contrast Guth (2006) reports diamond shaped patterns in SRTM data when comparing with the US National Elevation Dataset (NED) as a result of the flight path.

A more likely reason lies in the different methods of compiling GLOBE data applied within our test area. Since data from different sources and different algorithms have been used to compile GLOBE, some grid cells of GLOBE resemble median values of GTOPO data, while others have been compiled using spot sampling in the South-Western corner. In tests, systematically shifting data for different subregions lowered the overall deviation of GLOBE from SRTM, and increased correlation of error with topographic attributes. However, this shift is not constant for the different subregions, and an elimination of this systematic component in GLOBE DEM data was not within the scope of this dissertation. This systematic shift for different regions of the tested DEMs however resulted in directional effects and correlation of error with aspect, albeit that this correlation appears to be inhomogeneous and thus results in only medium correlation rates for global analysis.

Regression analysis for the three test areas however showed very similar results, supporting the hypothesis that a global dependency of GLOBE error on topographic characteristics can be deduced.

5.2 Modelling Uncertainty

5.2.1 Uncorrelated Noise

When trying to model DEM uncertainty, using a random normal distribution suggests itself where RMSE is the sole information about the amount and distribution of the values to be modelled, and this approach has been used by a number of authors (e.g. Wechsler, 2006; Fisher, 1998). Applying uncertainty simulated as spatially uncorrelated white noise to a DEM is viable when the assumption is that no trends, correlated components or systematic error are abundant. For DEMs, this component would be likely to stem from variations and flaws in the measurement process and is probably small compared to the contribution of other sources to the overall error. This approach of using uncorrelated noise works well for small amounts of uncertainty (small standard deviations of the normal distribution). However if the modelled uncertainty is large in relation to the cell to cell elevation differences of the underlying DEM, it results in very noisy, unrealistically and hydrologically incorrect topographies (compare Wechsler and Kroll, 2006), which in our case resulted in instabilities of the applied ice sheet model and crashes for uncertainties with standard deviations larger than 100m (compare section 5.1).
This confirms the fact that large DEM uncertainty, as given by RMSE of the size of

300m (e.g. GLOBE data for Antarctica and South America Hastings and Dunbar, 1998), consists of significant amounts of correlated and systematic error.

5.2.2 Random Cell Swapping

In our approach introducing spatial correlation to random noise surfaces (section 5.1.1) using random cell swapping (Fisher, 1998) we found that surfaces with global Moran's I values of 0.5 and above still showed a number of distinct outliers in the form of spikes and pits. While the overall appearance of the created error surfaces showed medium to longwave correlation, the surfaces still featured a noticeable amount of noise that propagated to the resulting DEM. While this is in general accordance with the assumption that uncertainty of DEMs consists of both correlated and uncorrelated components of potentially different wavelengths (Fisher and Tate, 2006), the derived topographies still resulted in occasional ice sheet model crashes, and the uncertainty was visually noticeable in the final DEMs. Using the random cell swapping approach, it was not possible to create smoother surfaces of higher spatial autocorrelation in sufficient numbers, because of the large data sets and the resulting high computational demands (compare Ehlschlaeger, 2002). The approach of random cell swapping might be made more effective by applying more advanced algorithms such as simulated annealing (Deutsch and Cockerham, 1994), or by combining it with filtering using spatial moving averages (Journel, 1996). The central problem of trying to model uncertainty based on simple RMSE figures remains given that no information on terrain dependencies or spatial autocorrelation is available.

5.2.3 Random Point Interpolation using IDW

In a next step we examined the uncertainty introduced to topography through resampling. The standard deviation of elevation values resampled using different origins showed a distinct dependency with elevation. In our approach to model this uncertainty we therefore used this formalised dependency to calculate standard deviations of normal distributions for random points on a DEM. An uncertainty value was then randomly drawn from this normal distribution at each location, and a surface was interpolated using IDW. This approach included two stochastic components – random selection of points on a DEM and the randomised sampling of the uncertainty value at each point from a normal distribution – which makes this method fit for use in MCS. The approach also included spatially correlated components, namely the dependency of the amount of uncertainty on elevation, and the spatial correlation introduced

through IDW interpolation. However, the amount and range of spatial autocorrelation in the created surfaces is based on the amount and density of the random points on the DEM, as well as the IDW weighting parameters, both of which could not be (were not) deduced from the analysis of the moving origin resampling results, and were therefore chosen somewhat arbitrarily. Additionally, the distribution of uncertainty at each location is again assumed to be normal, which might not be correct.

The surfaces created using IDW were smooth with no shortwave noise, as the wavelength of variation is determined via the minimum distance used in creating the random points. Adding these uncertainty surfaces to the DEM resulted in 'undisturbed' topographies – although this might not be a realistic assumption, it enabled us to run the GLIMMER ISM on these topographies without instabilities, and produce a sufficient large number of realisations for MCS because of the efficient computation. The approach could possibly be refined by adding an uncorrelated noise component to the surfaces, and by controlling the amount of spatial autocorrelation using empirical boundaries. In general, approaches based on geostatistics such as Kriging or stochastic imaging are much more common for the creation of continuous, correlated surfaces from point data for uncertainty or error modelling. However, since in our case no detailed information about the spatial distribution of uncertainty was available, these approaches would also be based on simple assumptions, at the cost of much higher computational demands, more complex usage and higher efforts for implementation.

The methods described in the three previous sections allow to create uncorrelated as well as correlated uncertainty surfaces of normal and near normal distribution (Hebeler and Purves, 2004). Correlation of DEM uncertainty with topographic characteristics of the DEM were implicitly introduced in the approach to model uncertainty from resampling, by using the relation of resampling variability and elevation to derive probability distributions for the magnitude of uncertainty. Nevertheless, spatial characteristics of the uncertainty distribution such as range and noise are still based on assumptions and depend on the parameters used in IDW, as well as the number and density of random points used in the method.

5.2.4 GLOBE DEM Uncertainty Model using Regression

In the approach to model GLOBE DEM uncertainty (Hebeler and Purves, in press, 2008a), regression analysis of DEM error derived using SRTM with topographic variables was conducted. During these analyses, the separation of magnitude and sign of uncertainty using simple linear and binary logistic regression, respectively, improved results over combined modelling of the two components. The regression part of the

model could possibly be further improved: using non-linear regression resulted in only marginal improvements with significantly higher computation times, but accounting for the observed systematic shift of GLOBE data relative to SRTM data is likely to improve regression results. Preliminary tests using an artificial neural network (ANN) approach showed r^2 of up to 0.7 in cross validation of simulated uncertainty surfaces and derived GLOBE error, while giving comparable semivariogram results.

At this point, the convolution filtering applied in our uncertainty model serves two purposes. Firstly, it ascertains a autocorrelation range in the uncertainty surfaces comparable to those of the error surfaces. Secondly, the filter eliminates excess amount of noise and outliers that could otherwise cause instabilities in the models applying the resulting DEMs. The applied filter is omnidirectional despite the directional trends that are observable in the error surfaces. However, the observed semivariogram ranges are small, likely due to the inhomogeneity of the error. Large areas of the DEM exhibit small scale error that gradually changes and contrasts with abrupt changes in error sign associated with the high error values in the high mountain areas. Thus directional filtering, or filtering using variable ranges that use information on a possible dependency of correlation range with terrain could further improve the uncertainty model. Alternatively, geostatistical methods with localised variograms might be another option (Kyriakidis, 2001). However, these more complex approaches require a distinct amount of knowledge and expertise, and are only likely to improve results when adequately adapted to the respective data. For large datasets of continental extent and for repeated application they might not be applicable, at least not by the general user.

It is important to note that the described GLOBE DEM uncertainty model does not calculate mean uncertainty values of zero for every grid cell when averaging over a large number of runs. This is due to the terrain dependency of uncertainty, where some cells feature topographic attributes that are more likely to result in an overall positive or negative amount of uncertainty. This can be explained by the systematic error component that is captured by the model. While normally any systematic error should be eliminated from the data where possible, for GLOBE DEM data this is not the case. Using the uncertainty model presented here, it is not possible to entirely eliminate systematic error, as the correlation rates are determined globally and are thus too low – furthermore it is not the intention of this model to correct or improve GLOBE DEM data. However, the total amount of simulated uncertainty for a larger DEM, averaged over a sufficiently large number of runs sums to zero, demonstrating that no systematic general bias is introduced. Moreover, the developed uncertainty model allows for the simulation of GLOBE DEM uncertainty suitable for MCS which can be produced

purely from a single (GLOBE) DEM, without the need for higher accuracy reference data. The model can therefore be used to analyse the impact of DEM quality on ISM results on Fennoscandia.

5.3 The Impact of Uncertainty

The most striking result of the first set of experiments is the influence of spatial correlation in modelled uncertainty on ISM results (Hebeler and Purves, 2004). While uncertainty introduced to the DEM as uncorrelated white noise with a mean of 0 and standard deviation of 30m resulted in a mean standard deviation of modelled ice extent between 1-2% (after 20-50k model years), correlated uncertainty of slightly lower standard deviation (25m on average, produced using IDW) resulted in standard deviations of ice extent around 5% (Fig. 4.4). Because of the use of IDW, the statistical distributions of the uncorrelated and correlated uncertainty surfaces are not identical, but the absolute amount of introduced uncertainty, as well as mean and standard deviations of the two distributions are comparable. However, interpolation using IDW resulted in higher kurtosis of the correlated uncertainty surfaces, while at the same time lowering the average standard deviation. Nevertheless the results suggest that the form of uncertainty, respectively its ability to influence/change existing landforms and their configuration is more important than the mere amount of uncertainty. This emphasises the fact that a sole accuracy figure such as RMSE is not suitable for estimating impact of uncertainty on a model.

Apart from the amount and spatial correlation of uncertainty, its impact in modelling clearly depends on the terrain characteristics as well as the influence of topography within the target model. This is also evident from the results of the geomorphological modelling experiment. Introducing GLOBE DEM uncertainty at 1km resolution had little effect on the derivation of global topographic attributes used to characterise a landscape. While the uncertainty locally influenced the calculation of slope and other attributes, key descriptive attributes for the global topography such as average stream length or mean watershed slope were not affected, because uncertainty effects apparently canceled themselves out over large areas. However, when delineating watershed boundaries, the effect of uncertainty on terrain became apparent. Because locally, correlated uncertainty can influence flow directions and elevate or lower small ridges and channels, small elevation changes can result in the rerouting of waterflow and thus an increase or decrease of derived watershed boundaries, as well as variation in the total number of delineated watersheds (Hebeler and Purves, in press).

Analysis of the different experiments investigating the **influence of topographic uncertainty on ice sheet models** (ISM) have found a number of factors besides the absolute amount of uncertainty and its spatial correlation to control the impact on ISM results:

- **Size of ice sheet** – as ice sheets grow, they superimpose the underlying bedrock topography and the ice surface becomes the relevant topography. Thus the impact of DEM uncertainty decreases with increasing relative ice sheet size. This effect was repeatedly shown in all experiments conducted for Fennoscandia. However, experiments carried out for Patagonia revealed different effects: while for small amounts of introduced uncertainties the overall size of the ice sheet hardly affected the standard deviation of modelled ice extent and volume in MCS, for larger modelled uncertainties the variation in ice extent and volume across MCS runs actually increased with increasing ice sheet sizes (Hebeler and Purves, 2005a). This effect is closely linked to the characteristics of the topography.
- **Characteristics of the topography** – the Fennoscandian topography is essentially dominated by the higher elevation of the southwest-northeast facing mountain ridge across Norway and Sweden, which provides a number of potential inception points for the ice sheet. The expansion of ice is limited by calving into the Atlantic in the west, and thus ice predominantly flows down the relatively gentle slopes to the east. DEM uncertainty primarily affects ice sheet configurations via inception and during the initial phase. Once a coalescent ice sheet has formed covering the Scandinavian ridge, topographic uncertainties that modify the form of ridges and valleys only have minor impact on the speed of the eastward ice extension. Patagonian topography, however, is dominated by the parallel running Andean ridges, and feature a large number of mountain tops that can act as potential inception points. Even at later stages of the ice sheet modelling, changes in the configuration of these Andean ridges and valleys through modelled uncertainty apparently have significant influence on the flow direction and thus the configuration of the ice sheet. Introducing increasing amounts of uncertainty therefore (to a threshold) has increased impact on modelled ice sheet configurations.
- **Configuration and phase of the ice sheet** – this point again is closely related to the topography; if the general form of underlying topography dominates the principal flow direction of the ice sheet such as in Fennoscandia, the impact of topographic uncertainty is less pronounced than for configurations where small changes in topography can alter the general flow direction or speed of a region in the ice sheet. In addition to that general configuration, the phase of the modelled ice sheet is also

important. Topographic uncertainty was found to have the largest impact during inception, where small changes in absolute elevation might or might not raise a mountain above the ELA, and thus support or prevent the formation of an ice cap. While with expanding ice sheets the influence of uncertainty wanes, during phases of ice retreat, even for larger ice sheets, the impact of topographic uncertainty increases.

- **Climate** – the climate, and above all temperature and thus the location of the ELA has a central impact on the effects of DEM uncertainty (Hebeler et al., in press). In a climate where all areas constantly experience temperatures below zero °C, elevation uncertainty has no impact on inception or ablation, and only influences the ice sheet configuration through changes in local slope and thus flow velocities. Equally, very warm climates acting on a single peak topography, where uncertainty is unlikely to create new inception points or prevent existing ones will show little response to DEM uncertainty.

In DEM uncertainty experiments using realistic climate scenarios on ISMs, the introduction of uncertainty results in a relatively low variation in the range of 2-5% of modelled ice extent of fully grown ice sheets on average. However, the absolute variation range covered by the minimum and maximum ice extent runs shows divergence of up to 25% (Hebeler et al., in press; Hebeler and Purves, 2008a, 2004), with significant differences in modelled ice sheet configurations.

Comparing these results with the impact from parametric uncertainty analysis allows one to relate the impact of DEM uncertainty to that of other internal and external ISM parameters. While the parametric uncertainty analysis (PUA) confirms the dominant impact of climate on modelled ice sheet configurations, it also shows DEM uncertainty to have equally distinct impact on model results as the tested ISM parameters. For the standard setup using a 12 °C temperature lowering compared to recent climate, the modelled DEM uncertainty resulted in variation of modelled ice sheet extent equal to that of a global 1 °C variation in temperature. Additionally, DEM uncertainty had similar or larger impacts on model results as a number of tested model parameters such as geothermal heat flux, flow enhancement factor or the refreezing fraction. For the setup using a warmer climate with only 10 °C temperature lowering and thus smaller overall ice sheets, DEM uncertainty was revealed to have a major influence, through triggering a bifurcation of modelled ice extent and volume: about 20% of the modelled ice sheets show a mean extent more than 15% larger than the rest of the runs, with a clear separation between the two maxima (Fig. 4.6A). This bifurcation effect is not observable for colder climates, underlining the dependency of

DEM uncertainty impact on climate, topography and ice sheet size. A closer examination of the model runs suggests this bifurcation is caused by the conflation of two smaller icecaps in the southwest. This conflation occurs where modelled uncertainty alters the local topography so it supports ice mass coalescence - either by lowering the elevation of obstructing ridges or by increasing the elevation of associated peaks - both of which can drive an increase in mass balance. The coalesced southern ice sheet can then expand further towards the east and west due to the further increase in accumulation enabled by the presence of a high elevation ice mass. The described effect is essentially due to the positive elevation-mass balance feedback (Paterson, 1994).

As ablation is known to be poorly represented in ISM, and resampling is an important source of topographic uncertainty in low resolution modelling, we investigated scale effects in melt modelling in order to better understand the dependencies of melt calculation, topography and scale, and consequently be able to develop improved approaches for modelling melt in an ISM. Since resampling in general lowers the average elevation of a DEM through averaging, one would expect an increase in calculated potential melt due to the lower elevations and the resulting higher temperatures. In contrast, the opposite is the case, and melt calculated at lower resolutions is found to significantly underestimate reference melt derived using higher resolutions - as much as 20% for high elevations above 2500m at 10km resolutions (Hebeler and Purves, 2008b). This effect is caused by the fact that the spatial variation of topography at high resolution is lost during resampling, and because melt is a nonlinear function of elevation in the tested cases of the temperature index model (TIM) and the enhanced temperature index model (eTIM), the mean melt for the topography within each low resolution cell is poorly estimated using just one resampled elevation value. For the simple TIM, where melt is a function of elevation, this could be easily compensated by adapting the melt function to calculate higher melt rates overall. However, this would potentially result in loss of melt-free areas, which are important for inception (Sugden et al., 2002). Applying a simple subgrid modelling approach (Marshall and Clarke, 1999) using three instead of one elevation values was found to considerably improve performance of the TIM, while offering the possibility of using the highest elevation subgrid cells for modelling of inception.

Because the eTIM models potential melt not as a simple function of elevation, but also takes into account gradient slope and aspect, scaling effects are more differentiated. While the simple elevation subgrid approach performs surprisingly well, it lacks a physically sound base, and tends to overestimate melt for lower areas. A subgrid parameterisation using elevation and average slope per cardinal direction on average

showed good performance, but was not scalable across all resolutions. Results varied for different resolutions and performance was poor for the 1km resolution, while the approach compared best for 5 and 10km resolutions. This is most likely caused by the fact that at 1km, the average slope length of the topography, which is crucial for melt calculation using the eTIM, is still captured well (Martin and Church, 2004). Hence little deviation in calculated potential melt compared to 100m resolution occur, while the averaging effect for 5km resolutions and above reflect on the calculated melt results at these resolutions. In general, the use of subgrids in modelling significantly improves calculated potential melt rates, and allows improved modelling of inception processes even at low elevations.

5.3.1 Minimising Uncertainty

In our experiments using subgrid melt modelling, we managed to reduce the impact of resampling DEMs to low resolutions on melt model results by applying subgrid parameterisation. By doing so, we reduced the impact of one of the main sources of topographic uncertainty on low resolution modelling. It is however important to note that the impact of DEM uncertainty on the subgrid modelling approach is slightly larger than that of the reference and baseline approaches, when comparing the relative standard deviation of calculated potential melt across 100 MCS runs. Because the subgrid parameterisation uses three elevation subgrids, each of the subgrids is subject to the introduced uncertainty and subsequently all three calculated melt values are biased. While for the reference approach, the uncertainty over a larger area is mostly cancelling itself out and thus only the net disturbance affects melt calculation, which results in melt deviations similar to that of the baseline approach. However considering the underestimation of the baseline approach, its lower absolute standard deviation results in the highest relative deviation. Additionally, the overall deviation across MCS runs for the baseline approach is lower, because potential melt is underestimated or even zero for elevations where both reference and subgrid approaches still calculate melt above zero. So, while overall the increase of absolute variation for the subgrid approach is small and is outweighed by the gain in performance, it is important to be aware of this effect, and consider it when developing parameterisations.

5.4 Quantifying and Communicating Uncertainty Impact

Where neither uncertainty nor its impact can be minimised, it is essential that it is communicated well. While especially topographic uncertainty should receive broader attention as a source of uncertainty, DEM uncertainty in general needs to be better communicated. Many authors have already stressed the importance of better communication of error and uncertainty in DEMs (e.g. Fisher and Tate, 2006; Kyriakidis and Goodchild, 2006; Wechsler, 2003; Carlisle, 2000; Shortridge and Goodchild, 1999; Ehlschlaeger and Goodchild, 1994). Compiling the needs and approaches to improving the generation and communication of uncertainty formalised by these authors can be concentrated into a scheme depicting the processes and data products involved (Fig. 5.1). The experiments carried out within the course of this dissertation confirmed that simple accuracy figures such as RMSE are inadequate for modelling uncertainty and analysing its impact on topographic process or form models. The distribution of explicit uncertainty models with DEMs would allow for sensitivity testing, but assessing the susceptibility of a model to topographic uncertainty appears to be inescapable, as our experiments confirmed that the impact of DEM uncertainty is not only depending on the amount and spatial correlation of uncertainty, but also on the form and configuration of the topography, as well as on the methods and algorithms applied on this topography within each model.

If the amount, form and dependencies of uncertainty, as well as its impact on model results are known and properly communicated, it ceases to be a problem. Uncertainty modelling can be a powerful tool in modelling and decision making, when assessing probabilities and reliability of a prognosis for example. Intentions, potentials and limitations of complex modelling and the consequent results could be communicated better; for example frequent discussions about how well model results fit empirical bounds (e.g. Hulton et al., 2002; Wenzens, 2003; Hulton et al., 2003) could probably be avoided.

At this point however, many users and researchers apparently associate the term ‘uncertainty’ with negative notions of fault, errors and inferior research results. While new and more effective ways of communicating and visualising uncertainty might be necessary (Oehler, 2005), these developments need to go hand in hand with a recognition that uncertainty in modelling is intrinsic and inevitable, and needs to be properly addressed in order to take advantage of it.

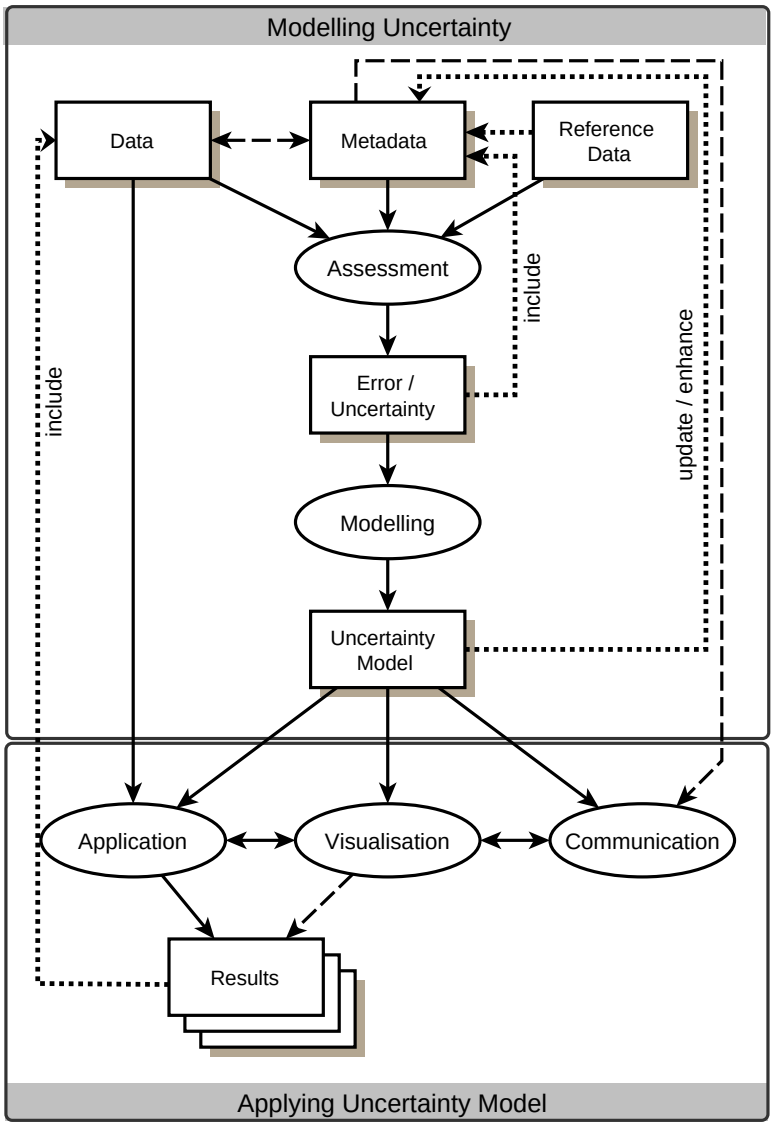

Figure 5.1: Processes, data and interdependencies in uncertainty assessment, modelling and application. Devillers et al. (2005) suggest a dynamic or proactive linkage of metadata and data. Once an uncertainty model has been developed for a certain dataset, it should be distributed as metadata, which will allow subsequent communication of the uncertainty (model) of the data without the need for assessment and model development.

Chapter 6

Conclusions and Outlook

6.1 Conclusions

Applications that employ digital elevation models encompass tasks that range from visualisation of continuous surfaces derived from elevation values, to modelling of physical processes which act upon or even alter these values. All of these applications are subject to a range of uncertainties, which can originate from the capture of elevation values, through processing of the data, to the representation of values within models. Uncertainty resulting from data accuracy is a concept that most users of spatial data are familiar with and aware of: the (unknown) accuracy and precision of a sensor and possible flaws or external influences can lead to deviations of the measurement from its actual value, termed error. Uncertainty is a result of data known to contain error, but the amount and/or spatial distribution of this error is unknown. Pre-processing of a DEM, for example the projection or interpolation of the data, can add additional uncertainty to the use of this DEM data. However, this uncertainty can be estimated, e.g. using reference point measurements. Additionally, DEMs are commonly distributed with accuracy figures such as RMSE.

Elevation values used in topographic models are usually supplied as single point values, distributed on a regular grid, (with the exception of TINs or contour lines). Therefore, any application that employs these single point values to represent topography, must implicitly or explicitly model surfaces.

Essentially, elevation values at locations where no measurements exist are approximated through interpolation, and the resulting topographic surfaces are dependent on the applied interpolation method, algorithm and parameters. These approximations are thus subject to uncertainty. Similarly, further processing, such as resampling to lower resolutions, again depends on parameters such as the source and target resolution, the

resampling algorithm, terrain characteristics, etc. Compared to uncertainty from DEM accuracy, this 'uncertainty of topographic representation' is a more abstract concept. It is often not understood by users of spatial data and rarely accounted for. Hardly any study using a DEM gives details such as the exact extent, coordinates of DEM origin, whether the map origin is given at the center of a cell or the boundary, which interpolation method has been applied including all parameters, the used software and version, etc. to an extent where no ambiguity remains.

Within this dissertation, the amount of uncertainty introduced to digital elevation models (DEM) through resampling to lower resolutions using different resampling origins and algorithms has been assessed. With mean standard deviations of 150m and more, these uncertainties were shown to be of comparable to or above those from accuracy figures of common DEMs such as SRTM, GLOBE or GTOPO30.

Assessing the error of GLOBE DEM data for three test areas using SRTM as a reference has shown the standard deviation of error to range between 70 and 80m. This is well in excess of the RMSE of 16m given for these areas (Hastings and Dunbar, 1999). Analyses also revealed these error surfaces to have non-normal distributions and strong dependencies with terrain characteristics such as elevation and roughness. Additionally, systematic shifts for different areas of GLOBE DEM data relative to SRTM were abundant. These findings confirm the limited use of simple global accuracy figures such as RMSE for DEM data. This fact is corroborated by the much larger impact of uncertainty modelled using correlated random error compared to that of uncorrelated white noise on ice sheet models. These results show the strong impact of the choice of a spatial correlation model for modelled DEM uncertainty.

Uncertainties from these various sources have been modelled in order to analyse their impact on ISM results. They were shown to result in noticeable variation in ice sheet sizes and configuration. Analysing the impact mechanisms of topographic uncertainty on ISM results, it was found that the amount of variation in model results is not only dependent on the amount and spatial distribution of uncertainty, but also by the importance of topography in the model under observation. For process models such as ISM, the impact of uncertainty was shown to vary over time: during phases of inception and ice retreat, uncertainty in topography had considerable influences on modelled ice sheet configurations, while the impact decreased with growing ice masses.

Analysing the impact of topographic uncertainty on ISM results, terrain type and configuration was shown to have a substantial influence. While for Fennoscandia, the relative impact of modelled uncertainty decreased with increasing ice sheet sizes, it remained constant and even increased with increasing ice sheets for Patagonia. This

effect is likely to be associated with the rugged terrain, and the stronger impact of modelled uncertainty on terrain configuration, e.g. rerouting of valleys, enlarging or decreasing of ridges and other features that control ice flow. For the relatively simple topography of Fennoscandia, major changes of topographic characteristics through modelled uncertainty are less likely. However, where climate results in smaller ice sheets, and thus the importance of topography is higher, modelled DEM uncertainty can result in a bifurcation of modelled ISM configurations, by controlling the coalescence of separate (smaller) ice sheets.

Sensitivity tests and parametric uncertainty analysis for the GLIMMER ISM using a steady-state climate comparable to that of the Last Glacial Maximum were conducted in order to compare the impact of DEM uncertainty. Findings showed that the influence of DEM uncertainty on modelled ice extent and volume ranges between 1 and 9% for different climate scenarios, and is comparable to that of model parameters such as the flow enhancement factor or basal traction. The variation of modelled ice extents are equivalent of a 1 °C climate change. Topographic uncertainty can thus have a significant influence on modelled ice sheets, and needs to be considered when ISM results are interpreted.

The impact of modelled uncertainty on topography-based models was also shown to depend on the type of information deduced from the perturbed topography. Global measures such as mean stream length, slope or the number of watersheds of an area varied little when subject to modelled DEM uncertainty. Local measures, such as the area or hypsometry of a specific delineated watershed on the contrary showed great variation.

Potential melt modelled across a range of scales using different models has been analysed. The loss of spatial information with decreasing resolutions was shown to cause systematic over- or underestimation of melt in different areas. For simple models such as the temperature index model (TIM), this effect has a near-linear scale dependency which could be accounted for once assessed. For more sophisticated approaches such as the TIM enhanced by a solar radiation component, the impact of this uncertainty is also complex and difficult to account for or compensate. Although the findings of this dissertation showed that resampling introduces uncertainty that can strongly influence results of low resolution modelling, it is rarely noticed or even accounted for in studies. The use of subgrids proved to minimise the effect of resampling on modelled potential melt, at little additional computational cost, and only slightly increases susceptibility to DEM uncertainty, at the gain of significantly improved modelled melt rates.

SRTM data has a higher resolution and accuracy than GLOBE, is compiled from a homogeneous data source and is freely available for large areas of the globe. Nevertheless, GLOBE is still the only global DEM for areas North of 60° N and South of 56° S. GLOBE therefore is the primary DEM basis for all medium to large scale cryospheric and related modelling, e.g. modelling of permafrost. In our experiments it was shown that differences in the GLOBE DEM production reflect on the DEM quality. As this systematic error appears to be traceable, it should be eliminated from the data if GLOBE is to be updated.

6.1.1 Key Findings

For each of the research questions forming this thesis, the key findings are summarised below:

1. What are the sources of uncertainty in/from topographic representation?
   - Sources of uncertainty in handling digital topographic data include data accuracy (DEM error), processing (such as resampling and projection) and the conceptual data model (e.g. resolution).
   - Topographic uncertainty originating from data processing and the conceptual model is potentially larger for large scale models than that from DEM accuracy.
2. How can topographic uncertainty be quantified and modelled?
   - Experiments have confirmed that topographic uncertainty (above a certain threshold) is likely to be spatially autocorrelated and dependent on topographic attributes such as elevation, slope and roughness.
   - GLOBE DEM error has been shown to be terrain dependent, and that these dependencies can be used to model uncertainty for GLOBE DEMs in areas where no reference data is available.
   - The statistical and spatial distribution of modelled uncertainty was shown to impact results of associated topography based models. Simple global accuracy measures given for DEM data such as RMSE lack information on spatial distribution of error and uncertainty – modelling uncertainty based on assumptions is therefore disputable and has to be applied with great care.
   - The developed uncertainty model for GLOBE DEM data, using SRTM as ground truth, works well in reproducing DEM uncertainty, and produces uncertainty surfaces suitable to be used within MCS simulations for areas where higher accuracy reference data is not available.

3. What impact does uncertainty from topographic representation have on topography-based modelling?

   - Uncertainty from DEM accuracy at 1 km propagates into model results at 10 and 20 km resolution (for the example of ice sheet modelling).
   - Topographic uncertainty has a larger impact on local/regional scale than on global scale terrain parameters in form models (e.g. topographic derivatives and indices)
   - The impact of modelled topographic uncertainty on a target model depends on the characteristics of the topography, the amount and spatial configuration of uncertainty and the relative importance of topography in the target model.

4. Where, when and how does uncertainty from topographic representation impact ice sheet modelling?

   - The impact of uncertainty in processes models such as ISM is context dependent (topography, boundary conditions) and can vary over time, e.g. the same amount of topographic uncertainty can have varying impact on results depending on the phase of the ISM:
   - in ISM the phases of inception and ice retreat are most susceptible to topographic uncertainty.
   - Topographic uncertainty has an impact on modelled ice extent and volumes comparable to that of internal model parameter. Additionally, a significant influence on spatial configurations of modelled ice sheets was observed.

5. How can the impact of uncertainty from topographic representation be quantified and communicated?

   - Parametric uncertainty analysis can be used for comparative impact analysis, and for testing uncertainty from multiple sources. PUA has been a suitable approach for assessing the uncertainty from model abstractions in ISM.
   - Frequency maps and probability function plots are suitable to convey uncertainty information.

6. How can the impact of uncertainty from topographic representation on ice sheet modelling be minimised?

   - The use of subgrid approaches can reduce the effects of scaling and the loss of spatial variation (uncertainty from processing and the data model), encountered in the downscaling of topography based models such as melt models. While the

uncertainty from resampling for these models is reduced, the use of subgrids showed an increased susceptibility to DEM uncertainty.

6.2 Outlook

Uncertainties associated with the use of digital elevation models (DEM) data can have significant impact on results of associated models. Both end-users and modellers have to be made aware of these uncertainties and their potential influence. It has also been shown that the spatial and statistical properties of modelled uncertainty influences results of associated topography based models. Thus uncertainty modelling based on simple global accuracy measures such as distributed with common DEMs, which is based on assumptions about the distribution of uncertainty, is inappropriate. This emphasises the demand for detailed information on DEM error to be distributed with the data formulated by a number of authors (e.g. Kyriakidis et al., 1999; Shortridge and Goodchild, 1999; Fisher, 1998; Ehlschlaeger and Goodchild, 1994). To achieve this, information on the amount and spatial distribution of uncertainty associated with a DEM have to be distributed together with the data. The distribution of an appropriate uncertainty model or of equiprobable surfaces with a dataset as proposed by Shortridge and Goodchild (1999) is one approach to foster the acceptance and application of uncertainty modelling. Even though uncertainty aware GIS are still not available, users and modellers are becoming more and more aware of the importance of uncertainty in spatial modelling, as shown by the increase of publications covering this topic over recent years.

The development of robust, easy to use uncertainty models that require less expertise than existing approaches of Kriging and stochastic simulations might be another option to propagate uncertainty awareness. The GLOBE uncertainty model developed within the course of this dissertation will continuously develop and improve as new applications emerge. One aim is to optimise regression of uncertainty and DEM attributes, for example by detrending the error surfaces prior to analysis, through the use of different terrain attributes with higher correlation coefficients, or by testing different approaches altogether. Preliminary experiments using an artificial neural network (ANN) approach to create uncertainty surfaces from GLOBE error for example showed significant improvement for the modelling of deterministic components. An improved way of selecting training areas to derive GLOBE error is also currently being researched.

Additionally, improved approaches to convey uncertainties in a simulation or model results need to be developed. Promising existing methods such as stochastic imaging need to be implemented in widespread GIS and made available to a wider public. These approaches need to include ways of documenting and communicating uncertainty in both DEMs and derived model results, e.g. by using visualisation techniques that are both simple to use and comprehend.

In the glaciological modelling domain, the importance of topographic uncertainty on modelled ice sheet configurations needs be realised and accounted for. Topographic uncertainty impacts both the fitting of ice sheet reconstructions to empirical boundaries, as well as the simulation of the behaviour of existing ice sheet to changing climates. Furthermore, parametric uncertainty analysis in ice sheet modelling was shown to be well suited to assess potential variation in modelling results, originating from uncertainty in the input data or from parameterisation. Using probability distribution functions for the analysed parameters allows to assign probabilities to model outcomes, and thus facilitates the communication of uncertainty in these results.

Where uncertainty and its impact on a model is understood, ways of minimising either the uncertainty itself or its impact can be sought. The possible application and integration of subscale modelling approaches for the calculation of mass balance within GLIMMER, for example using subgrid or quadtree approaches will intensely be researched, and funds for a follow-up project have been provided by the University of Zurich (Forschungskredit Nr 57060802, Project SuMo).

Appendices

Appendix A

Hebeler, F. & Purves, R.S. 2004: Representation of topography and its role in uncertainty: a case study in ice sheet modelling.
Proceedings of the GIScience 2004 conference, College Park, Maryland, Oct 19-24 2004, p.118-121

Representation of Topography and its Role in Uncertainty: A Case Study in Ice Sheet Modelling

Felix Hebeler and Ross S. Purves
Geographic Information Systems Division (GIS)
Department of Geography, University of Zurich (Irchel)
Winterthurerstr. 190
CH-8057 Zurich, Switzerland
{fhebeler, rsp}@geo.unizh.ch

As elevation and its derivatives are essential inputs for a wide range of process models, topography and its representation in environmental modelling is undoubtedly of key importance and as such has long been recognised in GIScience (e.g. Hutchinson & Gallant, 1999; 2000). Research areas include the variation in derived parameters with resolution, scale, and algorithms (Zhang *et al.*, 1999; Hutchinson & Gallant, 2000), appropriate models of terrain representation (Wood, 1998; Schneider, 2001), generalisation of topographic data (Weibel & Heller, 1991), and others. However, in the main this work has concentrated on so-called primary and composed topography indices (Beven & Moore, 1992), e.g. catchment areas (Hurtrez *et al.*, 1999) or feature extraction at variable scales (Fisher *et al.*, 2004). Sensitivity tests examining the influence of resolution are relatively common in process modelling, but generally do not explore issues of representation, with some notable exception (Tucker *et al.*, 2001).

In this paper the sensitivity of a large scale dynamic process model to topography and its representation is explored. Model intercomparisons are performed as a first step towards developing a set of experiments to explore the uncertainty introduced into a dynamic process model as a result of variations in representation of terrain. The topographies used as model inputs, the experiments chosen to identify the importance of terrain representation, and the model used are described as well as some initial results from these experiments.

A primary step in this work is to test model sensitivity to different aspects of terrain representation: resolution, DEM quality, generalisation and smoothing effects, and slope algorithms. As a case study, an ice sheet model (Boulton & Payne, 1992; Purves & Hulton, 2000) is run using a range of natural and artificial DEMs. Ice sheet modelling, in common with most numerical modelling, aims to improve our understanding of the real world through abstractions of reality. In this work we seek to investigate the importance of different abstractions of terrain properties on such models. In ice sheet modelling two key processes – nucleation (the initiation of an ice sheet through the forming of perennial ice) and ablation (the removal of mass from the ice sheet system, usually as melting or calving) – are highly susceptible to aspects of terrain representation. Ice sheet models (ISMs) therefore present an excellent example for sensitivity testing. Also, current ISMs run on resolutions of 5 to 20km, allowing the use of a range of possible higher resolution DEM data sets

for the testing of the influence of different methods of terrain generalisation effects.

Suitable elevation data is selected and DEMs from a total of three data sources are tested:

- DEM of Scandinavia created from GTOPO30 (USGS) and ETOPO2 (NGDC) data. This DEM has already been used together with a climate model (based on proxy records) for the simulation of the Fennoscandian ice sheet through the last glacial maximum by Hagdorn (2003)
- DEM generalized from high resolution data (SRTM90 data of Switzerland and southern South America)
- artificial topography of various resolution and amplitude

To test sensitivity of ISM to DEM quality, from each of the original DEM data sources, 150 topographies varying by error values derived from metadata are created to perform Monte Carlo Simulations. The ISM is run on every one of these topographies and ice volume and ice extent are compared between model runs at different timesteps.
To test the effect generalization of topography has on the model, different algorithms and methods are used to downscale the DEM sources to the resolution needed by the model (10 and 20km). As an example, the performance of simple linear interpolation is tested against more complex and demanding feature preserving methods, such as splining in conjunction with hydrological networks or generalising with surface networks (Hutchinson, 1993). Similarly, the impact of smoothing algorithms on DEMs is tested: numerical problems are often faced by models where slope is too steep in DEMs. These are countered by smoothing topography to prevent model crashes (Takeda *et al.*, 2002).
Finally, slope calculation plays a central role not only in ice sheet inception, but also in flow calculations. A number of papers have been written addressing the effects different algorithms have on the calculation of terrain derivatives (e.g. Jones, 1998; Schmidt *et al.* 2004). Furthermore, the effect of scaling on slope estimates is well known (Zhang *et al.*, 1999). In this paper, the effect of different slope calculation algorithms on the ISM will be tested by running the model using different algorithms (e.g. simple 'four nearest neighbours' method, Horn's method, Constrained Quadratic Surface Method, etc.). Alternatively, the residual errors determined for these methods in existing works like Jones (1998), can be calculated and applied to topographies the model is then run on.

Preliminary results show the nucleation process to be significantly affected by random errors of 30, 100, and 300 m standard deviation superimposed on Scandinavian topographies. For subsequent model timesteps, the standard deviations of modelled ice extent and volume over the set of model runs decrease, due to the smoothing effect the growing ice sheets have on the underlying topography. Because superimposing uncorrelated error fields on DEMs produces

noisy topographies, effects of sudden changes in altitude and slope on the ISM tend to lead to model instabilities. Thus, above a certain threshold (approx. 200 m STDV of error), these datasets are not well suited to simulate effects of generalisation or measuring errors. However, analysis of SRTM90 data, generalised to resolutions of 5 and 10km using bilinear interpolation, suggests the usage of error fields with standard deviations of more than 200m for the ISM simulations: the standard deviations of the high resolution (90m) grid cells contributing to one generalised, low resolution (5km) cell range from 100 to more than 500m for altitudes above 800m. Therefore, spatially correlated error fields, that prevent the introduction of extreme noise to the original topography, will be introduced for Monte Carlo Simulations using standard deviations of 100m and above.

Acknowledgements

This research is funded by the Swiss National Science Foundation (SNF Project Number 200021-100054). We are grateful for the ice sheet model and support provided by Dr. Nick Hulton, Dept. of Geography and Dr. Magnus Hagdorn, Grant Institute of the University of Edinburgh.

References

Beven K.J., Moore I.D. (Eds.), 1992: *Terrain Analysis and Distributed Modelling in Hydrology.* Wiley & Sons, Inc.

Boulton G., Payne A., 1992: Simulation of the European ice sheet through the last glacial cycle and prediction of future glaciation. Tech. Rep. SKB 93-14, Swedish Nuclear Fuel and Waste Management Co.

Fisher P.F., Cheng T., Wood J., 2004: Where is Helvellyn? Fuzziness of multi-scale landscape morphometry. *Transactions of the Institute of British Geographers*, 29: 106–128

Hagdorn M.K.M., 2003: *Reconstruction of the Past and Forecast of the Future European and British Ice Sheets and Associated Sea-Level Change.* unpublished PhD thesis, University of Edinburgh

Hurtrez J.E., Sol C., Lucazeau F., 1999: Effect of drainage area on hypsometry from an analysis of small-scale drainage basins in the Siwalik hills (central Nepal). *Earth Surface Processes and Landforms*, 24: 799–808

Hutchinson M., Gallant J., 1999: Representation of terrain. In: P. Longley, M. Goodchild, D. Maguire, D. Rhind (Eds.), *Geographical Information Systems: Principles and Technical Issues.*, vol. 1, pp. 105–124. Wiley & Sons, Inc.

Hutchinson M., Gallant J., 2000: Digital Elevation Models and representation of terrain shape. In: J. Wilson, J. Gallant (Eds.), *Terrain Analysis: Principles and Applications.*, pp. 29–50. Wiley & Sons, Inc.

Hutchinson M.F., 1993: Development of a continent-wide DEM with applications to terrain and climate analysis. In: M. Goodchild, B.O. Parks, L.T. Steyaert (Eds.), *Environmental Modeling with GIS.*, pp. 392–399. Oxford University Press, New York

Jones K.H., 1998: A comparison of algorithms used to compute hill slope as a property of the DEM. *Computers & Geoscience*, 24(4): 315–323

Purves R.S., Hulton N.R., 2000: Experiments in linking regional climate, ice-sheet models and topography. *Journal of Quaternary Science*, 15: 369–375

Schmidt J., Evans I.S., Brinkmann J., 2004: Comparison of polynomial models for land surface curvature calculation. *International Journal of Geographical Information Science*, 17(8): 797–814

Schneider B., 2001: On the uncertainty of local form of lines and surfaces. *Cartography and Geographic Information Science*, 28(4): 237–247

Takeda A., Cox S., Payne A.J., 2002: Parallel numerical modelling of the Antarctic ice sheet. *Computers & Geoscience*, 28: 723–734

Tucker G., Lancaster S., Gasparini N., Bras R., Rybarczyk S., 2001: An object-oriented framework for hydrologic and geomorphic modeling using Triangulated Irregular Networks. *Computers & Geoscience*, 27(8): 959–973

Weibel R., Heller M., 1991: Digital terrain modelling. In: D. Maguire, M. Goodchild, D. Rhind (Eds.), *Geographical Information Systems: Principles and Applications.*, pp. 269–297. Wiley & Sons, Inc.

Wood J.D., 1998: Modelling the continuity of surface form using Digital Elevation Models. In: T. Poiker, N. Chrisman (Eds.), *Proceedings, 8th International Symposium on Spatial Data Handling*, pp. 725–36

Zhang X., Drake N.A., Wainwright J., Mulligan M., 1999: Comparison of slope estimates from low resolution DEMs: scaling issues and a fractal method for their solution. *Earth Surface Processes and Landforms*, 24: 763–779

Appendix B

Hebeler, F. & Purves, R.S.: The influence of elevation uncertainty on derivation of topographic indices.
Geomorphology, in press

The influence of elevation uncertainty on derivation of topographic indices

Felix Hebeler and Ross S. Purves

University of Zurich, Department of Geography
Winterthurer Str. 190, 8057 Zurich
Switzerland

Geomorpholgy, accepted for publication June 21, 2007

Abstract

Digital elevation models at a variety of resolutions are increasingly being used in geomorphology, for example in comparing the hypsometric properties of multiple catchments. A considerable body of research has investigated the sensitivity of topographic indices to resolution and algorithms, but little work has been done to address the impact of DEM uncertainty and elevation value error on derived products. By using higher resolution data from the Shuttle Radar Topography Mission - of supposed higher accuracy - for comparison with the widely used GLOBE 1km data set, error surfaces for three mountainous regions were calculated. Correlation analysis showed that error surfaces related to a range of topographic variables for all three regions, namely roughness, minimum and mean extremity and aspect. This correlation of error with local topography was used to develop a model of uncertainty including a stochastic component, permitting Monte Carlo Simulations. These suggest that global statistics for a range of topographic indices are robust to the introduction of uncertainty. However, the derivation of watersheds and related statistics per watershed (e.g. hypsometry) is shown to vary significantly as a result of the introduced uncertainty.

1 Introduction

1.1 Digital elevation models

Representing the face of the earth as a continuous surface is a key task in research characterising the form of the earth's surface, modelling processes occurring on this surface or developing a better understanding of links explaining the relationship between process and form. Digital models of terrain can generally be categorised as either regular or irregular tessellations of point data, sometimes with additional ancillary information representing structural features such as breaks in slope or drainage divides (Weibel and Heller, 1991; Burrough and McDonnel, 1998). Since these models are usually taken to represent a continuous differentiable surface on which values of elevation and its derivatives (for example, slope and curvature) can be calculated at any point, some implicit or explicit scheme for interpolating or approximating values is required. Examples include linear

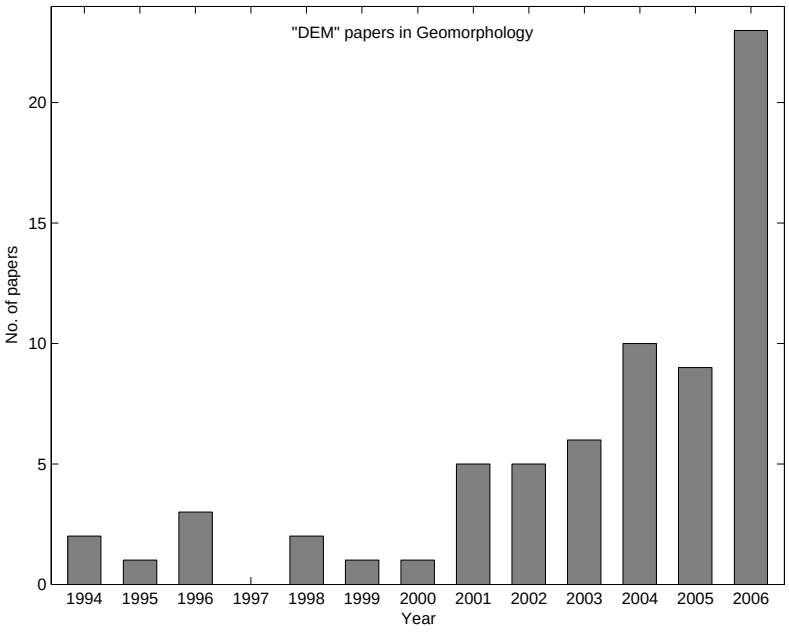

Figure 1: Number of papers mentioning "DEM" or "DTM" in their title, abstract or keywords in the journal Geomorphology, between Jan. 1994 and Dec. 2006 (Source: Web of Science Index)

interpolation, quadratic patches, thin-plate splines, Bezier splines and Coons patches. Within the GIScience community much attention has focussed on the veracity of the representation gained through different approaches (e.g. Schneider, 1998; Wood, 1998; Wise, 1998, 2000; Hutchinson and Gallant, 2000; Hugentobler et al., 2004; Chaplot et al., 2006); however, the wide availability of data which are regularly tesselated and the resulting ease of computation means that most research in the field of geomorphology using terrain data has been carried out on regular tessellations commonly known as Digital Elevation Models (DEMs), with some significant exceptions, (e.g. Tucker et al., 2001). In recent years the availability, resolution and coverage of digital data representing the surface of the earth has rapidly increased (Jarvis et al., 2004). So-called seamless datasets representing large parts of the earth's surface are available at resolutions ranging from approximately 1 km (GLOBE/GTOPO30) (USGS, 1996; GLOBE Task Team & others, 1999) down to 90 m and (for the contiguous USA) 30 m (SRTM, Rodriguez et al., 2005). Higher resolution data are collected by national mapping agencies in many countries as a component of national topographic databases, generally with resolutions of 10 - 50 m. Finally, in recent years very high resolution datasets consisting of LIDAR data with nominal resolutions of the order of meters have become available for specific locations (e.g. Staley et al., 2006). This increase in data availability and relative ease with which a wide range of topographic parameters may be derived has resulted in a steady increase in research within geomorphology which directly applies DEMs (Fig. 1). DEMs are, for instance, commonly used for extraction of a variety of forms (Herrington and Pellegrini, 2000; Fisher et al., 2004), fluvial geomorphic analysis at scales ranging from small catchments, through regional analysis to continental scales (Finlayson and Montgomery, 2003; Oksanen and Sarjakoski, 2005a), the modelling and validation of surface process models of long-term landscape evolution (Codilean et al., 2006) and as input data for ice sheet modelling at a range of scales (Bamber and Bindschadler, 1997; Lythe et al., 2001).

A relatively small number of topographic indices form the core of most descriptive use of DEMs within geomorphology. These include basic descriptive statistics of elevation (e.g. maximum, mean, minimum, standard deviation and hypsometry), local relief, gradient and aspect, curvature and

hydrological products such as flow direction, flow accumulation and watershed boundaries. As an input to numerical models, DEMs form a set of initial and boundary conditions for which numerical solutions to a set of driving equations are derived. For example, in ice sheet modelling elevation firstly determines locations at which positive mass balance will allow accumulation (Pollard, 1983; Marshall, 2002) and secondly surface slope and ice sheet thickness combine to allow derivation of the driving stress of the ice sheet through, for example, the Shallow Ice Approximation (Nye, 1957). It is therefore clear that DEMs, and topographic indices derived from them, are an increasingly important tool for both analysing forms and modelling processes in geomorphology.

1.2 Error and uncertainty in DEM

DEMs can be derived from a variety of sources requiring different processing methods, including the digitisation of contour maps, interpolation from spot height measurements collected in the field and processing of radar or laser measurement data. As such, any resultant DEM is subject to both the precision and accuracy of the measurement sensor together with the quality of digitising or interpolation methods (Heuvelink, 1998), and thus is subject to error, from these multiple sources. In this paper the term error implies the deviation of a measurement from its true value, implying that the elevation error of a DEM can only be determined if a set of more accurate reference data is available (Fisher and Tate, 2006).

Error is therefore implicitly associated with any DEM, but usually both the magnitude and spatial distribution of the error at any particular location are unknown. Error thus creates uncertainty, which can be approximated through the use of geostatistics or uncertainty models (Holmes et al., 2000). Here, the term uncertainty is used where a (modelled) value is expected to deviate from its true value, but it is uncertain to what extent, and is often associated with confidence intervals (Kyriakidis et al., 1999; Endreny and Wood, 2001; Shortridge, 2001).

Error and accuracy of DEM products and production methods have been the subject of much research and methods to both describe and reduce error have been developed (Wechsler, 2006). Different types of error are often listed, with Wise (2000) describing blunders, systematic and random errors as being typical in DEMs. Blunders are gross errors which occur less frequently in DEM products and can be the results of failing measuring equipment or digitising errors. Systematic errors show a common trend or dependency, and can be the results of processing or recording procedures, such as radar shadow effects (Shortridge, 2006) and terracing in poorly interpolated contour-derived DEMs (Wood, 1996). When known, systematic error can often be computationally reduced or eliminated by, for example, detrending data. Random error originates from a variety of sources, and no trend can be observed. Fisher and Tate (2006) summarise the three main sources of such DEM error as:

1. measurement and generation of source data;
2. data processing and DEM generation from source data; and
3. the properties of the terrain surface being modelled with respect to its representation in a DEM.

The third of these sources of error is particularly important since it emphasises a fundamental and often neglected consideration when working with DEMs: the resolution and representation of a terrain surface and the derivation of products from that terrain surface in themselves introduce ambiguities and can thus best be categorised as uncertainty (Schneider, 2001; Fisher and Tate,

2006).

Error surfaces can be generated for DEMs by using data which are assumed to have a higher accuracy. Subtracting this higher accuracy data from the DEM under study creates a surface that can be analysed to better understand the nature and sources of error. In such an analysis three components of error can be identified that are important for geostatistical modelling. The first is a random component, where no spatial dependency can be resolved (at the DEM's resolution). This component is also known as noise or nugget in semivariograms. The second component is related to the fact that terrain attributes (e.g. elevation, slope and roughness) typically change gradually over space, and this gradual change may also be reflected in the associated error surface. Error surfaces often exhibit characteristic ranges of spatial correlation, resulting in error patterns that stem from correlations with the underlying terrain (Hunter and Goodchild, 1997). A third component may be global trends superimposed on local patterns. These can often be detected using directional variograms, or profile plots (Liu et al., 1999; Holmes et al., 2000). Despite a recognition of the necessity for detailed error models and the suggestion that these be distributed with digital elevation data (Ehlschlaeger and Goodchild, 1994; Fisher, 1998), DEMs are still commonly distributed with at best global error or accuracy figures (Fisher, 1998), usually stating root mean squared error (RMSE) or standard deviation for vertical and horizontal accuracy (e.g. GLOBE, SRTM and most data from higher resolution DEMs provided by national mapping agencies). These global accuracy figures are of limited use since they contain no information on the spatial distribution of error, which, as discussed above, is often spatially correlated with topographic attributes such as altitude, slope or roughness (Holmes et al., 2000; Oksanen and Sarjakoski, 2005b). In order to geostatistically model the uncertainty inherent in DEMs, all three of the components of error observed in error surfaces should be taken into account.

Where no spatial dependency of error can be identified, e.g. because of the lack of higher accuracy reference data, assumptions about the spatial correlation of error must be made, or all of the error must be modelled as random noise. When modelling error using the RMSE supplied by the producers, it is often assumed to be normally distributed (Fisher, 1998; Oksanen and Sarjakoski, 2006; Wechsler, 2006). However, it has been suggested that this assumption is not generally valid (Holmes et al., 2000) and that more complex distributions of random errors should be modelled.

When information on the spatial autocorrelation of the error is known, it can be incorporated into an uncertainty model (Wechsler, 1999). Common methods include the use of global and local spatial correlation measures such as Moran's I that have been used, for example, in measuring the effect of random swapping of values (Fisher, 1998), or spatial moving averages that include correlation measures from variograms (Kyriakidis et al., 1999; Oksanen and Sarjakoski, 2006). While these methods introduce spatial correlation to the modelled uncertainty surfaces, correlation with the properties of the underlying surface is not explicitly accounted for.

1.3 Aims

The problem of uncertainty in results derived from digital elevation models has long been recognised and addressed in a variety of work. A number of experiments examine the robustness of descriptive indices of geomorphometric measures, such as slope and aspect (Evans, 1980; Burrough and McDonnel, 1998; Hodgson, 1998; Jones, 1998; Zhang et al., 1999), hypsometry (Strahler, 1952; Hurtrez et al., 1999), and hydrological catchment areas (Walker and Willgoose, 1999; Gallant and Wilson, 2000). While these studies generally focus on the effects of data models, resolutions and algorithms, the uncertainty stemming from elevation data itself, and the propagation and impact

on model results of this uncertainty compared to that introduced through data processing and model calculations has been largely ignored (Fisher and Tate, 2006).
Despite their widespread use, there are few studies examining the accuracy of either GTOPO30 or GLOBE DEMs (Harding et al., 1999) beyond the global figures provided by the data producers (GLOBE Task Team & others, 1999), but with the availability of data from the Shuttle Radar Topography Mission (SRTM), a number of studies have looked at the uncertainties inherent in different versions of SRTM data products. Accuracy studies have focused on technical issues of data acquisition (Heipke et al., 2002) or on comparison of SRTM data with higher resolution data such as spot height measurements, ICESat or LIDAR data (Sun et al., 2003; Carabajal and Harding, 2005). SRTM data appear to be sensitive to overestimating terrain height in densely vegetated areas due to scattered first returns from canopies (Shortridge, 2006). Incomplete data for a variety of reasons can lead to uncertainties resulting from the interpolation of "data holes" (Jarvis et al., 2004). However, in general SRTM data have a much higher accuracy than GLOBE DEM, and it has been implied that SRTM data may be used as ground truth for accuracy studies of GLOBE DEMs (Jarvis et al., 2004), when the focus is on generating a valid large-scale error model that can be generalised, rather than detailed analysis of regional uncertainties.
While SRTM data are available for large regions of the Earth's surface, for a number of reasons lower resolution DEM data (of supposed lower accuracy) is still being used in many applications. Large scale environmental models, such as global climate models and ice sheet models, run on resolutions of 1 to 20 km, and the use of higher resolution data is not sensible or even unpractical because of the demands on computational and memory capacity. Furthermore SRTM data are not available at latitudes above 60°N: models focussing on higher latitudes, such as permafrost, snowcover and ice sheet models are therefore still dependent on lower resolution data.
This paper therefore has two key aims: firstly, to develop a robust model of the error and/or uncertainty in GLOBE data and its relationship (if any) to the underlying terrain surface, and secondly, to illustrate the potential uses of this uncertainty model in geomorphometry through a simple case study. We first set out methods for deriving error surfaces of GLOBE DEM using SRTM as ground truth in regions where both data sets are available. These error surfaces are then used in the analysis of possible dependencies of GLOBE uncertainty on terrain properties. Where robust and generalisable dependencies are derived, this information can be incorporated using regression modelling to approximate error or uncertainty of GLOBE data for regions where no SRTM data is available, and to assess the impacts of uncertainty on previously completed studies. Finally, a case study assesses the impact of the modelled uncertainty on a standard set of geomorphometric analyses through Monte Carlo simulation.

2 Developing an uncertainty model

The development of a generalisable model of uncertainty in GLOBE elevation values was carried out through the following steps:

- Resampling and registration of higher accuracy data to allow a comparison with GLOBE data.
- Qualitative exploration of the variation in error values.
- Exploration of correlations of terrain parameters with error.

DEM	**Altitude**	**Mean**	**StDev**	**Skew**	**Kurt**	**Source**	**Size**(cells)
Alps	1 - 4570 m	692.8 m	624.8 m	1.65	5.46	DTED/SGN	1083108
Pyrenees	1 - 3276 m	651.9 m	481.2 m	0.86	3.86	DTED	720000
Turkey	1 - 4938 m	1066.5 m	738.4 m	0.55	2.29	DTED	816837

Table 1: Descriptive statistics of the GLOBE data used for the three study areas. (StDev = standard deviation; Skew = skewness, Kurt = kurtosis.

- Development of a model of terrain uncertainty.
- Generation of multiple uncertainty surfaces including a stochastic component.

2.1 Study areas and data sets

This work emerged from the need for a uncertainty model for GLOBE DEM data for Fennoscandia, to be used as input in Monte Carlo Simulations (MCS) for sensitivity testing of ice sheet model results (Hebeler and Purves, 2004). GLOBE data are produced using a variety of data sources and techniques, with the major contributors being USGS DEM data for the US, and digital terrain elevation (DTED) data and digital chart of the world (DCW) data for much of the rest of the northern hemisphere. While these sources are essentially the same as used for GTOPO30, the GLOBE data set has been refined over GTOPO30 by using higher accuracy data, where available (Hastings and Dunbar, 1998). For example, GLOBE has been refined using the local DEM of Italy provided by the Servizio Geologico Nazionale, which showed a slight improvement over DTED data for high altitudes, but much better agreement with actual terrain for lower elevations (GLOBE Task Team & others, 1999). The accuracy for GLOBE data sourced from DTED data is reported in meta-data as being around 18 m RMSE (USGS, 1996), decreasing to around 97 m RMSE for DCW data. For other areas, especially in South America much larger RMSE values have been reported. Fig. 2 shows the variation in source data for GTOPO30 data in different regions and an error surface calculated for South America showing the strong correlation of error magnitudes with different data sources. As the aim of this study was to develop and test a robust uncertainty model that is of general use for lower resolution data over large areas, GLOBE DEM data were selected over GTOPO30 because of their supposed higher accuracy and more recent production. Given this dependency of error on source data, study areas were chosen for their comparability with Fennoscandia - that is to say regions where GLOBE data were mostly derived from DTED data, with mountainous topography and spanning a similar range of altitudes to those found in Fennoscandia (between sea level and around 2500 m). The study areas selected are shown in Fig. 2 and include the European Alps, the Pyrenees and Turkey. Table 1 shows the descriptive statistics for these regions.

2.2 Data preparation

For our analysis, SRTM3 data provided by CGIAR-CIAT (Jarvis et al., 2006) were used. This data resembles the post-processed NASA SRTM data with voids filled using generated contours and auxiliary data, where available (Jarvis et al., 2004). In order to compare these SRTM data at a resolution of ∼100 m with GLOBE at ∼1 km, SRTM data were downsampled to fit the extent and resolution of the corresponding GLOBE data. While for some operations such as gradient calculation, it is necessary to work with projected data, any interpolation applied in projecting

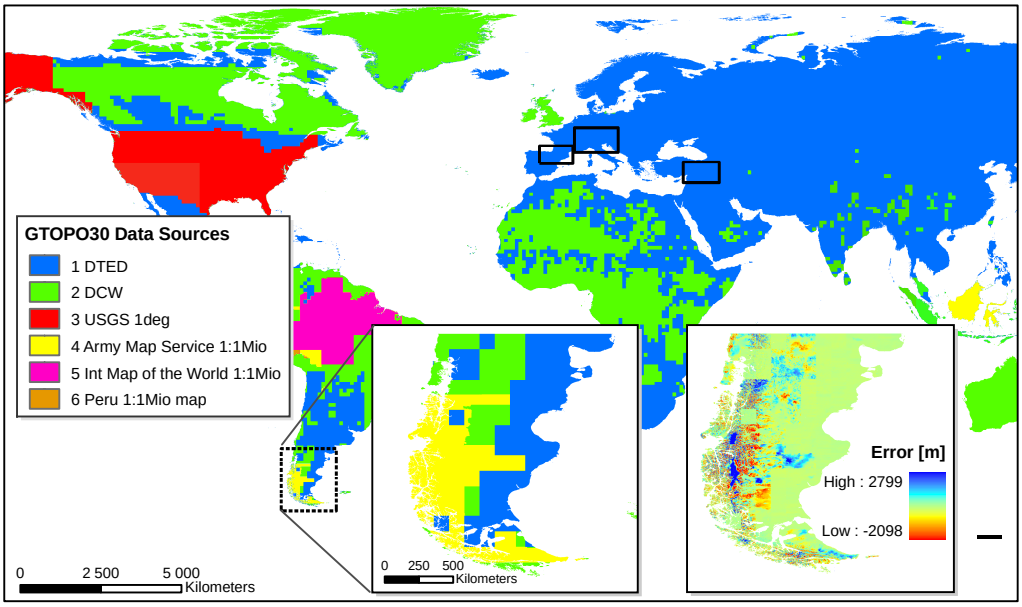

Figure 2: Sources used to compile GTOPO30 DEM data. The same source data, though with differing interpolation schemes were used in the production of GLOBE data. Study areas used in this paper marked solid black. Inset of Patagonia with data sources (left) and GLOBE deviation from SRTM (right). Note the variation in magnitude and spatial correlation of error for Patagonia (right inset), depending on the data sources used (left inset). Source: USGS 1996.

or resampling data alters the original data and introduces additional uncertainty (Montgomery, 2001). Our experiments indicated that error dependencies on terrain attributes varied relatively little between projected and unprojected data. Therefore bearing in mind that the values of some attributes calculated in the unprojected data were misleading, we carried out error analysis using the unprojected WGS84 spatial reference in which both SRTM and GLOBE data are distributed. To allow the derivation of error surfaces SRTM data were downsampled following the approach of Jarvis et al. (2004) by calculating the mean of all SRTM cells within the bounds of each GLOBE data cell. This approach is based on the assumption that GLOBE data represents the average altitude within each corresponding DEM cell, while SRTM data represents the maximum height at each posting, thus averaging of SRTM data should be used for downsampling when comparing with GLOBE. Both SRTM and GLOBE DEMs were then clipped to eliminate waterbodies before the calculation of error surfaces. Finally an error surface representing the deviation of GLOBE from the averaged SRTM data set was calculated by subtraction. For the purposes of our analysis, the higher accuracy SRTM data are assumed to be error free and thus a difference surface is assumed to completely describe the error in GLOBE data.

2.3 Error surfaces

Fig. 3 shows an error surface calculated for the Alps. Through visual examination a number of features become apparent. Most strikingly, it is clear that error values are strongly spatially correlated, following the boundaries of prominent features within the data set. In areas of low

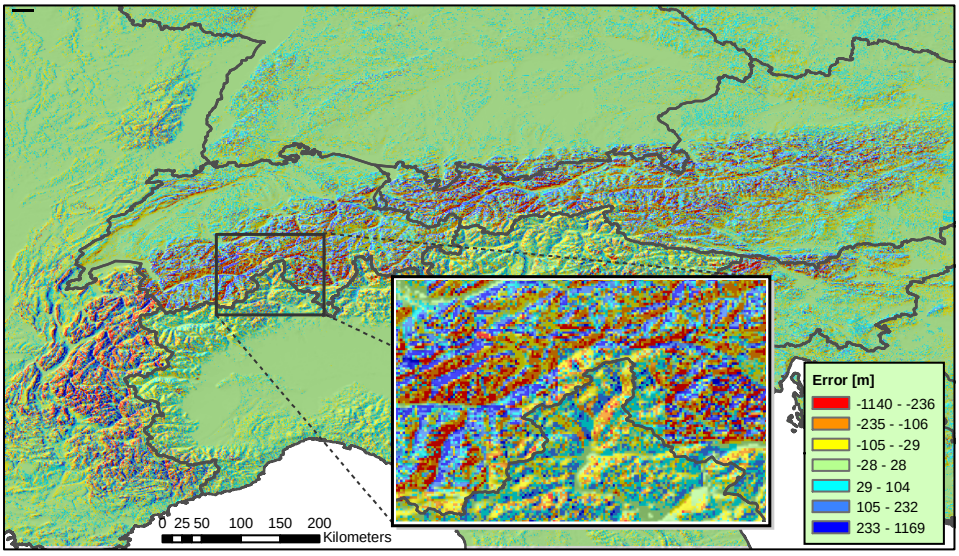

Figure 3: GLOBE error surface for the European Alps derived from SRTM data. Country borders and hillshade added for better visibility. Note that the overall amount of error is less for the Italian part of the Alps due to the use of higher accuracy local DEMs provided by the Servizio Geologico Nazionale in the compilation of GLOBE.

relief, relatively small errors of ±20 m with a short wavelength of variation are apparent. Finally, an observation can be made regarding the dependency of error with DEM source, as the magnitude of error appears to be less in the Italian part of the Alps - where different source data are used in the production of the DEM - than for the French or Swiss regions. This first examination of the error surface suggests a correlation of error with terrain features and attributes, but also indicates inhomogeneity in the error values and spatial correlation depending on both terrain type (high versus low relief) and data sources. Fig. 4 shows the semivariogram map for the error surface derived for the Alps. A general SW-NE trend is visible with high spatial autocorrelation indicated by low variance within a range of around three cells.

2.4 Correlating error with terrain parameters

Having carried out a visual analysis of error surfaces and considered previous work which has examined errors in terrain values at a range of scales, we could commence development of a model of error. The first step in developing this model was to examine the correlation of error with a range of terrain parameters. Table 2 shows the complete set of terrain parameters tested for correlation with GLOBE error. In practice, given the very large number of data points, all terrain parameters were statistically significantly correlated with the magnitude of error. In order to develop a useful error model, factor analysis was carried out to reduce the number of potential variables in the error model. Results from the factor analysis and the breakdown of intercorrelation of the variables suggested the variation in derived error to be best reproduced by two or three terrain parameters. Table 3 shows the correlation of a range of terrain parameters with the magnitude of error for the different study regions. Although parameters exhibited highest correlation coefficients with the

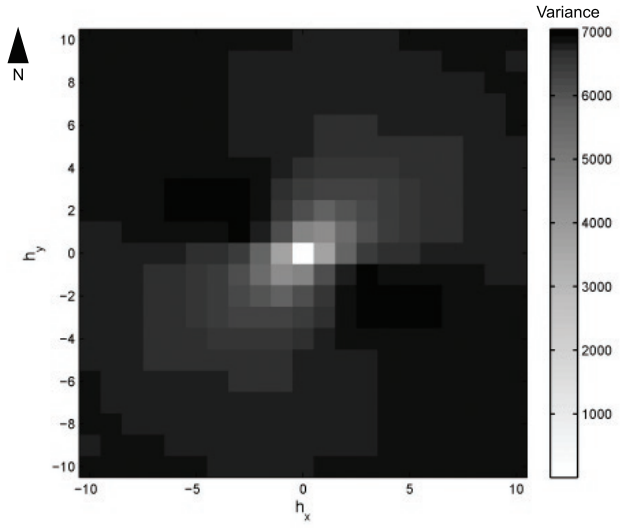

Figure 4: Semivariogram map of GLOBE error for the Alps. Variance in x and y direction is plotted for a 10 by 10 cell neighbourhood. Notice the SW-NE trend of lower variation, which is present in variogram maps of all three test areas.

magnitude of error, a relationship between aspect and the sign of the error is also visible in the error surfaces (Fig. 3) and was also used in the development of the uncertainty model described in the following section.

Attributes	Altitude	Value of GLOBE cell
	Error, absolute Error	(absolute) Deviation of GLOBE from mean SRTM value
Derivatives	Aspect	Direction of first derivative of elevation
	Slope	Magnitude of first derivative of elevation
	Plan Curvature	2nd derivative orthogonal to direction of steepest slope
	Profile Curvature	2nd derivative in direction of steepest slope
	Total Curvature	Compound curvature index
Indices (Neighbourhood Statistics)	Maximum/Mean/Minimum Extremity	Deviation of center cell from the maximum/mean/minimum of its 3x3 neighbourhood
	Roughness (Altitude)	Standard deviation of altitude in a 3x3 neighbourhood
	Roughness (Slope)	Standard deviation of slope in a 3x3 neighbourhood

Table 2: Attributes and indices calculated and tested for correlation with GLOBE error. Extremity calculated following Carlisle (2000).

DEM		**Altitude**	**Slope**	**Aspect**	**Rough Alt**	**Rough Slope**	**Extremity**			**Curvature**		
							Min	Max	Mean	Total	Plan	Profile
Pyrenees	Error	-0.067	-0.035	0.144	-0.028	-0.011	-0.249	-0.195	-0.427	-0.438	-0.398	0.385
	AbsError	0.397	0.586	0.003	0.636	0.563	0.537	-0.513	0.03	0.026	0.045	-0.001
Alps	Error	-0.056	0.005	0.11	0.004	0.006	-0.15	-0.153	-0.315	-0.331	-0.289	0.292
	AbsError	0.532	0.618	-0.003	0.663	0.581	0.579	-0.549	0.054	0.046	0.073	-0.01
Turkey	Error	-0.063	-0.012	-0.106	-0.008	0.006	-0.293	-0.273	-0.522	-0.521	-0.471	0.468
	AbsError	0.468	0.614	0.011	0.649	0.571	0.542	-0.52	0.034	0.023	0.047	0.005

Table 3: Correlation coefficients of calculated parameters with GLOBE error and magnitude of error (AbsError) for the three study sites.

Constant	Description
a	roughness of altitude (magnitude of error)
b	minimum extremity (magnitude of error)
c	constant (magnitude of error)
d	magnitude of error (residual regression)
e	constant(residual regression)
f	mean extremity (sign of error)
g	aspect (sign of error)
h	constant (sign of error)

Table 4: Constants used in the regression of error (a,b,c), the regression of the residuals (d,e) and the binary logistic regression of the error sign (f,g,h).

Variables	r^2	Coefficients				Constant c
4	0.453	0.753×a	0.034×b	0.0025×altitude	0.00002×slope	4.636
3	0.444	0.444×a	0.024×b	0.007×altitude		5.184
2	0.441	0.468×a	0.033×b			7.246
1	0.437	0.515×a				7.388

Table 5: Example of fitting the regression model for the Alps study area. The dependent variable is error magnitude; r^2 values and coefficients for different combinations of independent variables shown. Coefficients according to Table 4 where not explicitly given.

2.5 Building an uncertainty model

A simple linear regression model of error with terrain parameters was developed through the stepwise substitution of different combinations of parameters. Table 4 lists the parameters selected for the three regressions used in the uncertainty model. Table 5 shows an exemplary model fitting process with different combinations of parameters, and illustrates that most of the variation in the surface is explained by two terrain parameters, roughness and minimum extremity, with only a slight improvement with the use of three or four parameters. It was decided to include the second parameter into the regression, which improved r^2 by around 5-10 %, despite some intercorrelation of roughness and minimum extremity. By including a logistic regression the sign of the error was also simulated, using aspect and mean extremity. Both variables are uncorrelated, and it was found that correlation of sign of error with aspect could be slightly improved when transformed using a sine function. However, across the three test areas, no global transfer function could be found that resulted in an improvement for all three data sets. If the regression analysis had shown that the error surface was completely correlated with terrain parameters derived from the GLOBE data, it would have been possible to eliminate this error from the GLOBE data, and thus potentially reduce the uncertainty of terrain parameters derived from the GLOBE data. However, as shown in Table 6, whilst regression analysis showed strong correlations with the error surface, a significant quantity of the error is not explained. Thus, in order to model the uncertainty surface, stochastic elements were included, providing a suitable input for Monte Carlo simulation as every uncertainty surface produced will be different. In developing the model we used three qualitative and quantitative observations from the development of the error surfaces described above:

- Error surfaces are spatially autocorrelated with a range of approximately three grid cells.

Dataset	magnitude				sign			residual		
	r^2	a	b	c	r^2	d	e	f	g	h
Alps	0.441	0.468	0.033	7.25	0.559	0.559	-26.29	-0.005	0.002	-0.382
Pyrenees	0.405	0.617	0.032	7.09	0.595	0.595	-24.08	-0.015	0.003	-0.183
Turkey	0.423	0.502	0.028	9.33	0.577	0.577	-23.85	-0.017	0.001	-0.439
Global		0.52	0.032	7.6		0.58	-25.0	-0.012	0.002	-0.2

Table 6: Results of regression of the magnitude of error, the sign of error and the residuals of the error, with their corresponding constants (Table 4) for all study areas.

- Error magnitude can be described through terrain parameters, with all terrain parameters significantly correlated, and factor analysis suggesting that two to three parameters should adequately describe most of the variation.
- The sign of the error can be approximated from terrain parameters using a logistic regression.

The final error model consists of three parts, and took the following form. Regression of the modelled magnitude of error:

$$abs(\varepsilon') = \mathrm{a} \times roughness + \mathrm{b} \times extremity_{\min} + \mathrm{c} \tag{1}$$

where $abs(\varepsilon')$ is the magnitude of the derived error and a,b, and c are constants given in Table 4. Fig. 5 shows the residuals of this regression for the Alps. These residuals are correlated with the magnitude of the calculated error and can be described by the following linear equation:

$$res_1 = \mathrm{d} \times abs(\varepsilon) + \mathrm{e} \tag{2}$$

where res_1 is the residual of Eq. 1, and d and e are constants (Table 4). The residuals (res_2) of Eq. 2 are essentially random and can best be simulated by a transformed normal distribution $res_2 = N(0,1) \Rightarrow D(\mu = 0, \sigma = 30, \gamma_1 = 2, \gamma_2 = 6.8)$ which are then randomly added to res_1, introducing a first stochastic component to the model.
Finally, the sign s of the error is calculated as follows:

$$s = \mathrm{f} \times extremity_{\mathrm{mean}} + \mathrm{g} \times aspect + \mathrm{h} \tag{3}$$

where $-1 \leq s \leq 1$ and f,g and h are constants (Table 4). A random number r is then selected, where $0 \leq r \leq 1$, and applied to the following equation

$$\begin{aligned} s' &= -1 \qquad if\ r \leq |s|\ and\ s < 0 \qquad or \\ s' &= 1 \qquad if\ r \leq |s|\ and\ s \geq 0 \qquad or \\ s' &= -1 \qquad if\ r > |s|\ and\ s \geq 0 \qquad or \\ s' &= 1 \qquad if\ r > |s|\ and\ s < 0 \end{aligned} \tag{4}$$

to introduce a second, constrained random component to the model. The value of uncertainty in elevation at each cell U_{tot} is thus derived through the following equation:

$$U_{\mathrm{tot}} = (abs(\varepsilon) + res_1 + res_2) \times s' \tag{5}$$

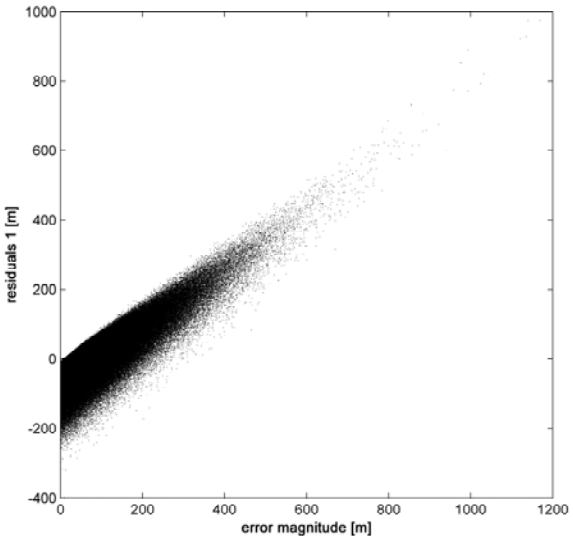

Figure 5: Plot of the residuals $res1$ from the regression of error magnitude with roughness and $extremity_{\min}$ against the magnitude of error, showing a good fit with a single factor linear regression.

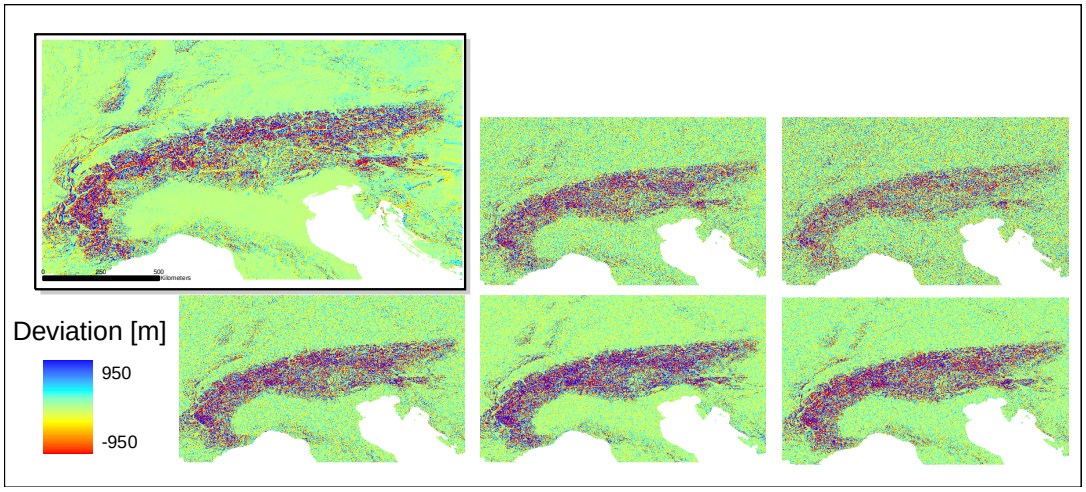

Figure 6: Error surface derived from GLOBE data for an approximately 200x300 km subset of the Alps study area (top left) together with five example uncertainty surfaces for the same area. While the main landscape features are detectable in both the error surface and all five uncertainty surfaces, the stochastic elements in the uncertainty surface, and the globally applied (low) omnidirectional spatial correlation result in a noisier structure of the uncertainty surfaces, when compared to the GLOBE error.

In order to take account of the spatial autocorrelation of the error surface shown in Fig. 3, the values of the error surface derived are transformed to a normal distribution and a convolution filter (Oksanen and Sarjakoski, 2005a) using a range derived from Fig. 4 is applied, in order to adjust spatial correlation of the modelled uncertainty to that of the original measured error, before the uncertainty surface is finally transformed back to its original distribution.
By adding the uncertainty surface to the original GLOBE data it is possible to examine the influence of this uncertainty on derived terrain parameters. Fig. 6 shows a set of five example uncertainty surfaces for a subset of the Alps together with the derived error surface. Distributions of modelled error against derived error for all three study regions are shown in Fig. 7.

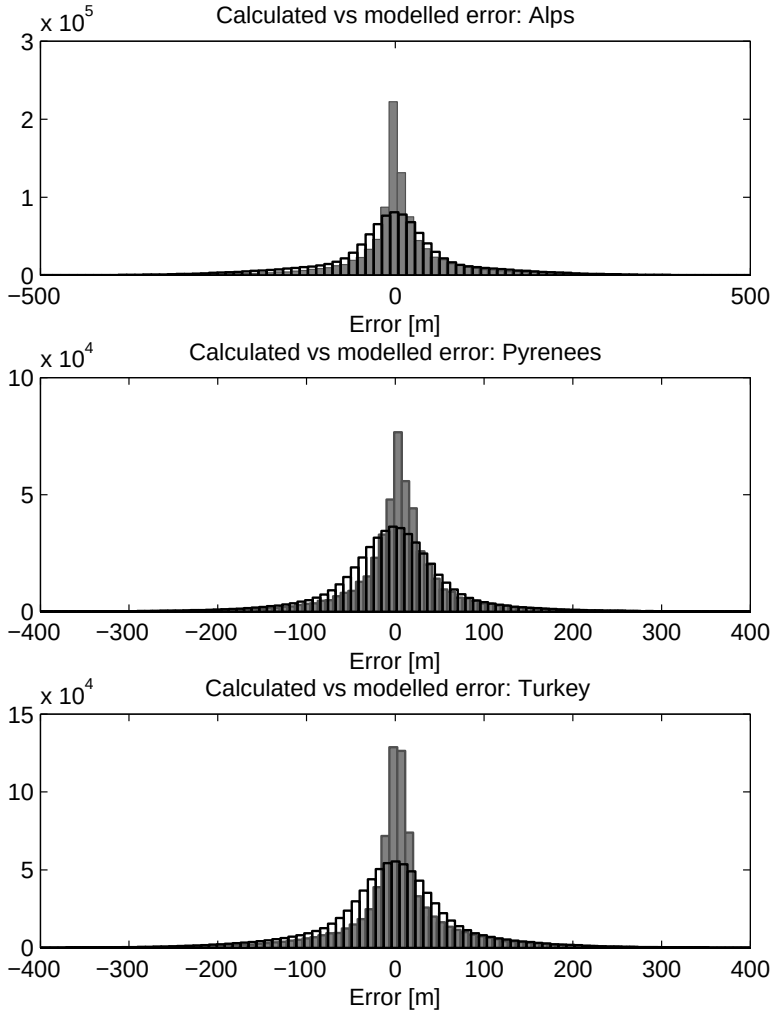

Figure 7: Distribution of GLOBE error surfaces derived using SRTM for all three datasets (solid gray bars), compared with distribution of modelled error (open black bordered bars). For better comparison, the tails of the distributions are not depicted, focusing on the distribution means.

3 Example Application

Having developed an uncertainty model, the next obvious step is to apply the model and determine whether it has any significant influence when deriving common topographic indices using GLOBE DEM data. In this case study we choose two approaches to examining the impact of uncertainty through the use of Monte Carlo Simulation (MCS). In the first experiment we derive a set of global parameters for the GLOBE DEM with 40 realisations of the uncertainty model added. In a second set of experiments the boundaries of individual watersheds were first derived before geomorphological indices per watershed were calculated for comparison. Finally, we examine in detail the differences within and between two large catchments defined through the MCS methods. For this example, all analysis was carried out on the Alps region shown in Fig. 3.

3.1 Methodology

A set of 40 uncertainty surfaces was created using the regressions described in section 2.5 and added to the original GLOBE DEM. As discussed earlier, to calculate meaningful topographic parameters these DEMs were projected, using bilinear interpolation, into an Albers Equal Area projection with the central meridian running through the centre of the DEM and two standard

Areal unit	Parameters calculated
per DEM	elevation, slope, number of watersheds, watershed delineation, Strahler order, stream length, hypsometric integral
per Strahler order	elevation, slope, stream length, relative area
per watershed	elevation, slope, stream length, area, hypsometric integral
per cell	watershed membership likelihood

Table 7: Geomorphological parameters calculated for the Alps using Monte Carlo Simulation.

parallels dividing the area into even thirds, thus minimising distortion. WGS84 was used as the reference ellipsoid and all further calculations were carried out using the projected DEM. To calculate meaningful hydrological indices, all sinks in the resulting DEMs were filled using ArcGIS. TARDEM (Tarboton, 1999) was used to calculate a set of parameters for every realisation (see Table 7). To delineate watersheds a pour point must be defined indicating a point on a stream network which accumulates all upstream flow. This process was automated by defining pour points to be the first cell encountered, of a given stream order, when travelling down the stream network of a given realisation, where first order streams are defined as those with no other cells draining into them and stream order is increased when two streams of equal order meet (Tarboton, 1999). Cells were then assigned a Strahler order based on the lowest order basin in which they were contained.

3.2 Results

3.2.1 Summary global statistics

Global statistics for the 40 different realisations of the Alps, as generated by Monte Carlo Simulation are shown in Fig. 8. The box and whisker plots divide the data into four quartiles with the median data value being displayed in the middle of the box plot (if the data are not skewed), the first and third quartiles the ends of the box and the minimum and maximum values displayed as the ends of the whiskers.
Fig. 8A,E show that global statistics of altitude and the distribution of altitude (shown through hypsometry) change very little for any of the MCS surfaces generated. However, some variation, particularly in the upper quantile, is visible in the global statistics of slope (Fig. 8B). Fig. 8C,D,F also show global statistics calculated per Strahler order as calculated for the network derived from the MCS realisations. Once again little variation is visible in elevation, but it is now revealed that most variation in slope occurs in cells which are assigned to the 1st order of the Strahler network or the headwaters of streams. Fig. 8F suggests that the number of cells assigned to each order of the Strahler network is relatively robust for the MCS.

3.2.2 Watershed derivation and derived statistics

The second set of experiments examined the robustness of watershed boundaries as a function of the uncertainty in elevation values in GLOBE. For these experiments, 6th order watersheds were delineated, where a watershed's pour point was defined as the first downstream point belonging to a 7th order stream. Thus each watershed contains cells with Strahler orders of 1 to 6. Fig. 9A shows the total number of watersheds derived, with all other results in Fig. 9B-F sorted according to this total number of watersheds. The notches in the center of the box plots indicate an estimate of the

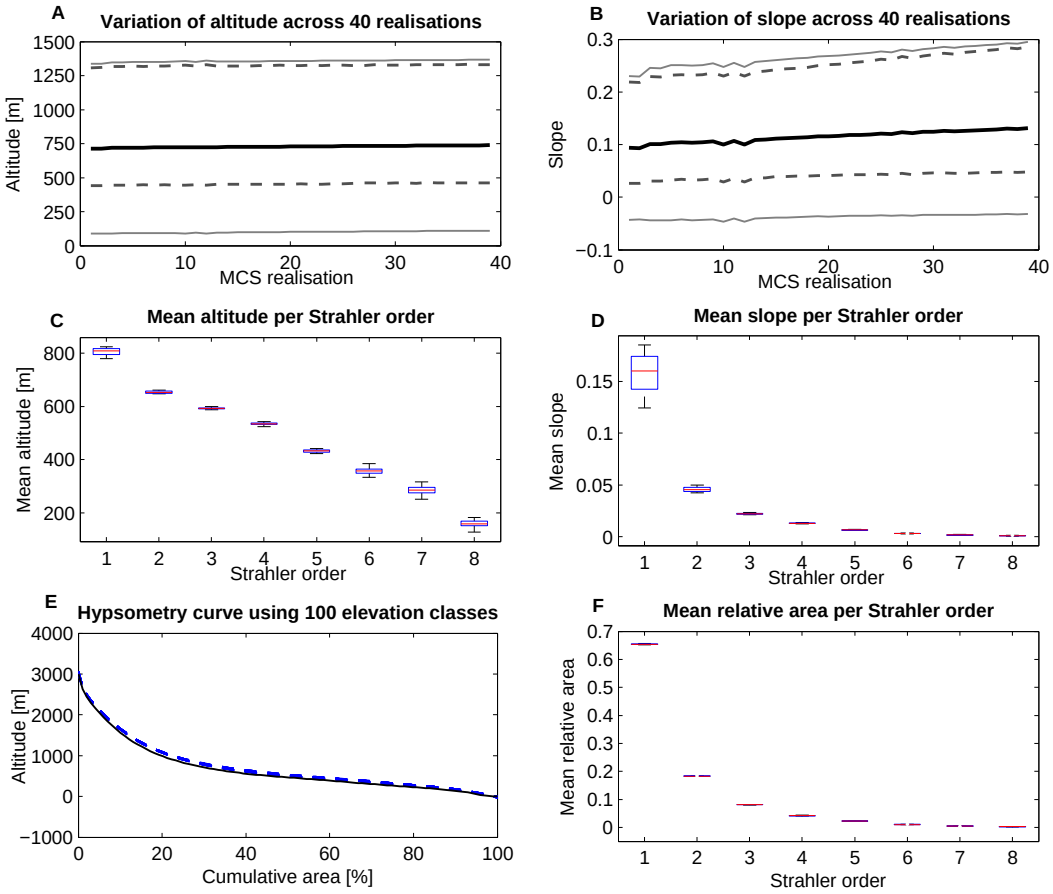

Figure 8: Global statistics for 40 MCS realisations using the uncertainty model. Variation of altitude (A) and slope (B) across all 40 DEMs are plotted depicting mean (solid black), quantiles at 0.33 and 0.66 (broken dark gray) and standard deviation (solid light gray). Boxplots of mean altitude (C), slope (D) and relative area (F) are plotted against the calculated Strahler order. Hypsometry curves using 100 elevation classes (E) are plotted for the 40 MCS DEMs (broken blue) as well as the original GLOBE DEM (solid black).

uncertainty around the medians. Boxes whose notches do not overlap indicate that the medians differ with a confidence of p = 0.05 (MATLAB, 2006). By examining these notched box plots it is clear, firstly, that most of the derived statistics are robust for all realisations. However, the box plots for slope show that on some occasions the median slope values are statistically significantly different (for example the 4th and 19th realisations of slope in Fig. 9B).

3.2.3 Comparison of two watersheds

Fig. 10 shows the membership likelihood of DEM cells belonging to one of two large, neighbouring watersheds (defined upstream of 7th order streams) when different uncertainty surfaces are applied. The variation in area is large with a variation of over 320% and 290% for W1 and W2, respectively. For both W1 and W2, most variation in watershed area is the result of the stream network capturing large areas of “flatlands”, though in the case of W1 some instability is also vis-

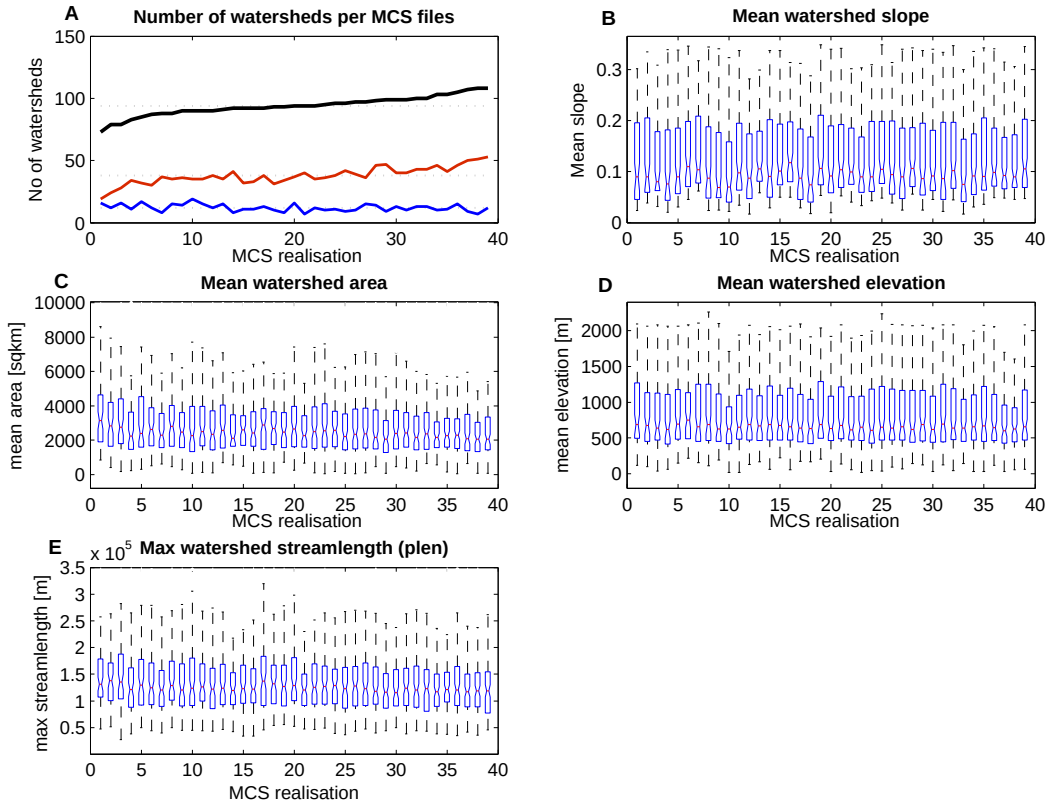

Figure 9: Watershed statistics for 40 MCS realisations using the uncertainty model. Number of 6th order watersheds (A), sorted by size. Absolute number (solid black) of delineated 6th order watersheds are plotted together with the number of watersheds with an area smaller than 2000 cells (solid red) and number of watersheds with areas larger than 5000 cells (solid blue). Mean across all 40 DEMs plotted in dotted light gray. Mean watershed slope (B), mean area (C), mean elevation (D) and mean maximum stream length (E, as given by plen using TARDEM) plotted across all 40 DEMs using box plots. For better visibility outliers are not drawn.

ible in the mountainous part of the catchment. Both catchments agree well with national borders, which in this region lie along the main ridge of the Alps, demonstrating the stability of catchment boundary definition in areas of high relief. Derivation of the elevation and slope statistics for the different watershed realisations (Fig. 11) show considerably more variability than that for the global statistics, since the region over which these statistics is calculated has itself considerable variation. Although more variation in catchment area was shown for W1, both elevation and slope vary more for W2.

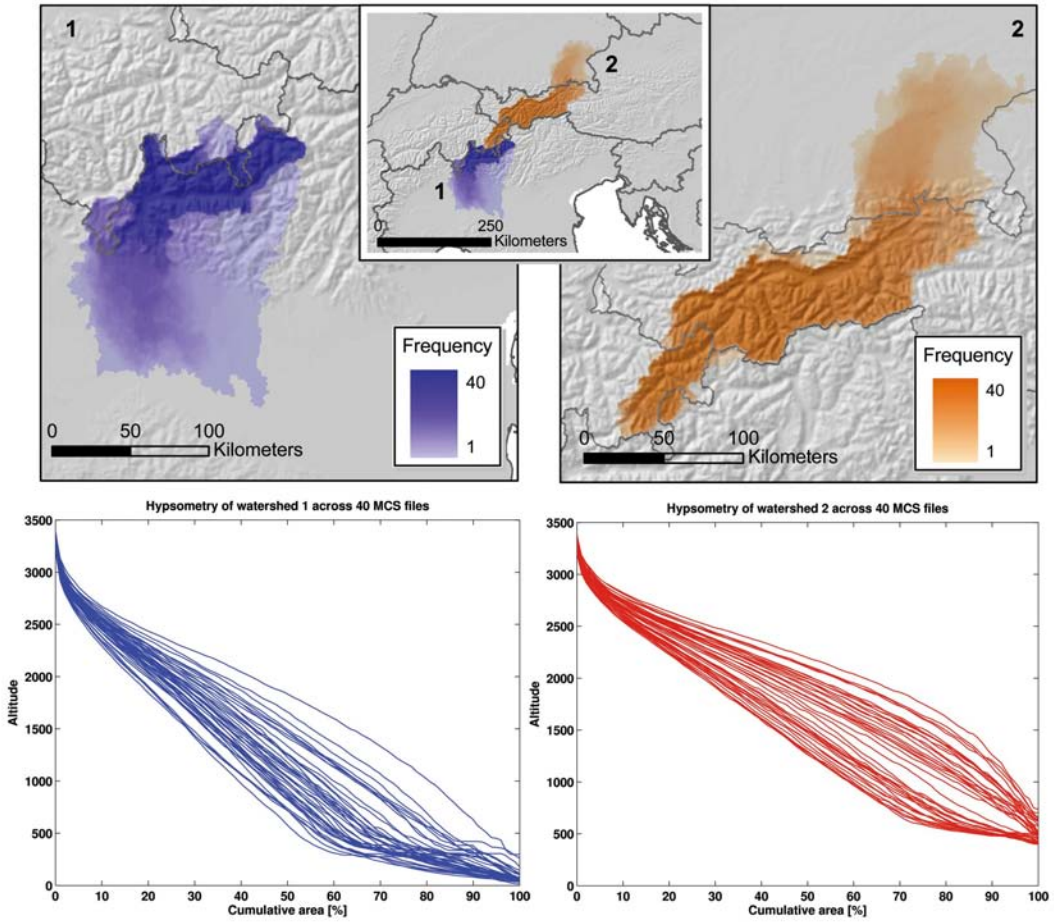

Figure 10: Frequency of cells belonging to two selected watersheds W1 (left) and W2 (right) across all 40 MCS runs (top). Most variation in watershed size is detectable in the lower regions of the catchment area, but some variation is also evident in the high mountain regions of both watersheds. Hypsometric curve (bottom) across 40 MCS runs for the two selected watersheds, showing a considerable amount of variation in form, depending on the size of lowland area 'captured' by a MCS simulation run.

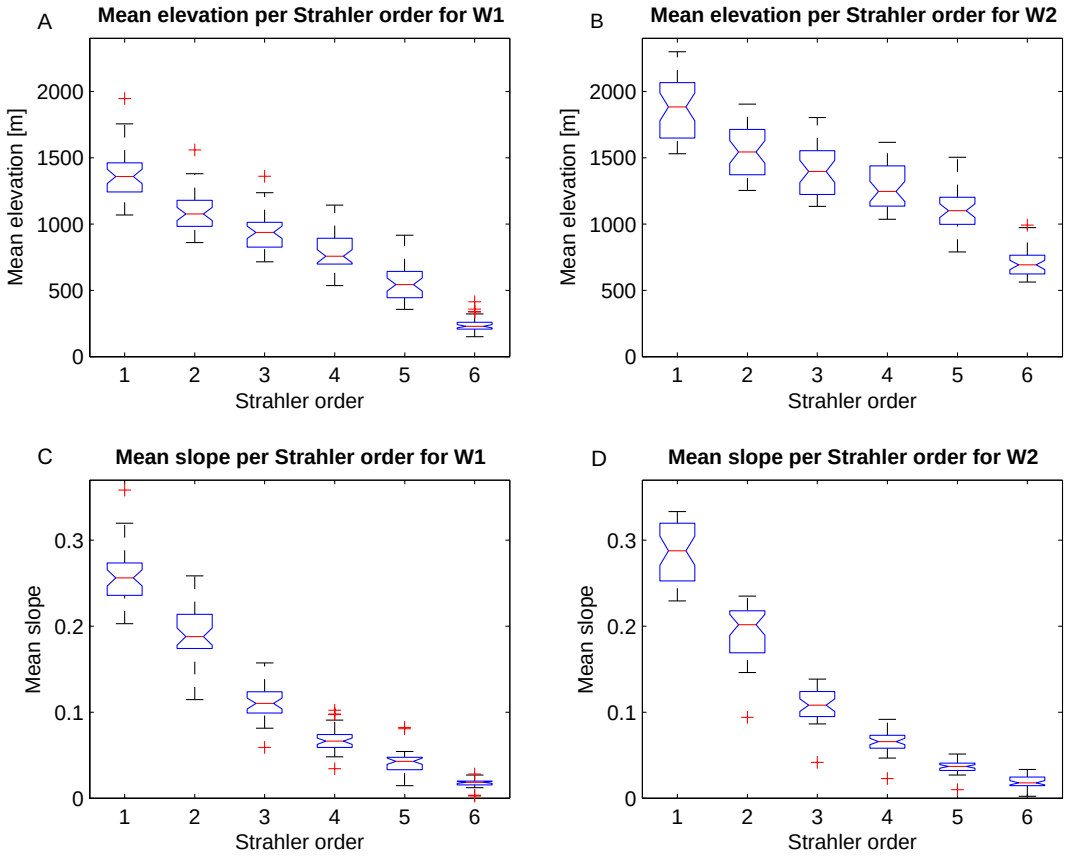

Figure 11: Variation of mean elevation (A,B) and mean slope (C,D) per Strahler order across 100 MCS realisations for the two selected watersheds W1 (A,C) and W2 (B,D).

4 Discussion

4.1 Uncertainty model

4.1.1 Data quality

On deriving the initial error surface for the Alps, a number of patterns presented themselves on a first visual inspection. Error appeared to be correlated with the underlying terrain, with large error values following the main ridge of the Alps. Error also appeared to be correlated with aspect, as different error signs appeared to be distributed on the either side of the major valleys. Comparable patterns were found for the other two test areas. This hints at luff side overestimation and lee side underestimation of elevation values by radar sensors, suggesting that our assumption of error free SRTM data may have been wrong. An equally likely cause would be a systematic misregistration between GLOBE and SRTM data. Tests confirmed that correlation of GLOBE and SRTM improves when their locations are systematically shifted, and consequently standard deviation of derived error decreases. However, the necessary shift is inconsistent across the three test areas and even across different subsets of the same test area, and the improvement is only minimal. In the Alps, the differences in GLOBE DEM production from DTED - median values from USGS/GTOPO in France versus spot sampling in the southwestern corner of the GLOBE

cell for the rest of the Alps excluding the Italian part (GLOBE Task Team & others, 1999) - become apparent as they result in different shifts of the data subsets in relation to SRTM. This heterogeneity, amongst other data quality issues, is likely to be the reason why error distributions showed only weak correlation with aspect when analysed, due to a significant scattering of the values, despite obvious visual dependency of error with aspect (Fig. 3). Furthermore, although correlation can be improved when using sinus transfer functions for aspect, the necessary functions vary considerably for the three areas, and global values that improve aspect-error correlation for all data sets could not be found. This again suggests a possible misregistration of GLOBE DEM data during the combination of different local sources. However, by using aspect only to predict the sign of error values, it proved to be a valuable parameter in locally autocorrelating error surfaces across areas of similar aspect.
Taking the above into consideration, it is unclear what causes the observable SW - NE trend in the spatial configuration of autocorrelation depicted in Fig. 4. While it corresponds with the general flight path of the Shuttle Radar Topography Mission (Eineder et al., 2001), Guth (2006) reported diamond shaped patters for error encountered in 1" SRTM data for the United States. At this point it is difficult to determine whether SRTM error is large enough to influence the regression analysis, as the overall vertical accuracy of SRTM for the selected study areas is reported to be less then 5 m (Rodriguez et al., 2005) which is much less than the reported RMSE values for GLOBE. By using CGIAR STRM data, voids in the original SRTM data have been filled, and interpolated values have thus been integrated in the regression analysis. Especially for the Alps data set, voids are common at very high altitudes. However, as these voids have been carefully filled and the respective altitude values are less important for the Fennoscandian study area, void-filled DEM data have been used for ease of processing and analysis. The use of SRTM30 for comparison with GLOBE would have been an alternative to the use of SRTM3, which would have avoided the problem of void-filling and resampling. Tests have shown that SRTM30-derived error surface show similar, yet slightly smaller correlations. Furthermore, a key aim in our experiments was to start with a dataset which had undergone as little preprocessing as possible and thus could be considered to be "ground truth" and SRTM3 was judged to be optimal for this task.
A further effect visible in the error surface for the Alps, is the pronounced change in error magnitude visible along the Italian border (Fig. 3), which confirms the suggested better agreement of the data source used for the compilation of the Italian part of the GLOBE data (Hastings and Dunbar, 1998) with SRTM data. This fact is not explicitly accounted for in the uncertainty model but was discussed as a possible error source in section 1.2.

4.1.2 Quality of the uncertainty model

While analysis suggests an overestimation of uncertainty by our model for the Italian part of the Alps, it suggests that our method of deriving error from averaged SRTM data is valid: the better accordance with terrain characteristics of the Italian data at 1km resolution is well captured by the derived error surfaces. At the same time, the global uncertainty model fits all three test areas equally well (Table. 6), suggesting the impact of this data heterogeneity to be tolerable. The correlation coefficients were broadly similar for the three datasets (Alps, Pyrenees and Turkey) over which they were derived and, based on this result, an uncertainty model was used in which it was assumed that the mean regression parameters for these three areas could be used for any areas with similar descriptive statistics and terrain types, given that the nominal data sources are the same. The distribution of the derived and modelled error align relatively well (Fig. 7), with

proportions of positive and negative error, mean and standard deviation and skewness of both distributions agreeing. However, the modelled errors have greater magnitudes (positive and negative) than the original error surface as suggested by its lower kurtosis. This is mainly due to the random proportion of error that can not be correlated with terrain attributes and constitutes the uncertainty of this unknown error proportion. Although it may be possible to tune the model to better replicate this feature of the distribution, a method to perform this tuning whilst preserving the dependence of error on terrain features in space proved difficult. This combination of deterministic and stochastic model components makes it difficult to definitively assess the quality of the uncertainty model compared to the derived error, particularly because of both the heterogeneity of the error and the need to consider both aspatial and spatial error distribution characteristics.

4.1.3 Improving the error model

Semivariogram maps of the derived error surfaces all show a characteristic directional trend, but with a very short range. This is due to the heterogeneity of the observed error, with large areas of small scale, gradually changing error, contrasting with the large error values that abruptly change sign, following the main valleys and ridges. Although directional effects were detected and directional variograms of the error surfaces shown to feature varying range values, the range of the convolution filter in the error model was derived from an omnidirectional variogram map. Using a directional variogram map to derive a convolution filter could improve simulation of correlation in spatial error. Alternatively, analysis of subregions and the application of local semivariograms to the modelled uncertainty data could also improve the simulation of the local amount of spatial autocorrelation. A correlation analysis of the range of autocorrelation of the error with respect to attributes of the underlying terrain would be the next step towards an advanced uncertainty model, e.g. following the approach of Kyriakidis et al. (1999) who used stochastic simulation with varying local uncertainty models. The model presented here does not calculate mean errors of zero for every grid cell when error surfaces are averaged over a large number of runs, as information on the likely sign and magnitude of error is included in the model. This suggests that such errors could be treated as systematic or trends as defined in section 1.2 and should be eliminated prior to analysing and modelling uncertainty. However, this result only holds for certain terrain types within the study data, and correlations were not good enough to clearly identify systematic errors and trends. The model presented aims to provide a means of estimating uncertainty for larger scales, and for the whole of the study area, the simulated uncertainty, averaged over a larger number of realisations, sums to zero for all tested DEMs.

If the model is to be transferred to areas without available SRTM reference data, such as Fennoscandia, the modelling of residuals from error magnitude regression (Eq. 2) can not be done using correlation with derived error. As the residual distribution is symmetric, a simulation using transferred random normal distribution might be possible.

Alternative concepts for modelling GLOBE error using artificial neural networks (ANN) (Behrens et al., 2005) have been explored for the Alps test area using the same set of derived terrain parameters. While the general, systematic error patterns were reproduced well after filtering of the training data, sensible integration of the filtered random error proved to be difficult. However, the use of ANNs might be a viable approach when trying to reproduce systematic, correlated DEM error.

4.2 Example application

The purpose of providing an example application to illustrate the use of an uncertainty model focussed on improving our understanding of the influence of uncertainty in elevation values of widely used digital elevation products on a range of popular topographic indices commonly calculated in the literature. We illustrate these examples on a DEM in the Alps, but we deliberately do not draw any conclusions on the geomorphological implications of these results - rather we restrict ourselves to commenting on differences between parameters for different realisations.

4.2.1 Summary global statistics

When calculating global statistics, it is clear that most of the illustrated terrain parameters are very robust to the uncertainty in elevation modelled. The single exception is the slope of the first order streams. This result makes sense, since first order streams are likely to be found in the roughest areas (where there is the least terrain convergence) and thus are also most susceptible to uncertainty in elevation values. These results do not however suggest that uncertainty is unimportant in considering terrain derivatives, but rather that when globally averaged the effects of uncertainty tend to cancel themselves out.

4.2.2 Watershed derivation and derived statistics

The results for the derivation of watersheds have some important differences from the global statistics calculated. Firstly, they show that the number of watersheds is sensitive to terrain uncertainty, with a considerable variation in the total number of watersheds derived (Fig. 9). Since not every pixel in the DEM is assigned to a watershed, the number of watersheds can grow whilst the number of larger watersheds remains roughly constant and the number of smaller watersheds increases. This result suggests that terrain uncertainties lead to a migration of pour points upstream and that edge effects are of potential importance in limiting the possible number of watersheds derived. Calculation of descriptive statistics per watershed show that, once again, these results are relatively robust with the exception of slope. In this case, statistically significant differences exist between median values of slope at the $p = 0.05$ level. Importantly, slope is no longer averaged according to Strahler order, but rather according to watersheds. However, since the majority of cells are assigned to first order streams, it is likely that the variability in these values strongly influences this statistic.

4.2.3 Comparison of two watersheds

The final set of comparisons between the two catchments show the greatest variability, and thus is perhaps of the most immediate importance to geomorphology. The spatial extents of W1 and W2 vary by over 320% and 290% respectively between their smallest and largest extents. This sensitivity in watershed area to elevation uncertainty is much larger than that reported by Jamieson et al. (2004) for changes in watershed delineation as a function of resolution. Changes in watershed area also have a significant impact on all other terrain variables summarised per basin. For example, hypsometric curves show considerable difference in form varying from convex to S-shaped (Fig. 10). These results are important, since comparison and interpretation of hypsometric curves are typical geomorphological tasks, and our result suggests that uncertainties in elevation may have a significant influence on the hypsometric curves. Where hypsometric curves and integrals are automatically derived, care is required to ensure that the results are robust to potential uncertainties

in elevation.
Furthermore, larger variations in topographic parameters occur not for W1, which varies the more in area, but W2 where the overall elevation is higher and thus the terrain surface is rougher and uncertainty is correspondingly greater. Furthermore, since most of the uncertainty in catchment area in W2 is found in relative "flatlands", the capture of small areas of relatively constant elevation can significantly change the distribution of both elevation and slope, especially those assigned to lower order streams. These values also vary for W1, but less markedly, presumably because uncertainty in elevation here results in the capture of areas of both high and low relief.
A proviso is required here - GLOBE data appear to have been fitted to a river network algorithmically. Thus, derivation of watershed areas with GLOBE tends to yield few surprises and authors have reported good agreement between GLOBE and other, higher resolution datasets (Jamieson et al., 2004). The modelled uncertainty surfaces result in considerable deviations from the watersheds derived by the hydrologically corrected GLOBE data. However, they provide a realistic estimate of the uncertainties present in a lower accuracy DEM product and, we believe, suggest a transferrable methodology for estimating the impacts of errors in elevation on the derivation of geomorphological indices.

5 Conclusions

This paper has introduced a methodology for, firstly, calculating an error surface and, secondly, based on regression with topographic indices, applying such error surfaces in developing uncertainty models which may be used in assessing the impact of uncertainty in elevation on specific geomorphological studies. The derivation of error surfaces is an important first step in assessing the likely sources of error, and where these errors are predominantly systematic, in suggesting ways to detrend data and thus reduce the influence of error. Where errors contain a significant stochastic component, as is the case here, the use of Monte Carlo Simulation provides a tractable tool for investigating the implications of uncertainty in elevation on both the derivation of geomorphological indices and, as is our intention in future work, the effects of uncertainty on more complex process models.
Application of the model to a case study showed that global statistics describing elevation, hypsometry and mean relative catchment area were relatively robust to uncertainty, though slope, particularly for low order streams showed large values of uncertainty. When comparative statistics for 6th order watersheds were calculated, some statistically significant differences in mean watershed slope were found, though most parameters were once again robust to uncertainty. The most striking results concerned the impact of uncertainty on two large watersheds, where hypsometric curves, catchment area, elevation and slope were all shown to have considerable uncertainty as a function of uncertainty in elevation values.

Acknowledgements

This research is funded by the Swiss National Science Foundation (SNF Project Number 200020-109449). We are grateful for useful discussions with Jo Wood and Pete Fisher (City University London), Phaedon Kyriakidis (Department of Geography, UCSB), Adrian Roellin (Institute for Mathematics, University of Zurich) and Oliver Korup (WSL, Davos) in formulating some of the

ideas in this paper. We would also like to thank Ian S. Evans and Peter L. Guth for their constructive reviews which helped us to considerably improve this paper.

References

Bamber, J. L., Bindschadler, R. A., 1997. An improved elevation dataset for climate and ice-sheet modelling: validation with satellite imagery. Annals of Glaciology 25, 439–444.

Behrens, T., Förster, H., Scholten, T., Steinrücken, U., Spies, E.-D., Goldschmitt, M., 2005. Digital soil mapping using artificial neural networks. Journal of Plant Nutrition and Soil Science 168, 21–33.

Burrough, P. A., McDonnel, R. A., 1998. Principles of Geographic Information Systems. Oxford University Press.

Carabajal, C. C., Harding, D. J., 2005. ICESat validation of SRTM C-band digital elevation models. Geophysical Research Letters 32, L22S01.

Carlisle, B. H., 2000. The highs and lows of DEM error - developing a spatially distributed DEM error model. In: Proceedings of the 5th International Conference on GeoComputation. University of Greenwich, United Kingdom, pp. 23–25.

Chaplot, V., Darboux, F., Bourennane, H., Leguédois, S., Silvera, N., Phachomphon, K., 2006. Accuracy of interpolation techniques for the derivation of digital elevation models in relation to landform types and data density. Geomorphology 77, 126–141.

Codilean, A. T., Bishop, P., Hoey, T. B., 2006. Surface process models and the links between tectonics and topography. Progress in Physical Geography 30, 307–333.

Ehlschlaeger, C. R., Goodchild, M. F., 1994. Uncertainty in spatial data: Defining, visualizing, and managing data errors. In: Proceedings of GIS/LIS 1994. Phoenix AZ, pp. 246–53.

Eineder, M., Breit, H., Adam, N., Holzner, J., Suchandt, S., Rabus, B., 2001. SRTM X-SAR calibration results. IEEE International Geoscience and Remote Sensing Symposium, 2001. IGARSS'01. 2, 748–750.

Endreny, T. A., Wood, E. F., 2001. Representing elevation uncertainty in runoff modelling and flowpath mapping. Hydrological Processes 15, 2223–2236.

Evans, I. S., 1980. An integrated system of terrain analysis and slope mapping. Zeitschrift für Geomorphologie Suppl. Bd. 36, 274–295.

Finlayson, D. P., Montgomery, D. R., 2003. Modeling large-scale fluvial erosion in geographic information systems. Geomorphology 53, 147–164.

Fisher, P. F., 1998. Improved modeling of elevation error with geostatistics. GeoInformatica 2:3, 215–233.

Fisher, P. F., Cheng, T., Wood, J., 2004. Where is Helvellyn? Fuzziness of multi-scale landscape morphometry. Transactions of the Institute of British Geographers 29, 106–128.

Fisher, P. F., Tate, N. J., 2006. Causes and consequences of error in digital elevation models. Progress in Physical Geography 30, 467–489.

Gallant, J., Wilson, J., 2000. Primary topographic attributes. In: Wilson, J., Gallant, J. (Eds.), Terrain Analysis: Principles and Applications. John Wiley & Sons, Chichester, pp. 51–85.

GLOBE Task Team & others, 1999. The Global Land One-kilometer Base Elevation (GLOBE) Digital Elevation Model, Version 1.0. Digital data base on the World Wide Web (URL: http://www.ngdc.noaa.gov/mgg/topo/globe.html) and CD-ROMs. National Oceanic and Atmospheric Administration, National Geophysical Data Center, 325 Broadway, Boulder, Colorado 80303, U.S.A.

Guth, P. L., 2006. Geomorphometry from SRTM: comparison to NED. Photogrammetric Engineering and Remote Sensing 72, 269–277.

Harding, D. J., Gesch, D. B., Carabajal, C. C., Luthcke, S. B., 1999. Application of the shuttle laser altimeter in an accurarcy assessment of GTOPO30, a global 1-kilometer digital elevation model. International Archives of Photogrammetry and Remote Sensing. 17-3/W14, 81–85.

Hastings, D. A., Dunbar, P. K., 1998. Development and Assessment of the Global Land One-km Base Elevation Digital Elevation Model (GLOBE). ISPRS Archives 32, 218–221.
URL `http://www.ifp.uni-stuttgart.de/publications/commIV/commIV.htm`

Hebeler, F., Purves, R. S., 2004. Representation of topography and its role in uncertainty: a case study in ice sheet modelling. In: GIScience 2004: Proceedings of the Third International Conference on Geographic Information Science. pp. 118–121.

Heipke, C., Koch, A., Lohmann, P., 2002. Analysis of SRTM DTM - methodology and practical results. In: Journal of the Swedish Society for Photogrammetry and Remote Sensing: Photogrammetry meets Geoinformatics. Vol. 2002:1. pp. 69–80.

Herrington, L., Pellegrini, G., 2000. An advanced shape of country classifier: Extraction of surface features from DEMs. In: 4th international conference on GIS and environmental modeling (GIS/EM4). Problems, Prospects and Research Needs. Banff, Alberta, Canada. pp. 2–8.

Heuvelink, G. B., 1998. Error propagation in environmental modelling with GIS. In: Fisher, P., Raper, J. (Eds.), Research Monographs in Geographic Information Systems. Taylor & Francis.

Hodgson, M. E., 1998. Comparison of angles from surface slope/aspect algorithms. Cartography & Geographic Information Systems 25, 173–185.

Holmes, K. W., Chadwick, O., Kyriakidis, P., 2000. Error in a USGS 30-meter digital elevation model and its impact on terrain modeling. Journal of Hydrology 233, 154–173.

Hugentobler, M., Purves, R. S., Schneider, B., 2004. Evaluating methods for interpolating continuous surfaces from irregular data: case study. In: Proccedings of the 11th International Symposium on Spatial Data Handling. University of Leicester, pp. 109–124.

Hunter, G. J., Goodchild, M. F., 1997. Modelling the uncertainty of slope and aspect estimates derived from spatial databases. Geographical Analysis 19, 35–49.

Hurtrez, J. E., Sol, C., Lucazeau, F., 1999. Effect of drainage area on hypsometry from an analysis of small-scale drainage basins in the Siwalik hills (central Nepal). Earth Surface Processes and Landforms 24, 799–808.

Hutchinson, M., Gallant, J., 2000. Digital elevation models and representation of terrain shape. In: Wilson, J., Gallant, J. (Eds.), Terrain Analysis: Principles and Applications. John Wiley & Sons, Chichester, pp. 29–50.

Jamieson, S. S. R., Sinclair, H. D., Kirstein, L. A., Purves, R. S., 2004. Tectonic forcing of longitudinal valleys in the Himalaya: morphological analysis of the Ladakh Batholith, North India. Geomorphology 58, 49–65.

Jarvis, A., Reuter, H., Nelson, A., Guevara, E., 2006. Void-filled seamless SRTM data V3, available from the CGIAR-CSI SRTM 90m Database: http://srtm.csi.cgiar.org. International Centre for Tropical Agriculture (CIAT).

Jarvis, A., Rubiano, J., Nelson, A., Farrow, A., Mulligan, M., 2004. Practical use of SRTM data in the tropics: Comparisons with digital elevation models generated from cartographic data. Working Document 198, 32 p., International Centre for Tropical Agriculture (CIAT), Cali, Columbia.

Jones, K. H., 1998. A comparison of algorithms used to compute hill slope as a property of the DEM. Computers & Geoscience 24, 315–323.

Kyriakidis, P. C., Shortridge, A., Goodchild, M., 1999. Geostatistics for conflation and accuracy assessment of digital elevation models. International Journal of Geographical Information Science 13, 677–707.

Liu, H., Jezek, K. C., Li, B., 1999. Development of an antarctic digital elevation model by integrating cartographic and remotely sensed data: A geographic information system based approach. Journal of Geophysical Research 104, 23199–23214.

Lythe, M., Vaughan, D. G., BEDMAP-Consortium, 2001. BEDMAP: A new ice thickness and subglacial topographic model of antarctica. Journal of Geophysical Research 106 (B6), 11335–11352.

Marshall, S. J., 2002. Modelled nucleation centres of the Pleistocene ice sheets from an ice sheet model with subgrid topographic and glaciologic parameterizations. Quaternary International 95-96, 125–137.

MATLAB, 2006. R2006b Documentation. The Mathworks Inc., 3 Apple Hill Drive Natick, MA 01760-2098 USA.

Montgomery, D. R., 2001. Slope distributions, threshold hillslopes, and steady-state topography. American Journal of Science 301, 432–454.

Nye, J., 1957. The distribution of stress and velocity in glaciers and ice sheets. Proceedings of the Royal Society of London Sr A 239, 113–133.

Oksanen, J., Sarjakoski, T., 2005a. Error propagation analysis of DEM-based drainage basin delineation. International Journal of Remote Sensing 26, 3085–3102.

Oksanen, J., Sarjakoski, T., 2005b. Error propagation of DEM-based surface derivatives. Computers & Geoscience 31, 1015–1027.

Oksanen, J., Sarjakoski, T., 2006. Uncovering the statistical and spatial characteristics of fine toposcape DEM error. International Journal of Geographical Information Science 20, 345–369.

Pollard, D., 1983. A coupled climate-ice sheet model applied to the quaternary ice ages. Journal of Geophysical Research - Oceans and Atmospheres 88 (NC12), 7705–7718.

Rodriguez, E., Morris, C. S., Belz, J. E., Chapin, E. C., Martin, J. M., Daffer, W., Hensle, S., 2005. An assessment of the SRTM topographic products. Technical Report JPL D-31639, Jet Propulsion Laboratory, Pasadena, California.

Schneider, B., 1998. Geomorphologically sound reconstruction of digital terrain surfaces from contours. In: Proceedings of the 8th International Symposium on Spatial Data Handling. pp. 657–667.

Schneider, B., 2001. On the uncertainty of local form of lines and surfaces. Cartography and Geographic Information Science 28, 237–247.

Shortridge, A. M., 2001. Characterizing uncertainty in digital elevation models. In: Hunsaker, C., Goodchild, M., Friedl, M., Case, T. (Eds.), Spatial Uncertainty in Eecology: Implications for Remote Sensing and GIS Applications. Springer, New York, pp. 238–257.

Shortridge, A. M., 2006. Shuttle radar topography mission elevation data error and its relationship to land cover. Cartography and Geographic Information Science 33, 65–75.

Staley, D. M., Wasklewicz, T. A., Blaszczynski, J. S., 2006. Surficial patterns of debris flow deposition on alluvial fans in death valley, ca using airborne laser swath mapping data. Geomorphology 74, 152–163.

Strahler, A. N., 1952. Hypsometric (area-altitude curve) analysis of erosional topography. Bulletin of the Geological Society of America 63, 1117–1141.

Sun, G., Ranson, K. J., Kharuk, V. I., Kovacs, K., 2003. Validation of surface height from shuttle radar topography mission using shuttle laser altimeter. Remote Sensing of Environment 88, 401–411.

Tarboton, D. G., 1999. TARDEM, a Suite of Programs for the Analysis of Digital Elevation Data. Utah State University, 8200 Old Main Hill, Logan, UT 84322-8200, USA.

Tucker, G. E., Lancaster, S. T., Gasparini, N. M., Bras, R. L., Rybarczyk, S. M., 2001. An object-oriented framework for hydrologic and geomorphic modeling using triangulated irregular networks. Computers & Geoscience 27, 959–973.

USGS, 1996. GTOPO30: Global 30 arc second elevation data. Online at http://edc.usgs.gov/products/elevation/gtopo30.html, EROS Data Center, Sioux Falls, SD.

Walker, J. P., Willgoose, G. R., 1999. On the effect of digital elevation model accuracy on hydrology and geomorphology. Water Resources Research 35, 2259–2268.

Wechsler, S. P., July 1999. Digital elevation model (DEM) uncertainty: Evaluation and effect on topographic parameters. In: ESRI User Conference 1999 Proceedings. San Diego, CA, online at http://www.gis.usu.edu/docs/protected/procs/esri/1999/PROCEED/abstracts/a262.htm.

Wechsler, S. P., 2006. Uncertainties associated with digital elevation models for hydrologic applications: a review. Hydrology and Earth System Sciences Discussions 3, 2343–2384.

Weibel, R., Heller, M., 1991. Digital terrain modelling. In: Maguire, D., Goodchild, M., Rhind, D. (Eds.), Geographical Information Systems: Principles and Applications. John Wiley & Sons, Chichester, pp. 269–297.

Wise, S. M., 1998. The effect of GIS interpolation errors on the use of digital elevation models in geomorphology. In: Lane, S. N., Richards, K. S., Chandler, J. H. (Eds.), Landform Monitoring, Modelling and Analysis. John Wiley & Sons, Chichester.

Wise, S. M., 2000. Assessing the quality for hydrological applications of digital elevation models derived from contours. Hydrological Processes 14, 1909–1929.

Wood, J. D., 1996. The geomorphological characterisation of digital elevation models. Ph.D. thesis, University of Leicester, UK.

Wood, J. D., 1998. Modelling the continuity of surface form using digital elevation models. In: Proceedings of the 8th International Symposium on Spatial Data Handling. pp. 725–36.

Zhang, X., Drake, N. A., Wainwright, J., Mulligan, M., 1999. Comparison of slope estimates from low resolution DEMs: scaling issues and a fractal method for their solution. Earth Surface Processes and Landforms 24, 763–779.

Appendix C

Hebeler, F. & Purves, R.S. 2008: Modelling DEM data uncertainties for Monte Carlo Simulations of Ice Sheet Models.
In: A. Stein, J. Shi & W. Bijker: Quality Aspects in Spatial Data Mining, CRC Press, Boca Raton, p.175-196

MODELLING DEM DATA UNCERTAINTIES FOR MONTE CARLO SIMULATIONS OF ICE SHEET MODELS

Felix Hebeler and Ross S. Purves

Department of Geography
University of Zurich
8057 Zurich, Switzerland
fhebeler@geo.unizh.ch, rsp@geo.unizh.ch

KEY WORDS: GIS, DEM/DTM, Error, Correlation, Impact Analysis, Modelling, Reference Data, Glaciology

ABSTRACT:

For realistic modelling of digital elevation model (DEM) uncertainty, information on the amount and spatial configuration is needed. However, common DEM products are often distributed with global error figures at best. Where no higher accuracy reference data is available, assumptions have to be made about the spatial distribution of uncertainty, that are often unrealistic. In order to assess the impact of DEM uncertainty on the results of an ice sheet model (ISM) for an area where no higher accuracy reference data was available, we quantified DEM error of comparable regions with available reference data. Deriving good correlation of error magnitude and spatial configuration with DEM characteristics, these dependencies were incorporated into an uncertainty model containing both deterministic and stochastic components. The developed uncertainty model proved to reproduce amount and spatial correlation of DEM error well while producing uncertainty surfaces suitable for Monte Carlo Simulations (MCS). Applying the model to a DEM of Fennoscandia, a MCS was conducted using an ISM during the first 40ka of the Last Glacial Maximum (LGM). Results showed DEM uncertainty to have significant impact on model results during nucleation and retreat of the ice sheet.

1 INTRODUCTION

All modelling is susceptible to the introduction of uncertainties to model results throughout the modelling chain. During data acquisition systematic error, measurement imprecision or limited accuracy of sensors can introduce ambiguities to measured values. Preprocessing and preparation of data to meet model needs, such as reprojecting, scaling or resampling the data introduces uncertainty. Finally, the methods and algorithms used as well as effects such as computational precision during modelling can introduce further uncertainties to results.

As all modelling is a mere abstraction of much more complex processes, that in many cases might not be fully understood, uncertainties are also an intrinsic part of the approach. Uncertainties are thus not necessarily a problem in modelling, but rather an inherent component of the process, as long as the sources and bounds of the uncertainties associated with individual models are known and understood. Where this is the case, sensitivity tests can be conducted to assess the susceptibility of model results to uncertainties in certain data, parameters or algorithms and compare these uncertainties with the sensitivity of model runs to variations in individual parameters. Decision makers have become increasingly familiar with such methodologies, through for example the scenarios presented in IPCC reports (IPCC, 2001).

While uncertainties inherent in spatial data have been the focus of a number of research projects in the GIScience community, many users of spatial data either completely neglect this source of uncertainty or consider it less important than for example, parameter uncertainties. However, even if a modeller is aware of the uncertainties introduced through, for instance a Digital Elevation Model (DEM), it is not always straightforward or even possible to assess them, e.g. when metadata from the data producers is incomplete, incorrect or missing. If this information cannot be reconstructed, assumptions have to be made that might or might not be realistic and sensible for testing the impact of uncertainties in spatial data on a model.

In this paper, we use the term 'error' when referring to the deviation of a measurement from it's true value. This implies that elevation error of a DEM can only be assessed where higher accuracy reference data is available (Fisher and Tate, 2006). Error is inherent in any DEM, but is usually not known in terms of both magnitude and spatial distribution, thus creating uncertainty. 'Uncertainty' is used in this context, where a value is expected to deviate from its true measure, but the extent to which it deviates is unknown, and can only be approximated using uncertainty models (Holmes et al., 2000).

1.1 Motivation

Ice sheet models, which are commonly used to explore the linkage between climate and ice extent either during past glacial periods, or to explore the response of the Earth's remaining large ice masses (the Greenland Ice Cap and the Antarctic Ice Sheet) to future climate change, run at relatively low resolutions of the order of 1-20km, for a number of reasons. Since the models run at continental or even global scales, computational capacities as well as assumptions in model physics limit possible modelling resolutions. Furthermore, climate models used to drive such models commonly run at even lower resolutions, and until recently the highest resolution global topographic datesets had nominal resolutions of the order of 1km. Ice sheet modellers commonly resample the highest available resolution data to model resolutions - for example in modelling ice extents in Patagonia a 1km resolution DEM was resampled to 10 and 20km respectively (Purves and Hulton, 2000). While it is often assumed that data accuracy of 1km source data is essentially irrelevant when resampled to 10 or 20km, previous work has suggested that these uncertainties can have a significant impact on modelled ice sheet extents and volumes (Hebeler and Purves, 2005).

Despite the recognised need (Kyriakidis et al., 1999), most DEM data is still distributed with little metadata - usually at best global values such as RMSE or standard deviation of error are given (Fisher and Tate, 2006). Information on spatial distribution of uncertainties is almost always not available, and assumptions made about the distribution of uncertainties are often debatable (Fisher and Tate, 2006, Wechsler, 2006, Oksanen and Sarjakoski, 2005, Weng, 2002, Holmes et al., 2000).

Following the approach of Hagdorn (2003) in reconstructing the Fennoscandian ice sheet during the last glacial maximum (LGM), we wanted to test the sensitivity of the model results to DEM data uncertainty. Hagdorn used GLOBE DEM data as input topography, for which accuracy figures are given as global values depending on the data source e.g. vertical accuracy of 30m at the 90% confidence interval for data derived from DTED (Hastings and Dunbar, 1998), with no information on spatial configuration or dependencies of uncertainties or error. Thus in order to assess the impact of uncertainty in the DEM on the ISM, a realistic model of GLOBE DEM uncertainty must also be developed which both describes dependencies of error values on the DEM and sensibly reconstructs the spatial configuration of uncertainty.

1.2 Aims

In this paper we set out to address three broad aims, which can be described as follows:

- To quantify the error in DEMs for a range of appropriate regions, using higher resolution data, and to assess the extent to which this error correlates with DEM characteristics.
- To develop a general model of DEM error for use in areas where higher resolution data are not available and simulate the spatial and numerical distribution of the remaining uncertainty stochastically.
- To apply the DEM uncertainty model in Monte Carlo Simulations of ISM runs for Hagdorn's experiments (Hagdorn, 2003) and assess the impact of modelled topographic uncertainty on ISM results.

The third aim can thus be considered as a case study of the application of a set of general techniques aimed at modelling DEM uncertainties and allowing their impact on model results to be compared with other potential sources of uncertainty.

2 MATERIALS & METHODS

The availability of SRTM data makes the evaluation of GLOBE and GTOPO30 data accuracy possible for large areas of the globe (Jarvis et al., 2004, Harding et al., 1999), and thus it is possible to retrospectively evaluate previous experiments that used GLOBE DEM as input data. However, since our study area of Fennoscandinavia lies outside the region covered by SRTM data (CIAT, 2006), no direct assessment of error using higher accuracy reference data is possible.
Our approach was thus as follows. Firstly, regions with similar topography and data sources to Fennoscandia, but lying within regions covered by SRTM data were identified. Secondly, error surfaces were generated by assuming the SRTM data to be a higher quality data source for these regions. A model of error, incorporating a stochastic component, which represents a generalised uncertainty model for all regions was then developed. Using this model it is possible to perform MCS simulations with the ISM, since the stochastic component of the uncertainty model means that multiple uncertainty surfaces can be generated.

2.1 DEM data

For the analysis of typical GLOBE DEM uncertainty, three datasets were selected based on previous tests which showed that uncertainty in the GLOBE DEM data was highest in high altitude and high relief areas. Such areas are also central to ice sheet inception (Marshall, 2002, Sugden et al., 2002) and thus likely to be particularly susceptible to uncertainty. To derive the uncertainty

DEM	Alps	Pyrenees	Turkey	Scand
Altitude	1 - 4570m	1 - 3276m	1 - 4938m	0 - 2191m
Mean	692.8m	651.9m	1066.5m	189.5m
STD	624.8m	481.2m	738.4m	207.4m
Skewness	1.65	0.86	0.55	3.09
Kurtosis	5.46	3.86	2.29	15.0
Source	DTED*	DTED	DTED	DTED
Size (cells)	1083108	720000	816837	6094816

Table 1: Descriptive statistics for the three test areas and the Fennoscandian study site used. * *Italian data provided by Servizio Geologico Nazionale (SGN) of Italy.*

model for Fennoscandia, GLOBE data for the European Alps, the Pyrenees and the eastern part of Turkey were selected. These regions have relatively similar properties in terms of hypsometry (Fig. 1) and statistics describing elevation values (Table 1) and were all compiled from DTED data, with the exception of the Italian part of Alps where data were sourced from the Italian national mapping agency (Hastings and Dunbar, 1998). For

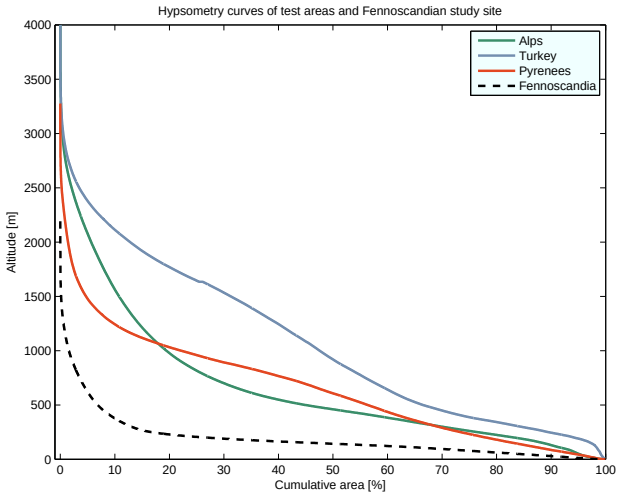

Figure 1: Hypsometry of the three selected test areas (solid lines) and the Fennoscandian study area (dashed), calculated from GLOBE DEM data at 1km resolution. Test areas show relative large proportions of the high areas that are of interest in the study site DEM of Fennoscandia. Altitudes above 4000m cropped for better visibility.

the three selected test areas, hole-filled SRTM data at 100m resolution (CIAT, 2006) were resampled to align with the GLOBE DEM at 1km resolution (GLOBE Task Team & others, 1999), using the mean of all SRTM cells within the bounds of the corresponding GLOBE data cell (Jarvis et al., 2004). Waterbodies were eliminated from all datasets, and error surfaces for the respective test areas were calculated by subtracting the GLOBE data from the averaged SRTM data. SRTM data in this approach is thus used as ground truth and considered error free. Like any data source, SRTM does of course contain errors (Sun et al., 2003, Heipke et al., 2002) - however their magnitude and spatial distribution was considered negligible for this experiment.
Calculations on the data sets were conducted using the original, unprojected WGS84 spatial reference which both SRTM and GLOBE DEM data are distributed in. For calculation of slope and related parameters, all DEMs were projected to Albers Equal Area projections (using WGS84 geoid), with the projection parameters chosen to minimise distortion for every region and minimise any further uncertainty introduced by the process (Montgomery, 2001).

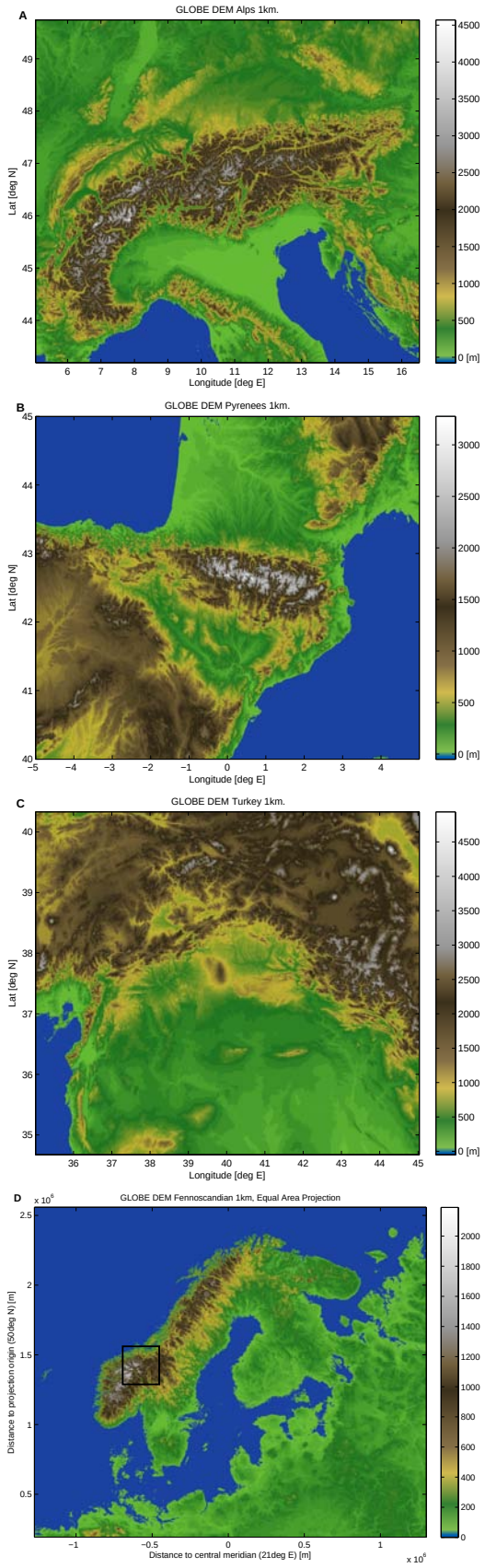

Figure 2: GLOBE DEM of the three test areas and the study site at 1km resolution. From top to bottom: (A) Alps, (B) Pyrenees, (C) Turkey (WGS84), (D) Fennoscandia (AEA).

2.2 Uncertainty model

Having derived error surfaces, they were first visually inspected. Descriptive statistics were calculated for each of the three areas and hypsometric curves and histograms compared. To assess spatial autocorrelation of both the DEM and the calculated error surfaces, semivariogram maps were derived for both the complete data sets as well as characteristic regions (e.g. for areas with high relief). Additionally, local Moran's I was calculated for all surfaces (Wood, 1996). Error, error magnitude and error sign were then tested for correlation with a set of terrain attributes and parameters (Table 2), where all neighbourhood analysis was conducted with a 3x3 window, which was found in to give the highest correlation values in pre-tests. Stepwise regression anal-

Altitude	Value of GLOBE cell
Error	Deviation of GLOBE from mean SRTM value
Error Magnitude	Magnitude of error
Sign	Sign of error (+1/-1)
Aspect	Direction of first derivative of elevation
Slope	Magnitude of first derivative of elevation
Plan Curvature	2nd derivative orthogonal to direction of steepest slope
Profile Curvature	2nd derivative in direction of steepest slope
Total Curvature	Compound curvature index
Maximum- Mean- extremity Minimum-	Deviation of center cell from max/mean/min of 3x3 neighbourhood
Roughness (Altitude)	Standard deviation of altitude in a 3x3 neighbourhood
Roughness (Slope)	Standard deviation of slope in a 3x3 neighbourhood

Table 2: Attributes, derivatives and indices used during correlation analysis. Extremity index calculated after Carlisle (2000).

ysis was used to find the best descriptive variables for modelling error in each of the three testing areas. The derived regression factors were averaged to formulate a general regression model for all three areas. Using this general regression, the residuals for each of the areas were also analysed to assess their dependency on the properties of the original DEM (Table 2). Again, a method to reproduce the characteristics common to the residuals of all three test area was sought, and combined with the first regression equation. In order to reproduce the spatial autocorrelation encountered in the original error surfaces, the uncertainty surfaces modelled using the above method were then transformed to a normal distribution and filtered using a Gaussian convolution filter (Ehlschlaeger et al., 1997, Hunter and Goodchild, 1997) using kernel sizes derived from autocorrelation analysis of the original error surfaces. The modelled uncertainty surfaces were next compared with the derived true error surfaces in terms of both their spatial and statistical distribution.
The developed uncertainty model was used to calculate a suite of 100 uncertainty surfaces for Fennoscandia that were superimposed on the original GLOBE DEM and used as input topographies for a MCS using the ISM.

2.3 Ice Sheet Model runs

The ISM used in these experiments is the GLIMMER model (Hagdorn et al., 2006), which was developed as part of GENIE (Grid Enabled Integrated Earth system model) and is freely available. For our experiments, we followed the approach of (Hagdorn, 2003) and ran simulations at 10km resolution for the 40 thousand years from approximately 120ka to 80ka BP. Climate forcing (essentially describing temperature and input mass) is based on an equilibrium line altitude (ELA) parameterisation (The ELA is the altitude at which net accumulation is zero - above the

	Range	Mean	STD	Skew.	Kurt.
Alps	-1140-1169m	3.3m	82.2m	0.05	11.61
Pyrenees	-920-797m	4.2m	68.8m	-0.14	14.23
Turkey	-817-964m	3.0m	70.7m	-0.04	11.29

Table 3: Descriptive statistics of derived GLOBE DEM error from three test areas.

Error Magnitude	Alps	Pyrenees	Turkey
Local Model	0.441	0.406	0.423
Global Model	0.430	0.393	0.422

Table 4: r^2 values of the regression modelling the amount of error for the three test areas. The good fit using the regression coefficients of the local model (top row) is retained when using the averaged global coefficients on each of the three areas (bottom row).

ELA mass accumulates, and below it ablates) derived from the Greenland ice core project (GRIP) data. Model runs have a time step of one year, and simulated ice thickness (and thus extents) are output to file every 500 years. Input topographies for the GLIMMER simulations consist of the GLOBE DEM data with added uncertainty surfaces derived from 1km uncertainty surfaces created by the uncertainty model, projected to Albers Equal Area projection and resampled to 10km resolution using bilinear interpolation. This method was chosen as it is a standard resampling technique applied by ice sheet modellers, and therefore is more representative for the study then the method of averaging of all contribution cells used in resampling SRTM to 1km (compare section 2.1).

3 RESULTS

3.1 Uncertainty model

Error properties Initial visual inspection of the derived error surfaces shows the high spatial correlation of error along prominent terrain features within the data set (compare Figures 2a and 3a), with reduced autocorrelation in areas of low relief. The distribution of error magnitude and sign also suggests some error dependencies on data sources, most visible through the lower overall error in the Italian part of the Alps seen in Figure 3a. Global autocorrelation analysis using semivariogram maps showed the range of autocorrelation to lie between 2 and 4km for each dataset, with directional trends following the orientation of prominent terrain features in the original DEMs. These semivariogram maps are strongly influenced by the semivariogram properties of high relief areas, since areas of low relief show little to no spatial autocorrelation at these resolutions. Calculated values of local Moran's I reinforce these findings. The statistic distribution of error (Table 3) shows comparable distributions for all three areas.

Error correlation Correlation analysis of error with the parameters presented in Table 2 showed relatively weak correlations with coefficients of between 0.2 and 0.5 for mean extremity, curvature and aspect for all datasets. Testing the magnitude of error for correlation resulted in higher correlation coefficients for minimum extremity, roughness of altitude, slope and altitude with values of up to 0.66. In a third analysis using binary logistic regression, the sign of error showed some correlation with aspect and minimum extremity, with 55-65% of the original error sign modelled correctly, depending on the test area. All parameters that exhibited a significant correlation with either error or error magnitude were included in a stepwise regression analysis. The best fit for modelling error was achieved with three parameters (mean extremity, curvature and aspect) yielding an r^2 of around 0.23. Regression of the magnitude of error gave an average r^2 of 0.42 (Table 4) using only two variables roughness (altitude) and minimum extremity. Taking the mean of the corresponding factors from all three test areas gave the following regression equation for modelling the amount of error:

$$abs(\varepsilon) = 0.53 \times roughness + 0.031 \times extremity_{min} + 7.6 \quad (1)$$

This regression was found to capture 50-70% of the measured error magnitude for the three test areas. As results of regression on error were considerably weaker, only the regression on error magnitude was used in the uncertainty model. Slope and its derivatives are therefore not used in the model and the analysis was continued on the unprojected WGS84 datasets.
Using 1, residuals were calculated for the three test areas and analysed. Residuals showed to be centered around a mean of 0 with a standard deviation of 43-50m, minimum values of around -300m and their maxima at 600-900m. This resulted in mildly skewed (skewness 1.7-2.4) distributions with high kurtosis of 10-18. The residuals were found to be well approximated using a modified random normal distribution ($N[0, 45]$). Squaring the residuals and randomly reassigning the signs to center the distribution around 0 again, then downscaling through a division by 100 proved to be a simple and satisfactory way to simulate regression residuals, while introducing a stochastic component to the uncertainty model.
Since only the magnitude of error showed a useful correlation, the sign of the modelled uncertainty was modelled separately for the uncertainty model. Although equation (2), derived from binary logistic regression showed agreement of only 55-65% of modelled against true error sign, the regression proved to capture the spatial correlation of the error sign well, at the cost of an overestimation of positive error of the order of 10-20%:

$$S = -0.0012 \times extremity_{mean} + 0.002 \times aspect - 0.2 \quad (2)$$

where $-1 \leq S \leq 1$. Further analysis confirmed that the closer the modelled values were to either +1 or -1, the higher the probability that the error's sign was modelled correctly. For the three test areas, almost all values higher than 0.6 or lower than -0.6, respectively, modelled the error sign correctly. Thus, a stochastic element was introduced for modelling error sign, where a random number r was drawn from a standard normal distribution for every value of S. Where $r \leq abs(S) + f$, with the correction factor $f = 0.35$, the modelled sign was kept, otherwise the sign was assigned randomly. This resulted in a ratio of positive to negative modelled error close to the measured error, while retaining most of the spatial characteristics of the sign distribution.
Combining the three steps, that is modelling the dependence of the error, residuals ($resid$) and error sign resulted in the following uncertainty model:

$$U_{tot} = (abs(\varepsilon) + resid) \times S \quad (3)$$

Finally, the modelled surfaces, though correctly representing the statistical distribution of error, did not yet take full account of the spatial autocorrelation of error. A Gaussian convolution filter (Oksanen and Sarjakoski, 2005) was thus applied to the modelled uncertainty raster by transforming the distribution of modelled uncertainty to a normal distribution and applying a convolution filter with a kernel range of 3km (3cells). After the filtering, the uncertainty raster was transferred back to its original distribution. QQ-plots show the distribution to be altered only minimally, with the added advantage that unrealistically noisy parts of the surface were effectively smoothed.

Modelled uncertainty surfaces Modelled uncertainty surfaces show a good correspondence in spatial configuration with the de-

	Mean	Max	Min	STD	Skew.	Kurt.	Sum
Mean	0.64	560	-561	40.5	0.0	8.7	$3.8E^6$
STD	0.02	54.8	53.7	0.02	0.0	0.03	$8.9E^4$

Table 5: Mean and standard deviation of the distribution statistics of 100 modelled uncertainty surfaces for Fennoscandia. Uncertainty modelled in meters.

rived error surfaces (Figure 3). The general dependencies visible in the derived error surfaces (Figure 3A) are generally preserved in the modelled uncertainty (Figure 3B), due to the regression component of the model. The small scale distribution of modelled uncertainty is generally noisier than that of the error, with the autocorrelation introduced through convolution filtering clearly visible (Figure 3B, inset). Comparing the histograms of

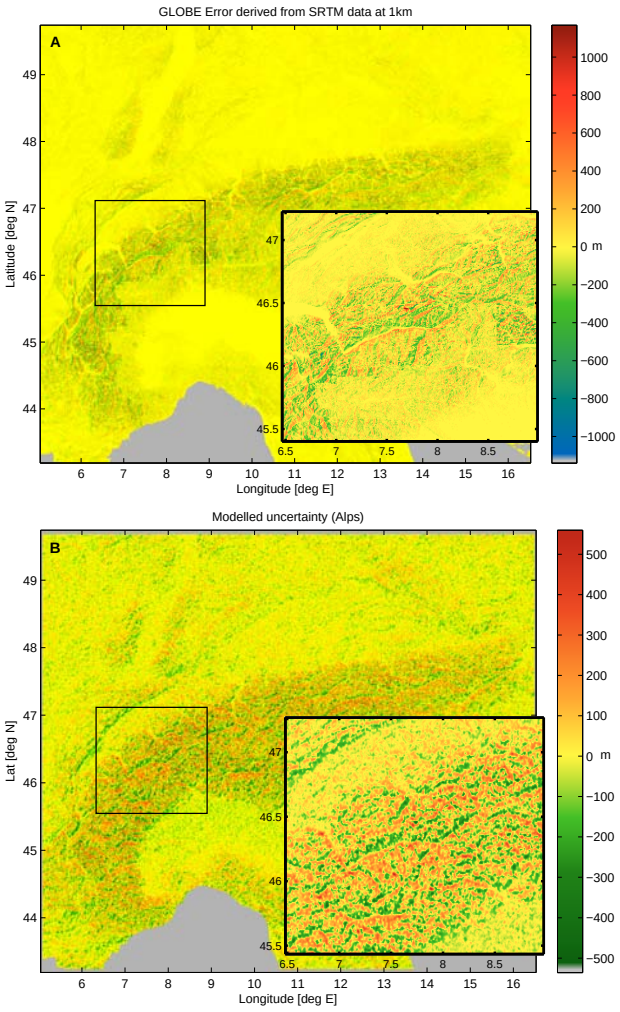

Figure 3: GLOBE error surfaces for the Alps derived using SRTM reference data (A), and modelled uncertainty surface (B) both with detail inset.

the derived error with the modelled uncertainty (Figure 4) shows good accordance, with an underestimation of values close to zero and an overestimation of values around the standard deviation of the distribution. Extreme error values are not reproduced by the uncertainty model, and the overall sum of the modelled uncertainty for any of the test areas is within 10% of the range of derived error. Modelling a suite of 100 uncertainty surfaces for Fennoscandia (2366x2576 cells), the descriptive statistics proved to vary little (Table 5). Calculating the mean, range and standard deviation of the modelled uncertainty for every raster cell across all 100 runs (Figure 5) illustrates the influence of the de-

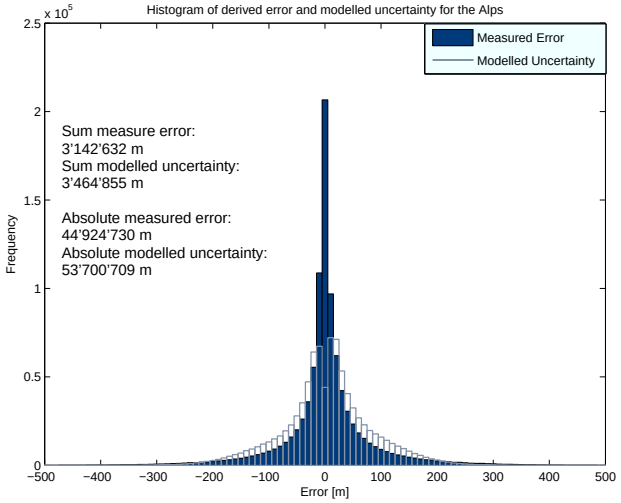

Figure 4: Histogram of the derived error for the Alps test area, compared to that of an example of a stochastically generated uncertainty surface for the same area.

terministic and the stochastic parts of the uncertainty model. For areas with mean positive or negative error, the strong influence of the sign regression results in predominately positive or negative errors. Likewise, areas of high uncertainty are likely to be the result of the regression modelling the magnitude of error following dominant landscape features. However, the two stochastic elements in the determination of error sign and modelling of the residuals introduce a stochastic component that results in imposition of noise across the raster, shown through the standard deviation and range of modelled uncertainty (Figure 5c,d).

3.2 Sensitivity study

Figure 6 and Figure 7 show a suite of representations of the influence of the modelled uncertainty in ISM results as a result of the driving temperature (Figure 6b) imposed together with the parameterisation of mass balance. Figure 6 shows the development through time of ice sheet extent and volume and the uncertainty induced in these values as a function of the DEM uncertainty, while Figure 7 illustrates the variation in ice sheet extent for a variety of snapshots in time.
These results clearly show that, firstly, uncertainty is greatest during ice sheet inception (standard deviation (STD) in extent $\sim$12%) , where uncertainties in elevation can raise or lower individual ice nucleation centres above or below the ELA. As ice centres grow and coalesce, the effects of uncertainty in topography decrease (STD in extent $\sim$3%), as the ice mass itself becomes the predominant topography. However, during periods of retreat (e.g around 20ka model years), uncertainty again increases.
Figure 7 clearly shows how with a mature ice sheet (e.g. after around 37ka model years), most uncertainty in ice sheet extent is found at the edges of the ice sheet. Once the ice sheet has reached a certain size, e.g. after approx 10ka model years, the range of uncertainty in the position of the ice front for these simulations varies between 40-100km for all later model stages. The variation is less at the NW ice front, as the bathometry rapidly lowers off the Norwegian coast and the ISM ablates ice all ice at altitudes lower than -500m. Variation of ice extent across the MCS runs is thus much higher towards Finnland and the Baltic Sea.

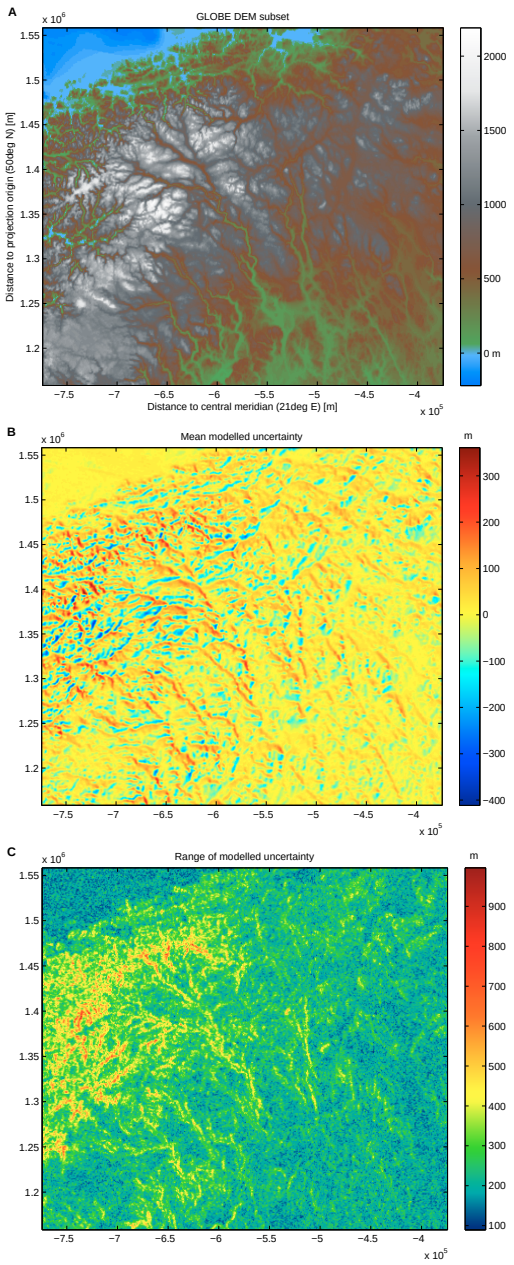

Figure 5: Part of the Fennoscandian DEM (A, inset in Figure 2D), with mean (B) and range (C) of modelled uncertainty for the area averaged over 100 surfaces.

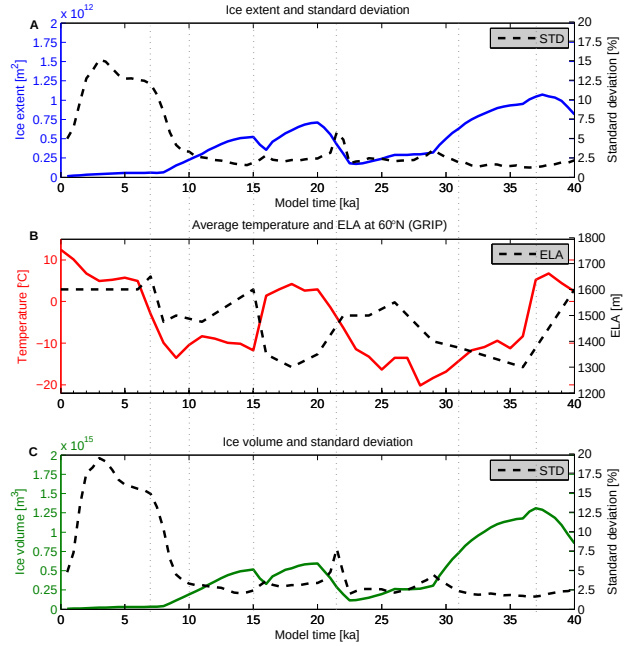

Figure 6: Mean ice extent (A) and volume (C) with their respective relative standard deviation (dashed lines) across 100 MCS runs plotted against modelling time. Climate forcing (temperature and ELA) shown in B, with vertical gray lines marking snapshot times shown in Figure 7.

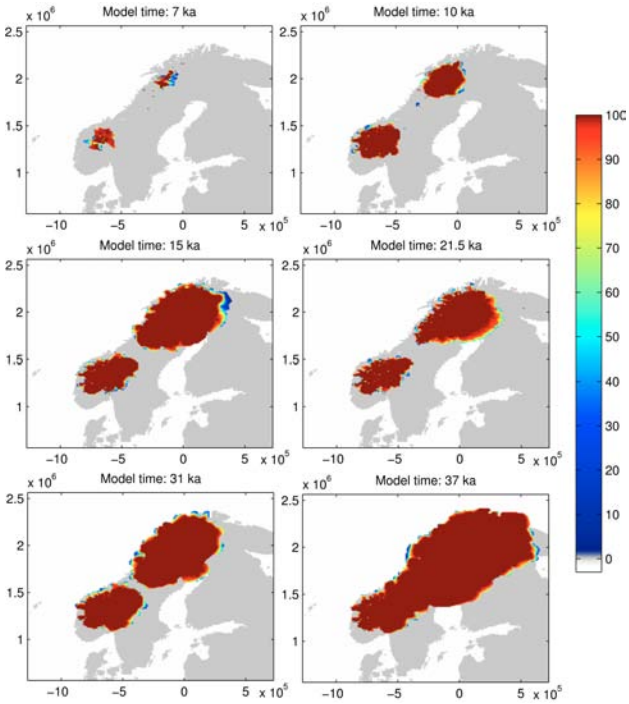

Figure 7: Frequency of DEM cells glaciated across 100 MCS runs after 7, 10, 15, 21.5, 31 and 37ka modeltime. Present time Fennoscandian coastline plotted for comparison.

4 DISCUSSION

In Section 1.2 we set out three broad aims for this work, namely to quantify DEM error for a variety of regions where higher quality data were available, to develop a general model of uncertainty based on these findings and, to apply this model to assess the uncertainty introduced into the results of ISM runs as a result of uncertainty in DEMs.

4.1 Quantifying DEM error

In assessing DEM error, we sought to identify areas which had broadly similar characteristics, based on the assumption that dependencies and characteristics of DEM error based on a DEM might be expected to be broadly similar for similar regions. Table 5 gives the descriptive statistics for error surfaces calculated for the three regions, which are broadly similar suggesting that this assumption is reasonable.

However, a further inherent assumption is that the variation in error is mainly described by terrain parameters within each region. In fact, this was found not to be the case in the Alpine region,

where error values notably decreased at the Swiss/Italian border in the Italian region of the Alps, where the original GLOBE data has a different source.
The error surfaces themselves (e.g. Figure 3a) show strong correlations of error with terrain features and, most strikingly, that error increases and is more spatially autocorrelated in areas of high relief. Initial attempts to correlate error with a range of parameters were relatively unsuccessful with low correlations, however the absolute error was found to be relatively strongly correlated with roughness and minimum extremity. Roughness in particular increases with relief, thus suggesting that the use of such a parameter is sensible. Local models with different coefficients were averaged for the 3 regions to create a global model (Equation 1) and the differences between the r^2 values generated by the local and global models found to be small, thus justifying the application of this global model in areas with similar terrain characteristics.
Examination of the residuals for the error model showed that no correlations with terrain parameters and no spatial autocorrelation. Thus this component of the error model was treated as uncertainty, along with the sign of the magnitude of error and is discussed further below.
The sign of the magnitude of the error was also examined for correlation with terrain parameters, and weak dependencies found (around 55-65% of the signs were correctly modelled by a binary logistic regression) based on aspect and mean extremity. These parameters, in particular aspect, introduce spatial autocorrelations to the error model similar to those seen running along terrain features. However, as discussed in Section 3.1 a purely deterministic approach to modelling error sign significantly overestimates positive errors, and thus a further stochastic term was introduced.

4.2 Developing an uncertainty model

The uncertainty model given in Equation 3 has three terms - absolute error, a residual and error sign. Of these 3 terms the first is purely deterministic, whilst the latter both contain stochastic elements, resulting in the generation of an uncertainty model.
Importantly for our application, the uncertainty model can be generated purely from a single DEM, thus allowing us to model uncertainty in regions where high quality data are not available. Figures 3 and 4 show a comparison between one uncertainty surface for the Alps and calculated error for the same region. The influence of the stochastic elements is immediately clear, with considerably more noise in areas of lower relief and overall, and overall greater total error (i.e the area under the curve in Figure 4). However, the range of error for the uncertainty surface is lower than that for the calculated error and the sum of positive and negative values (see Figure 4) similar.
Figure 5 shows how the uncertainty surfaces for Fennoscandinavia are themselves related to terrain features. For example, the mean modelled uncertainty is greatest in regions of high relief. The range of uncertainty illustrates clearly that areas where ice sheet inception is likely have the highest uncertainty in elevation (of the order of 800m).
The application of the convolution filter effectively smoothes extreme outliers and reduces the range of uncertainty within a given distance. This is important in many modelling applications, since outliers in particular, can lead to model instabilities (e.g. through unphysically steep slopes for a given resolution).
One important limitation of the model as it stands, lies in the similarity between the three test regions and Fennoscandinavia. Overall, Fennoscandinavia has less and lower areas of high relief by comparison to our three test regions, and therefore uncertainty may be overestimated. However, as long as this assumption is clearly stated, we believe that the application of the model is valid.
Since for Fennoscandinavia no higher accuracy reference data is available, other approaches of modelling DEM uncertainty including autocorrelation, such as stochastic conditional simulation (Kyriakidis et al., 1999) would be difficult to implement. However, if a measure of spatial autocorrelation of the error could be correlated to DEM attributes or compound indices, local information on spatial correlation could be used for improving the uncertainty surfaces produced, e.g. by using automated variogram analysis with stochastic conditional simulation (Liu and Jezek, 1999).

4.3 Case study - ISM in Fennoscandinavia

The developed uncertainty model proved to deliver surfaces that are both suitable for Monte Carlo Simulations through the inherent stochastic elements, as well as fit to run an ISM at a considerably low resolution of 10km. Earlier experiments (Hebeler and Purves, 2004) have shown that uncertainty modelled using random error in excess of 100m STD can destabilise the ISM at resolutions as low as 20km. This effect is mainly due to unreasonably high slope gradients introduced by the added uncertainty. By contrast the uncertainty model presented in this paper produces topographically sound surfaces by both incorporating information on the underlying topography as well as convolution filtering, thus avoiding unrealistic terrain configurations.
With a mean of zero and standard deviation of 40m, the introduced uncertainties for Fennoscandinavia are effectively smaller than those with standard deviations of up to 150m of previous experiments (Hebeler and Purves, 2005), but nevertheless prove to result in significantly different model results, especially during inception and retreat phases of the ISM. This implies that care has to be taken when interpreting results during these phases (Sugden et al., 2002). DEM uncertainties can influence model results in both ice sheet size and configuration during susceptible stages that may otherwise be attributed to climate or mass balance changes.
On the other hand, even though the relative variation of large ice sheets, e.g. the reconstructed Fennoscandian ice sheet after 15k and 31k model years, are relatively small in the order of 2-5% (Figure 6), the absolute difference in modelled extent is the order of 50-100km. Differences of modelled and empirically derived ice extent of ice sheets during the LGM of this order of magnitude have fueled debate over years (Hulton et al., 2002, Wenzens, 2003). In order to relate the impact of these DEM uncertainties to the effect other parameters have on ISM results, further sensitivity studies are necessary. For example stepwise variation of climate forcing, e.g. temperature and mass balance, could be applied and compared to the range of modelled ice sheet configurations this paper delivered.

5 CONCLUSIONS

In this paper, we have successfully captured the dependency of GLOBE DEM error for mountainous terrain with the underlying topography and to integrate this relationship into an uncertainty model. By applying this uncertainty model we produced spatially correlated, realistic uncertainty surfaces that are suitable for the use in Monte Carlo Simulations. Even though the amount of DEM uncertainty derived from GLOBE data was shown to have significant impact on ISM results for the Fennoscandian ice sheet during the LGM, sensitivity studies of ISM parameters and climate forcing are needed to relate the impact of DEM uncertainty e.g. to that of temperature change.
Future experiments will explore whether the developed uncertainty model could be improved by refining the selection of test

areas or through a better reproduction of local spatial autocorrelation. Porting the uncertainty model to other topographies and source data, and testing it on different resolutions, for example using SRTM and LIDAR data, will allow us to explore the sensitivity of other process models to DEM uncertainty.

ACKNOWLEDGEMENT

Felix Hebeler would like to thank Dr Phaedon Kyriakidis, UC Santa Barbara, Prof Peter Fisher and Dr Jo Wood (both City University London) as well as Dr Juha Oksanen (Finnish Geodetic Institute) for their advice and encouragement. This research is funded by the Swiss National Science Foundation (SNF Project Number 200021-100054).

REFERENCES

Carlisle, B. H., 2000. The highs and lows of DEM error - developing a spatially distributed DEM error model. In: Proceedings of the 5th International Conference on GeoComputation, University of Greenwich, United Kingdom, pp. 23–25.

CIAT, 2006. International Centre for Tropical Agriculture: Void-filled seamless SRTM data V3, available from the CGIAR-CSI SRTM 90m Database: http://srtm.csi.cgiar.org.

Ehlschlaeger, C. R., Shortridge, A. M. and Goodchild, M. F., 1997. Visualizing spatial data uncertainty using animation. Computers & Geoscience 23(4), pp. 387–395.

Fisher, P. F. and Tate, Nicholas, J., 2006. Causes and consequences of error in digital elevation models. Progress in Physical Geography 30(4), pp. 467–489.

GLOBE Task Team & others, 1999. The Global Land One-kilometer Base Elevation (GLOBE) Digital Elevation Model, Version 1.0. Digital data base on the World Wide Web (URL: http://www.ngdc.noaa.gov/mgg/topo/globe.html) and CD-ROMs. National Oceanic and Atmospheric Administration, National Geophysical Data Center, 325 Broadway, Boulder, Colorado 80303, U.S.A.

Hagdorn, M. K. M., 2003. Reconstruction of the Past and Forecast of the Future European and British Ice Sheets and Associated Sea-Level Change. unpublished PhD thesis, University of Edinburgh.

Hagdorn, M., Rutt, I., Payne, T. and Hebeler, F., 2006. GLIMMER - The GENIE Land Ice Model with Multiply Enabled Regions - Documentation. http://glimmer.forge.nesc.ac.uk/. Universities of Bristol, Edinburgh and Zurich.

Harding, D. J., Gesch, D. B., Carabajal, C. C. and Luthcke, S. B., 1999. Application of the shuttle laser altimeter in an accurarcy assessment of GTOPO30, a global 1-kilometer digital elevation model. International Archives of Photogrammetry and Remote Sensing. 17-3/W14, pp. 81–85.

Hastings, D. A. and Dunbar, P. K., 1998. Development & assessment of the global land one-km base elevation digital elevation model (GLOBE). ISPRS Archives 32(4), pp. 218–221.

Hebeler, F. and Purves, R. S., 2004. Representation of topography and its role in uncertainty: a case study in ice sheet modelling. In: GIScience 2004: Proceedings of the third international conference on geographic information science, pp. 118–121.

Hebeler, F. and Purves, R. S., 2005. A comparison of the influence of topographic and mass balance uncertainties on modeled ice sheet extents and volumes. In: Eos Trans. AGU, Fall Meet. Suppl., Vol. 86, pp. Abstract C23A–1154. No 52.

Heipke, C., Koch, A. and Lohmann, P., 2002. Analysis of SRTM DTM - methodology and practical results. In: A. Boberg (ed.), Journal of the Swedish Society for Photogrammetry and Remote Sensing: Photogrammetry meets geoinformatics, Vol. 2002:1, pp. 69–80.

Holmes, K. W., Chadwick, O. and Kyriakidis, P., 2000. Error in a USGS 30-meter digital elevation model and its impact on terrain modeling. Journal of Hydrology 233, pp. 154–173.

Hulton, N. R., Purves, R. S., McCulloch, R., Sugden, D. E. and Bentley, M., 2002. The Last Glacial Maximum and deglacation in southern South America. Quaternary Science Reviews 21, pp. 233–241.

Hunter, G. J. and Goodchild, M. F., 1997. Modelling the uncertainty of slope and aspect estimates derived from spatial databases. Geographical Analysis 19(1), pp. 35–49.

IPCC, 2001. Climate Change 2001: Synthesis Report. A Contribution of Working Groups I, II, and III to the Third Assessment Report of the Integovernmental Panel on Climate Change. Cambridge University Press, Cambridge, United Kingdom, and New York, NY, USA.

Jarvis, A., Rubiano, J., Nelson, A., Farrow, A. and Mulligan, M., 2004. Practical use of SRTM data in the tropics: Comparisons with digital elevation models generated from cartographic data. Working Document 198, Cali, International Centre for Tropical Agriculture (CIAT): 32.

Kyriakidis, P. C., Shortridge, A. and Goodchild, M., 1999. Geostatistics for conflation and accuracy assessment of digital elevation models. International Journal of Geographical Information Science 13(7), pp. 677–707.

Liu, H. and Jezek, K. C., 1999. Investigating dem error patterns by directional variograms and fourier analysis. Geographical Analysis 31, pp. 249–266.

Marshall, S. J., 2002. Modelled nucleation centres of the pleistocene ice sheets from an ice sheet model with subgrid topographic and glaciologic parameterizations. Quaternary International 95-96, pp. 125–137.

Montgomery, D. R., 2001. Slope distributions, threshold hillslopes, and steady-state topography. American Journal of Science 301(4-5), pp. 432.

Oksanen, J. and Sarjakoski, T., 2005. Error propagation of DEM-based surface derivatives. Computers & Geoscience 31(8), pp. 1015–1027.

Purves, R. S. and Hulton, N. R., 2000. Experiments in linking regional climate, ice-sheet models and topography. Journal of Quaternary Science 15, pp. 369–375.

Sugden, D. E., Hulton, N. R. and Purves, R. S., 2002. Modelling the inception of the patagonian icesheet. Quaternary International 95-96, pp. 55–64.

Sun, G., Ranson, K. J., Kharuk, V. I. and Kovacs, K., 2003. Validation of surface height from shuttle radar topography mission using shuttle laser altimeter. Remote Sensing of Environment 88(4), pp. 401–411.

Wechsler, S. P., 2006. Uncertainties associated with digital elevation models for hydrologic applications: a review. Hydrology and Earth System Sciences Discussions 3, pp. 2343–2384.

Weng, Q., 2002. Quantifying uncertainty of digital elevation models derived from topographic maps. In: D. Richardson and P. van Oosterom (eds), Advances in Spatial Data Handling, Springer, chapter 30, pp. 403–418.

Wenzens, G., 2003. Comment on: 'The Last Glacial Maximum and deglaciation in southern South America' by N.R.J. Hulton, R.S. Purves, R.D. McCulloch, D.E. Sugden, M.J. Bentley [Quaternary Science Reviews 21 (2002) 233-241]. Quaternary Science Reviews 22(5-7), pp. 751–754.

Wood, J. D., 1996. The Geomorphological Characterisation of Digital Elevation Models. PhD thesis, University of Leicester, UK.

Appendix D

Hebeler, F. & Purves, R.S. 2008: The influence of resolution and topographic uncertainty on melt modelling using hypsometric subgrid parameterisation.
Hydrological Processes 22(19), p.3887-4021

HYDROLOGICAL PROCESSES
Hydrol. Process. **22**, 3965–3979 (2008)
Published online 21 April 2008 in Wiley InterScience
(www.interscience.wiley.com) DOI: 10.1002/hyp.7034

The influence of resolution and topographic uncertainty on melt modelling using hypsometric sub-grid parameterization

Felix Hebeler* and Ross S. Purves
Department of Geography, University of Zurich, Winterthurer Str. 190, 8057 Zurich, Switzerland

Abstract:

Modelling of physical processes such as ablation or runoff at continental or global scales provides a key challenge: a high degree of abstraction is required in order to minimize computational demands, while spatial and temporal variability of key processes, often at the sub-scale level, need to be adequately captured and reproduced within a lower resolution model. For some approaches, such as temperature index models, downscaling to lower resolutions is straightforward. However a key issue when using these downscaled models is to assess the impact of scaling on model behaviour and results, including the associated uncertainties. We assess the impact of scaling on both a simple and an enhanced temperature index melt model from 100 m to 1, 5 and 10 km resolutions. Different sub-grid parameterization approaches are applied to both models across all resolutions and tested for their suitability against high-resolution reference data, with the aim of developing a robust, scalable and computationally undemanding parameterization. Results show patterns of over- and underestimation of potential melt rates for both models, with clear dependencies on scale, terrain roughness and variations of temperature thresholds, among other quantities. The sub-grid parameterizations tested in this article are found to effectively compensate these effects at little additional computational cost. Copyright © 2008 John Wiley & Sons, Ltd.

KEY WORDS melt modelling; sub-grids; parameterization; uncertainty; enhanced temperature index model; hypsometry

Received 21 September 2007; Accepted 21 February 2008

INTRODUCTION

Models are a key tool in understanding and exploring of a wide variety of systems. Since all models, by definition, are an abstraction of reality, choosing an appropriate degree of abstraction is a key task. While complex processes need to be abstracted sufficiently so they can be understood and modelled, their key properties and dependencies must be retained. The scale and complexity of the processes to be modelled as well as the target range of scales over which a model should be applicable determines a target model resolution—however, in practice both the resolution and complexity of a model are often trade-offs between our ability to understand the system, the complexity of numerical solutions at a given resolution and computational capacities (e.g. Martin and Church, 2004; Armstrong and Martz, 2003; Malanson, 1999).

One example of this challenge lies in the modelling of ablation at global scales, which is increasingly important in estimating future water resources and, for example, in deriving boundary conditions for models of the behaviour of large ice sheets. Many present day ice sheets have very narrow ablation zones in terms of typical ice sheet model resolutions and overall ice sheet extents—for instance in Greenland the ablation zone has a width of around 20–60 km in comparison to a total ice sheet width of approximately 800–1200 km and typical model resolutions of the order of 5–10 km (Alley *et al*., 2005; Ritz *et al*., 1997; Huybrechts *et al*., 1996, 1991).

A promising approach to meeting the challenge of matching models and processes of differing scales lies in the application of so-called sub-grid approaches. Sub-grid approaches involve the parameterization of properties or processes that are not resolved at the grid scale. Other methods of coping with this problem include coupled and nested modelling (e.g. Salzmann *et al*., 2007). Sub-grid modelling is characterized by storing additional layers of information on one variable while retaining the original model resolution. In geomorphological modelling,the use of hypsometric information (Strasser and Etchevers, 2003; Marshall, 2002; Marshall and Clarke, 1999) is a common approach. Rather than using one value of elevation for each model grid cell, attributes describing the hypsometry within each cell are also stored. This requires additional attributes per model cell, and attributes are most often stored in parallel grids. Sub-grid approaches can approximate information from much higher resolutions with relatively low additional computational costs for processing and storage.

If a new method of representing processes is developed, it must not only provide a means of resolving the process appropriately, its results should also be robust to uncertainty in its input parameters. This means that the inherent variation due to uncertainty in the input data should not trigger threshold effects, such as bifurcation of the model results, systematic over- or underestimation, or large deviation of model results for small variance in

* Correspondence to: Felix Hebeler, Department of Geography, University of Zurich, Winterthurer Str. 190, 8057 Zurich, Switzerland.
E-mail: felix.hebeler@geo.uzh.ch

input data. Therefore in this article we investigate three central questions:

- How does scaling impact potential melt rates calculated using temperature index models of different complexity?
- How can sub-grid approaches be used to effectively capture the variability of melt at low resolutions in mountainous regions?
- How sensitive are such approaches to typical uncertainties in input parameters?

Low resolution melt modelling

Simple temperature index models (TIM) (see for a review Hock, 2003) are often used for melt calculation in low resolution models running at continental or global scales, such as the GLIMMER ice sheet model (Hagdorn *et al*., 2006). TIMs parameterize the complex physical processes and feedbacks in melt modelling based on the observation that potential melt is related to the time a snow or ice mass is exposed to temperatures above 0 °C and the energy available for melting during this time. The potential melt energy is usually expressed as positive degree days (PDD). Melt is then calculated using a degree-day factor (DDF) which relates the temperature above 0 °C to a melt rate.

TIMs have been shown to estimate melt rates well where reference melt data to calculate DDFs and temperature data are available (Braithwaite, 1995), and can be run using a minimum of computational resources. TIMs have been applied across a variety of temporal and spatial resolutions ranging from hours and 10s of metres to decades and 10s of kilometres. However, if reference melt or temperature data is inaccurate or of insufficient spatial density, TIMs can significantly over- or underestimate melt and fail to reproduce observed spatial variation.

To overcome these limitations, TIMs have been extended by a variety of authors to incorporate a radiation component (Pellicciotti *et al*., 2005; Schneeberger *et al*., 2003; Hock, 1999; Williams and Tarboton, 1999; Cazorzi and Fontana, 1996). Via calculation of solar radiation, these extended models explicitly incorporate topographic parameters such as slope and aspect, horizon- and self-shading, as well as time of year and latitude. While *de facto* no additional input parameters are needed, potential melt distribution can be modelled at a greater level of detail, both temporally and spatially, at the cost of additional computational demands. However, calculation times as well as data requirements are low compared to those of full scale energy balance models, which is why enhanced TIMs are often favoured, especially when modelling over extended spatial and/or temporal domains.

Resolution effects and uncertainty

Where TIMs are used in low resolution models, the input topography usually has to be re-sampled, from resolutions typically in the range of 100 m to 1 km (e.g. SRTM or Global Land One-kilometre Base Elevation digital elevation models (GLOBE DEMs), Jarvis *et al*., 2006; Hastings and Dunbar, 1998) to resolutions as low as 5, 10 or even 20 km. The smoothing effect this resampling has on topography and consequently on any associated parameter has been widely noted and the subject of a number of experiments, ranging from calculation of derivatives (Florinsky, 1998; Zhang *et al*., 1999) to effects on spatial variability of parameters (Hu and Islam, 1997) and automatic analysis for environmental modelling (Albani *et al*., 2004). In hydrology, effects of scale and consequently methods to minimize these effects have been explored, for example by Armstrong and Martz (2003). The use of elevation bands and sub-grids are common approaches to preserving crucial DEM information across resolutions in hydrological and related modelling (Luce *et al*., 1999; Leung *et al*., 1996). However, scaling and parameterization can have significant impacts on model behaviour and results. In order to improve the parameterization or assess the uncertainty associated with the model results, it is important to qualify and quantify these impacts (Wechsler, 2007; Hebeler and Purves, 2008a; Endreny and Wood, 2001).

Aims

The aims of this study are thus as follows:

- To investigate the effect of varying resolutions on absolute values as well as uncertainties of calculated potential melt rates using different melt models.
- To derive a method for melt calculation at low resolutions that:
  - delivers improved melt rates (when compared to reference data)
  - is scalable
  - is robust with low overall uncertainty
  - has low computational demands

MATERIALS AND METHODS

For the experiments described in this article, potential melt for a study area is calculated using two models, namely a simple TIM and an enhanced temperature index model (eTIM), where an additional component models potential solar radiation. Potential melt is calculated at resolutions of 0·1, 1, 5 and 10 km and four sub-grid approaches using different parameterizations are compared. Figure 1 shows the schematic approach for calculating melt for each model, using different resolutions and parameterizations.

Additionally, to assess the robustness of the parameterization, the susceptibility of the different approaches to propagation of uncertainty in the input data is compared. Topographic uncertainty is simulated using a DEM uncertainty model, and its impact on calculated potential melt is explored using Monte Carlo simulation (MCS) (Hebeler and Purves, 2008a).

Hydrol. Process. **22**, 3965–3979 (2008)
DOI: 10.1002/hyp

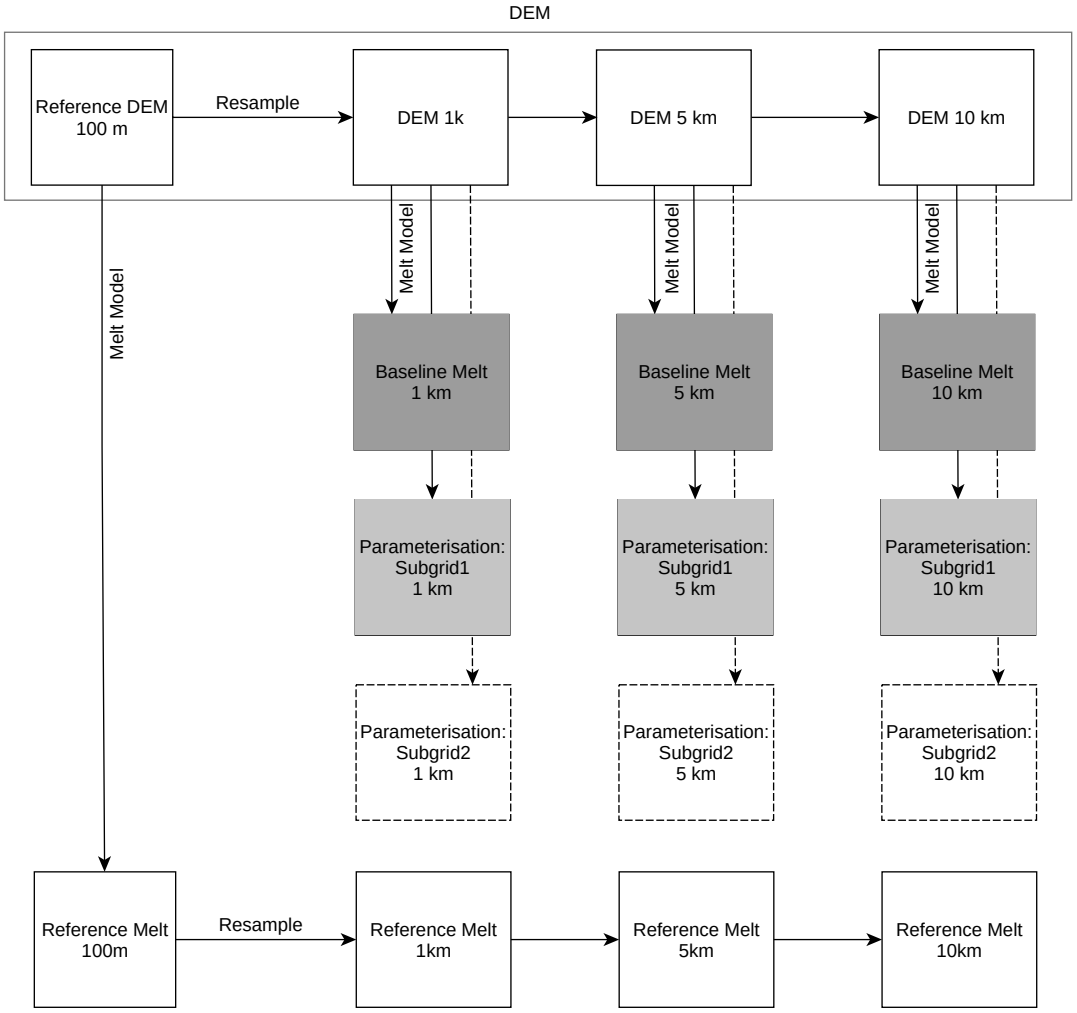

Figure 1. Experimental design: melt is calculated for resolutions of 100 m, 1, 5 and 10 km for both melt models following this scheme. At each resolution, a reference as well as an unparameterized baseline melt is calculated, and compared with alternative sub-grid parameterization approaches

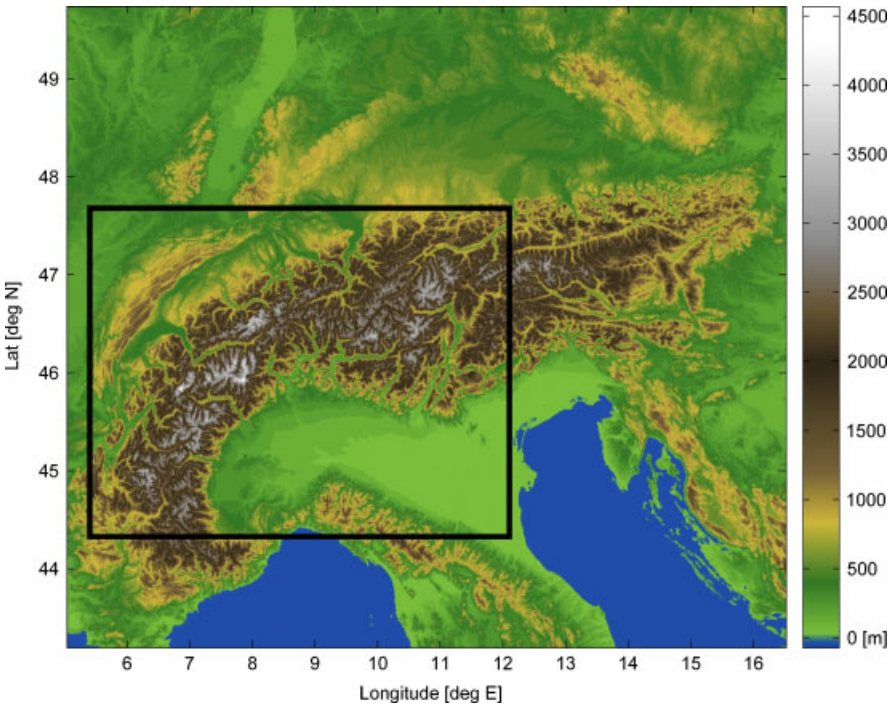

Figure 2. DEM of the European alps with the study area highlighted (solid black)

Hydrol. Process. **22**, 3965–3979 (2008)
DOI: 10.1002/hyp

Data

All model runs are conducted on a DEM of the European Alps (Figure 2). The study area lies between approximately 44 and 48°N latitude and 5 and 12°E longitude, with a total area of 201 000 km^2 and DEM altitudes ranging from sea level to 4654 m. All topography related calculations were conducted using hole-filled SRTM version 3 data at 3-arc-sec resolution (Jarvis *et al*., 2006), projected to an Albers equal area projection at 100 m resolution using bilinear re-sampling.

For the sub-grid experiments, the original DEM was re-sampled to resolutions of 1, 5 and 10 km, where the re-sampled elevation value was derived from the mean of all the 100 m grid cells within the target resolution grid cell.

Melt models

In our experiments, potential melt is calculated using a TIM and an enhanced version eTIM which includes the representation of potential solar radiation. Since a key aim of this work is to compare different sub-grid parameterization approaches for the TIM and eTIM, all model input parameters are assumed to be constant in time and space, with the exception of temperature and potential solar radiation. To avoid local effects and foster comparability, as well as limit the computational demands, a spatially constant mean annual air temperature at sea level was prescribed as input, and as a sinusoid with a period of 1 year and an amplitude of 5 °C. For each DEM grid cell, temperature is adjusted for elevation using a constant lapse rate of $-6{\cdot}5$ °C km^{-1} (Stone and Carlson, 1979).

Furthermore, since we do not wish to reproduce particular mass balance or run-off scenarios, but are investigating potential melt, only a single DDF instead of separate DDFs for ice and snow is used. If we wished to reproduce real melt rates within a glacier or ice sheet model, then such assumptions are unrealistic, as many authors have shown that DDFs for ice and snow vary between and within catchments (e.g. Braithwaite, 1995).

Temperature Index Model—TIM. A number of authors have applied simple TIMs, which all follow the basic form given by Braithwaite (1995)

$$M_{\text{pot}} = \begin{cases} DDFT & T > T_{\text{t}} \\ 0 & T \leq T_{\text{t}} \end{cases} \tag{1}$$

where DDF is the degree day factor in mm °C^{-1} d^{-1} and T is the temperature in °C. Potential melt M_{pot} is set to zero for temperatures below a certain threshold temperature T_{t}, in our case 0 °C. Melt is calculated daily for each grid cell and integrated over 1 year.

Enhanced Temperature Index Model–eTIM. In order to enhance the TIM with a component representing potential solar radiation, the approach of Pellicciotti *et al*. (2005) is adopted, and the same temperature forcing as for the simple TIM is applied. In addition to the parameterizing melt using PDD and a degree-day melt factor, this introduces a component that is directly dependent on potential direct shortwave radiation. Self- and horizon shading (Essery and Marks, 2007) are not considered in our model approach to minimize computation. Potential melt M_{pot} thus consists of a temperature term MT_{pot} and a radiation term MR_{pot}

$$M_{\text{pot}} = MT_{\text{pot}} + MR_{\text{pot}} \tag{2}$$

and is derived as:

$$M_{\text{pot}} = \begin{cases} F_{\text{t}} \cdot T + F_{\text{r}} \cdot (1-\alpha)R & T > T_{\text{t}} \\ 0 & T \leq T_{\text{t}} \end{cases} \tag{3}$$

where F_{t} is a temperature factor, T is the temperature, F_{r} is a radiation factor, α is albedo, R is the shortwave radiation at the surface and $T_{\text{t}} = 0$ °C is the threshold temperature for melt to occur (Table I). Note that the temperature factor (F_{t}) used in this equation is smaller than the commonly used DDFs (Pellicciotti *et al*., 2005). In our experiments, the potential clear-sky direct solar radiation at the surface corrected for the incidence angle I_{s} in Wm^{-2} is calculated following Kumar *et al*. (1997):

$$I_{\text{s}} = S_0 \cdot \left(1 + 0{\cdot}0344 \cos\left(\frac{360^{\circ} d}{365}\right)\right) \tau_{\text{b}} \cos i \tag{4}$$

where d[1..365] is the day of the year, τ_{b} is the atmospheric transmittance for beam radiation and i is the incident angle of the sun, which in turn is a function of the solar declination, slope and aspect. The total potential incoming solar radiation at the surface for each grid cell is then derived as follows:

$$R = I_{\text{s}} + I_{\text{d}} + I_{\text{r}} \tag{5}$$

where I_{s} is the potential direct radiation at the surface corrected for the incidence angle and atmospheric transmittance and I_d is the diffuse solar radiation, both calculated for clear-sky conditions. I_{r} is the radiation reflected from surrounding locations transmitted to the surface, calculated using a constant mean ground reflectance coefficient of 0·2, following Kumar *et al*. (1997).

Solar radiation R is calculated hourly for every grid cell and integrated over the calculated day length dt. Potential melt from solar radiation is then calculated according to Equation 3, using a relatively low, constant albedo of 0·4. While the albedos of snow, ice, debris and water range from 0·1 to 0·9 (Lefebre *et al*., 2003), a value of 0·4 attempts to represent the mean albedo over the area. At the same time, this low albedo ensures that potential melt from radiation is an important term in the eTIM model, providing a contrast with the TIM. Potential daily solar radiation is then converted to potential melt using F_{r} and added to potential daily melt derived using the daily mean temperature multiplied by the temperature factor F_{t}. As for the TIM, mean annual air temperature is varied over 1 year using a simple sinusoid function with an amplitude of 5 °C.

In this study, several simplifying assumptions have been made to facilitate computation and comparison of

Hydrol. Process. **22**, 3965–3979 (2008)
DOI: 10.1002/hyp

results, a number of which have been disputed in the literature:

- Spatially invariant input parameters are used such as sea-level temperatures, DDFs, reflectance coefficient and albedo (compare e.g. Essery and Etchevers, 2004, Hock, 2003; Lefebre *et al*., 2003).
- Potential melt is calculated using a single DDF, instead of 'real' ablation which would require a mass-balance (e.g. glacier) model and the use of separate DDFs for ice and snow (compare e.g. Hock, 2003; Braithwaite, 1995).
- A single mean albedo is used instead of different albedos for snow, ice, vegetated areas and barren ground (e.g. Pellicciotti *et al*., 2005; Lefebre *et al*., 2003), which again would necessitate a glacier model, the same holds for the reflectance coefficient.
- The threshold temperature for melt to occur is fixed at 0 °C, irrespective of the actual energy available for melt, which could cause this threshold to vary in time and space (e.g. Hock, 2005).
- Self- and horizon-shading is not considered in the radiation model, and conditions are assumed to be clear sky (e.g. Essery and Marks, 2007).

The cost of these simplifications inevitably is that any comparison with 'real' melt scenarios or observational data is not possible. However, in order to derive potential melt rates that lie within a realistic range, both melt models are tuned to approximately fit melt rates at selected locations reported by Strasser *et al.* (2004), by slightly adjusting the values for DDF and F_r used by Pellicciotti *et al.* (2005) for our case study. All adjusted parameters used in both models are given in Table I.

Method comparison

For each melt model at 1, 5 and 10 km resolution a *baseline* model run is performed without any sub-grid parameterization, that serves as a point of comparison. The aim of our sub-grid parameterizations is to give results close to the reference that mark an improvement over this baseline approach. All parameterized model runs are quantitatively compared with the baseline by calculating the root mean square error (RMSE) from the reference and qualitatively explored to describe and discuss differences between the methods.

Sub-grid parameterization

The aim of sub-grid parameterization is to capture the spatial variability of the modelled process at its original resolution, while reducing the demands for data and computation by approximating the process at a lower resolution. In the simple TIM, melt is a function of temperature, which in turn is determined by elevation via the prescribed sea-level temperature and the lapse rate. Potential melt is thus a linear function of altitude for temperatures above 0 °C. Because temperature is varied over time, a 'lower-threshold (LT altitude', equivalent to the absolute frost line) exists, which separates areas with temperatures above 0 °throughout the year, and areas where temperatures fall below zero for increasing time intervals during the year. As melt ceases during these intervals, the melt function becomes nonlinear for areas above LT. (Figure 3).

Potential melt calculated using the eTIM is influenced by temperature in a twofold manner: Firstly, the temperature dependent term of Equation 3 is equivalent to

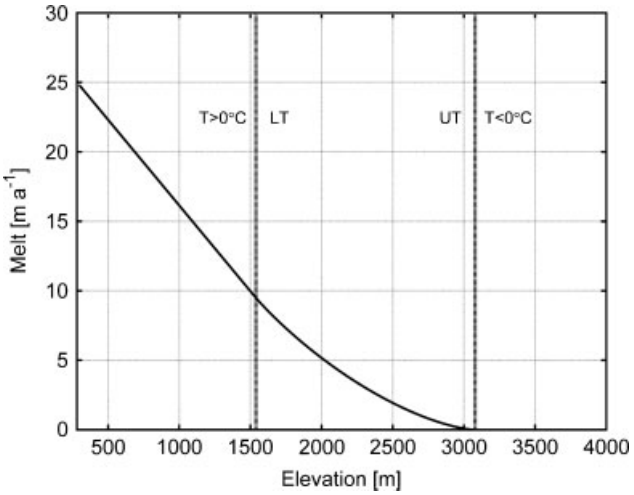

Figure 3. Potential melt as a function of altitude, calculated using the simple TIM over 1 year. Melt becomes nonlinear above a lower threshold (LT), the altitude above which temperature becomes 0 °C at least one day per year. Temperature is always below 0 for elevations above the upper threshold (UT)

Table I. Parameters used for the calculation of potential melt using the simple temperature index model and the enhanced solar radiation model

Symbol	Parameter	Value	Units
α	Albedo	0·4	
a_{seas}	Seasonal temperature amplitude	5·0	°C
DDF	Degree day factor	5·2	mm d^{-1} $°C^{-1}$
F_r	Shortwave radiation factor	0·012	m^2 mm W^{-1} h^{-1}
F_t	Temperature factor	0·05	mm h^{-1} $°C^{-1}$
lrate	Atmospheric lapse rate	−6·5	°C km^{-1}
MAAT	Mean annual air temperature at sea level	15·0	°C
r	Ground reflectance coefficient	0·2	
S_0	Solar constant	1367	W m^{-2}
T_t	Temperature threshold for melt	0	°C

Hydrol. Process. **22**, 3965–3979 (2008)
DOI: 10.1002/hyp

that of the TIM (Equation 1), and exhibits the same dependencies. Secondly, the radiation term is also influenced through temperature (Figure 4), because radiation incurred melt is also set to zero for days with temperatures below T_t (Pellicciotti *et al.*, 2005). Radiation melt can take on a range of values, for elevations below LT, as it is dependent on local slope and aspect. Because the atmospheric transmittance τ_b (Equation 4) increases with elevation, radiation melt slowly increases towards LT. Analogous to temperature inferred melt, the radiation melt decreases with elevation above LT, because temperatures fall below zero for increasing intervals during the year, and melt ceases (Figure 4).

Since in our case, the radiation melt term contributes approximately 60% of the total melt, besides elevation (through its influence on temperature), any parameterization approach must also consider the factors of slope gradient and aspect that influence the spatial variability of radiation (Figure 5).

All sub-grid approaches presented within this article are based on hypsometric parameterization, which attempts to capture the variability of elevation within a given area. Because the aim of this work is to develop and test a method that is scalable, melt is calculated for resolutions of 1, 5 and 10 km. Sub-grid values are calculated for each of these resolutions by calculating the hypsometric curve based on the topography resolved at 100 m within the respective low resolution cell. Three sub-grid layers are then created for each resolution, by storing the elevation values of the 0·15, 0·5 and 0·85 quantiles of the derived hypsometry for each cell. Thereby these sub-grids represent the mean altitude of the upper and lower 30% of elevation values and the median of all values. The thus derived elevation sub-grids are then used in all of the following parameterizations.

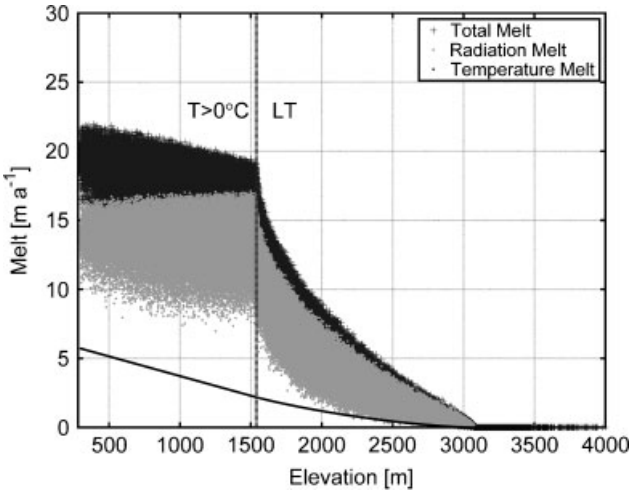

Figure 4. Potential melt plotted against elevation, calculated using the eTIM over 1 year. Below the 0 °C threshold (LT) melt values can take a range of values depending on slope and aspect. Radiation melt gradually increases with elevation (grey dots), while temperature melt (solid black line) decreases. For elevations above LT, potential radiation melt and thus total melt (dark grey +) decreases, because melt ceases for temperatures below 0 °C for increasing durations of the year

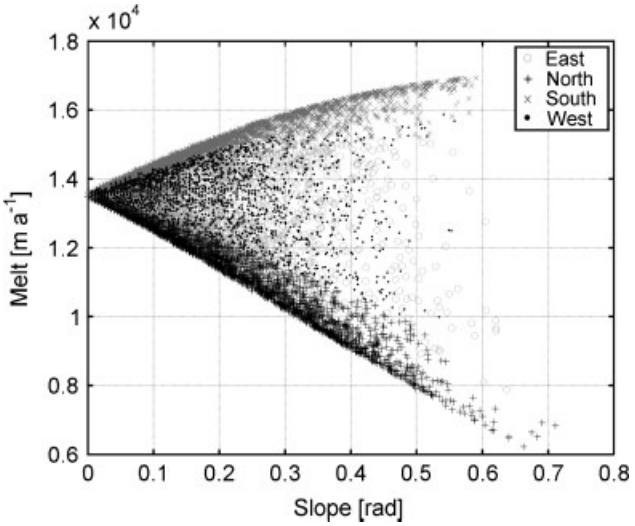

Figure 5. Potential melt from solar radiation versus slope per aspect quadrants (centred on the four cardinal directions). Melt calculated using the eTIM for elevations below the 0 °C threshold. Slope in radians. Melt increases with slope for south-facing slopes (grey x) and decreases for north-facing slopes (black +). The observable variation in calculated melt for a single slope value is caused by the variation of aspect within the respective 90° quadrant

- **Sub-grid 1** Melt is calculated separately for each of the three elevation sub-grids, weighted according to the relative hypsometric area of each sub-grid (0·3, 0·4, 0·3) and summed. For the eTIM, slope and aspect are calculated directly on each sub-grid. Because for the eTIM slope is calculated within each elevation sub-grid, the full elevation range of topography is not honoured, and the slope might be biased. While for the TIM only three sub-grids are needed, technically nine sub-grids are used for the eTIM, as slope and aspect have to be calculated for each sub-grid (Table II).
  Since the eTIM is dependent not only on elevation, but also on slope and aspect, sub-grid approaches that attempt to capture the variability of these parameters are introduced. These parameterizations are only applied to the eTIM, while sub-grid 1 is applied to both models:

Table II. Parameterization approaches used for the TIM and eTIM. All parameters/derivates not explicitly stated are calculated separately for every sub-grid

Name	Sub-grids	Description	Model
Sub-grid 1	3 (+3 + 3)	Elevation sub-grids (+ slope and aspect calculated on sub-grids for eTIM)	TIM and eTIM
Sub-grid 2	3 + 3 + 1	Elevation sub-grids + mean slope per elevation sub-grid + aspect	eTIM
Sub-grid 3	3 + 3 + 3	Elevation sub-grids + mean slope + mode of aspect per elevation sub-grid	eTIM
Sub-grid 4	5 + 4	Elevation sub-grids + mean slope per cardinal direction	eTIM

Hydrol. Process. **22**, 3965–3979 (2008)
DOI: 10.1002/hyp

- **Sub-grid 2** To avoid the biased calculation of slope within each sub-grid from the previous sub-grid 1 parameterization, for this approach slope is calculated at the reference resolution (100 m). Each cell is then classified into the elevation sub-grid class (either lower, median or upper third) to which they contribute at the low resolution (1, 5 or 10 km). The corresponding slopes are averaged for each of the sub-grids (Figure 6). While this requires one-time slope calculation at the highest resolution, slope is correctly calculated for each of the elevation sub-grids. Finally, one aspect value is calculated at the lower resolution for each cell. Thus, it is implicitly assumed that aspect values are more spatially auto-correlated and co-occur over larger areas, while the variation in slope is parameterized in the sub-grids. This gives a total of seven sub-grids for this approach (Table II).
- **Sub-grid 3** For the third approach, slope is calculated for each elevation sub-grid class identical to sub-grid 2. Additionally, we attempt to capture the variation of aspect in sub-grids. Since aspect is a 'circular' variable, no average value can be derived. In our approach, aspect is calculated at the 100 m resolution and classified into 12 nominal classes [1..12], each covering 30°. Cells are again masked at the high resolution, similar to slope (Figure 6). The mode of the aspect classes within each sub-grid elevation class (upper/median/lower) is then assigned to the corresponding sub-grid. Thus, for each elevation sub-grid cell at the lower resolution, aspect is determined by the aspect class of the majority of 100 m cells within each sub-grid elevation range.
- **Sub-grid 4** In this approach, solar radiation is calculated using four sub-grids containing the average slope in the four quadrants centred on the cardinal directions (north, south, east and west) calculated at the 100 m resolution. For each sub-grid, maximum potential melt from radiation $MR_{\max}$ is calculated irrespective of the temperature condition in Equation 3 (assuming T always $>T_t$), which delivers the maximum potential radiation melt, unreduced by temperature, over 1 year for the study area.

Additionally, five elevation sub-grids are used, adding the maximum and minimum elevation to the three previously used sub-grid elevations, giving a total of nine sub-grids for this approach (Table II). These values are then used to reduce maximum radiation melt for the amount influenced by temperature, by approximating the proportion of the area within each cell, which lies above the lower threshold (around 1500 m in Figure 4).

Potential radiation melt MR_{pot} (Equation 2) is thus calculated by reducing maximum radiation melt $MR_{\max}$ as follows:

$$MR_{\text{pot}} = MR_{\max} - MR_{\max} Q \tag{6}$$

The reduction factor Q is deduced using *reference* data calculated over 1 year at the 100 m resolution and re-sampled to the respective lower resolution of the sub-grids (compare Section 2.3). This (correctly reduced)

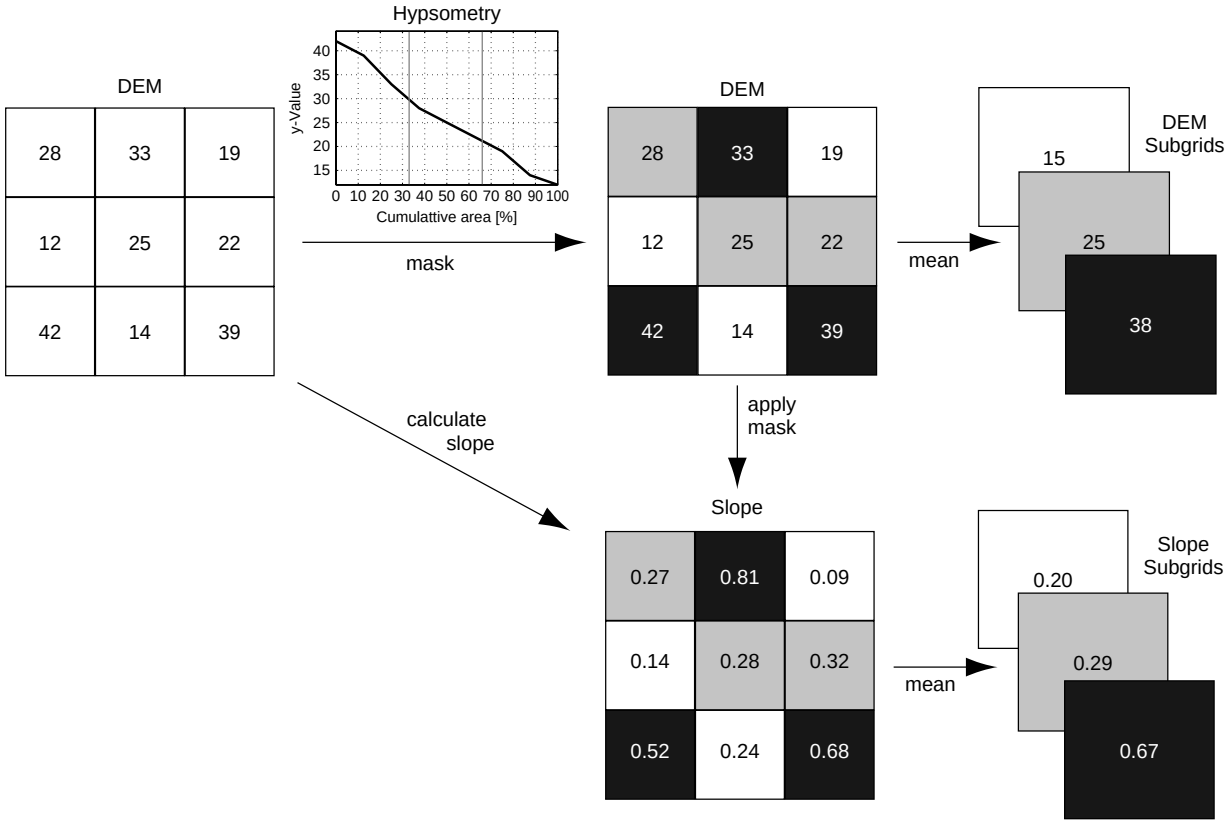

Figure 6. Scheme for calculating elevation and slope sub-grids (sub-grid 2): cells of the high-resolution DEM are masked according to the hypsometry class (upper/median/lower) they belong to at the respective lower resolution. DEM sub-grid values are directly derived using DEM quantiles, while slope is calculated per hypsometry class at the higher resolution

Hydrol. Process. **22**, 3965–3979 (2008)
DOI: 10.1002/hyp

reference radiation melt MR_{ref} is then subtracted from the unreduced radiation melt $MR_{\max}$ for each cell to derive the reduction factor Q as

$$Q = \frac{MR_{\max} - MR_{\text{ref}}}{MR_{\max}} \tag{7}$$

Q can be approximated using the following third order polynomial according to

$$Q = a_3 \cdot (t_{\text{frac}} + z_{\text{frac}})^3 + a_2 \cdot (t_{\text{frac}} + z_{\text{frac}})^2 + a_1 \cdot (t_{\text{frac}} + z_{\text{frac}}) + c \tag{8}$$

where $t_{frac}[0..1]$ is the fraction of the DEM above the LT within each cell and $z_{frac}[0..1]$ is the fraction of the DEM above the upper threshold (UT) (Figure 3).

A regression analysis to derive the terms of Equation 8 yielded similar results for the 5 and 10 km resolutions, with r^2 values above 0·96, while parameters for the 1 km resolution were outside the 99% confidence interval of both the 5 and 10 km regression, also giving a distinctively lower fit ($r^2 = 0{\cdot}84$). Parameters used for the regression in our experiments were thus chosen from the 10 km resolution regression to be $a_3 = 0{\cdot}467$, $a_2 = -1{\cdot}031$, $a_1 = -0{\cdot}114$, $c = -0{\cdot}007$. Without high-resolution reference, the fractions t_{frac} and z_{frac} have to be calculated using the five sub-grid elevations. As they have been calculated from the higher resolution hypsometry, the cumulative relative area for each sub-grid is known (0/0·15/0·5/0·85/1), and t_{frac} and z_{frac} can be approximated by linear interpolation between the cumulative area of the sub-grids below and above each threshold LT and UT.

Using t_{frac} and z_{frac} to calculate Q, the maximum radiation melt term $MR_{\max}$ can be corrected for temperature reduction to give MR_{pot} and added to the temperature melt term MT_{pot} (Equation 2), which is calculated similarly to the sub-grid 1 approach, using only the three original elevation sub-grids.

Table II summarizes the four sub-grid parameterization approaches and the total number of sub-grids required in each case.

Resolution experiments

Potential melt for both the TIM and eTIM is calculated in units of metres water equivalent per year (m w.e. a^{-1}). A set of melt rates was calculated for each model at 100 m resolution, and then re-sampled to 1, 5 and 10 km resolution by averaging melt, thus conserving mass (Figure 1). This gives a **reference** melt distribution derived from the melt rates calculated at the 100 m resolution in m w.e. a^{-1} for each resolution and model. These sets allow comparison by serving as a reference for assessing the effect of scaling, and the fit of different parameterization approaches.

Uncertainty analysis

As stated in the introduction, the aim of this work is not solely to develop an effective parameterization that gives improved results over the baseline approach, but also one that is robust towards uncertainty in the input data. Previous research (Hebeler and Purves, 2008a; Oksanen and Sarjakoski, 2005; Wechsler, 2000) has shown that sensitivity to DEM uncertainty is not constant and varies strongly for different parameters. It is therefore important to explore how sensitive sub-grid approaches are to DEM uncertainty. To assess this robustness, a DEM uncertainty model (Hebeler and Purves, 2008b) is used to simulate GLOBE DEM error. The GLOBE DEM became available at 30-arcsec resolution in 1998, and was derived from a number of different data sources. Although known to contain a number of flaws and errors, it is still widely being used and currently the only continuous DEM data set available for latitudes above 60°N. Applying the DEM uncertainty model, a suite of 100 uncertainty surfaces are produced at 1 km resolution, where each value represents the potential deviation of elevation at a location.

These surfaces are then added to the original topography and re-sampled to the corresponding target resolutions of 5 and 10 km, delivering a set of 100 different topographies for 1, 5 and 10 km resolution. Using a MCS approach, potential melt is then calculated using the simple TIM at 1 km resolution on each of the 100 surfaces and re-sampled to 5 and 10 km serving as a reference according to Section 2.5. For each 100 surfaces at 5 and 10 km, melt is also calculated using both an unparameterized (baseline) and a sub-grid approach. Finally, the mean and standard deviations of melt for each grid cell across each set of DEMs at the 5 and 10 km resolution are calculated, allowing comparison of the impact of uncertainty on melt variation across the different methods and resolutions.

RESULTS

Basic resolution effects

Comparing the **reference** potential melt across the varying resolutions, it is noticeable that melt ceases to be

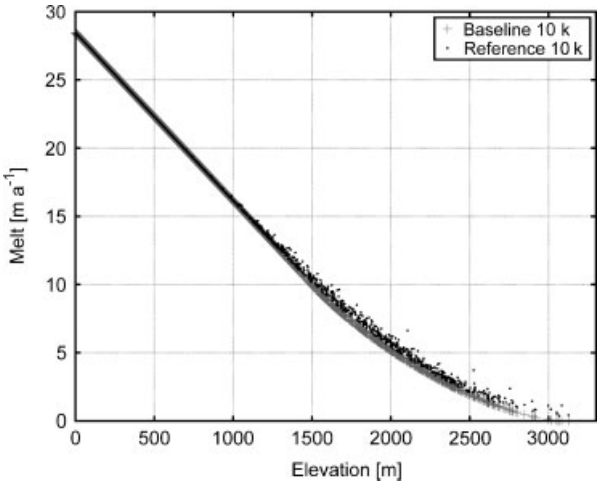

Figure 7. Baseline melt calculated on the 10 km DEM and reference melt averaged from 100 m to 10 km resolution, plotted against elevation

Hydrol. Process. **22**, 3965–3979 (2008)
DOI: 10.1002/hyp

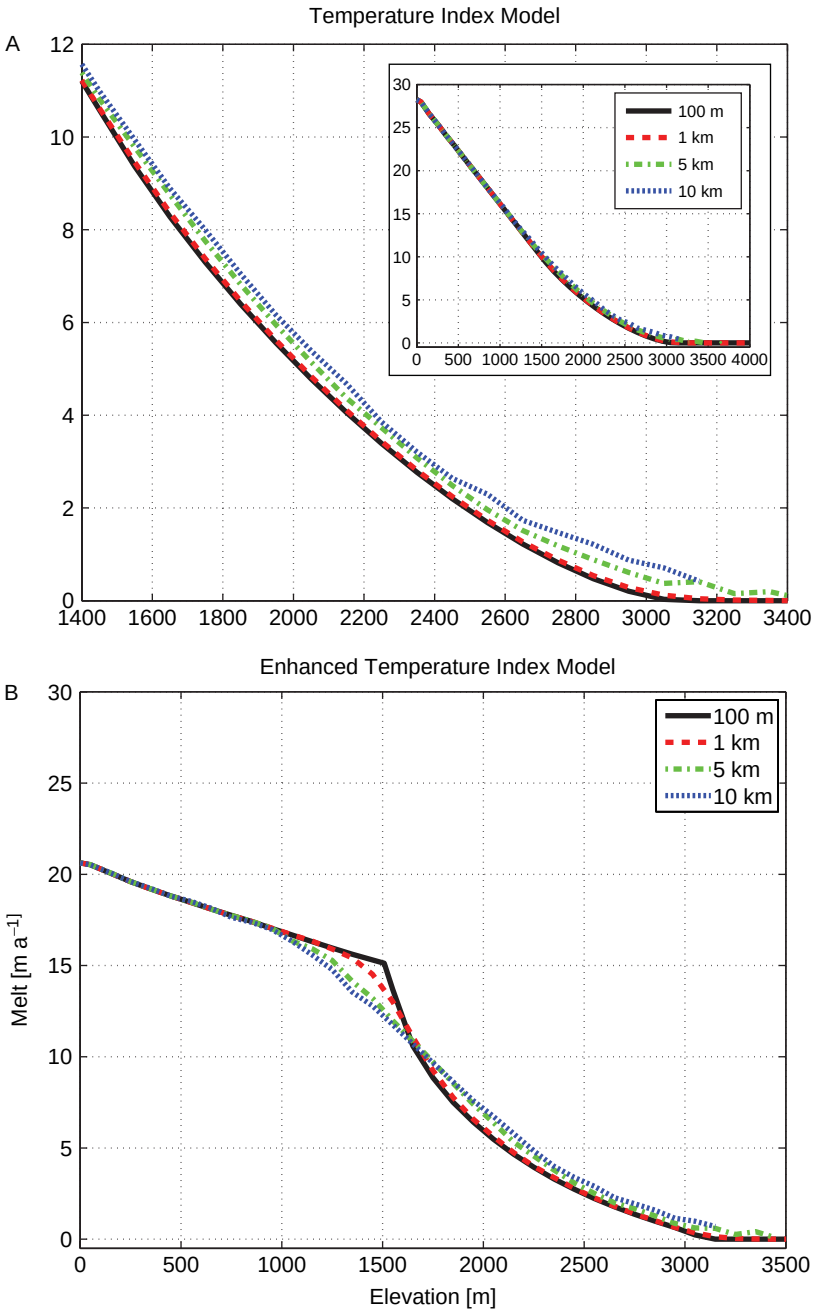

Figure 8. Mean melt versus altitude for the simple TIM (A) and the eTIM(B) for four different resolutions (0·1, 1, 5 and 10 km). For both models, the melt function becomes nonlinear above a threshold at approximately 1500 m at the reference resolution of 100 m. For areas above this threshold, temperatures are below 0 °C and melt becomes zero for increasing time spans during the year, and mean melt per altitude increases with decreasing resolution

a simple function of elevation for lower resolutions above a certain threshold elevation. Instead, potential melt can take on a range of values (Figure 7) when plotted against elevation. This effect is triggered by equifinality in the re-sampling: because of the nonlinear dependency of melt on elevation, different hypsometries at the 100 m resolution result in identical mean melt rates. While these identical melt rates are preserved through re-sampling to lower resolutions through averaging, the respective mean elevation values at the low resolution may differ. Hence different elevations at the low resolution can feature the same mean melt rates.

Figure 8A shows the mean melt within 100 m elevation bins range plotted against elevation for the different resolutions. Above a certain elevation threshold (around 1500 m in Figure 8A), for the TIM an increase in melt rates is observable for decreasing resolutions. While the same generally holds for the eTIM, there is a pronounced reduction in mean melt observable for elevations around 1500 m with decreasing resolution (Figure 8B). Compared to the high resolution reference calculated at 100 m, lower resolutions effectively show lower mean melt rates for elevations around 1500 m and higher mean melt rates for elevations above 1700 m.

Hydrol. Process. **22**, 3965–3979 (2008)
DOI: 10.1002/hyp

Table III. Mean melt and RMSE (in brackets) in m w.e. a^{-1} for the two approaches (baseline and sub-grid 1) across resolutions of 1, 5 and 10 km, compared to the corresponding reference melt for the TIM. Values are given for the whole of the study area for each resolution, as well as for areas above 1500 m and 2500 m, where temperature drops below 0 °C for increasing time spans during the year

TIM									
Resolution	1 km			5 km			10 km		
Model	All	≥1500	≥2500	All	≥1500	≥2500	All	≥1500	≥2500
Reference	17·29	4·63	0·93	17·29	5·23	1·33	17·29	5·65	1·69
Baseline	17·28 (0·38)	4·57 (0·74)	0·88 (0·66)	17·18 (0·44)	4·86 (0·84)	1·01 (0·76)	17·11 (0·34)	5·07 (0·64)	1·10 (1·65)
Sub-grid1	17·29 (0·31)	4·62 (0·34)	0·92 (0·20)	17·29 (0·19)	5·14 (0·23)	1·24 (0·02)	17·29 (0·13)	5·50 (0·17)	1·51 (0·20)

Sub-grid approaches

Figure 9A shows a comparison of calculations of potential melt modelled for the reference, baseline and sub-grid 1 approach using the TIM at 10 km resolution. Table III shows mean melt and the associated RMSE for the reference, baseline and sub-grid 1 parameterizations, while Figure 10 shows the spatial distribution of locations with no melt over the entire model region for all resolutions.

The following features are notable:

- Figure 9A shows that the relationship of melt to elevation is broadly similar for all realizations. However, above the LT elevation, Figure 9A clearly illustrates the better performance of the sub-grid 1 approach compared to the baseline.
- Table III shows that sub-grid 1 has lower RMSE values for all resolutions and elevation bands, and thus appears to better approximate the reference melt.
- The baseline and sub-grid 1 RMSE values for the 1 km model are very similar, however a significant improvement in performance is present for elevations above 1500 m and all elevation bands for the 5 and 10 km model runs.
- Areas without melt (Figure 10) are lost due to averaging using the reference approach, while the spatial pattern of melt-free areas is generally preserved using the baseline approach, with the absolute area decreasing by about half between the 1 and 10 km resolutions. Using the sub-grid 1 approach, the total number of cells without any melt (in all sub-grids) decreases with lower resolution, even though it is less pronounced than for the reference approach.

Table IV shows a comparison of three sub-grid parameterization approaches adopted for the **eTIM** with the baseline and reference potential melt. Since the sub-grid 2 and sub-grid 3 approach are very similar in their results and both have larger RMSEs than the baseline method for all resolutions, these are discarded in further reporting and comparisons are made with only sub-grids 1 and 4. Figure 9B shows the corresponding relationship between elevation and the reference, baseline and sub-grid approaches for the 10 km resolution.

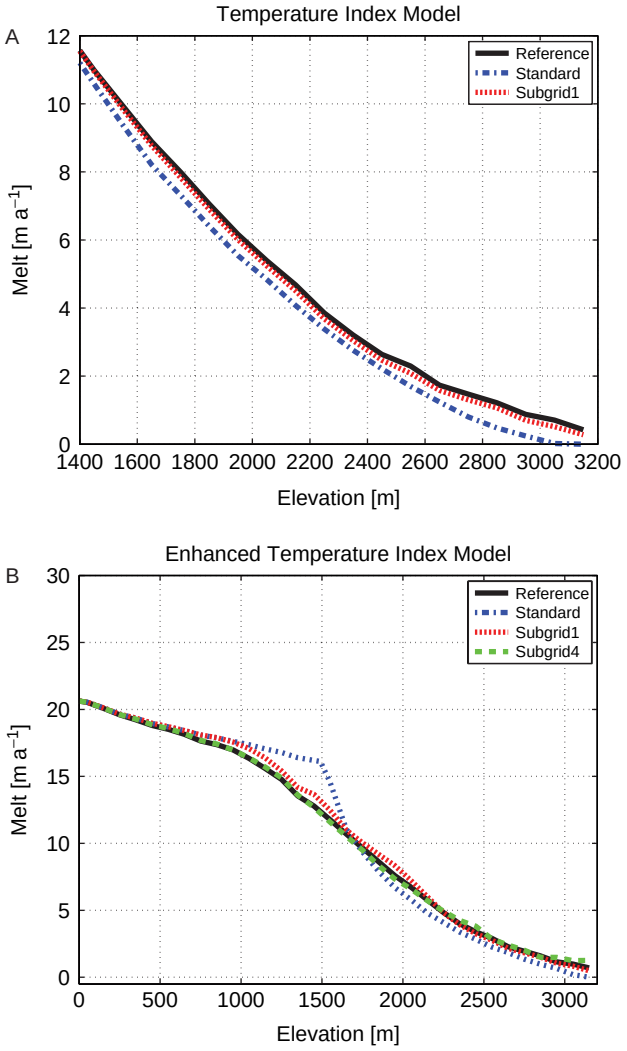

Figure 9. Mean melt versus altitude for different parameterizations of both the TIM (A) and eTIM (B) at 10 km resolution. Elevation ranges are similar to those in Figure 8

- In contrast to the TIM, Figure 9B shows a pronounced difference in melt for elevations between 1000 and 1600 m comparing the baseline with the reference and sub-grid approaches, while above ∼1700 m all realizations are broadly similar.
- Table IV shows that sub-grid 1 is clearly an improvement over the baseline approach for all resolutions and

Hydrol. Process. **22**, 3965–3979 (2008)
DOI: 10.1002/hyp

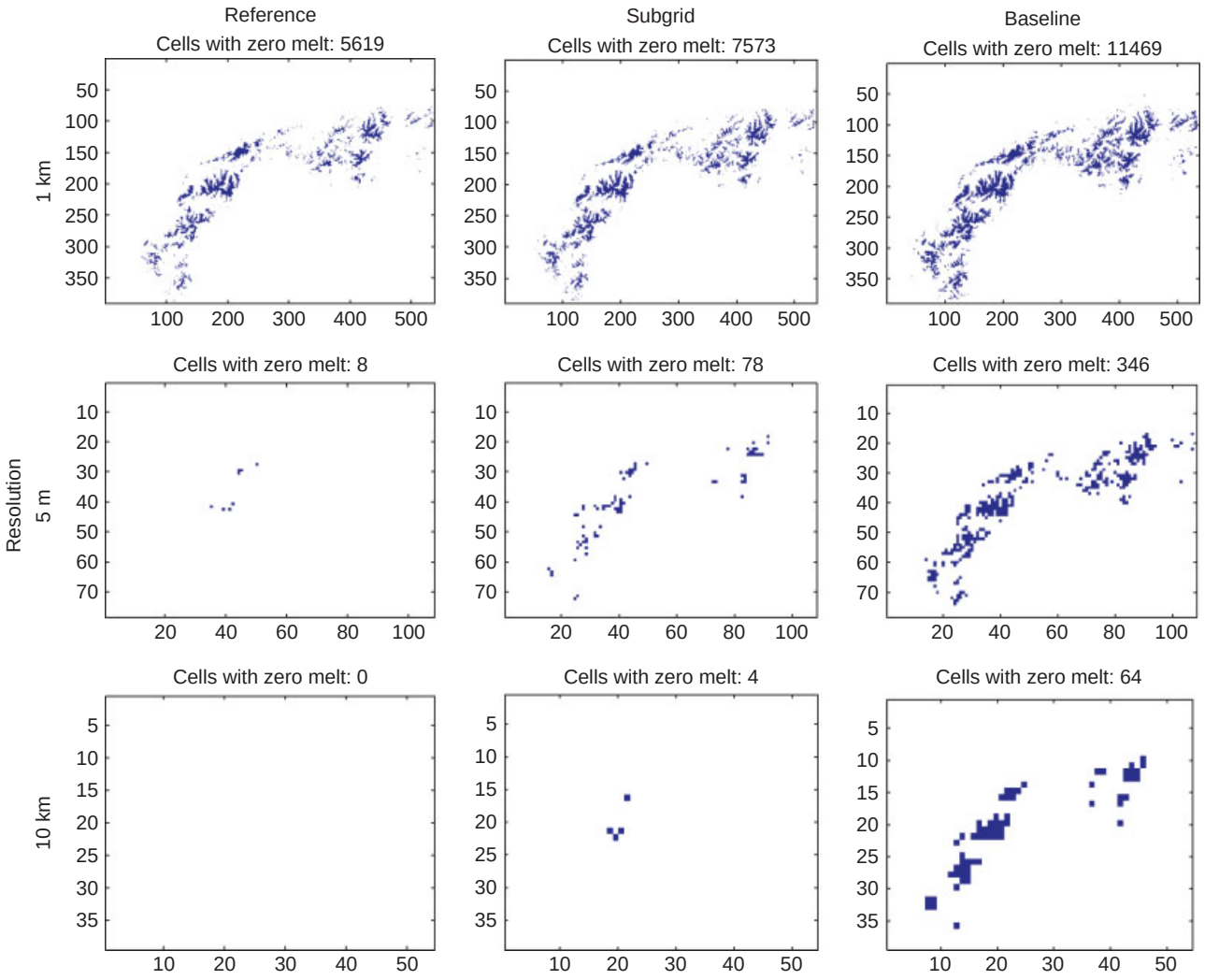

Figure 10. Matrix showing all cells with no melt across the model domain (Figure 2) in blue for the simple TIM. Different resolutions in rows, calculation methods in columns. For the reference melt (left column), the total area without melt decrease with lower resolutions, while the total melt per area is preserved. In the standard approach (right column), the pattern of melt-free cells is preserved. The sub-grid 1 approach (centre column) preserves some of the melt free cells

Table IV. Mean melt and RMSE (in brackets) in m w.e. a^{-1} for the four approaches (baseline and Sub-grid 1,2 and 4) across resolutions of 1, 5 and 10 km, compared to the corresponding reference melt for the eTIM. Values are given for the whole of the study area for each resolution, as well as for areas above 1500 m and 2500 m, where temperature drops below 0 °C for increasing time spans during the year. Optimal results feature a small difference in mean potential melt as well as low RMSE

	eTIM								
Resolution	1 km			5 km			10 km		
Model	All	≥1500	≥2500	All	≥1500	≥2500	All	≥1500	≥2500
Reference	15·27	5·84	1·37	15·27	6·50	1·78	15·27	6·91	2·19
Baseline	15·45 (0·63)	5·89 (0·70)	1·32 (0·24)	15·59 (0·99)	6·39 (1·11)	1·50 (0·39)	15·63 (1·14)	6·65 (1·23)	1·62 (0·68)
Sub-grid1	15·45 (0·56)	5·97 (0·58)	1·35 (0·23)	15·56 (0·57)	6·73 (0·59)	1·71 (0·20)	15·58 (0·55)	7·13 (0·52)	2·00 (0·24)
Sub-grid2	15·27 (0·77)	5·78 (0·87)	1·34 (0·40)	15·29 (1·18)	6·42 (1·45)	1·65 (0·66)	15·30 (1·27)	6·77 (1·56)	1·89 (0·82)
Sub-grid4	15·29 (1·08)	5·60 (2·07)	3·43 (2·25)	15·28 (0·47)	6·52 (0·89)	2·59 (1·10)	15·29 (0·34)	6·86 (0·61)	2·28 (0·61)

elevations, with significant improvements for the 5 and 10 km resolutions.

- Sub-grid 2 shows no improvement at any resolution.
- Sub-grid 4 shows the best overall fit with reference melt for the 5 and 10 km resolutions, demonstrated by the lowest RMSE values (Table IV), but a poor fit at the 1 km resolution.
- While Sub-grid 4 shows the best overall fit for the 5 km resolution, the quality of the fit decreases for higher elevations and overestimates melt for elevations above 2500 m at this resolution.

Hydrol. Process. **22**, 3965–3979 (2008)
DOI: 10.1002/hyp

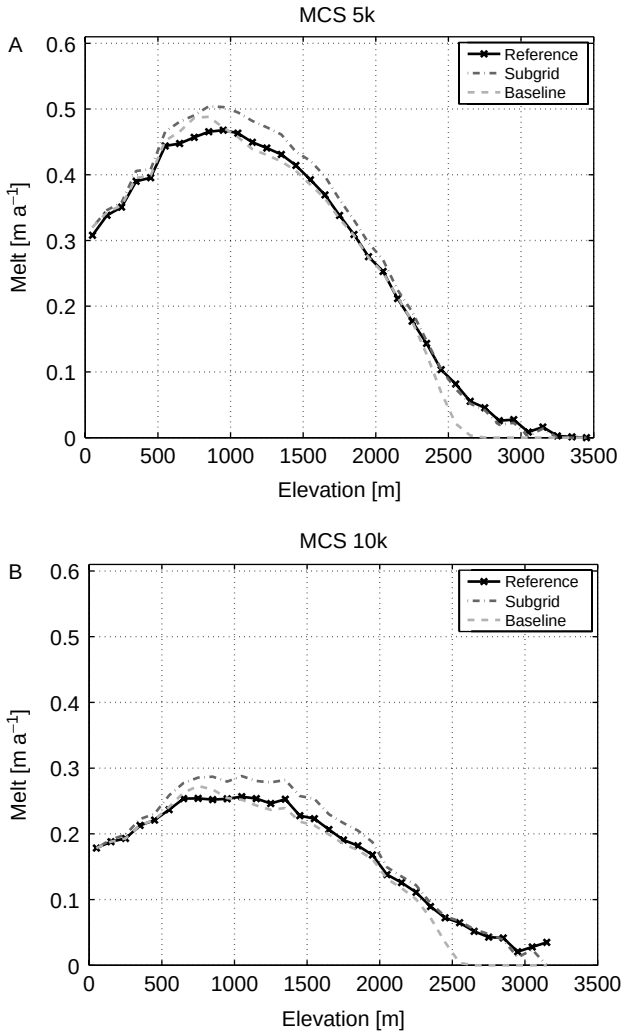

Figure 11. Standard deviation of melt over 100 MCS runs versus elevation bands for the baseline, reference and sub-grid 1 approach for the simple TIM at 5 km (A) and 10 km (B) resolution. The sub-grid approach shows increased susceptibility to DEM uncertainty for elevations below 2000 m, demonstrated by the higher standard deviation. For higher elevations, standard deviations of the sub-grid approach are comparable to the reference. Note that for the baseline approach, no melt is calculated above 2600 m, hence standard deviation becomes zero, while both sub-grid and reference methods show melt rates in the order of 0·5 m/a

Uncertainty analysis

Having run the TIM model at 5 and 10 km resolution on 100 topographies perturbed using simulated DEM uncertainty, the mean standard deviation across the 100 runs for elevation classes of 100 m range is plotted against elevation in Figure 11. It is apparent that the standard deviation of melt rates is about 5–10% higher for the sub-grid parameterized approach compared to the baseline for elevations below ~2000 m, for both resolutions of 5 and 10 km. Compared to absolute TIM reference melt rates (Figure 8A), the standard deviations amount to around 5% at 5 km resolution, and around 2·5% at 10 km resolutions, for elevations above 2000 m. For areas below 2000 m, the relative standard deviation becomes as low as 1%. For elevations above 2000 m, the standard deviation of the sub-grid 1 parameterization is almost identical to that of the reference approach. Note that the standard deviation for the baseline approach drops to zero around 2500 m (Figure 9), while both reference and sub-grid 1 values only become zero around 3200 m. This effect is due to the fact that the baseline approach underestimates melt rates, which therefore become zero earlier.

In general, it can be said that melt rates calculated using the TIM at low resolutions show variation of less than 5% when subject to typical GLOBE DEM data uncertainty.

DISCUSSION

Resolution effects

The resolution experiments, averaging the reference melt from 100 m to lower resolutions reveal potential melt to be dependent on terrain roughness (Figure 12). This effect is demonstrated by the scattering of potential melt rates as a function of elevation shown in Figure 7. Cells above the LT elevation will experience temperatures below zero during some interval of the year (described in the Section Method Comparison), which is when melt will become zero (Equations 1 and 3). When aggregated to lower resolution, cells at the 100 m resolution will therefore contribute less to the average melt than cells below LT. The mean melt at a low-resolution cell, averaged from 100 m, is therefore dependent on the number of cells with temperatures below zero during some interval of the year. Additionally, it is influenced by the length of that interval, which is determined by the seasonal temperature variation applied to the MAAT. This temperature variation is a nonlinear (sinusoidal) function, and is the reason for the nonlinear behaviour of the otherwise linear melt function.

Generally, the deviation of mean melt between two resolutions for a given elevation (Figure 8) depends on the amount of scaling, that is the difference in resolutions. The amount a TIM underestimates this reference melt, is dependent on the resolution with which it has originally been parameterized and the lower ‘target’ resolution.

While the origin resolution (in our case the reference at 100 m) should be adequately chosen to capture the scale of the parameterized model processes in order to ascertain sensible comparison of results (Martin and Church, 2004), the target resolution is usually determined by the computational demands of the model or the limitations associated with the input data. In the case of the simple TIM, the origin resolution should thus retain the hypsometry of a topography with minimal possible smoothing. Furthermore, the underestimation of melt will depend on the applied MAAT, lapse rate, and topographic properties such as overall elevation range and roughness, as MAAT and lapse rate control the elevation of the LT and UT.

Hydrol. Process. **22**, 3965–3979 (2008)
DOI: 10.1002/hyp

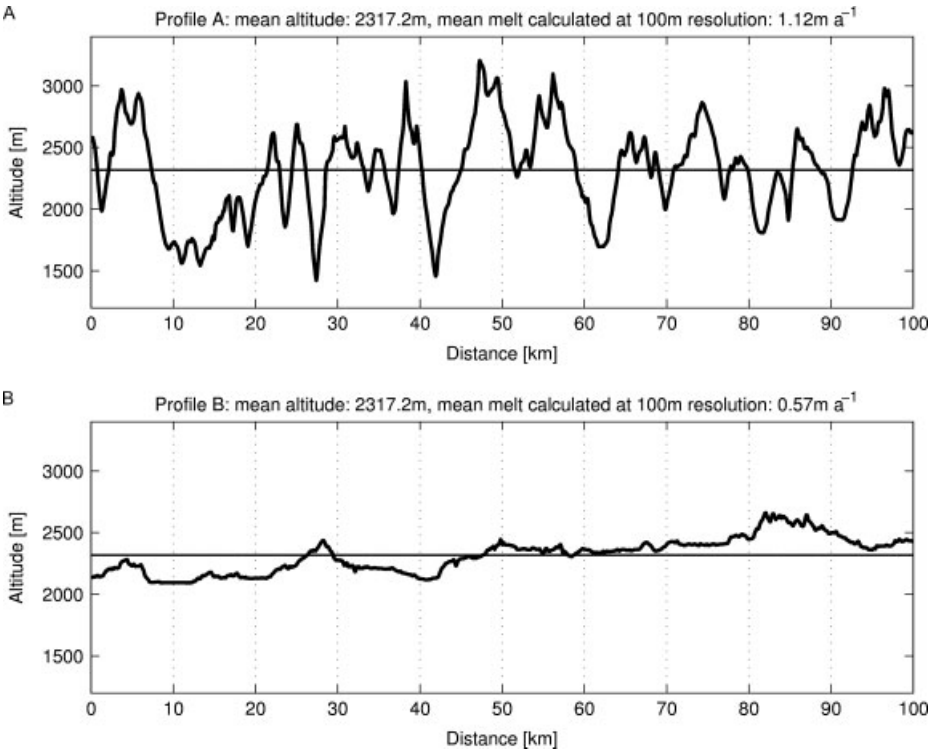

Figure 12. A 100 km profile of the central alps (A), with a mean elevation of 2317·2 m and an elevation range of more than 1500 m. Mean melt calculated for this profile using the TIM is 1·12 m/a. A much smoother profile taken from the South German midlands (B) with an elevation range of just above 600 m was raised to the same mean elevation. Because of the dependence of melt on terrain roughness, the mean potential melt rate calculated is only about half that of profile A at 0·57 m/a

For the eTIM, the effect scaling has on calculation of potential melt is more complex. The sharp transition at the 0 °C threshold at the 100 m reference resolution is gradually smoothed with decreasing resolution (Figure 8B). Using the baseline eTIM approach at low resolutions thus results in an overestimation of melt around the lower temperature threshold (~1500 m), which can be as much as 20% at a resolution of 10 km (Figure 8B). Simultaneously, an underestimation of melt for elevations above the threshold, similar to that encountered for the TIM can be observed. As for the TIM, a suitable reference resolution (origin) needs to retain topographic features that are important to characterizing the process of interest (Martin and Church, 2004). In the case of the eTIM this is elevation and the average slope length, which is necessary to capture the spatial variation of slope and aspect, used to calculate radiation based melt. For both the TIM and eTIM, the resolution of 1 km apparently captures the DEM properties of interest well, as the differences in melt compared to the 100 m resolution are small. The effect of averaging to 5 and 10 km resolution on topographic properties is much larger and reflected in the resulting deviation of melt rates.

Method comparison

TIM modelling approaches. Even though a simple underestimation of melt in the baseline *TIM* approach could easily be compensated by adapting the model parameters—for example DDF or temperature—this would require that the melt model was run at a higher resolution first in order to determine the optimal parameterization. However, looking at the pattern of melt-free cells modelled using the TIM (Figure 10), the dilemma of modelling melt at low resolutions becomes apparent: while the baseline approach retains the spatial pattern, thus keeping the overall area of melt-free cells approximately constant across resolutions, melt rates in these cells underestimate those rates derived at higher resolutions. A simple increase in melt at lower resolutions to fit the reference rates would again result in a loss of melt-free areas. These areas are important, for example, when modelling ice sheet inception or glaciers as global global runoff reservoirs, as it has been shown that even a small under- or overestimation of glacierized areas can have a significant influence on run-off regimes (Jansson *et al*., 2003; Kaser *et al*., 2003). The problem can be overcome by using the simple sub-grid 1 approach adopted in this article: while the sub-grid 1 parameterization produces melt rates close to the reference (Figure 9), it retains only few cells without any melt (Figure 10). However, the additional elevation information provided by the sub-grids can be included in modelling processes like inception (e.g. Marshall, 2002).

eTIM modelling approaches. Comparing the performance of the different sub-grid approaches applied to the eTIM (see Section on Sub-grid Parameterization), the performance of the simple sub-grid 1 parameterization is initially surprising (Table IV). The calculation of slope and aspect on the respective elevation sub-grids is somewhat arbitrary, and one would expect a better fit using

Hydrol. Process. **22**, 3965–3979 (2008)
DOI: 10.1002/hyp

averages from the high-resolution DEM (used in sub-grid 2 and 3). Looking at the dependencies of radiation melt on aspect and slope helps to explain the relatively good performance of the simple sub-grid 1 approach. Aspect has a strong influence on radiation melt (Figure 5), and the re-sampling of aspect to lower resolutions is difficult, as replacing a range of aspects at high resolution with just one value at a lower resolution will inevitably bias any result thus calculated. For the relatively low mean slopes in the range of 0·2–0·3 radians calculated for the sub-grid 1 approach, the resulting deviation in melt for different aspects is small, while high slopes in the range of 0·6–0·7 radians result in a much higher deviation, for example between south and north facing slopes. Averaged across all aspect values, a lower slope generally results in a higher mean melt for our experimental setup. This explains the slight overestimation of melt rates of the sub-grid 1 approach for elevations below 2000 m for the eTIM (Figure 9B), contrary to the slight underestimation of the sub-grid 1 approach for the TIM (Figure 9A).

The sub-grid 4 approach, using sub-grids for the four cardinal directions, performs well across the whole elevation range, with some overestimation of melt at higher elevations. However, while the approach proves to be effective for the 5 and 10 km resolutions, it is not valid for parameterization at the 1 km resolution (Table IV). This might be explained by the fact that average slope length is still captured well at the 1 km resolution, and thus pronounced elevation features, for example slopes predominantly facing one direction, are not averaged out at this scale. Thus, very distinct melt patterns can exist, which are not captured well enough at 1 km using our parameterization, leading to noticeable over- and underestimations for extreme cases. Additionally, while the sub-grid 4 approach shows the best overall fit at 5 km resolution, for elevations above 2500 m calculated potential melt considerably overestimates reference melt, and the approach provides no improvement over the baseline. However, this overestimation is likely to be due to the use of regression parameters for reduction of the radiation melt from the 10 km resolution. While this guarantees an optimal fit for all elevations at this resolution for the sub-grid 4 approach, results are sub-optimal for lower resolutions. While in general, the parameterization concept using directional sub-grids works well, the criteria (Section 1.3) of scalability is not completely fulfilled, and further investigation of the causes and the range of application scales, as well as a possible improvement of the method will be useful.

Uncertainty analysis

The sub-grid 1 approach shows a slightly increased susceptibility to DEM uncertainty, judged by the standard deviation of melt rates as a function of elevation (Figure 11), than the baseline or reference approaches. This can be explained by the fact that uncertainty introduced to the DEM has a threefold impact on the sub-grid approach, because elevation uncertainty affects all three sub-grid elevation values via the change of hypsometry. For the reference approach, the DEM uncertainty effects are more likely to be cancelled out over an area of 5 or 10 km. The same holds for the baseline approach, where uncertainties at the higher resolution are also averaged out. This increase in uncertainty of the sub-grid 1 parameterization relative to the reference and baseline approaches is at a maximum 10% for elevations below 2000 m. Because potential melt at these elevations plays a minor role in ablation calculations, this increased uncertainty is probably of little relevance. However, it is important to be aware of the effects of DEM uncertainty when using sub-grid approaches.

CONCLUSION

A parameterization using three hypsometric sub-grids has proven to be a simple, robust and scalable method for melt calculation at low resolutions using both simple and eTIMs. The use of sub-grids also provides additional information derived from higher resolution topographies, which can be used in a variety of modelling approaches, from simple masking to complex internal coupling, e.g. as in hydrological modelling across elevation bands.

The parameterization developed for the enhanced solar radiation model, using slope sub-grids for the cardinal directions, proved to provide the best modelling results for resolutions below 5 km, providing very good estimates of higher resolution reference melt rates, if regression parameters for adjusting radiation melt for temperature reduction are derived for each resolution. Performance is decreased if global regression parameters are used that have been derived for a range of resolutions, and the approach is therefore not fully scalable. Further experiments need to assess the threshold resolution for this parameterization approach, as well as the exact reasons for the existence of this threshold. Optimization of regression parameters for the reduction of radiation melt is also needed.

Our experiments using a DEM uncertainty model to test sensitivity of a simple TIM confirm that sub-grid parameterization can be used for modelling sub-scale processes, but care has to be taken when this form of parameterization is applied. Sensitivity studies should be conducted to assure the reliability of the model results is preserved.

ACKNOWLEDGEMENTS

This research was funded by the Swiss National Science Foundation SNF, project number 200020-109449. The comments of Dr Gwenn Flowers and the two anonymous reviewers greatly improved this article.

REFERENCES

Albani M, Klinkenberg B, Andison DW, Kimmins JP. 2004. The choice of window size in approximating topographic surfaces from digital

Hydrol. Process. **22**, 3965–3979 (2008)
DOI: 10.1002/hyp

elevation models. *International Journal of Geographical Information Science* **18**(6): 557–593.
Alley RB, Clark PU, Huybrechts P, Joughin I. 2005. Ice-sheet and sea-level changes. *Science* **310**: 456–460.
Armstrong RN, Martz LW. 2003. Topographic parameterization in continental hydrology: a study in scale. *Hydrological Processes* **17**(18): 3763–3781.
Braithwaite R. 1995. Positive degree-day factors for ablation on the Greenland ice sheet studied by energy-balance modelling. *Journal of Glaciology* **41**(137): 153–159.
Cazorzi F, Fontana GD. 1996. Snowmelt modelling by combining air temperature and a distributed radiation index. *Journal of Hydrology* **181**: 169–187.
Endreny TA, Wood EF. 2001. Representing elevation uncertainty in runoff modelling and flowpath mapping. *Hydrological Processes* **15**(12): 2223–2236.
Essery R, Etchevers P. 2004. Parameter sensitivity in simulations of snowmelt. *Journal of Geophysical Research* **109**: D20111.
Essery R, Marks D. 2007. Scaling and parametrization of clear-sky solar radiation over complex topography. *Journal of Geophysical Research* **112**: D10122.
Florinsky IV. 1998. Accuracy of local topographic variables derived from digital elevation models. *International Journal of Geographical Information Science* **12**(1): 47–61.
Hagdorn M, Rutt I, Payne T, Hebeler F. 2006. GLIMMER - The GENIE Land Ice Model with Multiply Enabled Regions - Documentation. http://glimmer.forge.nesc.ac.uk/, Universities of Bristol, Edinburgh, Zurich.
Hastings DA, Dunbar PK. 1998. Development and assessment of the Global Land One-km Base Elevation Digital Elevation Model (GLOBE). *ISPRS Archives* **32**(4): 218–221.
Hebeler F, Purves RS. 2008a. The influence of elevation uncertainty on derivation of topographic indices. *Geomorphology* (in press).
Hebeler F, Purves RS. 2008b. *Modelling DEM Data Uncertainties for Monte Carlo Simulations of Ice Sheet Models*. CRC press: (in press).
Hock R. 1999. A distributed temperature-index ice- and snowmelt model including potential direct solar radiation. *Journal of Glaciology* **45**(149): 101–111.
Hock R. 2003. Temperature index melt modelling in mountain areas. *Journal of Hydrology* **282**: 104–115.
Hock R. 2005. Glacier melt: a review of processes and their modelling. *Progress in Physical Geography* **29**(3): 362–391.
Hu Z, Islam S. 1997. Effects of spatial variability on the scaling of land surface parameterizations. *Boundary-Layer Meteorology* **83**: 441–461.
Huybrechts P, Letréguilly A, Reeh N. 1991. The Greenland ice sheet and greenhouse warming. *Global and Planetary Change* **3**(4): 399–412.
Huybrechts P, Payne A, Abe-Ouchi A, Calov R, Fabre A, Fastook J, Greve R, Hindmarsh R, Hoydal O, Jóhannesson T. 1996. The EISMINT benchmarks for testing ice-sheet models. *Annals of Glaciology* **23**: 1–12.
Jansson P, Hock R, Schneider T. 2003. The concept of glacier storage: a review. *Journal of Hydrology* **282**: 116–129.
Jarvis A, Reuter H, Nelson A, Guevara E. 2006. Void-filled seamless SRTM data V3, available from the CGIAR-CSI SRTM 90m Database, http://srtm.csi.cgiar.org, International Centre for Tropical Agriculture (CIAT).
Kaser G, Juen I, Georges C, Gómez J, Tamayo W. 2003. The impact of glaciers on the runoff and the reconstruction of mass balance history from hydrological data in the tropical Cordillera Blanca, Perú. *Journal of Hydrology* **282**: 130–144.
Kumar L, Skidmore AK, Knowles E. 1997. Modelling topographic variation in solar radiation in a GIS environment. *International Journal of Geographical Information Science* **11**: 475–497.
Lefebre F, Gallée H, van Ypersele J-P, Greuell W. 2003. Modeling of snow and ice melt at ETH camp (West Greenland): a study of surface albedo. *Journal of Geophysical Research* **108**(D8): 4231.
Leung LR, Wigmosta MS, Ghan SJ, Epstein DJ, Vail LW. 1996. Application of a subgrid orographic precipitation/surface hydrology scheme to a mountain watershed. *Journal of Geophysical Research* **101**(D8): 12 803–12 818.
Luce CH, Tarboton DG, Cooley KR. 1999. Sub-grid parameterization of snow distribution for an energy and mass balance snow cover model. *Hydrological Processes* **13**: 1921–1933.
Malanson GP. 1999. Considering complexity. *Annals of the Association of American Geographers* **89**(4): 746–753.
Marshall SJ. 2002. Modelled nucleation centres of the Pleistocene ice sheets from an ice sheet model with subgrid topographic and glaciologic parameterizations. *Quaternary International* **95–96**: 125–137.
Marshall SJ, Clarke G. 1999. Ice sheet inception: subgrid hypsometric parameterization of mass balance in an ice sheet model. *Climate Dynamics* **15**: 533–560.
Martin Y, Church M. 2004. Numerical modelling of landscape evolution: geomorphological perspectives. *Progress in Physical Geography* **28**(3): 317–339.
Oksanen J, Sarjakoski T. 2005. Error propagation of DEM-based surface derivatives. *Computers & Geosciences* **31**(8): 1015–1027.
Pellicciotti F, Brock B, Strasser U, Burlando P, Funk M, Corripio J. 2005. An enhanced temperature-index glacier melt model including the shortwave radiation balance: development and testing for Haut Glacier d'Arolla, Switzerland. *Journal of Glaciology* **51**(175): 573–587.
Ritz C, Fabre A, Letréguilly A. 1997. Sensitivity of a Greenland ice sheet model to ice flow and ablation parameters: consequences for the evolution through the last climatic cycle. *Climate Dynamics* **13**(1): 11–24.
Salzmann N, Frei C, Vidale P-L, Hoelzle M. 2007. The application of regional climate model output for the simulation of high-mountain permafrost scenarios. *Global and Planetary Change* **56**: 188–202.
Schneeberger C, Blatter H, Abe-Ouchi A, Wild M. 2003. Modelling changes in the mass balance of glaciers of the northern hemisphere for a transient $2\times$ CO_2 scenario. *Journal of Hydrology* **282**: 145–163.
Stone PH, Carlson JH. 1979. Atmospheric lapse rate regimes and their parameterization. *Journal of Atmospheric Sciences* **3**: 415–423.
Strasser U, Etchevers P. 2003. Using subgrid parameterization for topography and a forest canopy climate model for improving snowmelt flood simulations. In *Climatology and Hydrology of Mountain Areas*, de Jong C, Collins D, Ranzi R (eds). John Wiley and Sons Chichester.
Strasser U, Corripio J, Pellicciotti F, Burlando P. 2004. Spatial and temporal variability of meteorological variables at Haut Glacier d'Arolla (Switzerland) during the ablation season 2001: Measurements and simulations. *Journal of Geophysical Research* **109**: D03103.
Wechsler SP. 2000. Effect of DEM uncertainty on topographic parameters, DEM scale and terrain evaluation, Dissertation, State University of New York, College of Environmental Science and Forestry, Syracuse.
Wechsler SP. 2007. Uncertainties associated with digital elevation models for hydrologic applications: a review. *Hydrology and Earth System Sciences* **11**(4): 1481–1500.
Williams KS, Tarboton DG. 1999. The ABC's of snowmelt: a topographically factorized energy component snowmelt model. *Hydrological Processes* **13**: 1905–1920.
Zhang X, Drake NA, Wainwright J, Mulligan M. 1999. Comparison of slope estimates from low resolution DEMs: scaling issues and a fractal method for their solution. *Earth Surface Processes and Landforms* **24**(9): 763–779.

Hydrol. Process. **22**, 3965–3979 (2008)
DOI: 10.1002/hyp

Appendix E

Hebeler, F., Purves, R.S. & Jamieson, S.S.R.: The impact of parametric uncertainty and topographic error in ice sheet modelling.
Journal of Glaciology, in press

The impact of parametric uncertainty and topographic error in ice sheet modelling

Felix HEBELER,[1] Ross S. PURVES,[1] Stewart S.R. JAMIESON,[2]

[1] *University of Zurich, Department of Geography, Winterthurer Str. 190, 8057 Zurich, Switzerland*
E-mail: felix.hebeler@geo.uzh.ch
[2] *University of Edinburgh, School of Geosciences, Drummond Street, Edinburgh, EH8 9XP, UK*

ABSTRACT. Ice sheet models (ISM) developed to simulate the behaviour of continental scale ice sheets under past, present or future climate scenarios are subject to a number of uncertainties from various sources. These sources include the conceptualisation of the ISM and the degree of abstraction and parameterisations of processes such as ice dynamics and mass balance. Assumptions of spatially or temporally constant parameters such as degree day factor, atmospheric lapse rate or geothermal heat flux are one example. Additionally, uncertainties in ISM input data such as topography or precipitation propagate to the model results.

In order to assess and compare the impact of uncertainties from model parameters and climate on the GLIMMER ice sheet model, a parametric uncertainty analysis (PUA) was conducted. Parameter variation was deduced from a suite of sensitivity tests, accuracy information deduced from input data and the literature. Recorded variation of modelled ice extent across the PUA runs was 65% for equilibrium ice sheets.

Additionally, the susceptibility of ISM results to modelled uncertainty in input topography was assessed. Resulting variations in modelled ice extent of the range of 1-6.6% are comparable to that of ISM parameters such as flow enhancement, basal traction or geothermal heat flux.

INTRODUCTION

The aim of this paper is to investigate how uncertainty in modelled ice sheet configurations is affected by a range of possible uncertainties in model inputs. In particular, we focus on assessing the influence of uncertainties in the representation of the bed topography in comparison with uncertainties of key mass-balance and ice dynamic parameters input to a three dimensional thermodynamically coupled ice sheet model (ISM). We do this by carrying out parametric uncertainty analysis on these parameters as well applying modelled uncertainty to digital elevation models (DEMs) of an ice sheet bed. Since our aim is to explore and compare uncertainty as a function of these parameters, model runs were carried out using a steady-state climate. The model runs explore ice sheet extents and volumes in Fennoscandia, with mass-balances approximately in line with the Last Glacial Maximum (LGM). However, we emphasise that we are primarily concerned with the development of methodologies to assess uncertainties in ISM results rather than the exploration of a particular ice sheet reconstruction.

Uncertainty in ice sheet models

Uncertainty in ice sheet models has two main sources. Firstly, the modelled ice sheet is a function of the initial decisions made in abstracting the real system to a conceptual model. By abstracting reality, we are accepting that uncertainty will be inherent in the results of our model - users of numerical models will seek to minimalise this. For example a model which does not consider longitudinal stresses will fail to replicate particular aspects of the glacial system. Secondly, model uncertainty can arise from uncertainties in the input parameters, such as the choice of parameter values at the model initialisation. The first set of uncertainties can only be explored through comparisons of systems that use different levels of abstraction in constructing their model rules. Thus, for example Hubbard and others (2005) showed how the inclusion of longitudinal stresses led to considerable variation in modelled ice sheet extents in Patagonia as compared to previous results (Hulton and others, 2002, 1994), based around models using the shallow ice approximation (Nye, 1957).

Within the ice sheet modelling community, intercomparison experiments have sought to explore the sensitivity of modelled results to differences in implementation (and in principle abstraction). For example, the EISMINT experiments (Payne and others, 2000; Huybrechts and others, 1996) explored a variety of model types and their responses to a range of glaciological (e.g. steady state Greenland ice sheet under present conditions) and hypothetical experiments (e.g. ice stream formation on a hypothetical symmetric topography). In many modelling fields a similar approach, though motivated by a different philosophy, is applied in ensemble modelling. Here, a variety of models are usually run in parallel and the results are weighted to provide a probabilistic forecast (Anderson, 1996). Such approaches are arguably better suited for use in policy formulation, where the focus of interest is centred on risk estimation (Vaughan and Spouge, 2002).

In general, such model intercomparisons allow exploration of differences between models for a given scenario, and are important in moving models towards a consensus view. However, since intercomparisons are also often used as a benchmark towards which modellers aim in development, they cannot be said to be a means of quantifying uncertainty. Additionally,

sensitivity to 'external' (input) parameters are usually not the subject of those intercomparisons, leaving a gap in the understanding of uncertainties associated with ice sheet modelling, which we aim to fill. This second set of uncertainties, the focus of this paper, can be explored in a variety of ways. The most common approach employed in glaciological modelling is to carry out a sensitivity study. In such studies, all but one parameter are typically held constant whilst the parameter under investigation is varied through some range, and the response of the modelled ice sheet is visualised or quantified (e.g. Essery and Etchevers, 2004; Pattyn, 2003; Purves and Hulton, 2000; Huybrechts and de Wolde, 1999; Ritz and others, 1997; Fabre and others, 1995; van de Wal and Oerlemans, 1994). Sensitivity studies are important because they allow modellers to quantify which parameters, in isolation, have the greatest influence on model results. However, since all but the most trivial ice sheet models are inherently nonlinear, it is often difficult to properly quantify uncertainty or allow assignment of probabilities to particular outcomes (van der Veen, 2002).

Parametric uncertainty analysis

Currently, despite the increased importance of numerical modelling in policy making, relatively little research has explored ways in which uncertainties might be consistently calculated in individual ice sheet model results. Parametric uncertainty analysis (PUA), where all parameters are varied together, is one such approach. Marshall and others (2002) investigated the response of the North America Ice Sheet to a range of parameters, and completed a number of simulations where parameters were varied simultaneously. Tarasov and Peltier (2004) also explored the response of the North American Ice Sheet during the LGM to simultaneous variations in a range of parameters whilst geophysically constraining the modelled ice extents. However, in both of these experiments the variation of parameter values appears to have been based on a limited variation of parameter values over a pre-defined range. Such approaches allow the range of potential model responses to input parameters to be estimated, but these responses are not associated with probabilities.

Vaughan and Spouge (2002) carried out a full parametric uncertainty analysis of future ice sheet mass balance for the Greenland ice sheet using parameterisations of accumulation and ablation. A key difference in this approach is that probability distributions functions (PDFs) are estimated for each parameter, and used in the model runs to allow calculation of a final PDF for a chosen model output parameter. Probability density functions in general are used to associate a probability with a certain parameter value or model outcome. For example using a normal distribution as a PDF, values close to the mean are more likely to occur than values that deviate more from the mean – in the case of a normal distribution, 66% of all values are within one standard deviation of the mean. The advantage of using PDFs in parametric uncertainty analysis is that by including a (realistic) likelihood for a certain parameter value to occur, probabilities can be assigned to model outcomes. This in turn allows modellers, policy makers and users to identify in a more meaningful way how each parameter might affect the result, and estimate, for instance, the risk of extreme events. Typically, parametric uncertainty analysis is carried out using Monte Carlo simulation (MCS) which is a brute force technique, where large numbers of model runs are normally required to generate an ensemble of results from which PDFs can be calculated.

Topography in ice sheet models

In ice sheet modelling the bed topography on which models are run is generally treated as having no uncertainty associated with it. However, the data used in the generation of these bed topographies is often associated with large uncertainties which vary as a function of locale (Hebeler and Purves, 2008). Furthermore, the interpolation methods used to resample these data to resolutions appropriate for typical ISMs also introduce further uncertainties (Hebeler and Purves, 2004). Topography, as discussed by Kerr (1993), plays a key role in influencing ice sheet behaviour through its geometry whereby the mass-balance profile is controlled by relief (e.g. through orographic effects) and the topographic geometry (e.g. hypsometry). Topography also influences ice sheet configuration directly by facilitating or constraining ice flow - for example in a glacial trough (Jamieson and others, 2008). The sensitivity of modelled ice sheet extents to uncertainty in topography is consequently relevant to furthering our understanding of ice sheets, and to refining numerical models that seek to reconstruct such systems.

Aims

The objectives of this paper are therefore threefold:

1. to propose a generalisable set of methods for exploring the parametric uncertainty of ice sheet model results;
2. to explore the influence of uncertainty in bed topography on modelled ice extents and volumes; and
3. to compare the influence of topographic uncertainty to other sources of uncertainty – such as climatic or basal model inputs – on modelled ice extents and volumes.

The remainder of the paper is structured as follows. We briefly introduce the ice sheet model used in our experiments, before we describe a method for exploring uncertainty in bed topography. We then review the parameters and associated PDFs derived for the parametric uncertainty experiments. The results of the experiments are presented as plots of ice extent and volume through time and by visualisations of ice extent and volume from ice sheets in equilibrium, using probability maps. Additionally histograms of the associated PDFs are given. Finally, we discuss the significance of the results and their implications for those constructing, using and interpreting ice sheet models.

METHODOLOGY

The GLIMMER Ice Sheet Model

Physical laws relating to the dynamics of glaciers have long been incorporated into numerical models of ice flow so that predictions might be made about past, present and future ice sheet behaviour (e.g. Huybrechts and Le Meur, 1999; Oerlemans and others, 1998; Hulton and others, 1994). We aim to test how uncertainty in various model input parameters can affect the result of such ice sheet models. To achieve this, we employ a community ice sheet model called GLIMMER (General Land Ice Model for Multiply Enabled Regions (Payne, 1999)) which builds upon the foundations laid down by the modelling studies of Huybrechts (1986), Boulton and Payne

(1992) and Payne and Dongelmans (1997). Ice dynamics calculations implement the shallow ice approximation (Hutter, 1983), a widely used approach which assumes that bedrock and ice surface slopes are small enough that normal stress components can be neglected. The ice flow law parameter is handled by a three-dimensional thermomechanical model. A full outline of the numerics implemented in GLIMMER is provided by Hagdorn and others (2007) and Paterson (1994) provides additional context to the derivation of these mechanics.

The ability of a modelled ice sheet to grow and interact with its bed and climate is strongly dependant upon basal ice velocities. In GLIMMER, the velocities of the basal ice v_b at any one point are determined as a function of the basal shear stress (τ_b) and the effective pressure (N = ice overburden pressure - basal water pressure) thus:

$$v_\mathrm{b} = k\,\tau_\mathrm{b}^{p}\,N^{-q} \tag{1}$$

where k is a constant describing the thermomechanical properties of ice and p and q are positive integers (Paterson, 1994). The basal slip coefficient t_b, also known as the basal traction parameter, determines the dependence of the thermomechanical properties of ice upon N and therefore assumes that k and N^{-q} can be integrated as a single parameter. Equation 1 can therefore be simplified (Hagdorn and others, 2007) to:

$$v_\mathrm{b} = t_\mathrm{b}\,\tau_\mathrm{b} \tag{2}$$

Sliding is assumed to occur when ice temperature at the bed reaches pressure melting point (taking into account both a user defined geothermal heat flux - G_therm - and calculated frictional heat contributions) at which point the ice can detach from the bed and begin sliding due to the presence of water. Its ability to do so is a function of t_b which is calculated as a linear function of basal melt rate (b_melt):

$$t_\mathrm{b} = \min(t_\mathrm{bmax}\,, b_\mathrm{soft} + t_\mathrm{bslope} b_\mathrm{melt}) \tag{3}$$

The slope of the function is given by t_bslope, the softness of the bed is given by a parameter b_soft and the basal traction is limited from becoming too large by the value of t_bmax. Variability in the basal traction parameter will therefore alter the behaviour and form of the resulting ice mass.

At each timestep, the model requires spatial parameterisation of surface mass balance and air temperature as inputs. We follow the approach of Jamieson and Sugden (2008) to generate these inputs. The distinction between snowfall (which only occurs below a given temperature - t_snow) and rainfall across the model domain is determined using a positive degree day (PDD) model (Reeh, 1991). The PDD approach makes the assumption that melt at the ice or land surface is proportional to the number of days (integrated through time) in which the air temperature (T) rises above freezing point. The number of positive degree days is therefore proportional to the energy available for melting. Melt (w) is calculated by:

$$w = \mathit{DDF} \int^{year} \max(T, 0)\,dt \tag{4}$$

where *DDF* is the degree day factor describing the density and albedo of snow or ice (*DDF* is different for each). The melt calculation further assumes that there is an annual sinusoidal cyclicity (i.e. seasonality) to air temperature, which is calculated by taking the mean annual temperature and an associated half-range (t_range). Further diurnal deviations from the sinusoidally shifted mean annual temperature are accounted for by assuming that this variability has a normal distribution with a standard deviation of 5 °C. The mean annual air temperature (MAAT) at the land or ice surface is calculated given a MAAT at sea level which is then adjusted to the surface using an atmospheric lapse rate (*lrate*). The model also incorporates a firn model to account for the fraction (w_max) of melted snow that refreezes to become superimposed ice. The patterns of precipitation and MAAT used as inputs to this model are described in the section 'Climate Forcing' below.

The Earth can be approximated as a thin elastic layer (the lithosphere) that floats above the asthenosphere. GLIMMER treats these two components separately and can do so in a number of ways. The flexural rigidity of the lithosphere is modelled as it responds to changes in load (Lambeck and Nakiboglu, 1980). The response of the asthenosphere to changes in overburden is modelled so that mantle flow is approximated over time as an exponentially decaying hydrostatic response function (Hagdorn and others, 2007)

The model has been tested in the EISMINT experiments (Payne and others, 2000; Huybrechts and others, 1996), and it has been employed to gain better understanding of ice dynamics (e.g. Le Brocq and others, 2006). Furthermore, it has been used as a tool to reconstruct ice sheet configurations over numerous regions and time periods (Jamieson and Sugden, 2008; Lunt and others, 2008; Payne, 1999; Payne and Baldwin, 1999).

Study area

For the experiments, we use basal topography of Fennoscandia extracted from 30 arc-second resolution GLOBE DEM data (GLOBE Task Team & others, 1999) between 50 and 72° N and between 14° W and 56° E. This is merged with ETOPO2 bathymetric data (NGDC, 2006) at 2 minute resolution and transformed to Albers Equal Area projection. Thus the open water-bodies in GLOBE are filled by ETOPO2 data, and resampled to 10 km resolution. The model domain covers an area of 2580 by 2370 km, with a minimum elevation of -3882m and a maximum elevation of 1960 m.

Climate Forcing

The primary objective of the experiments described in this paper is to investigate the influence of uncertainty in topography, climate, and model parameters upon modelled ice sheet extent and volumes. To this end, we are concerned with generating ice sheets in which parameters are varied and which can be compared to a benchmark simulation of a Fennoscandian ice sheet.

For precipitation rates, CRU (2006) and IPCC (2006) observation data of recent climate were used to interpolate a precipitation scheme (Fig. 1), which can be scaled and varied over time. Notable features are high values of precipitation along the western coastal regions, with the highest precipitation of ca. 2.6 m per year occurring in the southwest fjords.

CRU and IPCC climate data from 30 year observation periods were also used to compile MAAT at sea-level for the study area. From this data, latitudinal dependencies were derived to construct an input temperature field at sea-level that matches the general trends from observation data and gets colder with increased latitude. For modelling steady state ice sheets on Fennoscandia, recent mean temperature was lowered by a constant value over the whole modelling domain (c.f. Forsström and Greve, 2004; Huybrechts and de Wolde, 1999).

Preliminary sensitivity tests for different temperature and precipitation schemes were run to determine an optimal climate setup for the DEM uncertainty analysis as well as the parametric uncertainty tests. Lowering of present-day temperature by 10 to 14 °C, approximately resembling the cooling during the Last Glacial Maximum (Ritz and others, 1997), proved to produce stable and sensible ice sheet extents.

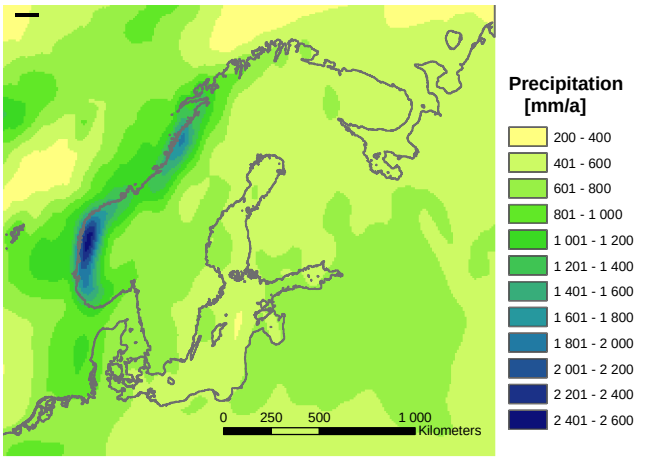

Fig. 1: Precipitation scheme for Fennoscandia compiled from present day CRU and IPCC observation data serving as baseline input for the GLIMMER ISM.

DEM Uncertainty Experiments

Digital elevation models (DEMs) are subject to uncertainties generated from sources such as resampling and data accuracy. GLOBE DEM data, commonly used for modelling in Fennoscandia, is known to contain substantial uncertainties originating from numerous data sources, from compilation methods and from measurement errors. Despite claims as to the need for detailed error models as an integral part of digital elevation data (Ehlschlaeger and Goodchild, 1994), common DEMs such as GLOBE are distributed with only global error or accuracy figures (Fisher, 1998) as described by the root mean squared error RMSE (Hastings and Dunbar, 1999). These global accuracy figures have proven unrealistic and are of limited use as they lack information on the spatial distribution of error which is often spatially correlated with topographic attributes such as altitude or slope (Oksanen and Sarjakoski, 2005; Holmes and others, 2000).

Therefore, in order to realistically model DEM uncertainty including spatial dependencies, higher order reference data is necessary where no explicit error model exists. Because of the limited availability of such reference data for large regions of Fennoscandia, a model for simulating GLOBE DEM uncertainty has been developed (Hebeler and Purves, in press,a, b). This model assesses GLOBE DEM error properties over a number of mountainous regions where higher order reference data (SRTM, Jarvis and others, 2006) is available. Using these regions, characteristics of error magnitude and spatial configuration, including its correlation with DEM characteristics such as elevation, slope and roughness, have been assessed. Analysis showed GLOBE error to be best modelled using deterministic components of uncertainty, modelled using regression, combined with stochastic elements. While the deterministic components reproduced the amount and spatial configuration of uncertainty well, the stochastic elements allow the produced uncertainty surfaces to be used within Monte Carlo Simulations. The resulting uncertainty surfaces are essentially surfaces of deviations from the original elevation data in meters, and are added to the GLOBE DEM.

Using this uncertainty model derived from areas with existing reference data, a suite of 150 uncertainty surfaces at 1 km resolution for Fennoscandia were produced. These uncertainty surfaces were then added to the original GLOBE DEM, resampled to 10 km and used as input to the GLIMMER ISM for Monte Carlo Simulations, thus allowing assessment of the impact of GLOBE DEM uncertainty on ISM results. The baseline model setup was used in our simulations, with present MAAT lowered by -10 °C, -12 °C and -14 °C, respectively, producing three sets of ISM runs. In order to determine the number of runs necessary to obtain stable and reliable results, the standard deviation of modelled ice extent across all model runs, as well as the standard deviation of this standard deviation, were plotted against the increasing number of runs, until both measures stabilised towards a constant value (Raaflaub and Collins, 2006). For each set, the mean and standard deviation of modelled ice extent and volume after 30ka model years across all runs were evaluated, and probability maps (Hunter and Goodchild, 1995) were compiled, as a measure of the frequency with which each cell was glaciated across a suite of MCS runs.

Parameter Sensitivity

Using the PDD approach for determining snow melt in GLIMMER, five parameters influence the temperature forcing. These are the mean annual air temperature at sea-level, the latitudinal dependency of temperature, the seasonal variation of temperature, the atmospheric lapse rate and the geothermal heat flux. Additionally, four parameters influence the ISM via their explicit or implicit dependence on temperature, namely the degree day factors for ice and snow, the threshold temperature for precipitation to fall as snow and the meltwater refreezing fraction (Fig. 2).

The following parameters were thus selected for initial sensitivity testing in order to identify sensible parameter ranges for PUA:

Mean annual air temperature and latitudinal dependency - *MAAT*

Atmospheric lapse rate - *lrate*

Annual temperature half-range (seasonal variation) - t_{range}

Precipitation - *precip*

Degree day factor for ice - DDF_{ice}

Degree day factor for snow - DDF_{snow}

Geothermal heat flux - G_{therm}

Threshold temperature for precipitation to fall as snow - t_{snow}

Meltwater refreezing fraction - w_{max}

The modelling of basal water and basal traction can influence ice sheet configuration due to their importance in controlling basal ice velocities. A flow enhancement factor is often used in ISMs as a tuning parameter to adjust ice flow properties, for example for layers of soft or warm ice. Thus, the following three additional parameters were tested, giving a total of 12:

Flow enhancement factor - *ffac*

Ice thickness threshold for resolving physics - *icelimit*

Basal traction rate - *btrc*

The influence of each of these parameters upon mass balance and ice dynamics and their interrelations within GLIMMER are schematically depicted in Figure 2.

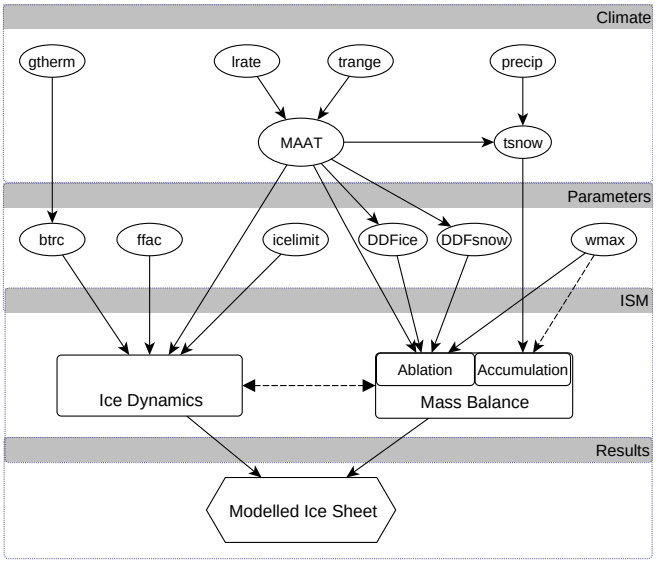

Fig. 2: Relational diagram of the ISM parameters used in the sensitivity and parametric uncertainty analyses.

For all parameters, initial values as well as variation ranges were derived from the literature and are described in detail in the following section. Additionally, for climate forcing, variation was derived from uncertainty in the input data, e.g. using differences between CRU and IPCC data and by accounting for uncertainty given in the respective metadata. Using information from the literature along with details of input data uncertainty and sensitivity, a probability density function (PDF) was derived for each parameter, in order to be used in the parametric uncertainty analysis. For this analysis, a suite of 510 input configurations for GLIMMER was created, whereby each of the 12 parameters listed above was randomly assigned a value according to the corresponding PDF.

SENSITIVITY TESTS

In this section, the sensitivity tests using the selected model parameters are presented and discussed, and probability density functions to be used within the parametric uncertainty analysis are deduced for each parameter.

Parameter ranges and PDFs

For each parameter the value range and selection criteria used within each sensitivity test are given here. A PDF to be used within the parametric uncertainty analysis for each parameter is deduced using the input criteria as well as the model sensitivity. An overview of both the tested parameter range as well as the resulting model sensitivity is given at the end of this section.

MAAT and latitudinal dependency

Differences found between the IPCC and CRU climate data sets used to derive MAATs lie in the range of -5 to +7 °C. This value range is similar to that reported by Christensen and others (1998) for CRU data compared against data from the Danish Meteorological Institute. Using these mapped differences as a basis, MAATs were varied in steps of 1 °C for the sensitivity tests, spanning a range from -8 to -16 °C cooling relative to present sea-level MAAT. Because the latitudinal variability of temperature is implicitly captured within the variation of MAAT compiled from the CRU and IPCC observations, model sensitivity to latitudinal temperature dependency was not explicitly tested and was kept constant for the PUA.

Probability Distribution Function for MAAT:
Sensitivity tests for MAAT (Fig. 3a) revealed that temperature reductions of less than 8 °C prevented any ice growth, because high ablation rates prevented ice nucleation at these temperatures. Temperature decreases of 9 °C resulted in the formation of small ice caps, but high ablation rates still prevented the formation of larger ice sheets. For temperature reductions of more than 16 °C, modelled ice sheets reached the borders of the modelling domain. Modelled ice extent after 30ka years shows an almost linear dependency with temperature decreases between -9 and -16 °C, thus indicating the relatively large influence of MAAT on model results within this range.

Because the baseline scenario, using a reduction from present day temperature of -12 °C, proved to give stable results for all parameter variations, it was chosen as the mean for the MAAT PDF in the PUA. Because the probability of temperature scenarios above or below this mean should decrease towards the extreme ends of -8 and -16 °C, a normal distribution with a standard deviation of 1.5 °C (N[-12,1.5]) was chosen as the PDF for the PUA. Thus, 95% (the 2 standard deviation range) of all temperatures lie between -9 to -15 °C (Fig. 4a).

Seasonal temperature variation

To account for seasonal variation of air temperature, the MAAT imposed on the ISM is altered using a sinusoidal function with a default half-range of 9 °C. This corresponds to an overall range in yearly mean temperatures of 18 °C, a range characteristic of present day maritime and semi-continental climates. According to Christensen and others (1998) current seasonal variation over Scandinavia ranges between 10 and 20 °C. The seasonal temperature range however is known to be strongly dependent on continentality and MAAT, and thus can take on higher values for continental locations or lower ranges for extremely cold climates. For the initial sensitivity testing, seasonal temperature amplitudes between 3 and 15 °C have therefore been used (Fig. 3b).

Probability Distribution Function for t_{range}:
Seasonal variation in temperature (t_{range}) proved to have a large influence on ISM results. For the baseline approach with a -12 °C temperature reduction, the variation of the seasonal temperature amplitude exhibited a non-linear dependency on the modelled ice extent. Because higher seasonal variations are more likely to raise temperatures above freezing and thus cause ablation during parts of the year for a certain location, elevation threshold effects are likely to play a role in the sen-

sitivity results (Hebeler and Purves, in press,b). Variations in t_{range} of between 3 and 11 °C resulted in stable, sensible ISM results. While slightly higher variations are still supported by the sensitivity results (Fig. 3b), a half range of less then 3 °C results in unrealistically large ice sheet configurations. The seasonal temperature range amplitude was therefor varied according to a normal distribution around a mean of 9 °C N[9,2]. This yields a PDF with the two standard deviation range (95%) between approx. 5 and 13 °C (Fig. 4b).

Lapse rate

The input temperature that is used to force ice sheet growth is the air temperature at the upper surface. Surface elevation is equivalent to the bedrock elevation for ice-free areas - for glaciated areas ice thickness is added - and surface temperature is extrapolated from sea-level MAAT using an atmospheric lapse rate, which is commonly taken to be 6.5 °C km^{-1} (Stone and Carlson, 1979). However, the moist adiabatic lapse rate is subject to seasonal and latitudinal variation as well as being dependent on height and atmospheric stability, and is suggested to be a better approximation to the atmospheric lapse rate in the middle and lower troposphere (Stone and Carlson, 1979). The lapse rate also varies with air moisture content, and increases up to 9.8 °C km^{-1} for dry air. For cold, high latitude regions, lapse rates have been shown to be fairly constant and nearly sub moist adiabatic.

Air pressure, seasonal variation or temperature/precipitation dependencies of the lapse rate are not explicitly considered in our climate forcing. However, variation of the lapse rate for the sensitivity testing was chosen to reflect the maximum influence that these factors might have upon lapse rate variability. Most models in very cold, dry environments such as Antarctica are generated using lapse rates of 7-9 °C km^{-1} (Jamieson and others, 2008; van der Veen, 2002; Thompson and Pollard, 1997). For their climate simulation, Christensen and others (1998) use a temporally variable lapse rate which ranges by between 5 and 6 °C km^{-1} across the year, and Charbit and others (2007, 2002) apply a lapse rate of 8 °C km^{-1} for their model of the Fennoscandian ice sheet. Reeh (1991) suggests a lapse rate of 8 °C km^{-1} for polar regions. Given the uncertainty regarding appropriate lapse rates over different regions, we select the maximum and minimum previously used rates of between 5 and 9 °C km^{-1} for use in our sensitivity analysis (Fig. 3c).

Probability Distribution Function for *lrate*:
Because of its direct relationship to temperature, modelled ice sheet extent and volume is highly sensitive to lapse rate (Fig. 3c) within the tested parameter range. An increase of the lapse rate from 5 to 6.5 °C km^{-1} almost doubles ice extent and volume, while a further increase to 8 °C km^{-1} results in a smaller magnitude response. Because of the cold climate conditions, the mean lapse rate for our experiment was assumed to be slightly higher than the commonly chosen value of 6.5 °C km^{-1} and was set to 7 °C km^{-1}. For the PUA, a PDF based on a normal distribution around this mean of 7 °C km^{-1} with a standard deviation of 1 °C km^{-1} was selected (N[7,1]). The value range deduced from the literature (5-9 °C km^{-1}) is thus covered within the 95% interval of the PDF (Fig. 4c).

Precipitation

The range and distribution of precipitation derived from CRU and IPCC data compares well with that given by Christensen and others (1998). However their reported bias of CRU precipitation data compared to observation varies for different regions by between 15 and 30%. This range was used to derive values for initial sensitivity tests and served as a basis for parametric variation. Precipitation over Fennoscandia ranges from about 0.4 m to 2.5 m per year, where most regions receive a mean of ca. 1 m of precipitation. In order to preserve the spatial precipitation scheme, and to avoid unreasonably large changes to areas that had either high or low precipitation, precipitation rates for the sensitivity tests were scaled as a percentage of the derived baseline scheme.

For the sensitivity test, variations in the range of -40% to +40%, relative to present day distribution were applied. As the impact of precipitation is strongly dependant on the mean temperature, sensitivity tests were conducted for three temperature scenarios, where recent MAAT has been lowered by 10, 12 and 14 °C, respectively (Fig. 3d-3f), in order to ascertain stable model runs for combinations of high precipitation rates and low temperatures.

Probability Distribution Function for *precip*:
As expected, the impact of varying precipitation proved to be closely related to MAAT. Scaling of precipitation in the range of -40 to +40% showed near linear dependencies with modelled ice extent for the -10 and -12 °C scenarios. For the -14 °C scenario, the relationship became slightly nonlinear, resulting in unstable model runs for increases in precipitation of more than 40%, for which ice reached the domain boundaries. Perturbing precipitation between -40 and +40 % however produced stable equilibrium results for MAAT lowering between -10 and -14 °C. The baseline precipitation was therefore used as the mean precipitation for the PUA PDF, and a global value for perturbing precipitation was drawn from a normal distribution around a mean of 0, with a standard deviation of 15% (N[0,0.15]) (Fig. 4d). This resulted in variations of precipitation between -30 and +30% in 95% of all cases. This slightly more conservative range was chosen to ensure model stability, while the 15% standard deviation still corresponds well with the mean deviation of 20% of the CRU data to meteorological observations as reported by Christensen and others (1998).

Degree day factors for ice and snow

Degree day factors used for temperature index modelling have been shown to vary for different regions, due to a range of factors such as seasonal and daily temperature amplitude, prevailing macro climate, albedo and continentality. Where temperature index models are used in glaciological modelling, different DDFs are commonly used for ice and snow. Hock (2003) compiled a list of snow and ice DDFs derived from a range of regional studies. DDFs for ice were shown to vary between 5.4 and 20 mm d^{-1} °C^{-1}, with most values lying in the range between 6 and 10 mm d^{-1} °C^{-1}. Commonly, an average DDF_{ice} of 8 mm d^{-1} °C^{-1} is used for modelling ice melt, where DDFs can not be derived from observations. The values compiled by Hock (2003) for DDF_{snow} range from a minimum of 2.5 to 11.6 mm d^{-1} °C^{-1}, with most values in the interval of 3-6 mm d^{-1} °C^{-1}.

For the sensitivity tests, the DDF for ice and snow were

varied between 6 and 10 mm d^{-1} °C^{-1} and between 3 and 8 mm d^{-1} °C^{-1}, respectively.

Probability Distribution Function for DDF_{ice} and DDF_{snow}:
Again, being closely related to temperature, variation of the DDFs has a large influence on the configuration of the modelled ice sheets (Fig. 3g & 3h). Increasing the DDF for snow from 3 to 4 mm d^{-1} °C^{-1} results in a decrease of modelled ice sheet extent and volume by almost 10% in the -12°C scenario.

For the parametric uncertainty analysis, the PDF for DDF_{ice} was centered around the standard value of 8 mm d^{-1} °C^{-1} which was used as a mean. A normal distribution with a sigma of 1 was used to cover the range identified in the literature of between 6 and 10 mm d^{-1} °C^{-1} (N[8,1]) within the 95% interval (Fig. 4e). As the standard value for DDF_{snow} marks the lower end of the variation range, an exponential distribution was chosen in this case, using a mean (μ) of 1 following the form

$$y = f(x|\mu) = \frac{1}{\mu} e^{\frac{x}{\mu}} \tag{5}$$

The default value of 3 mm d^{-1} °C^{-1} was added to the distribution, resulting in an effective range from 3 to approx. 10 mm d^{-1} °C^{-1} and a mean of 4 mm d^{-1} °C $^{-1}$, covering the range of values from the literature with decreasing probabilities for extreme values (Fig. 4f).

Geothermal heat flux

For geothermal heat flux, most ice sheet model experiments assume a value of 42 mW m^{-2}, which is a standard value for the average heat flux of Precambrian shields. However, Pollack (1982) states that heat flux is dependent on the continental age and location. Näslund and others (2005) have calculated the average geothermal heat flux to be 49 mW m^{-2} for the Fennoscandian ice sheet, with regional variations ranging from 30 to 83 mW m^{-2}. In their sensitivity tests, Ritz and others (1997) also use values of 50 and 60 mW m^{-2}, the latter being the standard value for continents. Greve and Hutter (1995) vary the heat flux by ±30% in their Greenland sensitivity experiments, using values of 29.4, 42 and 54.6 mW m^{-2}. For our sensitivity tests, a variation of the geothermal heat factor of between 35 and 65 mW m^{-2} was chosen (Fig. 3i).

Probability Distribution Function for G_{therm}:
Ice velocity depends upon the geothermal heat flux via the basal melt rates and resultant water pressures, which in turn determine rates of ice sliding. However, we find that changes in G_{therm} have negligible influence on modelled ice extent and volume (Fig. 3i). For very cold MAAT and thus low ice temperatures, the influence of geothermal heat on the thermal regime of the ice sheet is relatively small, which may explain the insensitivity to variation of this factor. However preliminary sensitivity tests with different temperature setups showed that variation of G_{therm} within the given range could influence modelled ice volume, and therefore G_{therm} was included in the PUA, and varied normally around a mean of 49 mW m^{-2} using N[49,7] (Fig. 4g).

Snow temperature threshold

The threshold temperature t_{snow} below which precipitation is assumed to fall as snow thus contributing to accumulation for mass balance modelling varies little in the literature. For example Fabre and others (1998) and Charbit and others (2007) use a threshold of 2 °C and Schneeberger and others (2003) use a threshold of 1.5 °C with linear interpolation of the rain/snow ratio from 0.5 to 2.5°C. Most other models employ a fixed threshold of 1°C. Sensitivity testing thus covered this range of between 0.5 and 2.5 °C (Fig. 3j).

Probability Distribution Function for t_{snow}:
The influence of the air temperature threshold for precipitation to fall as snow is slightly larger on modelled ice volumes than extents. Furthermore, we observe nonlinear behaviour in our models due to the spatial distribution of precipitation, which result in local effects overlying global response patterns. This suggests that variation of the threshold temperature is a potentially important factor despite the relatively low overall impact compared to that of MAAT. For the PDF, the standard value of 1 °C was assumed to have the highest probability. As the upper and lower end of the variation range are physically constrained, and are not symmetric around the mean of 1, a lognormal distribution ($\mu = 0.1, \sigma = 0.3$) was chosen for the PUA, with maxima and minima constrained to 3 and 0.5, respectively. For simplicity, random values below 0.5 or above 3 were set to 1, explaining the slight peak in the PDF (Fig. 4h).

Refreezing fraction

The refreezing fraction $w_{\max}$ prescribes the amount of melted snow that refreezes to form superimposed ice. The default value of 0.6 thus states that the first 60% of snow melted by the potential ablation forms superimposed ice, while the rest is lost as runoff. The model is designed so that if potential ablation is greater than the volume of precipitation (as snow), superimposed ice first melts, before ice itself melts. The ratio of 0.6 has been used in a suite of papers on Greenland ice sheet modelling in the early 1990's (Huybrechts and others, 1991; Letréguilly and others, 1991a,b). Even though some models and measurements suggest lower values might be appropriate or that no superimposed ice forms (e.g. Lefebre and others, 2003), a ratio of 0.6 is commonly applied in the modelling of large ice sheets. We tested refreezing fractions of between 0.4 and 0.8 for their impact on ISM results (Fig. 3k).

Probability Distribution Function for $w_{\max}$:
The refreezing fraction had a considerable influence when varied within the range tested (Fig. 3k), and is an important factor for uncertainty analysis. This is because as $w_{\max}$ is applied globally over the model domain, it is uncoupled from influencing factors such as climate, ice rheology and topography. Within our PUA, the refreezing fraction is therefore varied around the standard value of 0.6 using a normal distribution N[0.6,0.065] (Fig. 4i).

Basal traction constant / Basal sliding

In reality, as basal traction is dependent upon such factors as basal hydrology, the presence of deformable sediment or bedrock and basal sediment saturation (Jamieson and others, 2008), one global constant is unlikely to represent the different conditions prevailing under an ice sheet. Basal traction specifies the dependence of the thermomechanical properties of ice upon effective pressure. By prescribing basal traction as a function of basal melt rate b_{melt}, as we do here, spatial variations in the thermal field of the ice sheet become more gradual than if it were prescribed purely by the presence or not of water at the bed. Above a certain threshold of basal melt rate, basal sliding is at a constant maxi-

mum in our model. Ritz and others (1997) use a constant of 3×10^{-8} m a^{-1} Pa^{-2}, Payne (1995) applies a sliding multiplier of 5×10^{-3} m a^{-1} Pa^{-1}, the standard value of the EISMINT experiments is 1×10^{-3} m a^{-1} Pa^{-1} (Payne and others, 2000). Jamieson and others (2008) use basal traction constants of 2×10^{-3} and 5×10^{-3} m a^{-1} Pa^{-1} to explore ice sheet behaviour. For our sensitivity tests, two different ways of calculating basal traction were used to test the importance of the inclusion of a basal melt rate parameterisation. In a first approach, a constant basal traction value was applied where basal ice is at the pressure melting point. This set of results was used to determine the range of basal sliding rates to test with the second approach, where basal sliding is a function of basal melt water (Eq. 3). In this second sensitivity test, both minimum and maximum basal traction rates (t_{bmax}) as well as the slope of the linear relationship between melt rate and basal traction (t_{bslope}) were varied in order to determine optimal model setup (e.g. Fig. 3l).

Probability Distribution Function for *btrc*:
Changes in basal traction values have a considerable impact on ISM results and behaviour setup, through their influence on model stability via velocity calculations. If basal sliding is modelled using a constant where basal ice is at melting point (e.g. sliding and basal traction are set to either on or off), an initial increase from 0.1×10^{-3} to 1×10^{-3} m a^{-1} Pa^{-1} results in growth of ice volume and extent. Increasing the basal traction constant then reduces both volume and extent, and triggers oscillation of the ice sheet margins. This instability is due to the lack of transition between zero and maximum values of basal sliding, and was identified previously by Payne and Dongelmans (1997). For high basal sliding constants, this on/off scenario locally results in enhanced ice flow over the base, which in turn results in a rapid drawdown of ice, which decreases ice thicknesses locally. This continues until a threshold minimum ice thickness and in turn driving stress is reached, whereby the warm streaming features shut down while ice thicknesses again build up, to a state whereby rapid flow can once again be initialised. Because of these instabilities, very high basal sliding rates (enabled by high *btrc* constants) do not lead to increases in overall ice extent. However, the impact of changes in basal traction very much depends on the method used for handling basal water in the ice sheet, and on local bedrock topography. If the basal sliding is modelled as a linear function of basal melt rate, with transition zones between areas of maximum and zero sliding, these instabilities are dampened, and the basal traction configuration has less influence on the modelled ice extent and volume (Fig. 3l).

While oscillating behaviour can be found in real ice streams, in ice sheet models not accounting for longitudinal stresses it is likely to be a numerical artefact, especially where basal traction is uncoupled from basal melt rates (Payne and Baldwin, 2000). As model instabilities, which are the result of numerical limitations, can influence results, for the PUA a conservative setup was chosen, using a (minimum) basal traction constant of 0.1×10^{-3} m a^{-1} Pa^{-1}, a slope of 0.02 and variation of the maximum basal traction constant drawn randomly from a log-normal distribution ($\mu = 1e^{-05}, \sigma = 0.75$ [m a^{-1} Pa^{-1}]), suitable for covering the wide range of possible values between 0.1×10^{-3} m a^{-1} Pa^{-1} and approximately 7×10^{-3} m a^{-1} Pa^{-1} (Fig. 4j).

Flow enhancement factor

A flow enhancement factor *ffac* is commonly used as a tuning factor. While a standard factor of 1 is often applied in ice sheet models (e.g. Pattyn, 2003), higher factors are often used to simulate changes in the physical properties of ice, for example Fabre and others (1995) used this factor to represent layers of softer Weichselian ice in the Greenland ice sheet. In their sensitivity study of a Greenland ISM, Ritz and others (1997) used flow enhancement factors of 1, 3 and 5, values also used in previous experiments (e.g. Greve and Hutter, 1995; Fabre and others, 1995; Huybrechts and others, 1991; Letréguilly and others, 1991a). Sensitivity of ice extent and volume to flow factors of between 0.5 and 5 have therefore been explored in our sensitivity tests (Fig. 3m).

Probability Distribution Function for *ffac*:
The sensitivity tests showed ice extent to be relatively insensitive to changes in flow factor, while the volume varied by up to 10% with each 0.5 point change in flow factor (between values of 0.5 and 1.5), while flow factors larger than 2 have less effect on the ice volume (Fig. 3m). This effect can be explained by the lower viscosity of ice simulated through an increased flow enhancement factor. The 'softer' ice thus flows faster to lower elevations, where it is ablated, thus preventing the build up of ice at higher elevations. This results in comparable ice extent yet decreased volume. Based on these results and the commonly used values for the flow enhancement factor, the PDF was chosen to vary around the default value of 1. As the parameter range of the flow factor around this standard value is asymmetric, a lognormal distribution was chosen for the PUA, with $\mu = 0.1$ and $\sigma = 0.36$. The distribution was limited to a minimum of 0.5 by setting values below 0.5 to 1, explaining the peak in the PDF plot (Fig. 4k).

Ice limit

Because for small ice thicknesses, only minimal deformation will occur, the full thermodynamic equations need not to be solved. For computational efficiency, a minimum ice thickness threshold exists in GLIMMER, above which ice dynamics are solved. The default limit is 500 m, which corresponds to a maximum slope of 2.5% at 20 km resolution or 5% at 10 km. Using the shallow ice approximation, it has been shown that ISMs become unstable when dealing with slopes above 10%, corresponding to an ice thickness change of 1000 m at the resolution of 10 km used in these experiments. Lowering the threshold results in an increased computational demand for little gain in the predictive ability of the model because flow rates at very low slopes are negligible. Sensitivity tests were thus performed using conservative thresholds of between 200 and 600 m (Fig. 3n).

Probability Distribution Function for *icelimit*:
As expected, the impact of changing the ice limit threshold has little effect on the modelled configuration of ice sheets, while the calculation time significantly increased for low values (up to 30% for limits of 200 m instead of the default 500 m). However, variation of the ice limit results in nonlinear behaviour, and has a slightly higher influence on modelled ice volume than on extents.
Despite the limited sensitivity of modelled ice masses to these effects, the ice limit threshold is nevertheless included in the PUA for completeness. As no distribution can be deduced from the literature, and the parameter does not represent

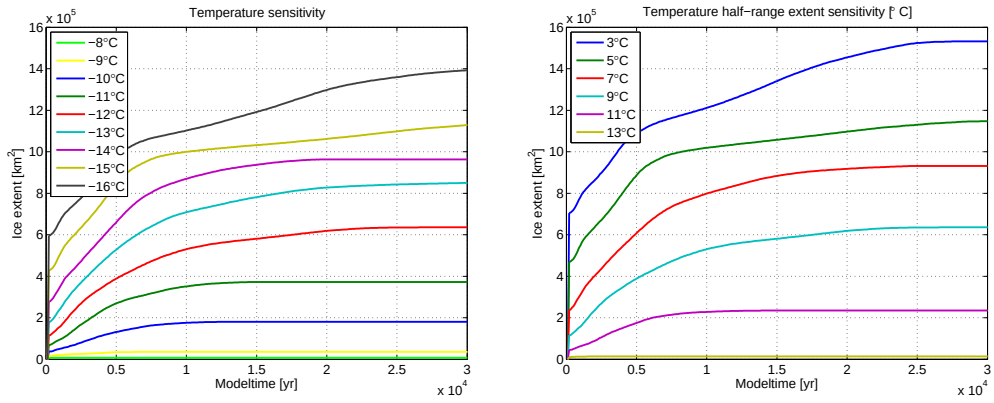

(a) Temperature

(b) Seasonal temperature variation

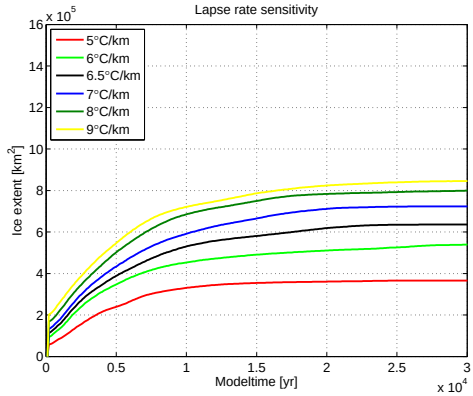

(c) Lapse rate

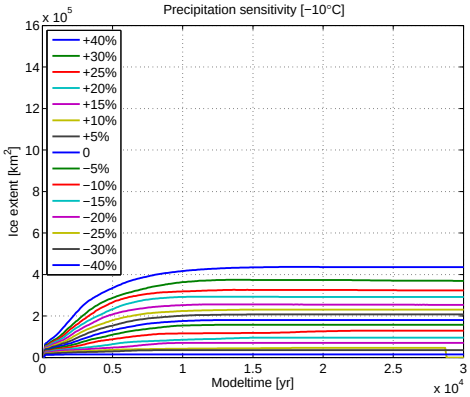

(d) Precipitation at -10 °C

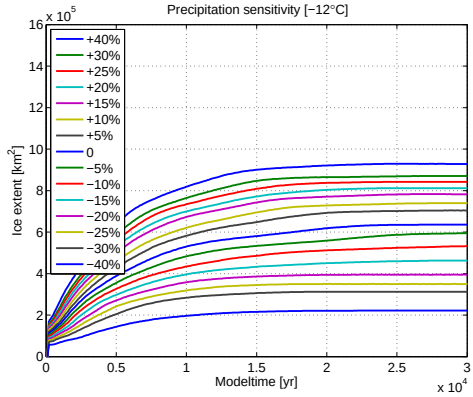

(e) Precipitation at -12 °C

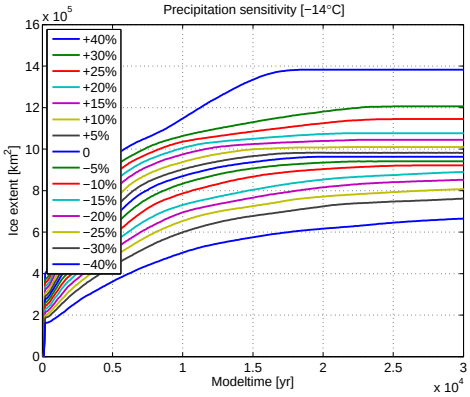

(f) Precipitation at -14 °C

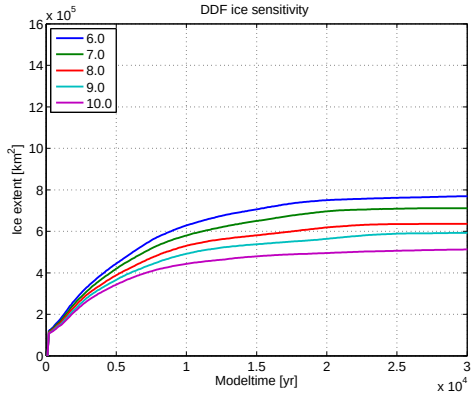

(g) DDF of ice

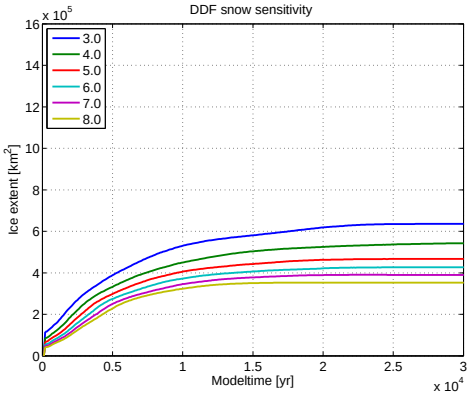

(h) DDF of snow

Fig. 3: (a-h) Sensitivity of modelled ice sheet extents to variation in input parameters MAAT, seasonal temperature variation, lapse rate, precipitation at -10, -12 and -14 °C, and DDF for ice and snow.

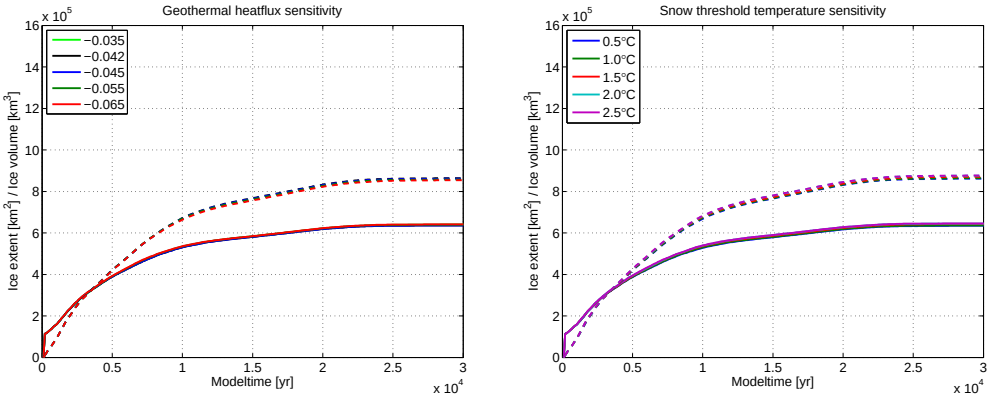

(i) Geothermal heat flux

(j) Snow threshold temperature

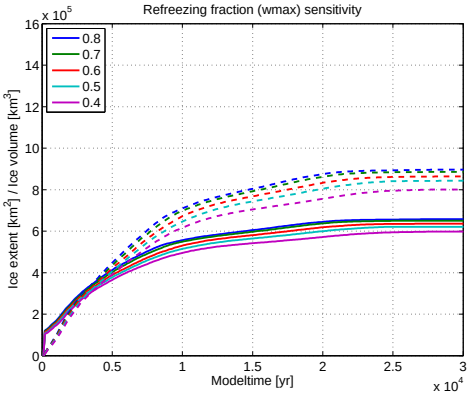

(k) Refreezing fraction

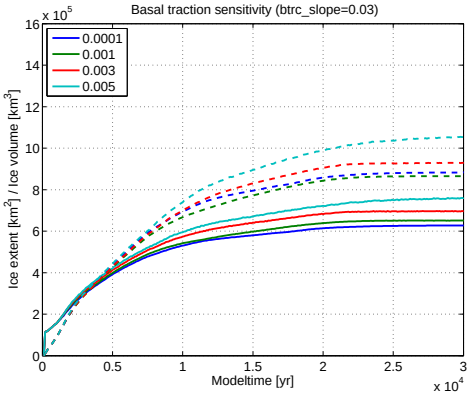

(l) Basal traction as a function of basal melt

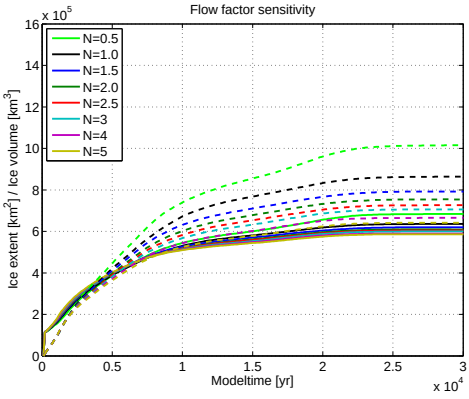

(m) Flow enhancement factor

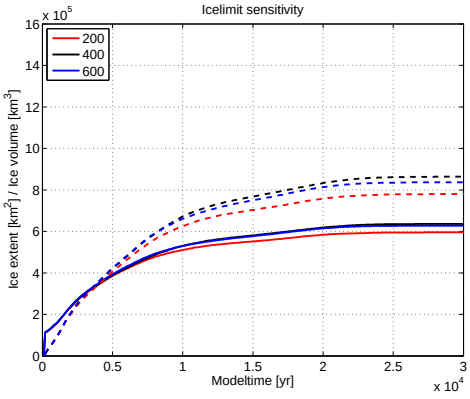

(n) Ice limit

Fig. 3: (i-n) Sensitivity of modelled ice sheet extents (solid) and volume (dashed) to variation in geothermal heat flux, snow threshold temperature, refreezing fraction, basal traction (as a function of basal melt rate), flow enhancement factor and the ice thickness threshold to solve ice dynamics.

a physical process, a uniform distribution between 200 and 600 m was chosen for the PUA (Fig. 4l).

Results and Discussion of Sensitivity Tests

The sensitivity tests conducted prior to the PUA indicate that the modelled ISM extent and volumes are most sensitive to input parameters that influence mass balance (compare Fig. 2, Tab. 1): the tested range of mean annual air temperature (Fig. 3a) and seasonal variation in air temperature (Fig. 3b) resulted in the largest variations in modelled extent (up to 200%) in the sensitivity tests. Up to a 100% change was recorded for variation in precipitation for the -12 and -14 °C scenarios (Fig. 3e,3f). The impact of lapse rate (Fig. 3c), precipitation at -10 °C and the DDFs of ice and snow (Figs. 3g & 3h) was of the range of 40-75%.

Model parameters that control ice dynamics have less influence over ice sheet model results, variation of basal traction (Fig. 3l), the flow enhancement factor (Fig. 3m) and the refreezing factor (Fig. 3k) had an impact upon modelled ice extent of around 10-20%. Additionally, the variation of both the geothermal heat flux (Fig. 3i) and snow threshold temperature (Fig. 3j) parameters within their tested ranges were found to have limited influence on both modelled ice extent and volume (around 1-2%). Varying the ice thickness threshold (Fig. 3n) for resolving of dynamics had a low to medium nonlinear impact on model results, which varied by about

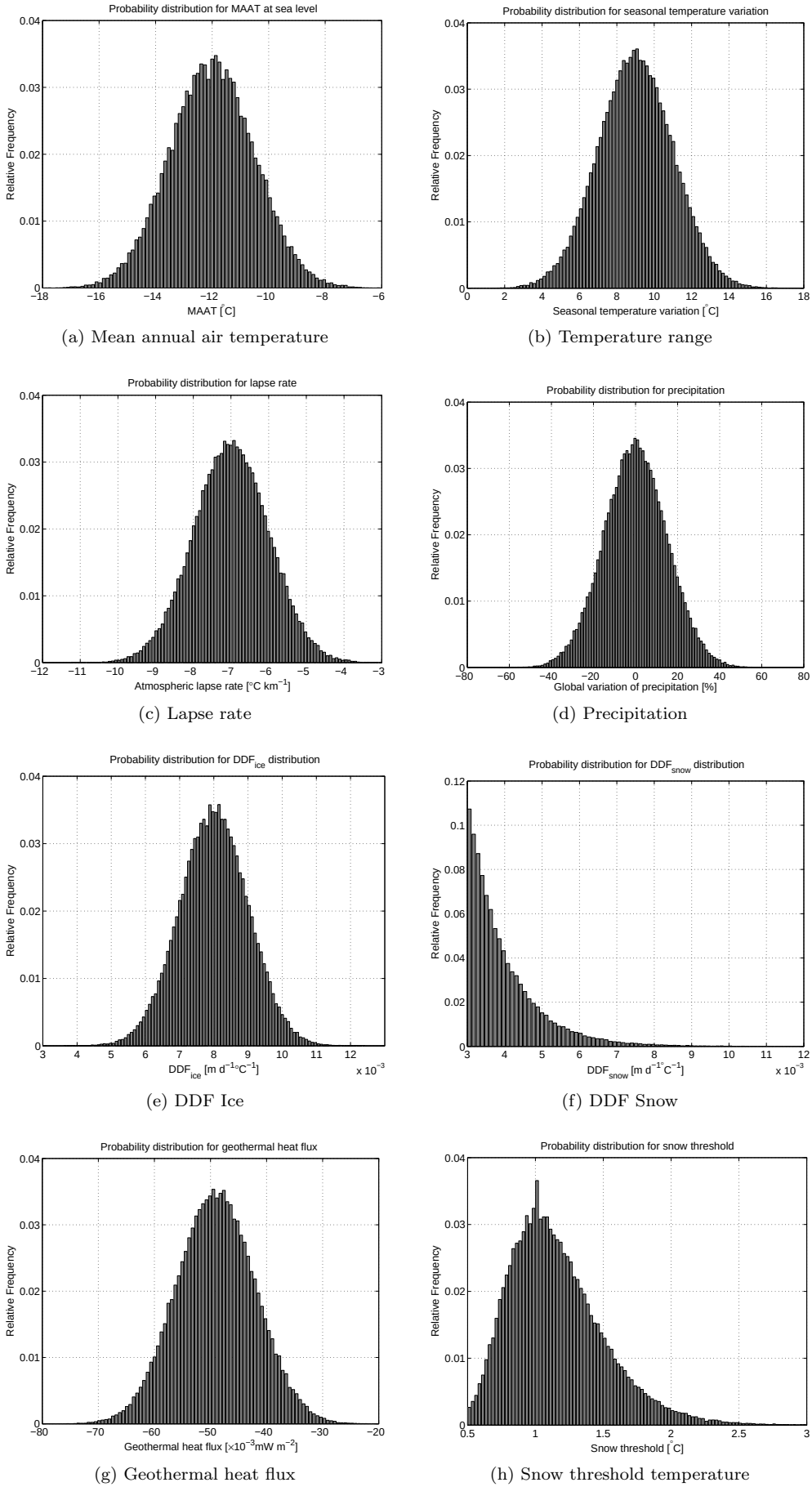

(a) Mean annual air temperature

(b) Temperature range

(c) Lapse rate

(d) Precipitation

(e) DDF Ice

(f) DDF Snow

(g) Geothermal heat flux

(h) Snow threshold temperature

Fig. 4: Probability distribution functions of the tested model parameters mean annual air temperature, seasonal temperature range, lapse rate, precipitation, DDF for ice and snow, geothermal heat flux and snow threshold temperature used in the parametric uncertainty function.

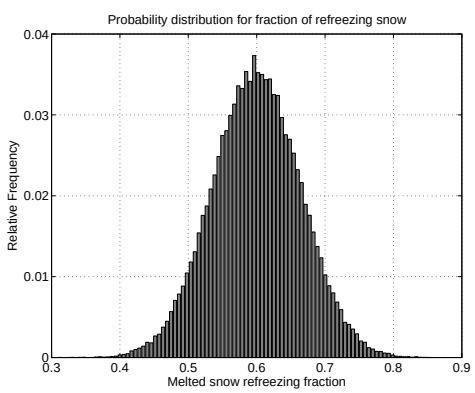

(i) Refreezing fraction

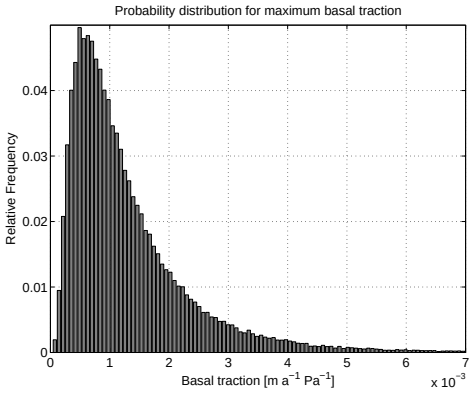

(j) Maximum basal traction

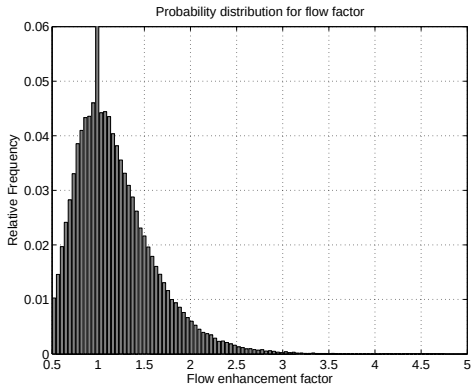

(k) Flow factor

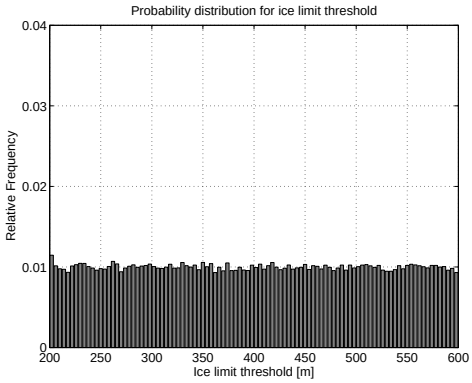

(l) Ice limit

Fig. 4: (*continued*) Probability distribution functions of the tested model parameters refreezing fraction, maximum basal traction, flow factor and ice limit used in the parametric uncertainty function.

5%. In general the impact of changing the above parameters is slightly smaller on extent than volume.

While 'external' climate parameters have a greater influence on ice sheet configurations, the 'internal' parameters that control ice dynamics can influence model stability, shown by our sensitivity tests for different basal traction configurations. The effect these parameters have on model stability can be observed when examining ice sheet behaviour. For example particular selections of parameter values can generate oscillations in ice flow. Therefore parameter setups have been chosen that are unlikely to trigger model instabilities, and because of the use of these more conservative value ranges, the influence of internal ice dynamics model parameters associated with internal ice dynamics might be low compared to those of the climate forcing module.

While the strong influence of climate parameters concurs with previous findings (Huybrechts and de Wolde, 1999), the sensitivity of modelled ice sheets to some other parameters is more controversial. For instance Huybrechts and de Wolde (1999) have found basal melt rates to have a large influence on mass balance of the Antarctic and Greenland ice sheets, and melt rates of 10-30m/a have been found for ice shelves (Rignot and Thomas, 2002; Huybrechts and de Wolde, 1999). For grounded ice, basal melt rates are heavily determined by the geothermal heat flux, and high basal melt rates under the Antarctic and Greenland ice sheets are explained by multiples of the normally assumed fluxes of 56 mW m^{-2}. Fahnestock and others (2001) report local basal melt rates of up to 1m/a for the Greenland ice sheet. In our experiments however, maximum basal melt rates lie in the range of 0.5 to 1 m/a, and variation of the geothermal heat flux showed little impact on modelled ice extent or volume, in agreement with findings by Ritz and others (1997). This inconsistency could be explained by the conservative selection of parameter variation values, but since the applied values are averages over the whole modelling domain, higher rates appeared to be unreasonable and unsupported by the literature. Another possible explanation is that in our model setups, ice thickness variation (and therefore topography) is a dominant factor influencing basal melt rates through overburden pressure. Because rapid variations in ice thickness are driving large differences in overburden pressure, they may overlay the impact of changes in geothermal heat flux. In this case higher variations in G_{therm} than the ones applied in our studies (which we assumed to be unrealistic) would show a greater impact on modelled ice extents and volumes.

Our experiments showed that increasing flow enhancement factors had a considerable effect on reducing modelled ice volume and to a lesser amount ice extent. In contrast Ritz and others (1997) experienced a slight increase in modelled ice extent for initial increases of the flow factor for their Greenland experiments. Similar behaviour can be observed for variation in basal sliding comparing the two sets of experiments. Possible explanations may lie both in the topography and the climate configurations. For example, the Greenland ice sheet margin positions are not only limited through high ablation in lower areas, but also by mass transport from the accumulation areas. In this case the lower ice viscosity simulated

Parameter		Unit	Baseline Value	Range	Impact (% deviation from baseline) Extent	Volume	Ratio	Fig.
Temperature	*MAAT*	°C	-12	-8 - -16	217.8	250.0	0.87	3a
Seasonal temperature variation	t_{range}	°C	9	3 - 15	238.7	263.5	0.91	3b
Lapse rate	*lrate*	°C/km	6.5	5 - 9	75.4	105.3	0.72	3c
Precipitation -10 °C	*precip*	% [m/a]	100	60 - 140	241.7	315.1	0.77	3d
Precipitation -12 °C	*precip*	% [m/a]	100	60 - 140	111.1	147.8	0.75	3e
Precipitation -14 °C	*precip*	% [m/a]	100	60 - 140	74.6	126.2	0.59	3f
Degree day factor for ice	DDF_{ice}	mm/d °C	8	6 - 10	40.3	49.2	0.82	3g
Degree day factor for snow	DDF_{snow}	mm/d °C	3	3 - 8	44.6	51.3	0.87	3h
Geothermal heat flux	G_{therm}	mW/m^2	45	35 - 65	0.8	2.4	0.33	3i
Snow threshold temperature	t_{snow}	°C	1	0.5 - 2.5	1.7	1.7	1.03	3j
Refreezing fraction	w_{max}		0.6	0.4 - 0.8	9.5	11.1	0.86	3k
Maximum basal traction	*btrc*	m/a Pa	0.0001	0.0001 - 0.007	21.2	21.7	0.98	3l
Flow enhancement factor	*ffac*		1	0.5 - 5	15.5	43.3	0.36	3m
Ice dynamic limit	*icelimit*	m	500	200 - 600	5.0	7.7	0.65	3n
DEM uncertainty -10 °C	DEM	m	0	*-1044 - 1044*	26.5	37.3	0.71	
DEM uncertainty -12 °C	DEM	m	0	*-1044 - 1044*	16.9	23.4	0.72	
DEM uncertainty -14 °C	DEM	m	0	*-1044 - 1044*	3.3	5.8	0.57	

Table 1: Sensitivity test parameters: default values of the baseline approach, tested parameter range, and impact on modelled ice extent and volume. Impact is measured as the deviation range from the baseline (default) value after 30 ka in percent. Ratio is the ratio of relative impact of parameter variation on extent when compared to volume. Precipitation [m/a] for each of the three temperature scenarios is varied in percent relative to the baseline input scenario. Maximum basal traction modelled using a slope of 0.02 for the basal melt function. Results of the DEM uncertainty test shown for comparison, with local maximum and minimum modelled uncertainty in meters, are discussed in the DEM uncertainty section.

by a higher flow factor would allow ice to flow further without being ablated. The relatively large seasonal temperature variations in our model setup make it likely for an area to experience ablation during some time of the year, especially for lower elevations. Therefore increases in ice extent during colder periods of the year may ablate during the summer, and not contribute to the long-term expansion of the ice sheet.

The baseline parameters and their range examined in our sensitivity tests have been carefully compiled. However both parameter ranges and parameter PDFs are approximations or still based on assumptions. The impact on modelled ice extent and volume of varying parameters across the ranges given in Table 1 are therefore not applicable for a direct comparison with each other or results from other studies. Nevertheless the impact and the impact ratio (impact on extent/volume, measure as deviation from mean in percent) for each parameter can be used to compare the relative influence of each of the factors on ISM results. The derived impact ratio (Tab. 1) can also be used to compare whether parameters have a predominant influence either on modelled ice extent or volume. This is an important consideration in understanding the mechanisms through which these parameters influence the ISM.

In general, the impact ratio of parameter variation on modelled ice extent and volume is around 0.8 (Tab. 1). This slightly higher impact of uncertainty on modelled ice volume can be explained by the fact that ice extent is a two dimensional measurement. By contrast the calculation of ice volume is three dimensional and the variation of ice thickness is explicitly included. Because of the influence of topographic uncertainty on the calculation of ice thickness, its direct impact is likely to be reflected in modelled ice volume. Parameters with a low impact ratio have a greater influence on modelled ice volume than extent, such as the flow enhancement factor and the geothermal heat flux, via its influence on basal sliding. Both

parameters influence ice velocity, through changes in either ice viscosity or sliding behaviour. Increased ice velocities support the accelerated flow of ice to lower elevations, where it is more likely to be ablated. At the same time, because ice flows away from the accumulation areas faster, ice build up is inhibited. Thus, if mass balance gradients at the edges of the ice mass are very steeply negative (i.e. high ablation rates occur near the ELA) then ice extent may not change significantly with increasing ice velocities. At the same time ice thickness (and thus volume) decreases because the ice transports ice from the accumulation zone to the ablation zone more rapidly.

Conversely, the maximum basal traction rate and the threshold temperature for precipitation to fall as snow have impact ratios close to 1 (Tab. 1). This means their influence on modelled ice extent is larger than on volume when compared to other parameters. While the overall impact of t_{snow} might be too small to support detailed analysis, it is interesting that higher rates of basal traction appear to favour changes in ice extent rather than volume. This is opposite to the effect of geothermal heat flux, a parameter that controls basal sliding via its dependence on basal melt. One explanation for this possible contradiction could lie in the fact that variation in geothermal heat flux effects the entire ice sheet, resulting in an overall change in the area of basal ice at melting point. Changes in basal traction rate on the other hand only influence areas that already are at the pressure melting point and are experiencing basal sliding. As this phenomenon occurs mostly in stream patterns and towards the edges of the ice sheet, where the ELA is positioned, changes in ice volume generated by the spatial pattern of ice velocity through basal traction may be relatively slow. At the same time ice extent may be influenced more strongly through local advances of ice stream outlets: because concentrated patches of thicker ice do not melt away as quickly as homogenously distributed, but thinner, slow moving ice advance would. However, differences as well as overall values of basal traction rate impact on modelled ice extent and volume are small, which means that a small relative changes in model results can have strong influences on the associated impact ratio.

It is interesting to note the observable decrease of the impact ratio (Tab. 1) for the precipitation variation at -14 °C. In comparison to the warmer climates tested, the impact upon volume versus extent increases. This may be due to the impact of air temperature on ice temperature and thus velocity. For the cold -14 °C scenario, the ice sheet boundary is strongly influenced by (low) ice velocities caused by the low temperatures as well as the high ice thickness dampening steeper slopes of the bedrock topography. This in turn results in areas of positive mass balance with increasing ice thickness, where ice cannot flow to ablation areas, thus direct changes in mass balance mainly act on ice volume, rather than extent. Effectively, the stiffer, slower flowing ice results in the buildup of a higher ice dome compared to higher temperature scenarios.

PARAMETRIC UNCERTAINTY ANALYSIS

The mean modelled ice extent and volume across all 510 ISM runs comprising the PUA stabilised after around 200 runs. However variance in standard deviations of both extent and volume remained high, with more than 5% difference in standard deviation of modelled ice volume being generated between the 450th and 510th model runs. Analysis of the suite of ISM runs carried out for the PUA revealed that 6 out of 510 configurations resulted in unreasonably large ice masses that reached the boundaries of the modelling domain, with ice extents in excess of 18x10^{5}km^2 (three times the standard deviation above the mean). All 6 configurations featured combinations of low temperatures (-14 °C or lower) and small seasonal temperature variations, in conjunction with normal to increased precipitation rates. In 4 out of 510 cases, the PUA configuration prevented the growth of any ice at all due to high temperatures (-7 to -9 °C) and/or low precipitation. Upon removal of these 10 outliers, despite the high variance in input parameters, and the high sensitivity of modelled ISM results to these parameters, the variation in standard deviation modelled ice volume dropped below 5% after 200 runs (Fig. 5).

Ice Extent [x10^{5}km^2]				**Ice Volume** [x10^{5}km^3]			
Mean	STD	Min	Max	Mean	STD	Min	Max
5.66	3.70	0.02	15.58	8.02	6.06	1.24	31.36

Table 2: Mean, standard deviation (STD), maximum and minimum equilibrium (after 30k model years) ice extent and volume for the parametric uncertainty analysis.

The small number of outliers (10 in total) comprise less than 2% of the runs, suggesting that PUA configuration was appropriate in most cases. The fact that only 6 configurations resulted in ice sheets that grew out of the domain suggests a conservative selection of parameter ranges towards their upper end. At the same time, the PDF plot (Fig. 6) shows more than 40 runs with ice extents smaller than 0.35x10^{5}km^2, which essentially feature only a small number of glaciated mountain peaks and no significant ice sheets. This suggests the variation of input parameter ranges may be biased towards the lower end.

This is supported by the mean ice extent and volume of the PUA (Tab. 2), which lie below that of the -12 °C baseline scenario (Tab. 3): the mean modelled ice extent of the remaining 500 ice sheets which reach equilibrium (after 30ka model years), is approx. 5.7x10^{5}km^2 with a standard deviation of 3.7x10^{5}km^2, equivalent to slightly more than 65% of the mean (Tab. 2). Possible explanations for the smaller average ice extent compared to that of the -12 °C baseline scenario include the unchanging spatial pattern of the precipitation scheme, where scaling of the precipitation below a certain threshold is more likely to inhibit ice nucleation in general. Another factor might be the PDFs of the input parameters. While most PDFs are symmetric around the default parameter values of the baseline configuration (e.g. MAAT, precipitation, lapse rate), the PDFs of DDF_{snow}, the flow enhancement factor and the snow threshold temperature (Fig. 4f,4k,4h) are asymmetric, with a higher probability of selecting values that result in relatively smaller ice sheets. However, the relatively low sensitivity of modelled ice sheets to these last three factors, and the high susceptibility to climatic factors makes it more likely the aforementioned ice mass configurations are the result of either high air temperatures and/or low precipitation.

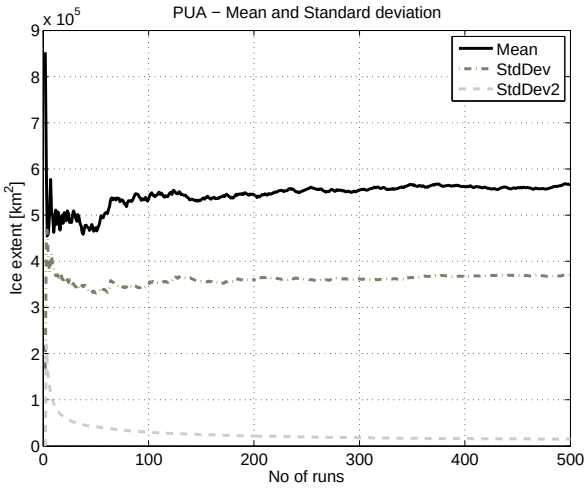

Fig. 5: Mean (solid) and standard deviation (broken) of ice extent after 30k model years across PUA runs plotted against number of runs. Standard deviation of standard deviation plotted dashed light gray.

Indeed, a closer examination of the model setup configurations of the runs that resulted in no significant ice sheets, showed that almost all of them had sea-level temperatures above -10 °C (relative to present day climate) in combination with high values of seasonal temperature variation. Sensitivity tests show that only small ice caps form for temperature lowering of less than 9 °C (Fig. 3a) and, even for lower temperatures, high ablation rates during summer, as a result of large seasonal temperature variations, prevent the expansion of ice from the highest peaks. This underlines the fact that temperature is probably the most important parameter for the ISM, especially because it affects not only mass balance, but also ice dynamics, and has multiple feedback and coupling mechanisms (compare Fig. 2).

The model configurations generated for our parametric uncertainty analysis models cover a wide range of possible ice sheet configurations (Fig. 7), and approximately half of all runs results in a single ice sheet stretching across the Fennoscandian ridge. This is reflected in a relative standard deviation of extent of 92% over all runs during the inception phases, which decreases with ice sheet growth, and slowly increases again after 12 kyrs to around 65% (Fig. 8).

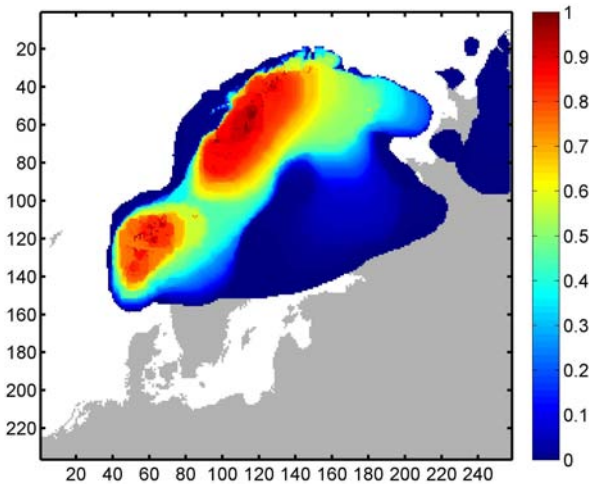

Fig. 7: Probability map of modelled equilibrium ice extent across the PUA. Likelyhood of a cell to be glaciated after 30ka across a suite of 500 model runs. Size of model area in cells for the x and y-axis.

Apart from the peak in the PUA resulting from the runs where only small ice caps formed, the PUA shows a bifurcation of modelled equilibrium ice extent above and below 6x10^{5}km^2. The probability map (Fig. 7) indicates that the cause is likely to be the coalescence of the two separate ice sheets in the northeast and southwest of the Fennoscandian ridge, which form in over 80% of all runs. In about 50% of all model runs, these two ice masses coalesce to form a single large ice sheet. Probability drops sharply to values below 5% along the northwest coastal margin. A more gradual decrease is observed at the southeast ice sheet margin in southern Sweden and towards the Russian mainland. A relatively small number of runs (less than 10%) shows considerably larger ice sheets reaching further into the Atlantic and covering the Baltic sea, as well as forming independent ice caps towards the eastern boundary of the modelling domain.

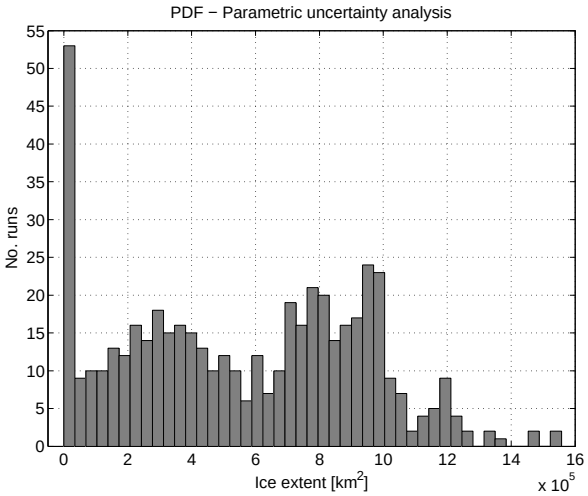

Fig. 6: PDF of modelled ice extent of the parametric uncertainty analysis.

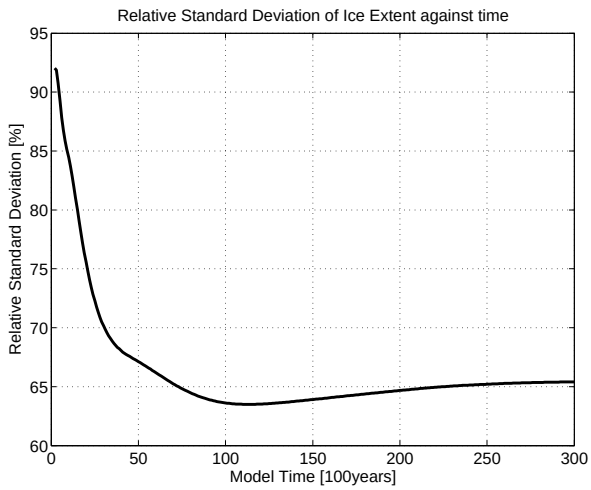

Fig. 8: Relative standard deviation [%] of modelled ice extent over time for parametric uncertainty analysis.

DEM UNCERTAINTY TESTS

Plotting the standard deviation of the standard deviation of modelled ice extent against increasing numbers of Monte Carlo simulations for the DEM uncertainty test shows the value stabilises after around 100 to 150 model runs under all three temperature scenarios (Fig. 9); consequently, the maximum number of conducted MCS runs for all scenarios was limited to 150. This number is considerably larger than the number of runs used in some other MCS. For example Davis and Keller (1997) conducted 50 runs for slope stability prediction modelling, and Openshaw (1989) suggests 20-30 runs would be sufficient if only summary statistics are required. For our DEM uncertainty runs, an estimation of the mean of modelled ice sheets using only 50 runs would produce largely sensible results: the mean of the first 50 runs for the -10 °C scenario is within 2.6% of that all 150 runs (-12 °C:1.2%, -14 °C:0.3%). However an estimation of standard deviation after only 50 runs show as much as 31% change from the value derived after 150 model runs for the -10 °C scenario (-12 °C:14.5%, -14 °C:1.8%, compare Fig. 9). The requirement for an increased number of model runs to obtain a stable set of results is likely to be caused by the complexity of both the ISM and the model used to simulate DEM uncertainty, in comparison to, for example, a slope stability model.

Modelled ice extent and volume for the three temperature scenarios (Tab. 3) show the total range of modelled ice extent (the difference between the minimum to maximum run) to be ca. 22% around the mean for the -10 °C scenario, ca. 16% for the -12 °C scenario and ca. 3% for the -14 °C scenario. The variation for modelled ice volumes is notably higher, with values of approximately 31%, 23% and 6% for the -10, -12 and -14 °C scenarios.

An increased cooling from -10 to -12 °C relative to recent temperatures, results in an almost threefold increase in modelled ice extent. The absolute standard deviation of modelled ice extents and volume under these cooler conditions only increases by about a third (Tab. 3, Fig. 9), which is equivalent to a drop of relative standard deviation from 6.5% to approx. 3% (and equivalent to a drop from 9.2% to 3.8% in modelled ice volume). While further cooling of -14 °C increases the size of the modelled ice sheet by about another 50%, absolute standard deviation also decreases and relative standard deviation drops to around 1% (Fig. 10). The the impact of DEM uncertainty as represented by relative standard deviation is larger on modelled ice volume than it is on extent.

This decreasing impact of DEM uncertainty on ISM results with increasing total ice sheet size, as measured by the relative standard deviation of ice extent and volume across MCS runs (Fig. 10), is consistent with previous findings (Hebeler and Purves, 2008), as is the larger impact of DEM uncertainty on modelled ice volume than on ice extent. These results reflect the shrinking influence of bedrock topography in models where ice sheet configurations result in larger ice masses.

This fact is also supported by the probability distribution functions of modelled ice extent for the three temperature scenarios shown in Figure 9, which are classified into 30 equally distributed classes between the respective minimum and maximum modelled ice extent. In the -10 °C scenario (Fig. 9b) a bifurcation in the PDF is observable, where a third of the modelled ice sheets are about 20% larger than the rest.

Looking at the associated probability map for the -10 °C setup (Fig. 11A) show the main ice masses in northern Norway (Fig. 11A), with two smaller ice caps in the southwest with high glaciation probabilities. These are surrounded by an irregular probability distribution, showing that relatively large areas have relatively low probabilities of becoming glaciated. This suggests the bifurcation in the PDF is caused by the coalescence of the two southwestern icecaps. This occurs where local topography supports ice mass coalescence – either by lowered elevation of obstructing ridges or by increased elevation of associated peaks – which can drive an increase in mass balance. The coalesced Southern ice sheet can then expand further towards the East and West due to the further increase in accumulation enabled by the presence of a high elevation ice mass. This positive elevation-mass balance feedback occurs because as the two ice caps meet, the area between them is rapidly filled with ice, and instead of the bedrock, the elevated ice surface determines air temperature, resulting in increased likelihood of precipitation falling as snow and in turn less ablation, which thus increases mass balance of the ice sheet. The additional ice then flows towards lower elevations, thus driving ice expansion in the west and east.

A clear peak and a slight right skew characterises the PDF of the -12 °C scenario (Fig. 9), with only 9 runs featuring modelled ice extents of 10% or more below the mean. The associated probability map (Fig. 11B) features two glaciation centers in the northeast and southwest, with glaciation probabilities being high over the majority of the potentially glaciated area but decreasing rapidly towards the ice margins, dropping to zero within an average range of ca. 3-5 cells. This rapid transition of probability over a few cells indicates a relatively certain position of the ice margin. An exception to this is a considerable area of medium to high probability glaciated cells located between the northeastern and southwestern ice sheets. In ca. 10-15 of the 150 runs, these ice sheets are not fully connected and the described elevation-mass balance feedback is not initiated, resulting in substantially smaller ice sheet extents. This reflects uncertainty in the coalescence of the two ice masses. In the northeastern corner a similar pattern exists, where glaciation probability gradually decreases towards the ice margin over ca. 20-30 cells. In these areas, the position of the ice margin is less certain, resulting in a higher sensitivity to uncertainty in bed topography. While, because of the large overall ice masses, the relative difference in size is comparably small, the configuration of the modelled ice sheets is significantly different, namely two separate ice sheets in almost 10% of all cases as compared to a single large ice sheet.

With a further decrease in temperature to -14 °C, the influence of DEM uncertainty, measured as both relative and absolute standard deviation, becomes negligible, resulting in an evenly distributed PDF with an absolute variation of 3.5% from the mean. The probability map for this scenario (Fig. 11C) shows a single ice mass stretching over the Fennoscandian ridge with centrally high probabilities of glaciation and again a rapid decrease in probability towards the edges. Here, ice extent is mainly limited by calving into the Atlantic and the Baltic Sea, as well as higher ablation rates in Southern Sweden. The influence of topography on ice flow is limited to a relatively small area in the north east, where the glaciation probability decreases more gradually towards the Russian mainland (Fig. 11C).

Since ice sheet models are commonly run at resolutions of 5-20 km, an order of magnitude lower than the most common DEMs of the earth's surface (e.g. SRTM, GLOBE, GTOPO30),

	Ice Extent [x10^5km^2]					**Ice Volume** [x10^5km^3]				
Temp	Mean	Std. Dev.	rel. Std. Dev. [%]	Min	Max	Mean	Std. Dev.	rel. Std. Dev. [%]	Min	Max
-10 °C	2.160	0.143	6.6	1.942	2.420	2.170	0.198	9.1	1.864	2.536
-12 °C	6.517	0.202	3.1	5.724	6.800	8.816	0.366	4.2	7.390	9.410
-14 °C	9.360	0.071	0.8	9.196	9.515	14.028	0.162	1.2	13.479	14.331

Table 3: Mean, absolute and relative standard deviation, maximum and minimum equilibrium ice extents and volume after 30k model years for the three DEM uncertainty MCS scenarios, as generated after mean temperature lowering of 10, 12 and 14 °C.

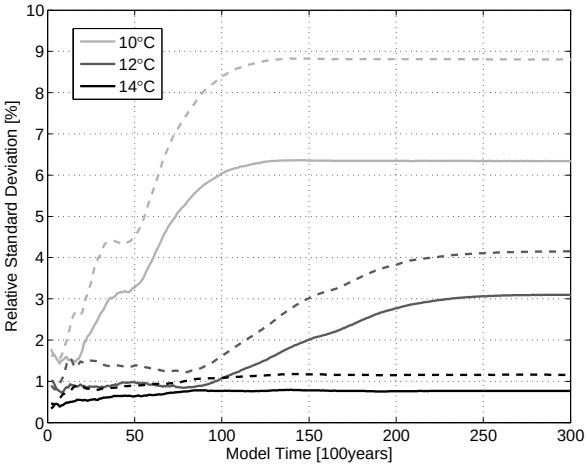

Fig. 10: Relative standard deviation [%] of modelled ice extent (solid) and volume (dashed) for the three temperature scenarios of the DEM uncertainty MCS.

DEM accuracy is often assumed to be irrelevant. Our analysis has shown this assumption to be misleading, because uncertainty such as that simulated for the GLOBE DEM has an impact upon model results that is similar in scale to that of other key ISM parameters such as the flow enhancement factor, basal traction or the refreezing fraction. Additionally, because of the necessary resampling of DEMs during preparation for use as ISM input, key landform features and attributes are often lost due to the inherent smoothing. This in turn may lead to unrealistic tuning of an ISM or its climate driver parameters in order to force ice growth.

COMPARISON OF RESULTS

The aim of this work is to systematically investigate the effect of uncertainty in model parameterisation and input data, and to develop generalisable set of methods for exploring this parametric uncertainty in ice sheet model results rather than to investigate the uncertainties associated with a particular ice sheet reconstruction. The conducted model test are valid primarily for the selected baseline parameter values, which makes a comparison of the absolute model results with that from other experiments, or even with work from other authors difficult. The main reason for this is that the impact of uncertainty in one parameter can strongly depend on a number of other model parameters. Modelling of Fennoscandian ice sheet using different models, climate data or topographic resolution is likely to produce different results, which is partly triggered by the large degree of approximation applied in large scale physical ice sheet models. Despite this, a comparison of the results obtained throughout our experiments with empirical data such as compiled by Svendsen and others (2004) can help to integrate our findings with previous work.

In general, the ice sheet configuration obtained by applying our baseline climate compares well to those compiled by Svendsen and others (2004) for the LGM in Fennoscandia, except for the eastern ice margin, where modelled ice sheets reach to the Gulf of Bothnia and northern Finland, while the recorded LGM maximum is further east, reaching across the White Sea into Russia. The smaller ice sheets modelled within our experiments are presumably the result of the climate distribution (temperature and precipitation) based on present day observations, which are likely to differ from those of the LGM. Additionally, because we did not aim at reconstructing the LGM ice sheet, boundary conditions were not adjusted for this task. Earlier experiments on Fennoscandia that applied climate time series based on GRIP data (Dahl-Jensen and others, 1998) as well as global sealevel changes reproduced ice sheet configurations well in line with recorded LGM extents (Hagdorn, 2003). Because open water of more than 250 m depth restrains ice advance through the associated calving rates applied within the model, the Baltic Sea prevents ice flow towards the east. Applying local sea level lowering that prevailed during the LGM would have facilitated the filling of the Baltic Sea and consequent ice flow eastwards, and modelled ice sheets and associated uncertainties would have likely been larger. This assumption is sustained by the fact that for PUA runs with very cold climate and increased precipitation, which account for the maximum modelled ice extent (Fig. 7), the Gulf of Bothnia is ice covered despite the unchanged sea level, and maximum ice extent reaches into the White Sea and Russia (Fig. 7), giving a closer resemblance to the maximum ice limits mapped by Svendsen and others (2004).

While for the DEM uncertainty experiments, the spatial distribution of the input topography was varied, for the PUA parameters were varied globally. The changes in topographic configuration as a result of DEM uncertainty influenced ice sheet configuration both through impact on inception points and ice flow. Alteration of ridges and troughs control the coalescence of ice masses and resulted in different configurations

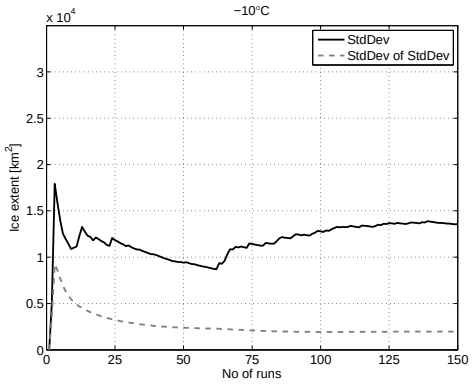

(a) Standard deviations of ice extent - DEM uncertainty -10 °C scenario

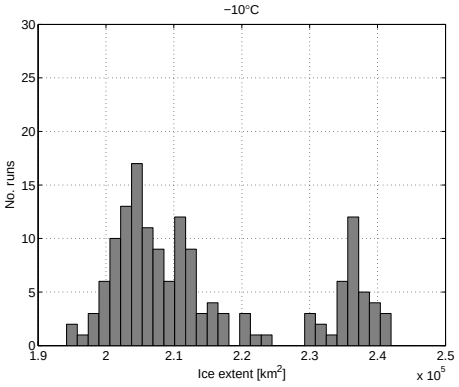

(b) PDF - DEM uncertainty -10 °C scenario

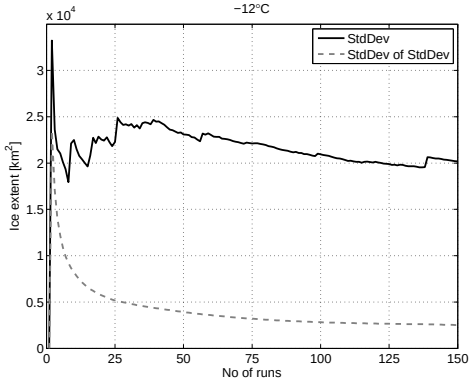

(c) Standard deviations of ice extent - DEM uncertainty -12 °C scenario

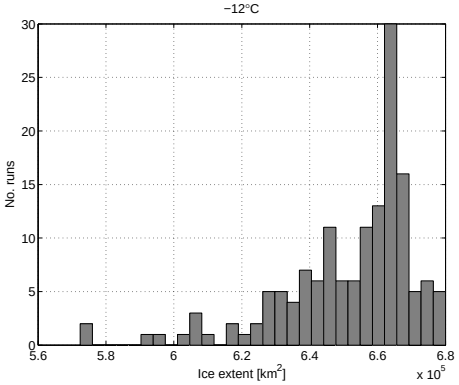

(d) PDF - DEM uncertainty -12 °C scenario

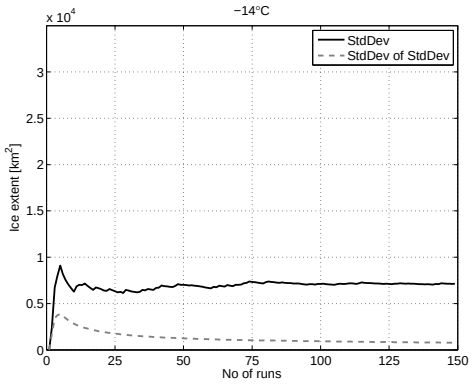

(e) Standard deviations of ice extent - DEM uncertainty -14 °C scenario

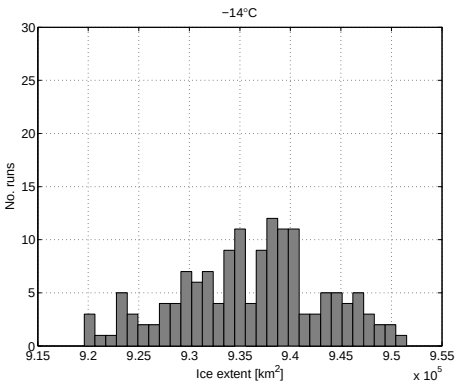

(f) PDF - DEM uncertainty -14 °C scenario

Fig. 9: The left-hand column shows the standard deviations of modelled ice extent across an increasing number of MCS runs for the -10, -12 and -14 °C scenarios (Figures a,c,e). Standard deviation of ice extent plotted solid, standard deviation of the standard deviation in light gray, dashed. The right-hand column shows the PDFs of modelled ice extents for the -10, -12 and -14 °C temperature scenarios of the DEM uncertainty analysis (Figures b,d,f) using 30 equal sized classes (note the different horizontal scales).

(two isolated vs. one continuous ice sheet, Fig. 11A,B), represented by the bifurcation of the associated PDFs (Fig. 9). This same bifurcation can be seen in the PUA results (Fig. 6), where the influence of topography on ice sheet configuration is determined by the prevailing climate. While the patterns are comparable, the variation of modelled ice extent and volume encountered in the PUA is much larger than that of the DEM uncertainty tests.

CONCLUSIONS

1. We have proposed a generalisable set of methods for exploring the parametric uncertainty of ice sheet model results. The approach of compiling a range of possible parameter values from the literature as well as climate input data, and the derivation of associated probability functions to be used as input to a parametric uncertainty analysis allows numerous stable models of ice sheets to be generated and analysed. While the 510 runs conducted

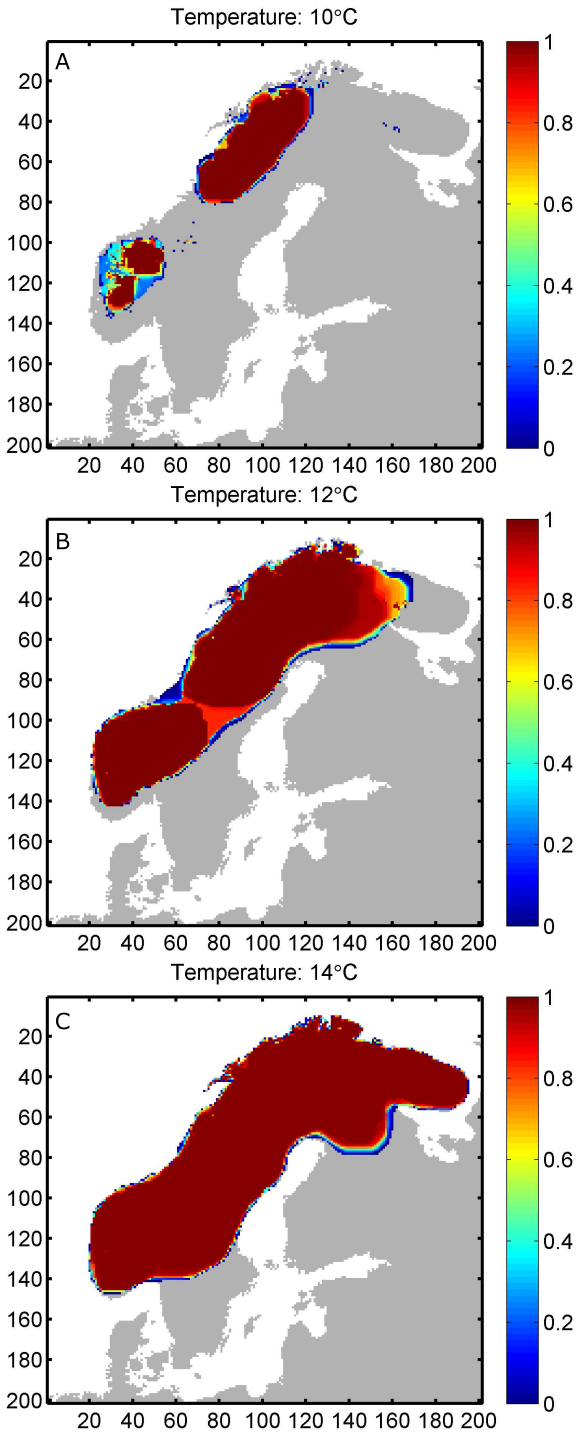

Fig. 11: Probability maps of modelled ice extent of the DEM uncertainty MCS runs, for the three temperature scenarios of -10 °C (A), -12 °C (B) and -14 °C (C). Probability of each grid cell being glaciated across 150 runs is plotted on top of the Fennoscandian coastline. X- and y-axis given in number of cells.

for the PUA require considerable amounts of time and computing power, it was shown that if extreme outliers are eliminated during the analysis, for example through visual inspection, the overall number of necessary runs can be reduced to 200-250. Comparison of the relative impacts of tested parameters as well as their impact ratio on modelled ice extent and volume aids understanding of uncertainty impact mechanisms as well as the explanation of PUA results.

A comprehensive selection of ISM parameters were used to generate ice sheets of Fennoscandia, and the majority of these resulted in stable ice masses. This allowed us to identify the importance of particular parameters upon ice sheet extent and volume. The approach presented here provides a reproducible method for sensitivity testing of ISM, in order to determine their susceptibility to uncertainty in input data and to the choice of model parameters.

2. Applying an uncertainty model in the simulating of DEM error allowed us to explore the impact of uncertainty in bed topography on modelled ice sheets. Across Monte Carlo Simulation (MCS) runs, for ice sheets in equilibrium recorded variations were in the range of 0.8 to 6.6% for modelled extent, and between 1.2 and 9.1% for modelled volume, depending on the applied temperature scenario. Even though these variations are relatively small, experiments suggest the effect that topographic uncertainty can have on model results, especially during phases of inception and for smaller ice sheets sizes, is significant and can result in substantially different ice sheet configurations. Using an ISM that employs the shallow ice approximation in combination with a complex uncertainty model such as the GLOBE DEM uncertainty model applied in this study showed that a minimum of 100-150 MCS runs is required in order to deliver a stable and reliable set of results that inform the user about the probability of particular areas being glaciated.

3. Using different climate scenarios, the dependency of the impact of topographic uncertainty on the overall size of an ice sheet was determined. The influence of DEM uncertainty on ISM is comparable to that of (other) parameters, such as the flow enhancement factor or basal traction. Parameters influencing mass balance directly, such as mean annual air temperature, precipitation and degree day factors were confirmed to have the largest impact on modelled ice extent and volume. Uncertainty from model parameters, assessed by a full parametric uncertainty analysis, revealed large variations in modelled ice sheet extents, with a relative standard deviation of 65% across MCS runs for equilibrium ice sheets. Modelled ice sheet configurations exhibited a bifurcation, induced by characteristics of the bedrock topography.

Acknowledgements

This research was funded by the Swiss National Science Foundation SNF, project number 200020-109449. The authors would like to thank J. Fastook and an anonymous reviewer, as well as the scientific editor R. Greve for their help in improving this paper.

References

Anderson, J. L., 1996. A Method for Producing and Evaluating Probabilistic Forecasts from Ensemble Model Integrations., *Journal of Climate*, **9**(7), 1518–1530.

Boulton, G.S. and A. Payne, 1992. Simulation of the European ice sheet through the last glacial cycle and prediction of future glaciation., *Tech. Rep. SKB 93-14*, Swedish Nuclear Fuel and Waste Management Co.

Charbit, S., C. Ritz, G. Philippon, V. Peyaud and M. Kageyama, 2007. Numerical reconstructions of the Northern Hemisphere ice sheets through the last glacial-interglacial cycle., *Climate of the Past*, **3**, 15–37.

Charbit, S., C. Ritz and G. Ramstein, 2002. Simulations of Northern Hemisphere ice-sheet retreat: sensitivity to physical mechanisms involved during the Last Deglaciation., *Quaternary Science Reviews*, **21**, 243–265.

Christensen, O. B., J. H. Christensen, B. Machenhauer and M. Botzet, 1998. Very High-Resolution Regional Climate Simulations over Scandinavia - Present Climate., *Journal of Climate*, **11**, 3204–3229.

CRU, 2006. Climatic Research Unit, School of Environmental Sciences, University of East Anglia: 5x5 degree gridded temperature and precipitation data., http://www.cru.uea.ac.uk/, accessed 20.8.2006.

Dahl-Jensen, D., K. Mosegaard, N. Gundestrup, G. D. Clow, S. J. Johnsen, A. W. Hansen and N. Balling, 1998. Past temperatures directly from the Greenland ice sheet., *Science*, **282**(5387), 268–271.

Davis, T. J. and C. P. Keller, 1997. Modelling uncertainty in natural resource analysis using fuzzy sets and Monte Carlo simulation: slope stability prediction., *International Journal of Geographical Information Science*, **11**(5), 409–434.

Ehlschlaeger, C. R. and M. F. Goodchild, 1994. Uncertainty in Spatial Data: Defining, Visualizing, and Managing Data Errors., Proceedings of GIS/LIS 1994, Phoenix AZ, 246–53.

Essery, R. and P. Etchevers, 2004. Parameter sensitivity in simulations of snowmelt., *Journal of Geophysical Research*, **109**, D20111.

Fabre, A., A. Letréguilly, C. Ritz and A. Mangeney, 1995. Greenland under changing climates: sensitivity experiments with a new three-dimensional ice-sheet model., *Annals of Glaciology*, **21**, 1–7.

Fabre, A., G. Ramstein, C. Ritz, S. Pinot and N. Fournier, 1998. Coupling an AGCM with an ISM to investigate the ice sheets mass balance at the last glacial maximum., *Geophysical Research Letters*, **25**(4), 531–534.

Fahnestock, M., W. Abdalati, I. Joughin, J. Brozena and P. Gogineni, 2001. High Geothermal Heat Flow, Basal Melt, and the Origin of Rapid Ice Flow in Central Greenland., *Science*, **294**(5550), 2338–2342.

Fisher, P. F., 1998. Improved Modeling of Elevation Error with Geostatistics., *GeoInformatica*, **2:3**, 215–233.

Forsström, P.-L. and R. Greve, 2004. Simulation of the Eurasian ice sheet dynamics during the last glaciation, *Global and Planetary Change*, **42**, 59–81.

GLOBE Task Team & others, 1999. The Global Land One-kilometer Base Elevation (GLOBE) Digital Elevation Model, Version 1.0. Digital data base on the World Wide Web (URL: http://www.ngdc.noaa.gov/mgg/topo/globe.html) and CD-ROMs., National Oceanic and Atmospheric Administration, National Geophysical Data Center, 325 Broadway, Boulder, Colorado 80303, U.S.A.

Greve, R. and K. Hutter, 1995. Polythermal three-dimensional modelling of the Greenland ice sheet with varied geothermal heat flux, *Annals of Glaciology*, **21**, 8–12.

Hagdorn, M. K. M., 2003. Reconstruction of the Past and Forecast of the Future European and British Ice Sheets and Associated Sea-Level Change., unpublished PhD thesis, University of Edinburgh.

Hagdorn, M. K. M., I. Rutt, T. Payne and F. Hebeler, 2007. GLIMMER - The GENIE Land Ice Model with Multiply Enabled Regions - Documentation. http://glimmer.forge.nesc.ac.uk/, Universities of Bristol, Edinburgh and Zurich.

Hastings, D. A. and P. K. Dunbar, 1999. Global Land One-kilometer Base Elevation (GLOBE) Digital Elevation Model, Documentation, Volume 1.0. Key to Geophysical Records Documentation (KGRD) 34., National Oceanic and Atmospheric Administration, National Geophysical Data Center, 325 Broadway, Boulder, Colorado 80303, U.S.A., 1.0 ed.

Hebeler, F. and R. S. Purves, 2004. Representation of topography and its role in uncertainty: a case study in ice sheet modelling., GIScience 2004: Proceedings of the Third International Conference on Geographic Information Science., 118–121.

Hebeler, F. and R. S. Purves, 2008. Modeling DEM Data Uncertainties for Monte Carlo Simulations of Ice Sheet Models., Stein, A., J. Shi and W. Bijker, eds., Quality Aspects in Spatial Data Mining., CRC Press, Boca Raton, 175–196.

Hebeler, F. and R. S. Purves, in press,a. The influence of elevation uncertainty on derivation of topographic indices., *Geomorphology*.

Hebeler, F. and R. S. Purves, in press,b. Parameterisation of low resolution melt modelling using hypsometric subgrids and its susceptibility to uncertainty., *Hydrological Processes*.

Hock, R., 2003. Temperature index melt modelling in mountain areas., *Journal of Hydrology*, **282**, 104–115.

Holmes, K. W., O. A. Chadwick and P. C. Kyriakidis, 2000. Error in a USGS 30-meter digital elevation model and its impact on terrain modeling., *Journal of Hydrology*, **233**, 154–173.

Hubbard, A., A. S. Hein, M. R. Kaplan, N. R. J. Hulton and N. Glasser, 2005. A modelling reconstruction of the Last Glacial Maximum ice sheet and its deglaciation in the vicinity of the Northern Patagonian Icefield, South America., *Annals of Glaciology*, **87 A**(2), 375–391.

Hulton, N. R. J., R. S. Purves, R. D. McCulloch, D. E. Sugden and M. J. Bentley, 2002. The Last Glacial Maximum and deglacation in southern South America., *Quaternary Science Reviews*, **21**, 233–241.

Hulton, N. R. J., D. E. Sugden, A. Payne and C. M. Clapperton, 1994. Glacier modeling and the climate of Patagonia during the last glacial maximum., *Quaternary Research*, **42**, 1–19.

Hunter, G. J. and M. F. Goodchild, 1995. Dealing with error in spatial databases: a simple case study., *Photogrammetric Engineering and Remote Sensing*, **61**(5), 529–537.

Hutter, K., 1983. Theoretical Glaciology. Mathematical Approaches to Geophysics., D. Reidel Publishing Company, Dordrecht, Boston, Lancaster.

Huybrechts, P., 1986. A three-dimensional time-dependant numerical model for polar ice sheets; some basic testing with a stable and efficient finite difference scheme., *Tech. rep.*, Geografisch Instituut, Vrije Universiteit Brussel, Belgium.

Huybrechts, P. and E. Le Meur, 1999. Predicted present-day evolution patterns of ice thickness and bedrock elevation over Greenland and Antarctica., *Polar Research*, **18**(2), 299–306.

Huybrechts, P., A. Letréguilly and N. Reeh, 1991. The Green-

land ice sheet and greenhouse warming., *Global and Planetary Change*, **3**(4), 399–412.

Huybrechts, P., A. Payne, A. Abe-Ouchi, R. Calov, A. Fabre, J. L. Fastook, R. Greve, R. C. A. Hindmarsh, O. Hoydal and T. Jóhannesson, 1996. The EISMINT benchmarks for testing ice-sheet models., *Annals of Glaciology*, **23**, 1–12.

Huybrechts, P. and J. de Wolde, 1999. The dynamic response of the Greenland and Antarctic ice sheets to multiple-century climatic warming., *Journal of Climate*, **12**(8), 2169–2188.

IPCC, 2006. Intergovernmental Panel on Climate Change Data Distribution Center: The Climatic Research Unit Global Climate Dataset - mean 1961-90 climatology., http://www.ipcc-data.org/, accessed 20.7.2006.

Jamieson, S. S. R., N. R. J. Hulton and M. K. M. Hagdorn, 2008. Modelling landscape evolution under ice sheets., *Geomorphology*, **97**(1-2), 91–108.

Jamieson, S. S. R. and D. E. Sugden, 2008. Landscape evolution of Antarctica., Cooper, A.K. and C. Raymond, eds., Antarctica: A Keystone in a Changing World - Proceedings of the 10th International Symposium on Antarctic Earth Sciences., The National Academies Press, Washington D.C., 39–54.

Jarvis, A., H. I. Reuter, A. Nelson and E. Guevara, 2006. Void-filled seamless SRTM data V3, available from the CGIAR-CSI SRTM 90m Database: http://srtm.csi.cgiar.org, International Centre for Tropical Agriculture (CIAT).

Kerr, A., 1993. Topography, climate and ice masses: a review., *Terra Nova*, **5**(4), 332–342.

Lambeck, K. and S. M. Nakiboglu, 1980. Seamount loading and stress in the ocean lithosphere., *Journal of Geophysical Research*, **85**, 6403–6418.

Le Brocq, A. M., A. J. Payne and M. J. Siegert, 2006. West Antarctic balance calculations: Impact of flux-routing algorithm, smoothing algorithm and topography., *Computers & Geoscience*, **32**(10), 1780–1795.

Lefebre, F., H. Gallée, J.-P. van Ypersele and W. Greuell, 2003. Modeling of snow and ice melt at ETH Camp (West Greenland): A study of surface albedo., *Journal of Geophysical Research*, **108**(D8, 4231).

Letréguilly, A., P. Huybrechts and N. Reeh, 1991a. Steady-state characteristics of the Greenland ice sheet under different climates., *Journal of Glaciology*, **37**, 149–157.

Letréguilly, A., N. Reeh and P. Huybrechts, 1991b. The Greenland ice sheet through the last glacial-interglacial cycle., *Global and Planetary Change*, **4**(4), 385–394.

Lunt, D. J., P. J. Valdes, A. Haywood and I. C. Rutt, 2008. Closure of the Panama Seaway during the Pliocene: implications for climate and Northern Hemisphere glaciation., *Climate Dynamics*, **30**(1), 1–18.

Marshall, S. J., T. S. James and G. K. C. Clarke, 2002. North American Ice Sheet reconstructions at the Last Glacial Maximum, *Quaternary Science Reviews*, **21**(1-3), 175–192.

Näslund, J.-O., P. Jansson, J. L. Fastook, J. Johnson and L. Andersson, 2005. Detailed spatially distributed geothermal heat-flow data for modeling of basal temperatures and meltwater production beneath the Fennoscandian ice sheet., *Annals of Glaciology*, **40**(1), 95–101.

NGDC, 2006. National Geophysical Data Center, 2-Minute Gridded Global Relief Data (ETOPO2v2), www.ngdc.noaa.gov/mgg/global/ , accessed 1.6.2006.

Nye, J. F., 1957. The distribution of stress and velocity in glaciers and ice sheets., *Proceedings of the Royal Society of London Sr A*, **239**, 113–133.

Oerlemans, J., B. Anderson, A. Hubbard, P. Huybrechts, T. Jóhannesson, W. H. Knap, M. Schmeits, A. P. Stroeven, R. S. W. van de Wal, J. Wallinga and Z. Zuo, 1998. Modelling the response of glaciers to climate warming., *Climate Dynamics*, **14**, 267–274.

Oksanen, J. and T. Sarjakoski, 2005. Error propagation of DEM-based surface derivatives., *Computers & Geoscience*, **31**(8), 1015–1027.

Openshaw, S., 1989. Accuracy of Spatial Databases., Taylor & Francis, London, chap. Learning to live with errors in spatial databases., 263–276.

Paterson, W. S. B., 1994. The Physics of Glaciers., Pergamon Press, Oxford, 3 ed.

Pattyn, F., 2003. A new three-dimensional higher-order thermomechanical ice sheet model: Basic sensitivity, ice stream development, and ice flow across subglacial lakes., *Journal of Geophysical Research - Solid Earth*, **108**(B8), art.no.2382.

Payne, A. J., 1995. Limit cycles in the basal thermal regime of ice sheets., *Journal of Geophysical Research*, **100**(B3), 4249–4263.

Payne, A. J., 1999. A thermomechanical model of ice flow in West Antarctica., *Climate Dynamics*, **15**, 115–125.

Payne, A. J. and D.J. Baldwin, 1999. Thermomechanical modelling of the Scandinavian ice sheet: implications for ice-stream formation., *Annals of Glaciology*, **28**, 83–89.

Payne, A. J. and D. J. Baldwin, 2000. Analysis of ice-flow instabilities identified in the EISMINT intercomparison exercise., *Annals of Glaciology*, **30**, 204–210.

Payne, A. J. and P. W. Dongelmans, 1997. Self-organization in the thermomechanical flow of ice sheets., *Journal of Geophysical Research*, **102,B6**, 12219–12233.

Payne, A. J., P. Huybrechts, A. Abe-Ouchi, R. Calov, J. L. Fastook, R. Greve, S. J. Marshall, I. Marsiat, C. Ritz, L. Tarasov and M. P. A. Thomassen, 2000. Results from the EISMINT model intercomparaison: the effects of thermomechanical coupling., *Journal of Glaciology*, **46**(153), 227–238.

Pollack, H. N., 1982. The heat flow from the continents., *Annual Review of Earth and Planetary Sciences*, **10**, 459–481.

Purves, R. S. and N. R. J. Hulton, 2000. A climatic-scale precipitation model compared with the UKCP baseline climate., *International Journal of Climatology*, **20**, 1809–1821.

Raaflaub, L. D. and M. J. Collins, 2006. The effect of error in gridded digital elevation models on the estimation of topographic parameters., *Environmental Modelling and Software*, **21**(5), 710–732.

Reeh, N., 1991. Parameterization of melt rate and surface temperature on the Greenland ice sheet., *Polarforschung*, **59**(3), 113–128.

Rignot, E. and R. H. Thomas, 2002. Mass balance of polar ice sheets., *Science*, **297**(5586), 1502–1506.

Ritz, C., A. Fabre and A. Letréguilly, 1997. Sensitivity of a Greenland ice sheet model to ice flow and ablation parameters: consequences for the evolution through the last climatic cycle., *Climate Dynamics*, **13**(1), 11–24.

Schneeberger, C., H. Blatter, A. Abe-Ouchi and M. Wild, 2003. Modelling changes in the mass balance of glaciers of the northern hemisphere for a transient 2x CO_2 scenario., *Journal of Hydrology*, **282**, 145–163.

Stone, P. H. and J. H. Carlson, 1979. Atmospheric Lapse Rate Regimes and Their Parameterization., *Journal of Atmospheric Sciences*, **3**, 415–423.

Svendsen, J. I., H. Alexanderson, V. I. Astakhov, I. Demidov, J. A. Dowdeswell, S. Funder, V. Gataullin, M. Henriksen, C. Hjort, M. Houmark-Nielsen, H. W. Hubberten, O. Ingolfsson, M. Jakobsson, K. H. Kjaer, E. Larsen, H. Lokrantz, J. P. Lunkka, A. Lysa, J. Mangerud, A. Matiouchkov, A. Murray, P. Moller, F. Niessen, O. Nikolskaya, L. Polyak, M. Saarnisto, C. Siegert, M. J. Siegert, R. F. Spielhagen and R. Stein, 2004. Late Quaternary ice sheet history of northern Eurasia., *Quaternary Science Reviews*, **23**(11-13), 1229–1271.

Tarasov, L. and W. R. Peltier, 2004. A geophysically constrained large ensemble analysis of the deglacial history of the North American ice-sheet complex, *Quaternary Science Reviews*, **23**(3-4), 359–388.

Thompson, S. L. and D. Pollard, 1997. Greenland and Antarctic Mass Balances for Present and Doubled Atmospheric CO_2 from the GENESIS Version-2 Global Climate Model., *Journal of Climate*, **10**(5), 871–900.

Vaughan, D. G. and J. R. Spouge, 2002. Risk Estimation of Collapse of the West Antarctic Ice Sheet, *Climate Change*, **52**(1), 65–91.

van der Veen, C.J., 2002. Polar ice sheets and global sea level: how well can we predict the future?, *Global and Planetary Change*, **32**, 165–194.

van de Wal, R. S. W. and J. Oerlemans, 1994. An Energy-Balance Model for the Greenland Ice-Sheet., *Global and Planetary Change*, **9**, 115–131.

Bibliography

Aerts, J. C. J. H., Clarke, K. C., Keuper, A. D., 2003. Testing popular visualization techniques for representing model uncertainty. Cartography and Geographic Information Science 30 (3), 249–261.

Agumya, A., Hunter, G. J., 2002. Responding to the consequences of uncertainty in geographical data. International Journal of Geographical Information Science 16 (5), 405–417.

Albani, M., Klinkenberg, B., Andison, D. W., Kimmins, J. P., 2004. The choice of window size in approximating topographic surfaces from digital elevation models. International Journal of Geographical Information Science 18 (6), 557–593.

Alley, R. B., Clark, P. U., Huybrechts, P., Joughin, I., 2005. Ice-sheet and sea-level changes. Science 310, 456–460.

Anandakrishnan, S., Catania, G. A., Alley, R. B., Horgan, H. J., 2007. Discovery of till deposition at the grounding line of Whillans ice stream. Science 315 (5820), 1835–1838.

Anselin, L., 1995. Local indicators of spatial association - LISA. Geographical Analysis 27 (2), 93–115.

Armstrong, R. N., Martz, L. W., 2003. Topographic parameterization in continental hydrology: a study in scale. Hydrological Processes 17 (18), 3763–3781.

Arrell, K., Fisher, P. F., Tate, N. J., Bastin, L., 2007. A fuzzy c-means classification of elevation derivatives to extract the morphometric classification of landforms in Snowdonia, Wales. Computers & Geoscience 33 (10), 1366–1381.

Benn, D. I., Evans, D. J., 1998. Glaciers and Glaciation. Arnold, London.

Bertin, J., 1983. Semiology of graphics: Diagrams, networks, maps. University of Wisconsin Press, Madison, Wisconsin.

Beven, K., 2007. Towards integrated environmental models of everywhere: uncertainty, data and modelling as a learning process. Hydrology and Earth System Sciences 11 (1), 460–467.

Beven, K., Kirkby, M., 1979. A physically based variable contribution area model of basin hydrology. Hydrological Science Bulletin 24, 43–69.

Blatter, H., 1995. Velocity and stress fields in grounded glaciers: A simple algorithm for including deviatoric stress gradients. Journal of Glaciology 41, 333–343.

Boulton, G., Payne, A., 1992. Simulation of the European ice sheet through the last glacial cycle and prediction of future glaciation. Tech. Rep. SKB 93-14, Swedish Nuclear Fuel and Waste Management Co.

Box, J. E., Bromwich, D. H., Veenhuis, B. A., Bai, L.-S., Wang, S.-H., Stroeve, J. C., Haran, T., Rogers, J. C., Steffen, K., 2006. Greenland ice sheet surface mass balance variability (1988-2004) from calibrated polar MM5 output. Journal of Climate 19 (12), 2783–2800.

Braithwaite, R., 1995. Positive degree-day factors for ablation on the Greenland ice sheet studied by energy-balance modelling. Journal of Glaciology 41 (137), 153–159.

Budd, W., Jenssen, D., 1975. Numerical modelling of glacier systems. IAHS Publications 104, 257–291.

Budd, W., Jenssen, D., Smith, I., 1984. A three-dimensional time-dependent model of the west antarctic ice sheet. Annals of Glaciology 5, 29–36.

Burrough, P. A., McDonnell, R. A., 1998. Principles of Geographic Information Systems. Oxford University Press, Oxford.

Burrough, P. A., van Gaans, P. F. M., Hootsmans, R., 1997. Continuous classification in soil survey: spatial correlation, confusion and boundaries. Geoderma 77 (2-4), 115–135.

Burrough, P. A., van Gaans, P. F. M., MacMillan, R. A., 2000. High-resolution landform classification using fuzzy k-means. Fuzzy Sets and Systems 113 (1), 37–52.

Buttenfield, B. P., 1993. Representing data quality. Cartographica 30 (2-3), 1–7.

Buttenfield, B. P., 2000. Mapping ecological uncertainty. In: Hunsaker, C., Goodchild, M., Friedl, M. A., Case, T. J. (Eds.), Spatial Uncertainty in Ecology. Springer, Berlin, pp. 116–132.

Calov, R., Marsi, I., 1998. Simulations of the northern hemisphere through the last glacial-interglacial cycle with a vertically integrated and a three-dimensional thermomechanical ice-sheet model coupled to a climate model. Annals of Glaciology 27, 169–176.

Calov, R., Savvin, A., Greve, R., Hansen, I., Hutter, K., 1998. Simulation of the Antarctic ice sheet with a three-dimensional polythermal ice-sheet model, in support of the EPICA project. Annals of Glaciology 27, 201–206.

Carabajal, C. C., Harding, D. J., 2005. ICESat validation of SRTM C-band digital elevation models. Geophysical Research Letters 32, L22S01.

Carlisle, B. H., 2000. The highs and lows of DEM error - developing a spatially distributed DEM error model. In: Proceedings of the 5th International Conference on GeoComputation. University of Greenwich, United Kingdom, pp. 23–25.

Cazorzi, F., Fontana, G. D., 1996. Snowmelt modelling by combining air temperature and a distributed radiation index. Journal of Hydrology 181, 169–187.

Chaplot, V., Darboux, F., Bourennane, H., Leguédois, S., Silvera, N., Phachomphon, K., 2006. Accuracy of interpolation techniques for the derivation of digital elevation models in relation to landform types and data density. Geomorphology 77, 126–141.

Charbit, S., Ritz, C., Philippon, G., Peyaud, V., Kageyama, M., 2007. Numerical reconstructions of the Northern Hemisphere ice sheets through the last glacial-interglacial cycle. Climate of the Past 3, 15–37.

Charbit, S., Ritz, C., Ramstein, G., 2002. Simulations of Northern Hemisphere ice-sheet retreat: sensitivity to physical mechanisms involved during the last deglaciation. Quaternary Science Reviews 21, 243–265.

Codilean, A. T., Bishop, P., Hoey, T. B., 2006. Surface process models and the links between tectonics and topography. Progress in Physical Geography 30 (3), 307–333.

Collins, W. D., Bitz, C. M., Blackmon, M. L., Bonan, G. B., Bretherton, C. S., Carton, J. A., Chang, P., Doney, S. C., Hack, J. J., Henderson, T. B., Kiehl, J. T., Large, W. G., McKenna, D. S., Santer, B. D., Smith, R. D., 2006. The community climate system model version 3 (CCSM3). Journal of Climate 19 (11), 2122–2143.

Comber, A. J., Fisher, P. F., Harvey, F., Gahegan, M., Wadsworth, R., 2006. Using metadata to link uncertainty and data quality assessments. In: Riedl, A., Kainz, W., Elmes, G. A. (Eds.), Progress in Spatial Data Handling. 12th International Symposium on Spatial Data Handling. Vol. 6. Springer, Berlin, pp. 279–292.

Corripio, J. G., 2003. Vectorial algebra algorithms for calculating terrain parameters from DEMs and solar radiation modelling in mountainous terrain. International Journal of Geographical Information Science 17 (1), 1–23.

Couclelis, H., 1996. Towards an operational typology of geographic entities with ill-defined boundaries. In: Burrough, P. A., Frank, A. U. (Eds.), Geographic Objects with Indeterminate Boundaries. Taylor & Francis, London, pp. 45–55.

Couclelis, H., 2003. The certainty of uncertainty: GIS and the limits of geographic knowledge. Transactions in GIS 7 (2), 165–175.

CRU, 2006. Climatic Research Unit, School of Environmental Sciences, University of East Anglia: 5x5 degree gridded temperature and precipitation data. http://www.cru.uea.ac.uk/, accessed 20.8.2006.

Davis, T. J., Keller, C. P., 1997a. Modelling and visualizing multiple spatial uncertainties. Computers & Geoscience 23 (4), 397–408.

Davis, T. J., Keller, C. P., 1997b. Modelling uncertainty in natural resource analysis using fuzzy sets and Monte Carlo simulation: slope stability prediction. International Journal of Geographical Information Science 11 (5), 409–434.

Debreu, L., Blayo, E., 2002. AGRIF: Adaptive grid refinement in fortran. Technical Report 0262, Institut National de Recherche en Informatique et en Automatique.

DeConto, R. M., Pollard, D., 2003. A coupled climate-ice sheet modeling approach to the Early Cenozoic history of the Antarctic ice sheet. Palaeogeography, Palaeclimatology, Palaeoecology 198, 39–52.

Deutsch, C. V., Cockerham, P. W., 1994. Practical considerations in the application of simulated annealing to stochastic simulation. Mathematical Geology 26 (1), 67–82.

Devillers, R., Bédard, Y., Jeansoulin, R., 2005. Multidimensional management of geospatial data quality information for its dynamic use within GIS. Photogrammetric Engineering and Remote Sensing 71 (2), 205–215.

Duckham, M., Mason, K., Stell, J., Worboys, M., 2001. A formal approach to imperfection in geographic information. Computers, Environment and Urban Systems 25 (1), 89–103.

Ehlschlaeger, C. R., 2002. Representing multiple spatial statistics in generalized elevation uncertainty models: moving beyond the variogram. International Journal of Geographical Information Science 16 (3), 259 – 285.

Ehlschlaeger, C. R., Goodchild, M. F., 1994. Uncertainty in spatial data: Defining, visualizing, and managing data errors. In: Proceedings of GIS/LIS 1994. Phoenix AZ, pp. 246–53.

Ehlschlaeger, C. R., Shortridge, A. M., Goodchild, M. F., 1997. Visualizing spatial data uncertainty using animation. Computers & Geoscience 23 (4), 387–395.

Eineder, M., Breit, H., Adam, N., Holzner, J., Suchandt, S., Rabus, B., 2001. SRTM X-SAR calibration results. IEEE International Geoscience and Remote Sensing Symposium, 2001. IGARSS'01. 2, 748–750.

Endreny, T. A., Wood, E. F., 2001. Representing elevation uncertainty in runoff modelling and flowpath mapping. Hydrological Processes 15 (12), 2223–2236.

Engelhardt, H., Humphrey, N., Kamb, B., Fahnestock, M., 1990. Physical conditions at the base of a fast moving antarctic ice stream. Science 248 (4951), 57–59.

Essery, R., 2003. Aggregated and distributed modelling of snow cover for a high-latitude basin. Global and Planetary Change 38, 115–120.

Essery, R., Etchevers, P., 2004. Parameter sensitivity in simulations of snowmelt. Journal of Geophysical Research 109, D20111.

Essery, R., Marks, D., 2007. Scaling and parametrization of clear-sky solar radiation over complex topography. Journal of Geophysical Research 112, D10122.

Evans, B. J., 1997. Dynamic display of spatial data-reliability: does it benefit the map user? Computers & Geoscience 23 (4), 409–422.

Evans, I. S., 1980. An integrated system of terrain analysis and slope mapping. Zeitschrift für Geomorphologie Suppl. Bd. 36, 274–295.

Fabre, A., Letréguilly, A., Ritz, C., Mangeney, A., 1995. Greenland under changing climates: sensitivity experiments with a new three-dimensional ice-sheet model. Annals of Glaciology 21, 1–7.

Fabre, A., Ramstein, G., Ritz, C., Pinot, S., Fournier, N., 1998. Coupling an AGCM with an ISM to investigate the ice sheets mass balance at the last glacial maximum. Geophysical Research Letters 25 (4), 531–534.

Farr, T. G., Rosen, P. A., Caro, E., Crippen, R., Duren, R., Hensley, S., Kobrick, M., Paller, M., Rodriguez, E., Roth, L., Seal, D., Shaffer, S., Shimada, J., Umland, J., Werner, M., Oskin, M., Burbank, D., Alsdorf, D., 2007. The Shuttle Radar Topography Mission. Reviews of Geophysics 45, RG2004.

Finlayson, D. P., Montgomery, D. R., 2003. Modeling large-scale fluvial erosion in geographic information systems. Geomorphology 53, 147–164.

Fischer, U. H., Clarke, G. K. C., 2001. Review of subglacial hydro-mechanical coupling: Trapridge Glacier, Yukon Territory, Canada. Quaternary International 86, 29–43.

Fisher, P. F., 1993. Algorithm and implementation uncertainty in viewshed analysis. International Journal of Geographical Information Science 7 (4), 331–347.

Fisher, P. F., 1996. Propagating effects of database generalization on the viewshed. Transactions in GIS 1 (2), 69–81.

Fisher, P. F., 1998. Improved modeling of elevation error with geostatistics. GeoInformatica 2:3, 215–233.

Fisher, P. F., 1999. Models of uncertainty in spatial data. In: Longley, P. A., Goodchild, M. F., Maguire, D. J., Rhind, D. W. (Eds.), Geographical information systems: principles, techniques, management and applications. John Wiley & Sons, Inc., Chichester, pp. 191–205.

Fisher, P. F., 2000. Sorites paradox and vague geographies. Fuzzy Sets and Systems 113 (1), 7–18.

Fisher, P. F., Cheng, T., Wood, J., 2004. Where is Helvellyn? Fuzziness of multi-scale landscape morphometry. Transactions of the Institute of British Geographers 29 (1), 106–128.

Fisher, P. F., Cheng, T., Wood, J., 2007. Higher order vagueness in geographical information: Empirical geographical population of type n fuzzy sets. GeoInformatica 11 (3), 311–330.

Fisher, P. F., Tate, N. J., 2006. Causes and consequences of error in digital elevation models. Progress in Physical Geography 30 (4), 467–489.

Florinsky, I. V., 1998. Combined analysis of digital terrain models and remotely sensed data in landscape investigations. Progress in Physical Geography 22 (1), 33–60.

Florinsky, I. V., 2002. Errors of signal processing in digital terrain modelling. International Journal of Geographical Information Science 16 (5), 475–501.

Foody, G. M., 2003. Uncertainty, knowledge discovery and data mining in gis. Progress in Physical Geography 27, 113–121.

Foody, G. M., Atkinson, P. M., 2002. Uncertainty in Remote Sensing and GIS. John Wiley & Sons, Inc., Chichester.

Glen, J., 1958. The flow law of ice. International Association of Scientific Hydrology Publication 47, 169–170.

GLOBE Task Team & others, 1999. The Global Land One-kilometer Base Elevation (GLOBE) Digital Elevation Model, Version 1.0. Digital data base on the World Wide Web (URL: http://www.ngdc.noaa.gov/mgg/topo/globe.html) and CD-ROMs. National Oceanic and Atmospheric Administration, National Geophysical Data Center, 325 Broadway, Boulder, Colorado 80303, U.S.A.

Goodchild, M. F., 1992. Geographical Information Science. International Journal of Geographical Information Science 6 (1), 31–45.

Goovaerts, P., 1997. Geostatistics for Natural Ressources Evalutation. Oxford University Press, Oxford, New York.

Greve, R., 1997. Application of a polythermal three-dimensional ice sheet model to the greenland ice sheet: Response to steady-state and transient climate scenarios. Journal of Climate 10 (5), 901–918.

Griethe, H., Schumann, H., 2006. The visualization of uncertain data: Methods and problems. In: Simulation und Visualisierung - SimVis'06. pp. 143–156.

Guth, P. L., 2006. Geomorphometry from SRTM: comparison to NED. Photogrammetric Engineering and Remote Sensing 72 (3), 269–277.

Hagdorn, M., Rutt, I., Payne, T., Hebeler, F., 2007. GLIMMER - The GENIE Land Ice Model with Multiply Enabled Regions - Documentation. http://glimmer.forge.nesc.ac.uk/. Universities of Bristol, Edinburgh and Zurich.

Hagdorn, M. K. M., 2003. Reconstruction of the past and forecast of the future European and British ice sheets and associated sea-level change. unpublished PhD thesis, University of Edinburgh.

Harrower, M., 2004. Representing uncertainty: Does it help people make better decisions? In: UCGIS Workshop: Geospatial Visualization and Knowledge Discovery Workshop. National Conference Center, Landsdowne, VA.

Hastings, D. A., Dunbar, P. K., 1998. Development and assessment of the Global Land One-km Base Elevation Digital Elevation Model (GLOBE). ISPRS Archives 32 (4), 218–221.

Hastings, D. A., Dunbar, P. K., 1999. Global Land One-kilometer Base Elevation (GLOBE) Digital Elevation Model, Documentation, Volume 1.0. Key to Geophysical Records Documentation (KGRD) 34. National Oceanic and Atmospheric Administration, National Geophysical Data Center, 325 Broadway, Boulder, Colorado 80303, U.S.A., 1st Edition.

Hebeler, F., 2003. Methoden zur objektiven auswahl repräsentativer untersuchungsstandorte für physiogeographische und bodenkundliche fragestellungen mittels geographischer informationssysteme. Diplomarbeit Geographie, Universität Giessen, Institut für Bodenkunde und Bodenerhaltung.

Hebeler, F., Purves, R. S., 2004. Representation of topography and its role in uncertainty: a case study in ice sheet modelling. In: GIScience 2004: Proceedings of the Third International Conference on Geographic Information Science. pp. 118–121.

Hebeler, F., Purves, R. S., 2005a. A comparison of the influence of topographic and mass balance uncertainties on modeled ice sheet extents and volumes. In: Eos Trans. AGU. Vol. 86 of Fall Meet. Suppl. No 52.

Hebeler, F., Purves, R. S., 2005b. GIS in ice sheet modelling: assessing the impact of topographic uncertainties. In: Proceedings of the Swiss Geoscience Meeting 2005.

Hebeler, F., Purves, R. S., 2007a. Estimating the impacts of DEM uncertainty on ice sheet model results. In: Geophysical Research Abstracts. Vol. 9-08333.

Hebeler, F., Purves, R. S., 2007b. Modelling DEM data uncertainties for Monte Carlo simulations of ice sheet models. In: Proceedings of the 5th International Symposium on Spatial Data Quality. ITC, Enschede, The Netherlands.

Hebeler, F., Purves, R. S., 2008a. Modeling DEM data uncertainties for monte carlo simulations of ice sheet models. In: Stein, A., Shi, J., Bijker, W. (Eds.), Quality Aspects in Spatial Data Mining. CRC Press, Boca Raton, Ch. 14, pp. 175–196.

Hebeler, F., Purves, R. S., 2008b. Parameterisation of low resolution melt modelling using hypsometric subgrids and its susceptibility to uncertainty. Hydrological Processes 22 (19), 3965–3979.

Hebeler, F., Purves, R. S., in press. The influence of elevation uncertainty on derivation of topographic indices. Geomorphology.

Hebeler, F., Purves, R. S., Hagdorn, M., Hulton, N. R., 2005. Experiments on the sensitivity of modelled extent of Fennoscandian icesheet to representation of topography. In: Geophysical Research Abstracts. Vol. 7-07637.

Hebeler, F., Purves, R. S., Jamieson, S. S. R., in press. The impact of parametric uncertaintiy analysis and dem error in ice sheet modelling. Journal of Glaciology.

Herrington, L., Pellegrini, G., 2000. An advanced shape of country classifier: Extraction of surface features from DEMs. In: 4th International Conference on GIS and Environmental Modeling (GIS/EM4). Problems, Prospects and Research Needs. Banff, Alberta, Canada. pp. 2–8.

Heuvelink, G. B., 1998. Error propagation in environmental modelling with GIS. In: Fisher, P., Raper, J. (Eds.), Research Monographs in Geographic Information Systems. Taylor & Francis, London.

Heuvelink, G. B., Burrough, P. A., Stein, A., 1989. Propagation of errors in spatial modelling with GIS. International Journal of Geographical Information Science 3, 303–322.

Hindmarsh, R. C., 1993. Modelling the dynamics of ice sheets. Progress in Physical Geography 17 (4), 391–412.

Hock, R., 1999. A distributed temperature-index ice- and snowmelt model including potential direct solar radiation. Journal of Glaciology 45 (149), 101–111.

Hock, R., 2003. Temperature index melt modelling in mountain areas. Journal of Hydrology 282, 104–115.

Hofton, M., Dubayah, R., Blair, J., Rabine, D., 2006. Validation of srtm elevations over vegetated and non-vegetated terrain using medium footprint lidar. Photogrammetric Engineering and Remote Sensing 72 (3), 279–285.

Holmes, K. W., Chadwick, O., Kyriakidis, P. C., 2000. Error in a USGS 30-meter digital elevation model and its impact on terrain modeling. Journal of Hydrology 233, 154–173.

Horn, B., 1981. Hill shading and the reflectance map. Proceedings of the IEEE 69, 14–47.

Hu, Z., Islam, S., 1997. Effects of spatial variability on the scaling of land surface parameterizations. Boundary-Layer Meteorology 83, 441–461.

Hubbard, A., 1999. High-resolution modeling of the advance of the Younger Dryas ice sheet and its climate in Scotland. Quaternary Research 52, 27–43.

Hubbard, A., Hein, A. S., Kaplan, M. R., Hulton, N. R., Glasser, N., 2005. A modelling reconstruction of the Last Glacial Maximum ice sheet and its deglaciation in the vicinity of the Northern Patagonian Icefield, South America. Annals of Glaciology 87 A (2), 375–391.

Hugentobler, M., 2004. Terrain modelling with triangle based free-form surfaces. Phd, Dept. of Geography, University of Zurich.

Hugentobler, M., Purves, R. S., Schneider, B., 2004. Evaluating methods for interpolating continuous surfaces from irregular data: case study. In: Proccedings of the 11th International Symposium on Spatial Data Handling. University of Leicester, pp. 109–124.

Hulton, N. R., Purves, R. S., McCulloch, R., Sugden, D. E., Bentley, M., 2002. The Last Glacial Maximum and deglacation in southern South America. Quaternary Science Reviews 21, 233–241.

Hulton, N. R., Sugden, D. E., Payne, A., Clapperton, C., 1994. Glacier modeling and the climate of Patagonia during the last glacial maximum. Quaternary Research 42, 1–19.

Hulton, N. R., Sugden, D. E., Purves, R. S., 2003. Author's response to the comments by G.Wenzens. Quaternary Science Reviews 22, 755–757.

Hunter, G. J., Goodchild, M. F., 1995. Dealing with error in spatial databases: a simple case study. Photogrammetric Engineering and Remote Sensing 61 (5), 529–537.

Hunter, G. J., Goodchild, M. F., 1997. Modelling the uncertainty of slope and aspect estimates derived from spatial databases. Geographical Analysis 19 (1), 35–49.

Hutchinson, M., Gallant, J., 2000. Digital elevation models and representation of terrain shape. In: Wilson, J., Gallant, J. (Eds.), Terrain Analysis: Principles and Applications. John Wiley & Sons, Inc., Chichester, pp. 29–50.

Hutter, K., 1983. Theoretical Glaciology. Mathematical Approaches to Geophysics. D. Reidel Publishing Company, Dordrecht, Boston, Lancaster.

Huybrechts, P., 1986. A three-dimensional time-dependant numerical model for polar ice sheets; some basic testing with a stable and efficient finite difference scheme. Tech. rep., Geografisch Instituut, Vrije Universiteit Brussel, Belgium.

Huybrechts, P., 1990. A 3-D model for the Antarctic ice sheet: a sensitivity study on the glacial-interglacial contrast. Climate Dynamics 5, 79–92.

Huybrechts, P., 2004. Mass balance of the cryosphere: observations and modelling of contemporary and future changes. Cambridge University Press, Cambridge, Ch. Antarctica: modelling, pp. 491–523.

Huybrechts, P., de Wolde, J., 1999. The dynamic response of the Greenland and Antarctic ice sheets to multiple-century climatic warming. Journal of Climate 12 (8), 2169–2188.

Huybrechts, P., Payne, A., Abe-Ouchi, A., Calov, R., Fabre, A., Fastook, J., Greve, R., Hindmarsh, R., Hoydal, O., Jóhannesson, T., 1996. The EISMINT benchmarks for testing ice-sheet models. Annals of Glaciology 23, 1–12.

IPCC, 2006. Intergovernmental panel on climate change data distribution center: The climatic research unit global climate dataset - mean 1961-90 climatology. http://www.ipcc-data.org/, accessed 20.7.2006.

IPCC, 2007. Intergovernmental Panel on Climate Change - Fourth Assessment Report: Climate Change 2007 - Working Group II: Impacts, Adaptation and Vulnerability. Intergovernmental Panel on Climate Change, United Nations, Geneve.

Jamieson, S. S. R., Hulton, N. R. J., Hagdorn, M., 2008. Modelling landscape evolution under ice sheets. Geomorphology 97 (1-2), 91–108.

Jamieson, S. S. R., Sugden, D. E., 2008. Landscape evolution of Antarctica. In: Cooper, A., Raymond, C. (Eds.), Antarctica: A Keystone in a Changing World - Proceedings of the 10th International Symposium on Antarctic Earth Sciences. The National Academies Press, Washington D.C., pp. 39–54.

Jansson, P., Hock, R., Schneider, T., 2003. The concept of glacier storage: a review. Journal of Hydrology 282, 116–129.

Jarvis, A., Reuter, H., Nelson, A., Guevara, E., 2006. Void-filled seamless SRTM data V3, available from the CGIAR-CSI SRTM 90m Database: http://srtm.csi.cgiar.org. International Centre for Tropical Agriculture (CIAT).

Jarvis, A., Rubiano, J., Nelson, A., Farrow, A., Mulligan, M., 2004. Practical use of SRTM data in the tropics: Comparisons with digital elevation models generated from cartographic data. Working Document 198, 32 p., International Centre for Tropical Agriculture (CIAT), Cali, Columbia.

Johnsen, S., Clausen, H. B., Dansgaard, W., Fuhrer, K., Gundestrup, N. Hammer, C. U., Iversen, P., Jouzel, J., Stauffer, B., Steffensen, J. P., 1992. Irregular glacial interstadials recorded in a new greenland ice core. Nature 359, 311–313.

Jones, K. H., 1998. A comparison of algorithms used to compute hill slope as a property of the DEM. Computers & Geoscience 24 (4), 315–323.

Journel, A. G., 1996. Modelling uncertainty and spatial dependence: Stochastic imaging. International Journal of Geographical Information Science 10 (5), 517–522.

Kaser, G., Juen, I., Georges, C., Gómez, J., Tamayo, W., 2003. The impact of glaciers on the runoff and the reconstruction of mass balance history from hydrological data in the tropical Cordillera Blanca, Perú. Journal of Hydrology 282, 130–144.

Kerr, A., 1990. The initiation of maritime ice sheets. Zeitschrift für Gletscherkunde und Glazialgeologie 26 (1), 69–79.

Kerr, A., 1993. Topography, climate and ice masses: a review. Terra Nova 5 (4), 332–342.

Keuper, A. D., 2004. The influence of uncertainty metadata on decision-making using geographic data products. Unpublished phd thesis, University of California, Santa Barbara.

Kienzle, S., 2004. The effect of DEM raster resolution on first order, second order and compound terrain derivatives. Transactions in GIS 8 (1), 83–111.

Kuhn, M., 2003. Redistribution of snow and glacier mass balance from a hydrometeorological model. Journal of Hydrology 282, 95–103.

Kumar, L., Skidmore, A. K., Knowles, E., 1997. Modelling topographic variation in solar radiation in a GIS environment. International Journal of Geographical Information Science 11, 475–497.

Kyriakidis, P. C., 2001. Spatial Uncertainty in Ecology: Implications for Remote Sensing and GIS Applications. 175-213. Springer, Berlin, Ch. Geostatistical Models of Uncertainty for Spatial Data.

Kyriakidis, P. C., Goodchild, M. F., 2006. On the prediction error variance of three common spatial interpolation schemes. International Journal of Geographical Information Science 20 (8), 823–855.

Kyriakidis, P. C., Shortridge, A., Goodchild, M., 1999. Geostatistics for conflation and accuracy assessment of digital elevation models. International Journal of Geographical Information Science 13 (7), 677–707.

Laube, P., van Kreveld, M., Imfeld, S., 2005. Developments in Spatial Data Handling. Springer, Berlin, Ch. Finding REMO - Detecting Relative Motion Patterns in Geospatial Lifelines., pp. 201–215.

Lee, J., 1996. Digital elevation models: Issues of data accuracy and applications. In: Proceedings of the 1996 ESRI International User Conference. Palm Springs, CA, USA.

Lefebre, F., Gallée, H., van Ypersele, J.-P., Greuell, W., 2003. Modeling of snow and ice melt at ETH camp (West Greenland): A study of surface albedo. Journal of Geophysical Research 108 (D8, 4231).

Leung, L. R., Wigmosta, M. S., Ghan, S. J., Epstein, D. J., Vail, L. W., 1996. Application of a subgrid orographic precipitation/surface hydrology scheme to a mountain watershed. Journal of Geophysical Research 101 (D8), 12803–12818.

Li, Z., Zhu, Q., Gold, C., 2005. Digital Terrain Modelling: Principles and Methodology. CRC Press, Boca Raton.

Liston, G. E., 2004. Representing subgrid snow cover heterogeneities in regional and global models. Journal of Climate 17 (6), 1381–1397.

Liu, H., Jezek, K. C., 1999. Investigating DEM error patterns by directional variograms and fourier analysis. Geographical Analysis 31, 249–266.

Longley, P. A., Goodchild, M. F., Maguire, D. J., Rhind, D. R., 2005. Geographic Information Systems and Science. John Wiley & Sons, Inc., Chichester.

Luce, C. H., Tarboton, D. G., 2001. Modeling snowmelt over an area: Modeling subgrid scale heterogeneity in distributed model elements. In: Proc. MODSIM.

Luce, C. H., Tarboton, D. G., Cooley, K. R., 1999. Sub-grid parameterization of snow distribution for an energy and mass balance snow cover model. Hydrological Processes 13, 1921–1933.

Lythe, M., Vaughan, D. G., BEDMAP-Consortium, 2001. BEDMAP: A new ice thickness and subglacial topographic model of antarctica. Journal of Geophysical Research 106 (B6), 11335–11352.

MacEachren, A. M., Robinson, A., Hopper, S., Gardner, S., Murray, R., Gahegan, M., Hetzler, E., 2005. Visualizing geospatial information uncertainty: What we know and what we need to know. Cartography and Geographic Information Science 32 (3), 139–160.

MacMillan, R. A., McNabb, D. H., Jones, R. K., 2000. Automated landform classification using dems: a conceptual framework for a multi-level, hierarchy of hydrologically and geomorphologicaly oriented physiographic mapping units. In: 4th International Conference on GIS and Environmental Modeling (GIS/EM4). Problems, Prospects and Research Needs. Banff, Alberta, Canada.

Malanson, G. P., 1999. Considering complexity. Annals of the Association of American Geographers 89 (4), 746–753.

Marshall, S. J., 2002. Modelled nucleation centres of the Pleistocene ice sheets from an ice sheet model with subgrid topographic and glaciologic parameterizations. Quaternary International 95-96, 125–137.

Marshall, S. J., Clarke, G., 1999. Ice sheet inception: subgrid hypsometric parameterization of mass balance in an ice sheet model. Climate Dynamics 15, 533–560.

Martin, Y., Church, M., 2004. Numerical modelling of landscape evolution: geomorphological perspectives. Progress in Physical Geography 28 (3), 317–339.

Martinoni, D., 2002. Models and experiments for quality handling in digital terrain modelling. Ph.D. thesis, University of Zurich, Dept. of Geography.

Matheron, G., 1969. Principles of geostatistics. Economical Geology 58, 1246–1266.

Monmonier, M., 2006. Cartography: uncertainty, interventions, and dynamic display. Progress in Human Geography 30 (3), 373–381.

Moore, I., Grayson, R., Ladson, A., 1991. Digital terrain modelling: A review of hydrological, geomorphological, and biological applications. Hydrological Processes 5 (1), 3–30.

Moran, P., 1950. Notes on continuous stochastic phenomena. Biometrika 37, 17–23.

Murray, T., 1997. Assessing the paradigm shift: deformable glacier beds. Quaternary Science Reviews 16 (9), 995–1016.

Nye, J., 1957. The distribution of stress and velocity in glaciers and ice sheets. Proceedings of the Royal Society of London Sr A 239, 113–133.

Oehler, S., 2005. Visualisierung von unsicherheiten unter einbezug grossraeumiger modellierungsdaten. Diplomarbeit, Geographisches Institut der Universitaet Zuerich.

Oerlemans, J., 1980. Model experiments on the 100,000-yr glacial cycle. Nature 287, 430–432.

Oerlemans, J., 2002. On glacial inception and orography. Quaternary International 95 96, 5–10.

Oerlemans, J., Hoogendoorn, N., 1989. Mass balance gradients and climatic change. Quaternary Science Reviews 35 (121), 399–405.

Ohmura, A., Kasser, P., Funk, M., 1992. Climate at the equilibrium line of glaciers. Journal of Glaciology 38 (130), 397–408.

Oksanen, J., Sarjakoski, T., 2005a. Error propagation analysis of DEM-based drainage basin delineation. International Journal of Remote Sensing 26 (14), 3085–3102.

Oksanen, J., Sarjakoski, T., 2005b. Error propagation of DEM-based surface derivatives. Computers & Geoscience 31 (8), 1015–1027.

Oksanen, J., Sarjakoski, T., 2006. Uncovering the statistical and spatial characteristics of fine toposcape DEM error. International Journal of Geographical Information Science 20 (4), 345–369.

Oliver, M., Webster, R., 1990. Kriging: a method of interpolation for geographical information systems. International Journal of Geographical Information Science 4 (3), 313–332.

Otto-Bliesner, B. L., 1996. Initiation of a continental ice sheet in a global climate model (GENESIS). Journal of Geophysical Research 101 (D12), 16909–16920.

Otto-Bliesner, B. L., Brady, E. C., Clauzet, G., Tomas, R., Levis, S., Kothavala, Z., 2006. Last glacial maximum and Holocene climate in CCSM3. Journal of Climate 19 (11), 2526–2544.

Paterson, W., 1994. The Physics of Glaciers., 3rd Edition. Pergamon Press, Oxford.

Pattyn, F., 2003a. Ice-sheet modelling at different spatial resolutions: focus on the grounding zone. Annals of Glaciology 31, 211–216.

Pattyn, F., 2003b. A new three-dimensional higher-order thermomechanical ice sheet model: Basic sensitivity, ice stream development, and ice flow across subglacial lakes. Journal of Geophysical Research - Solid Earth 108 (B8), art.no.2382.

Payne, A. J., 1999. A thermomechanical model of ice flow in West Antarctica. Climate Dynamics 15, 115–125.

Payne, A. J., Dongelmans, P., 1997. Self-organization in the thermomechanical flow of ice sheets. Journal of Geophysical Research 102,B6, 12219–12233.

Payne, A. J., Huybrechts, P., Abe-Ouchi, A., Calov, R., Fastook, J., Greve, R., Marshall, S., Marsiat, I., Ritz, C., Tarasov, L., Thomassen, M., 2000. Results from the EISMINT model intercomparaison: the effects of thermomechanical coupling. Journal of Glaciology 46 (153), 227–238.

Payne, A. J., Sugden, D. E., 1990. Topography and ice sheet growth. Earth Surface Processes and Landforms 15, 625–639.

Pellicciotti, F., Brock, B., Strasser, U., Burlando, P., Funk, M., Corripio, J., 2005. An enhanced temperature-index glacier melt model including the shortwave radiation balance: development and testing for Haut Glacier d'Arolla, Switzerland. Journal of Glaciology 51 (175), 573–587.

Pike, R. J., 2000. Geomorphometry - diversity in quantitative surface analysis. Progress in Physical Geography 24 (1), 1–20.

Plewe, B., 2002. The nature of uncertainty in historical geographic information. Transactions in GIS 6 (4), 431–456.

Pollard, D., 1982. A simple ice-sheet model yields realistic 100 kyr glacial cycles. Nature 296 (5855), 334–338.

Pollard, D., DeConto, R., 2007. Grounding line behavior in a heuristically coupled ice sheet-shelf model. In: Geophysical Research Abstracts. Vol. 9-03103.

Pollard, D., Thompson, S. L., 1997. Climate and ice-sheet mass balance at the last glacial maximum from the genesis version 2 global climate model. Quaternary Science Reviews 16 (8), 841–863.

Purves, R., Clough, P., Joho, H., 2005. Identifying imprecise regions for geographic information retrieval using the web. In: Billen, R., Drummond, J., Forrest, D., Joao, E. (Eds.), Proceedings of the 13th GIS Research UK: GISRUK 2005. Glasgow.

Purves, R. S., Hulton, N. R., 2000a. A climatic-scale precipitation model compared with the UKCP baseline climate. International Journal of Climatology 20, 1809–1821.

Purves, R. S., Hulton, N. R., 2000b. Experiments in linking regional climate, ice-sheet models and topography. Journal of Quaternary Science 15, 369–375.

Purves, R. S., Mackaness, W. A., Sugden, D. E., 1999. An approach to modelling the impact of snow drift on glaciation in the cairngorm mountains, scotland. Journal of Quaternary Science 14 (4), 313–321.

Raaflaub, L. D., Collins, M. J., 2006. The effect of error in gridded digital elevation models on the estimation of topographic parameters. Environmental Modelling and Software 21 (5), 710–732.

Raper, J., Livingstone, D., 1995. Development of a geomorphological spatial model using object-oriented design. International Journal of Geographical Information Science 9 (4), 359–383.

Reeh, N., 1991. Parameterization of melt rate and surface temperature on the Greenland ice sheet. Polarforschung 59 (3), 113–128.

Reinke, K., Hunter, G. J., 2002. Spatial Data Quality. Taylor & Francis, London, Ch. A Theory for Communicating Uncertainty in Spatial Databases., pp. 76–101.

Ritz, C., Fabre, A., Letréguilly, A., 1997. Sensitivity of a Greenland ice sheet model to ice flow and ablation parameters: consequences for the evolution through the last climatic cycle. Climate Dynamics 13 (1), 11–24.

Ritz, C., Mazauric, C., Peyaud, V., Debreu, L., 2007. A mesh refinement approach, AGRIF, to take into account small scale processes in the GRISLI large scale ice sheet model. In: Geophysical Research Abstracts. Vol. 9-09892.

Saito, F., Abe-Ouchi, A., Blatter, H., 2003. Effects of first-order stress gradients in an ice sheet evaluated by a three-dimensional thermomechanical coupled model. Annals of Glaciology 37 (1), 166–172.

Saito, F., Abe-Ouchi, A., Blatter, H., 2006. European ice sheet modelling initiative (EISMINT) model intercomparison experiments with first-order mechanics. Journal of Geophysical Research 111, F02012.

Salzmann, N., Frei, C., Vidale, P.-L., Hoelzle, M., 2007. The application of regional climate model output for the simulation of high-mountain permafrost scenarios. Global and Planetary Change 56, 188–202.

Santos, J., Lodwick, W. A., Neumaier, A., 2002. A new approach to incorporate uncertainty in terrain modeling. In: Egenhofer, M. J., Mark, D. M. (Eds.), Geographic Information Science, Second International Conference. Vol. 2478 of Lecture Notes in Computer Science. Springer, Berlin.

Schmidt, J., Evans, I. S., Brinkmann, J., 2003. Comparison of polynomial models for land surface curvature calculation. International Journal of Geographical Information Science 17 (8), 797–814.

Schneeberger, C., Blatter, H., Abe-Ouchi, A., Wild, M., 2003. Modelling changes in the mass balance of glaciers of the northern hemisphere for a transient 2x CO_2 scenario. Journal of Hydrology 282, 145–163.

Schneider, B., 2001a. On the uncertainty of local form of lines and surfaces. Cartography & Geographic Information Systems 28 (4), 237–247.

Schneider, B., 2001b. Phenomenon-based specification of the digital representation of terrain surfaces. Transactions in GIS 5 (1), 39–52.

Schneider, B., Martinoni, D., 2001. A distributed geoprocessing concept for enhancing terrain analysis for environmental modeling. Transactions in GIS 5 (2), 165–178.

Schoof, C., 2007a. Ice sheet grounding line dynamics: steady states, stability and hysteresis. Journal of Geophysical Research 112, F03S28.

Schoof, C., 2007b. Marine ice-sheet dynamics. part 1. the case of rapid sliding. Journal of Fluid Mechanics 573, 27–53.

Schytt, D., 1969. A study of 'ablation gradient'. Geografski Annaler 49A, 327–332.

Shary, P. A., 1995. Land surface in gravity points classification. Mathematical Geology 27 (3), 373–390.

Shary, P. A., Sharaya, L. S., Mitusov, A. V., 2002. Fundamental quantitative methods of land surface analysis. Geoderma 107, 1–32.

Shortridge, A. M., 2001. Characterizing uncertainty in digital elevation models. In: Hunsaker, C. T., Goodchild, M. F., Friedl, M. A., Case, T. J. (Eds.), Spatial Uncertainty in Ecology: Implications for Remote Sensing and GIS Applications. Springer, Berlin, New York., pp. 238–257.

Shortridge, A. M., 2006. Shuttle radar topography mission elevation data error and its relationship to land cover. Cartography and Geographic Information Science 33 (1), 65–75.

Shortridge, A. M., Clarke, K. C., 1999. On some limitations of square raster cell structures for digital elevation data modeling. In: Lowell, K., Jaton, A. (Eds.), Spatial Accuracy Assessment: Land Information Uncertainty in Natural Resources. Ann Arbor Press, Michigan.

Shortridge, A. M., Goodchild, M. F., 1999. Communicating uncertainty for global data sets. In: Shi, W., Goodchild, M. F., Fisher, P. F. (Eds.), International Symposium on Spatial Data Quality. Hong Kong, pp. 59–65.

Slaymaker, O., Kelly, R. E., 2007. The Cryosphere And Global Environmental Change. Blackwell Publishing, Oxford.

Smith, M. J., Clark, C. D., 2005. Methods for the visualization of digital elevation models for landform mapping. Earth Surface Processes and Landforms 30 (7), 885–900.

Stokes, C. R., Clark, C. D., Lian, O. B., Tulaczyk, S., 2007. Ice stream sticky spots: A review of their identification and influence beneath contemporary and palaeo-ice streams. Earth Science Reviews 81 (3-4), 217–249.

Strasser, U., Corripio, J., Pellicciotti, F., Burlando, P., 2004. Spatial and temporal variability of meteorological variables at Haut Glacier d'Arolla (Switzerland) during the ablation season 2001: Measurements and simulations. Journal of Geophysical Research 109, D03103.

Strasser, U., Etchevers, P., 2003. Using subgrid parameterization for topography and a forest canopy climate model for improving snowmelt flood simulations. In: de Jong, C., Collins, D., Ranzi, R. (Eds.), Climatology and Hydrology of Mountain Areas. John Wiley & Sons, Inc., Chichester.

Sugden, D. E., Hulton, N. R., Purves, R. S., 2002. Modelling the inception of the Patagonian icesheet. Quaternary International 95 96, 55–64.

Sun, G., Ranson, K. J., Kharuk, V. I., Kovacs, K., 2003. Validation of surface height from shuttle radar topography mission using shuttle laser altimeter. Remote Sensing of Environment 88 (4), 401–411.

Swisstopo, 2007. DTM-AV 2m Grid. www.swisstopo.ch, accessed 24.1.2008.

Tarboton, D. G., 1997. A new method for the determination of flow directions and upslope areas in grid digital elevation models. Water Resources Research 33 (2), 309–319.

Tarboton, D. G., 1999. TARDEM, a Suite of Programs for the Analysis of Digital Elevation Data. Utah State University, 8200 Old Main Hill, Logan, UT 84322-8200, USA.

Tobler, W. R., 1970. A computer movie simulating urban growth in the Detroit region. Economic Geography 46, 230–240.

Tucker, G. E., Whipple, K. X., 2002. Topographic outcomes predicted by stream erosion models: Sensitivity analysis and intermodel comparison. Journal of Geophysical Research 107 (B9), 2179.

U.S. Geological Survey, 1996. GTOPO30: Global 30 arc second elevation data. Online at http://edc.usgs.gov/products/elevation/gtopo30.html, eROS Data Center Distributed Active Archive Center (EDC DAAC), Sioux Falls, SD.

van de Wal, R. S. W., Oerlemans, J., 1994. An energy-balance model for the Greenland ice-sheet. Global and Planetary Change 9, 115–131.

van der Veen, C., 2002. Polar ice sheets and global sea level: how well can we predict the future? Global and Planetary Change 32, 165–194.

Veregin, H., 1989. Accuracy of Spatial Databases. Taylor & Francis, London, Ch. Error modelling for the map overlay operation., pp. 3–18.

Walker, J. P., Willgoose, G. R., 1999. On the effect of digital elevation model accuracy on hydrology and geomorphology. Water Resources Research 35 (7), 2259–2268.

Wechsler, S. P., 2003. Perceptions of digital elevation model uncertainty by DEM users. URISA Journal 15 (2), 57–64.

Wechsler, S. P., 2006. Uncertainties associated with digital elevation models for hydrologic applications: a review. Hydrology and Earth System Sciences Discussions 3, 2343–2384.

Wechsler, S. P., Kroll, C. N., 2006. Quantifying DEM uncertainty and its effects on topographic parameters. Photogrammetric Engineering and Remote Sensing 72 (9), 1081–1090.

Weibel, R., Buttenfield, B. P., 1992. Improvement of GIS graphics for analysis and decision-making . International Journal of Geographical Information Science 6 (3), 223–245.

Weibel, R., Heller, M., 1991. Digital terrain modelling. In: Maguire, D., Goodchild, M., Rhind, D. (Eds.), Geographical Information Systems: Principles and Applications. John Wiley & Sons, Inc., Chichester, pp. 269–297.

Wenzens, G., 2003. Comment on: 'The Last Glacial Maximum and deglaciation in southern South America' by N.R.J. Hulton, R.S. Purves, R.D. McCulloch, D.E. Sugden, M.J. Bentley [Quaternary Science Reviews 21 (2002) 233-241]. Quaternary Science Reviews 22 (5-7), 751–754.

Williams, K. S., Tarboton, D. G., 1999. The ABC's of snowmelt: a topographically factorized energy component snowmelt model. Hydrological Processes 13, 1905–1920.

Wise, S. M., 1998. The effect of GIS interpolation errors on the use of digital elevation models in geomorphology. In: Lane, S. N., Richards, K. S., Chandler, J. H. (Eds.), Landform Monitoring, Modelling and Analysis. John Wiley & Sons, Inc., Chichester.

Wise, S. M., 2000. Assessing the quality for hydrological applications of digital elevation models derived from contours. Hydrological Processes 14 (11), 1909–1929.

Wood, J. D., 1996. The geomorphological characterisation of digital elevation models. Ph.D. thesis, University of Leicester, UK.

Wood, J. D., 1998. Modelling the continuity of surface form using digital elevation models. In: Poiker, T., Chrisman, N. (Eds.), Proceedings, 8th International Symposium on Spatial Data Handling. pp. 725–36.

Wood, J. D., Fisher, P. F., 1993. Assessing interpolation accuracy in elevation models. IEEE Computer Graphics & Applications 13 (2), 48–56.

Zadeh, L. A., 1965. Fuzzy sets. Information and Control 8, 338–353.

Zevenbergen, L. W., Thorne, C. R., 1987. Quantitative analysis of land surface topography. Earth Surface Processes and Landforms 12, 47–56.

Zhang, X., Drake, N. A., Wainwright, J., Mulligan, M., 1999. Comparison of slope estimates from low resolution DEMs: scaling issues and a fractal method for their solution. Earth Surface Processes and Landforms 24 (9), 763–779.

Zhou, Q., Liu, X., 2004. Analysis of errors of derived slope and aspect related to DEM data properties. Computers & Geoscience 30, 369–378.

Ziadat, F. M., 2007. Effect of contour intervals and grid cell size on the accuracy of DEMs and slope derivatives. Transactions in GIS 11 (1), 67–81.